Arne Wolpers

Advances in chain-growth control and analysis of polymer

Boosting iodine-mediated polymerizations and mastering band-broadening effects in size-exclusion chromatography

Advances in chain-growth control and analysis of polymer: boosting iodine-mediated polymerizations and mastering band-broadening effects in size-exclusion chromatography

Dissertation

zur Erlangung des mathematisch-naturwissenschaftlichen Doktorgrades

Doctor rerum naturalium

der Georg-August-Universität Göttingen

im Promotionsprogramm Catalysis for Sustainable Synthesis (CaSuS)

der Georg–August University School of Science (GAUSS)

vorgelegt von

Arne Wolpers

aus Hildesheim

Göttingen, 2014

Betreuungsausschuss

Prof. Dr. Philipp Vana, MBA	*Institut für Physikalische Chemie, Georg-August-Universität Göttingen*
Prof. Dr. Michael Buback	*Institut für Physikalische Chemie, Georg-August-Universität Göttingen*
Prof. Dr. Dietmar Stalke	*Institut für Anorganische Chemie, Georg-August-Universität Göttingen*

Mitglieder der Prüfungskommission

Referent

Prof. Dr. Philipp Vana, MBA	*Institut für Physikalische Chemie, Georg-August-Universität Göttingen*

Korreferent

Prof. Dr. Michael Buback	*Institut für Physikalische Chemie, Georg-August-Universität Göttingen*

2. Korreferent

Assoc.-Prof. Dr. Gregory T. Russell	*Department of Chemistry, University of Canterbury*

Weitere Mitglieder der Prüfungskommission

Prof. Dr. Dietmar Stalke	*Institut für Anorganische Chemie, Georg-August-Universität Göttingen*
Prof. Dr. Peter Botschwina	*Institut für Physikalische Chemie, Georg-August-Universität Göttingen*
Prof. Dr. Burkhard Geil	*Institut für Physikalische Chemie, Georg-August-Universität Göttingen*
Jun.-Prof. Dr. Ricardo Mata	*Institut für Physikalische Chemie, Georg-August-Universität Göttingen*

Tag der mündlichen Prüfung: 10. November 2014

Abstract

In the present thesis, various novel iodine-mediated *reversible-deactivation radical polymerization* (RDRP) techniques were investigated. In addition, effects of instrumental band broadening (BB) in size-exclusion chromatography (SEC) on molar-mass analysis of polymers were theoretically evaluated.

Mechanistically, in *iodine-transfer polymerizations* (ITPs) and *reverse ITPs* (RITPs), control of chain-growth is generally achieved by a *degenerative chain transfer* (DT) of iodine end-groups between two macromolecules. While in ITP systems, iodine is introduced by an iodo *chain-transfer agent* (CTA), in RITP systems, more highly activated iodo CTAs are generated in situ. In the case of *reversible chain-transfer catalyzed polymerizations* (RTCPs), a catalyst added to an ITP or RITP system is proposed to lead to an additional reversible chain-transfer mechanism of iodine between a macromolecule and a catalyst molecule, resulting in an improved chain-growth control.

In this thesis, for poly(methyl methacrylate) (polyMMA) produced by several RITP-based RTCPs, the beneficial impact of the used catalysts on chain-growth control was confirmed by molar-mass analysis via SEC. End-group analysis via *electrospray ionization mass spectrometry* (ESI-MS) indicated that chain-growth control is exclusively achieved by terminal iodine atoms, supporting the proposed RTCP mechanism and potentially enabling further polymer processing by end-group conversion reactions. Contribution of the catalysts to either initiation or termination reactions—leading to their undesired depletion or to rate retardation—can also be excluded. In addition to the thorough ESI-MS studies, a strategy was presented to effectively reduce the adverse inhibition period of RITP by the use of a radical-initiator cocktail.

In a novel approach, the application of UV initiation was developed for iodine-mediated polymerizations. Systems of *n*-butyl acrylate (BA), *n*-butyl methacrylate (BMA) and styrene (St) were irradiated in the presence of an iodo CTA and a UV initiator. Their respective potentials to generate well-defined iodine-functionalized polymer at room temperature was studied. The underlying mechanism and kinetics of the systems were thoroughly investigated both analytically and by kinetic simulations. While UV polymerization of St at room temperature is slow, systems of BA and BMA produced well-defined polymer within a few hours (BMA) or even less (BA). Polymerizations were governed by irradiation, with no polymer generated in the dark periods, demonstrating high potential as photoswitchable "on–off" systems. Furthermore, UV irradiation was shown to be highly beneficial for polymerizations of BMA. Significant incessant cleavage of the weak tertiary carbon–iodine bond in polyBMA and successive ultrafast reversible termination with free iodine constitute an additional reversible deactivation mechanism coexisting with DT, thus boosting chain-growth control. UV initiation at elevated temperatures was presented as a tool to increase polymerization rates while fully retaining molar-mass control.

In the second part of this thesis, BB effects in the ubiquitously employed SEC technique were investigated with special regard to the analysis of polymer obtained from *(quasi-)living polymerizations* ((Q)LPs), such as well-controlled RDRPs. To this end, the influence of several experimental operating parameters on the extent of BB was determined by SEC analysis of narrow-distribution polymer. The shape of BB (the so-called *BB function,* BBF) is known to be skewed. An isolated quantification of symmetric broadening and asymmetric skewing was achieved by using the *exponentially-modified Gaussian* (EMG) model as BBF. It was shown that (i) a change of the analyte's injection mass only affects symmetric broadening and (ii) a change of either the flow rate of the eluent or the column temperature only affects skewing. This correspondence between the two parameters and their independent physical drivers underlines the applicability of the EMG model and is in accordance with existing theories of BB mechanisms.

The impact of BB on molar-mass analysis was then evaluated by simulating a series of SEC experiments. This included both (i) the simulation of the calibration process with narrow-distribution polymer standards and (ii) the subsequent molar-mass determination of simulated analytes' *molar-mass distributions* (MMDs). For respective sets of simulations, predetermined extents of BB (EMG) were systematically applied. Obtained characteristic values of the analytes' MMDs—i.e., the *number-average molar mass,* $\overline{M}_\mathrm{n}$, and

the *dispersity*, $Đ$—for the cases of no BB were then compared to the respective cases of applied BB. It was found that BB, in particular skewing and especially during the calibration process, leads to a significant experimental underestimation of the $\overline{M}_n$ values. This effect becomes disproportionately more pronounced with larger $\overline{M}_n$ values. In combination with potentially increasing $Đ$ values, these trends echo those commonly obtained from the analysis of RDRP systems, suggesting that BB has been making a hitherto unsuspected contribution to deviations from ideal behavior in such systems. The impact on molar-mass determination was well-understood and universally quantified over the complete molar mass range for given extents of BB. Methods to fully or partially correct SEC results by taking into account the examined effects were suggested.

Structural overview

This thesis is generally divided in two major parts: the investigation of various novel iodine-mediated *reversible-deactivation radical polymerization* (RDRP) systems in Part II (page 7) and the evaluation of effects of instrumental *band broadening* (BB) in *size-exclusion chromatography* (SEC) on molar-mass analysis of polymers in Part III (page 137). They are preceded by an Introductory Part (page 1), where the general scientific background and underlying motivation for the conducted research are outlined. For an easier understanding of the presented results, more detailed theoretical aspects will be respectively given at the beginning of the parts (page 9 and page 139). First results on iodine-mediated polymerizations are presented for *reverse iodine-transfer polymerizations* (RITPs) and RITP-based *reversible chain-transfer catalyzed polymerizations* (RTCPs) in Chapter 3 (page 29), which will be mainly done in terms of end-group analysis via *electrospray ionization mass spectrometry* (ESI-MS). Conclusions on the there obtained findings are given at the end of the chapter. In the second chapter of this part, UV-initiated iodine-mediated polymerizations are presented. Three different monomers, *n*-butyl acrylate (BA, page 66), *n*-butyl methacrylate (BMA, page 102), and styrene (St, page 124), are investigated and the results are presented in three individual sections. Rather than combined conclusions on these three monomers at the end of the chapter, individual concluding remarks are given at the end of each monomer section in order to emphasize and refresh the gained knowledge, which provides the basis for a better understanding of the following monomer sections. Future perspectives combining the findings of all investigated iodine-mediated systems are given at the end of the part.

In the second major part, BB effects in SEC are investigated. After theoretical aspects about SEC and BB, the extent of BB is experimentally determined for various instrumental operating conditions in Chapter 7 (page 153). In the following chapter, the impact of BB on molar-mass determination of polymer is investigated by a series of simulations (page 173). Individual concluding remarks are presented at the end of the respective chapters. Future perspectives on correction techniques of the obtained effects are briefly given at the end of the part.

Eventually, experimental information on used materials, analytical methods, and experimental procedures are provided.

Contents

Part I

Introductory part

This part gives a brief introduction to the subjects of the present thesis. It clarifies the motivation behind the conducted research and presents its general scientific context. This thesis is divided into two major subjects, namely (i) the investigation of iodine-mediated polymerization systems (Part II starting on page 7) and (ii) the investigation of band-broadening effects in size-exclusion chromatography (Part III starting on page 137). While both will be briefly introduced in the following, further scientific context and underlying theoretical aspects will be individually presented at the beginning of the respective parts.

CHAPTER 1

Introduction and motivation

Polymeric materials are composed of macromolecules, which themselves consist of multiple covalently linked low-molar-mass repeating units, so-called monomers. About one century after the pioneering and groundbreaking research on polymer chemistry by Hermann Staudinger,[1] today's life would be unimaginable without artificially produced polymeric materials. The various industrial applications of synthetic polymers span domains such as packaging, housewares, clothing, paints, infrastructure, sports equipment, as well as the construction and automotive industry.[2] Because of the ever-increasing and diverse demands that are put on the high-performance materials of modern society, it is essential to precisely control polymer characteristics. Polymer characteristics, in turn, are determined by the macromolecular structures, which clarifies the craving for tools that allow for accurate tailoring of individual and complex macromolecular architectures. At the same time, along with the required precision of the polymer characteristics, the accuracy of analysis methods becomes increasingly important to the same degree.

Radical polymerization (RP) of vinyl monomers is arguably the most commonly used technique to produce synthetic polymer in both industry and academia,[3] which is due to its extensive range of accessible monomer classes, low price, operational ease, as well as its tolerance toward most impurities and toward a wide range of reaction conditions. However, as the *conventional* RP process involves continuous initiation of rapidly growing

macroradicals, which irreversibly terminate very shortly after[4] to form dead polymer, individual manipulation of chains is not possible and broad molar-mass distributions (MMDs) are generally obtained.

The *reversible-deactivation radical polymerizations*[5] (RDRPs, formerly and commonly known as *controlled radical polymerizations,* CRP),[6] which arose in the 1990s, resolve these limitations while preserving the advantages of conventional RP systems. They allow for the facile production of polymer with well-defined molar masses and complex architectures from common industrial monomers. RDRPs are based on the recurring reversible deactivation of the growing macroradicals by special mediating agents, which enables a controlled and even growth of living (potential growing)[7] chains with extended lifetimes. The fraction of dead chains is massively reduced, while the controlling agents also act as chain-end functionalities which can fulfill a chemical function in the system or act as attack points for further processing steps.

A central subject of the present thesis were RDRPs that are based on the reversible deactivation of macroradicals by terminal iodine atoms—so-called iodine-mediated polymerizations.[8] Iodine has the advantage over mediating agents in other well-established RDRP techniques, such as *atom-transfer radical polymerization* (ATRP)[9–11] or *reversible addition–fragmentation chain-transfer* (RAFT) polymerization,[12,13] that it is cheap, nontoxic, environmentally friendly and odorless. Since the iodine atoms constitute the polymer end-groups after the polymerization, one can benefit from the rich iodine chemistry for further conversion.[8,14,15] In all employed iodine-mediated polymerization techniques in this thesis, the iodine atom is originally introduced by a low-molar-mass iodo *chain-transfer agent* (iodo CTA). In the most common iodine-mediated system, iodine atoms are transferred between two living chains, which is referred to as *degenerative-chain-transfer* (DT) mechanism and *iodine-transfer polymerization* (ITP).[16] Implementation of ITPs is universal, robust, requires only little experimental effort, and is already realized in industrial processes.[17,18] Until now, several architectures could already be obtained in ITPs[19,20] or by post-processing of ITP products.[21–23]

Despite the benefits, the ITP technique inherently entails the major drawbacks that (i) highly activated iodo CTAs—needed to control growth of poly(methacrylates), for example—are fairly unstable and that (ii) DT of iodine is generally rather slow and thus molar-mass control inferior to other RDRP techniques. The development of more sophisticated iodine-mediated systems helped to tackle these handicaps. The most successfully

applied are (i) the *reverse iodine-transfer polymerization* (RITP)[24,25] and (ii) the *reversible chain-transfer catalyzed polymerization* (RTCP).[26,27] In RITP systems, highly activated iodo CTAs are conveniently generated in situ, giving access to a wider range of monomer classes. In RTCP systems, iodine transfer is thought to also occur between macromolecules and additionally introduced low-molar-mass catalysts via a superimposed reversible chain-transfer mechanism, providing a higher control of chain-growth.

In this thesis, the effect of different RTCP catalysts added to an RITP system was systematically investigated with special regard to the end-groups of the produced polymer chains. This information is available via electrospray ionization mass spectrometry (ESI-MS). While these systems were mainly investigated in terms of MMDs and chain-growth control in the literature,[27–29] little research has been conducted so far to identify the end-groups of the obtained polymer. The results of the ESI-MS studies do not only contribute to the elucidation of special mechanistic aspects of RTCP. Detailed knowledge of the obtained polymer's end-group functionality is an indispensible prerequisite for further processing steps.

The use of photoirradiation rather than heat as initiating stimulus has already gained comprehensive access to RPs in academic and industrial research[30–32] and receives gaining interest in the world of RDRPs.[33,34] By allowing RDRPs to proceed under mild thermal conditions, degradation of functional end-groups and undesirable side reactions can be minimized. In addition, photoirradiation offers a simple way to control the generation of radicals and can even enhance chain-growth control via promotion of the activation–deactivation frequency of a living chain. Since the pioneering work of Otsu et al. on photoiniferters,[35,36] UV/vis radiation has been applied to several RDRP systems including the above-mentioned ATRP,[33,37,38] and RAFT polymerization.[39,40]. In contrast, examples of iodine-mediated photosystems exist but are rare,[41–43] as it is arguably shied away from the fact that organoiodine compounds are known to readily decompose upon photoinduced cleavage of the carbon–iodine bond. However, as this might also lead to a promotion of activation events of living chains and thus chain-growth control, these systems seemed especially worthwhile to study in this work, so as to potentially extend the scope of iodine-mediated polymerizations.

In today's polymer research, most conclusions for the elucidation of the kinetics and mechanisms of polymerization processes and structure–property relationships of polymeric products are drawn from the analysis of the MMDs of the obtained polymers. *Size-exclusion chromatography*[44,45] (SEC,

also referred to as *gel-permeation chromatography*, GPC)[46] is undisputedly the most powerful tool and the overwhelmingly used method for the determination of MMDs of synthetic polymer worldwide. As every chromatographic method, SEC is subject to inevitable band broadening (BB),[47,48] possibly altering the obtained chromatograms in a significant way. **The systematic investigation of the effect of BB** on MMDs obtained via SEC, in order to reveal and prevent potential pitfalls in their interpretation, is another central subject of the present thesis. Special focus is directed on the analysis of polymers obtained from (quasi-)living polymerization ((Q)LP) systems, such as well-controlled RDRPs, for which the polymers' MMDs commonly evolve through a wide region of molar masses and range of SEC separation. To this end, typical extents of BB shall be experimentally determined while impact of BB on molar-mass results is envisaged to be determined by systematical simulations of SEC experiments.

.

Part II

Iodine-mediated polymerizations

In this first major part of the thesis, iodine-mediated *reversible-deactivation radical polymization* (RDRP) systems are studied. After a theoretical background on the mechanism and kinetics of the underlying *iodine-transfer polymerization* (ITP), the results of the investigated *reverse ITP* (RITP) and RITP-based *reversible chain-transfer catalyzed polymerizations* (RTCPs) will be presented in Chapter 3 (page 29). Conclusions on the obtained findings are given at the end of the chapter. In Chapter 4 (page 61), UV-initiated iodine-mediated polymerizations are presented. The results for the three different investigated monomers *n*-butyl acrylate (BA, page 66), *n*-butyl methacrylate (BMA, page 102), and styrene (St, page 124) are given in individual sections. Concluding remarks are respectively given at the end of each section. Further perspectives combining the finding of all investigated iodine-mediated systems are given in the last chapter of this part (page 133). A part of the content of the presented chapters has already been published and is reused with permisson from Wolpers, A.; Vana, P. *Macromolecules* **2014**, *47*, 954–963.

CHAPTER 2

Theoretical background: mechanism and kinetics of iodine-transfer polymerizations

Since the investigated iodine-mediated polymerizations in this part are based on ITPs, a theoretical background for ITP systems will be given in this chapter. Special focus will be laid on its kinetic and mechanistic features as a member of RDRPs. As it will be frequently addressed in the present thesis, the general mechanism of (conventional) radical polymerizations (RPs) as well as their distinction from RDRPs will be concisely described. In this context, it should be stated that the term *conventional* RP will be recurrently used to emphasize the difference from RDRP systems. Mechanistic and kinetic information on the RTCP will be given eventually.

2.1 Conventional radical polymerizations

2.1.1 Mechanism

The mechanism of RPs is based on successive chain growth. As in every chain-growth polymerization, there are three key steps: (i) initiation, (ii) propagation, and (iii) termination. They are presented in Scheme 2.1 on the following page and briefly described in the following.

The **initiation** reaction can be divided into two distinct processes. In Reaction I, the initiator decomposes (e. g., thermally, chemically, photochem-

radical formation & initiation

(I) $\text{initiator} \xrightarrow{k_{dec},\, f} 2\ \text{In}^{\bullet}$

(II) $\text{In}^{\bullet} + \text{monomer} \xrightarrow{k_{ini}} \text{polymer}^{\bullet}(1)$

propagation

(III) $\text{polymer}^{\bullet}(n) + \text{monomer} \xrightarrow{k_p} \text{polymer}^{\bullet}(n+1)$

termination

disproportionation

(IV) $\text{polymer}^{\bullet}(n) + \text{polymer}^{\bullet}(m) \xrightarrow{k_{td}} \text{polymer}^{=}(n) + \text{polymer}^{H}(m)$

combination

(V) $\text{polymer}^{\bullet}(n) + \text{polymer}^{\bullet}(m) \xrightarrow{k_{tc}} \text{polymer}(n+m)$

transfer

(VI) $\text{polymer}^{\bullet}(n) + \text{R–X} \xrightarrow{k_{tr}} \text{polymer–X}(n) + \text{R}^{\bullet}$

X = e. g., H, Hal

Scheme 2.1 General reactions in a radical-polymerization system including their respective rate coefficients.

ically) (reaction-rate coefficient: k_{dec}), while the initiator efficiency, f, gives the percentage of decomposing initiator that provides initiating radicals, $\text{In}^{\bullet}$. In Reaction II (k_{ini}), $\text{In}^{\bullet}$ adds to a monomer molecule and initiates a growing polymer chain with a chain length of 1, $\text{polymer}^{\bullet}(1)$. In Reaction III ($k_p$), the successive addition of monomer to $\text{polymer}^{\bullet}$ leads to **propagation** of the chain. The propagation is eventually stopped by the **termination** reaction of two $\text{polymer}^{\bullet}$. There are two different mechanisms for this process, namely the disproportionation reaction (Reaction IV, k_{td}) and the combination reaction (Reaction V, k_{tc}). Disproportionation gives an unsaturated and a saturated polymer species, $\text{polymer}^{=}(n)$ and $\text{polymer}^{H}(m)$, respectively, whereas combination leads to only one $\text{polymer}(n+m)$. The overall rate coefficient of the termination reaction is given by

$$k_t = k_{td} + k_{tc} \tag{2.1}$$

while the ratio of k_{td} and k_t is referred to as the termination mode δ_t:

$$\delta_t = \frac{k_{td}}{k_t}\ . \tag{2.2}$$

According to an *ideal* RP, the presented reactions are all assumed to be (i) irreversible, while (ii) their rate coefficients remain constant and do not depend on quantities such as chain lengths or monomer conversion. Furthermore, (iii) monomer molecules are involved only in propagation steps while (iv) the radical concentration remains constant throughout the polymerization.

During the polymerization process, nonideal reactions can lead to a **transfer** of the radical function of polymer$^\bullet$ onto other molecules (Reaction VI, k_{tr}, R–X, e. g., monomer, initiator, solvent; X = e. g., hydrogen, halogen atom). This reaction plays a fundamental role in the mechanism of RDRPs, in which agents are intentionally added to the system so as to induce (reversible) transfer reactions, which will be presented below.

2.1.2 Ideal polymerization rate

On the assumption of a constant radical concentration, the rate of the radical-*producing* decomposition reaction, R_{dec}, has to equal the rate of the radical-*consuming* termination reaction, R_t (Reaction I and Reaction IV and V in Scheme 2.1). Considering Equation 2.1 on the preceding page, this leads to

$$\begin{aligned} R_{dec} &= \frac{\mathrm{d}\,[\mathrm{In}^\bullet]}{\mathrm{d}t} = 2 \cdot k_{dec} \cdot f \cdot [\mathrm{initiator}] \\ &= R_t = -\frac{\mathrm{d}\,[\mathrm{polymer}^\bullet]}{\mathrm{d}t} = 2 \cdot k_t \cdot [\mathrm{polymer}^\bullet]^2 \ . \end{aligned} \tag{2.3}$$

The ideal rate of the propagation reaction, R_p, which can be regarded as the polymerization rate, can then be expressed as

$$\begin{aligned} R_p &= -\frac{\mathrm{d}\,[\mathrm{monomer}]}{\mathrm{d}t} = k_p \cdot [\mathrm{monomer}] \cdot [\mathrm{polymer}^\bullet] \\ &= k_p \cdot [\mathrm{monomer}] \cdot \sqrt{\frac{k_{dec}}{k_t} \cdot f \cdot [\mathrm{initiator}]} \ . \end{aligned} \tag{2.4}$$

reversible-deactivation mechanism in RDRPs

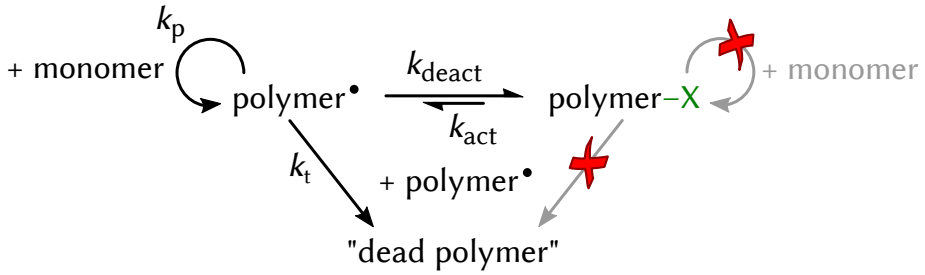

Scheme 2.2 General pseudo-first-order reversible-deactivation mechanism in RDRPs with respective rate coefficients: deactivation of polymer• gives the dormant species polymer–X.

2.2 Reversible-deactivation radical polymerizations

2.2.1 General mechanism

RDRPs[6] are based on the reversible deactivation of polymer• with a *capping agent* X, forming the *dormant* species polymer–X (see Scheme 2.2). In contrast to polymer•, polymer–X does not undergo reactions such as propagation with monomer or undesirable irreversible termination with another polymer•. In a typical successful RDRP, the pseudo-first-order rate coefficients of the activation and deactivation reaction are $k_{act} = 10^{-3}$–$10^{-1}\ s^{-1}$ and $k_{deact} = 10^{2}$–$10^{4}\ s^{-1}$, respectively.[49] In the context of the reversible-deactivation equilibrium

$$k_{act} \cdot [\text{polymer–X}] = k_{deact} \cdot [\text{polymer}^\bullet]\ , \tag{2.5}$$

this illustrates that there is about 10^5 times more polymer–X than polymer•, or in other words, a single living chain is active for only 10^{-5} of its entire lifetime. In order to ensure an evenly growth of all chains and narrow molar-mass distributions (MMDs), a high activation–deactivation frequency is crucial for a successful RDRP. There are two main mechanisms of reversible deactivation, namely (i) reversible termination (RT) and (ii) degenerative (or reversible) chain transfer (DT),[49,50] which will both be described in the following.

(a) general reversible-termination (RT) mechanism

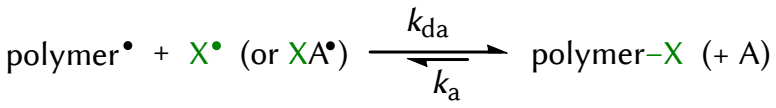

(b) nitroxide-mediated polymerization (NMP)

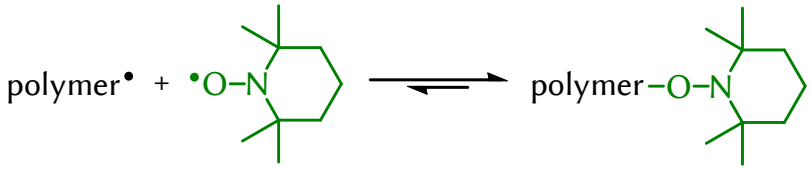

(c) atom-transfer radical polymerization (ATRP)

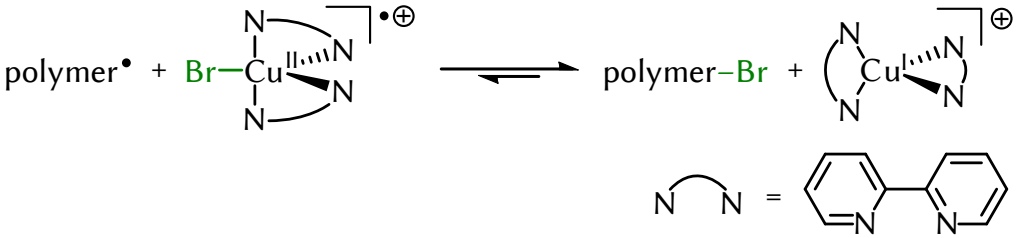

Scheme 2.3 (a) General RT mechanism in RDRP, (b) exemplary RT with a TEMPO radical in an NMP, and (c) exemplary RT with a Cu–bipyridine complex in an ATRP.

2.2.2 Reversible termination

In the RT mechanism, polymer• is deactivated by a reversible termination reaction with X• (or XA•) (see Scheme 2.3). Prominent examples are the *nitroxide-mediated polymerization* (NMP, with X = nitroxyl group, Scheme 2.3b),[51] first reported by Georges et al. in 1993,[52] and the *atom-transfer radical polymerization* (ATRP, with X = e. g., Cl, Br and A = transition-metal complex, Scheme 2.3c),[11] first reported independently by Matyjaszweski et al.[9] and Sawamoto et al.[10] in 1995. RT systems are based on the *persistent-radical effect* (PRE):[53] in contrast to polymer•, the persistent radical X• (or XA•) does not undergo irreversible self-termination. This leads to an accumulation of X• and thus an increased probability for polymer• to reversibly react with X• rather than irreversibly with another polymer•.

(a) general degenerative chain-transfer (DT) mechanism

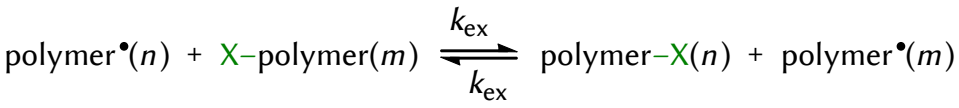

(b) reversible addition–fragmentation chain-transfer (RAFT) polymerization

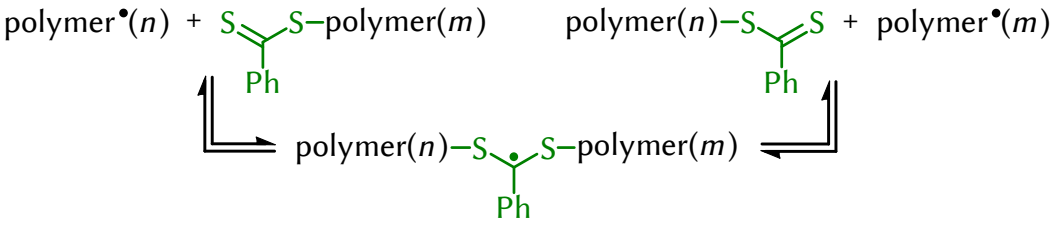

(c) iodine-transfer polymerization (ITP)

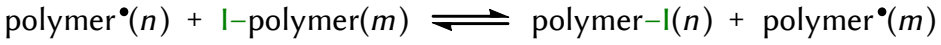

Scheme 2.4 (a) General DT mechanism in RDRP, (b) exemplary DT with a dithiocarbonylthio group in a RAFT polymerization, and (c) exemplary DT with an iodine atom in an ITP.

2.2.3 Degenerative chain transfer

In DT, polymer• is deactivated by the transfer of X from another polymer–X (see Scheme 2.4). More generally, this process is a *reversible* chain transfer. However, in order to emphasize that transfer occurs between two chemically (almost) identical polymer chains, the process was termed *degenerative.*[54] Prominent examples are the *reversible addition–fragmentation chain-transfer* (RAFT, with X = e. g., thiocarbonylthio group, Scheme 2.4b) polymerization,[13] first reported by Rizzardo et al. in 1998,[12] and the ITP (with X = I, Scheme 2.4c),[8] first reported by Matyjaszewski et al. in 1995.[16] In this context, the RAFT process is termed after the unique mechanism of consecutive addition and fragmentation, leading to a fairly stable intermediate radical. In contrast, for ITP, the iodine atom is directly transferred from one chain to the other. The principles of ITP are described in more detail in Section 2.4 on page 17.

2.3 Molar-mass distributions

2.3.1 Characteristic values

An important characteristic to describe polymeric products are their MMDs. Since they are mainly influenced by the reaction kinetics, MMDs help to gain deeper understanding of a polymerization process. Characteristic values of an MMD that are frequently reported on include its average molar masses—in particular the number-average molar mass, $\overline{M}_\mathrm{n}$, and the weight-average molar mass, $\overline{M}_\mathrm{w}$—as well as the dispersity, $Đ$. $\overline{M}_\mathrm{n}$ is the arithmetic average of the MMD and therefore defined as

$$\overline{M}_\mathrm{n} := \frac{\sum_i N_i \cdot M_i}{\sum_i N_i} \,, \tag{2.6}$$

with the number, N_i, and the molar mass, M_i, of chains exhibiting a chain length of i. $\overline{M}_\mathrm{w}$ is the arithmetic average of the MMD, when every N_i value is weighted with M_i. Therefore it is defined as

$$\overline{M}_\mathrm{w} := \frac{\sum_i N_i \cdot M_i^2}{\sum_i N_i \cdot M_i} \,. \tag{2.7}$$

The ratio between $\overline{M}_\mathrm{w}$ and $\overline{M}_\mathrm{n}$ is an expression for the broadness of the MMD and defined as

$$Đ := \frac{\overline{M}_\mathrm{w}}{\overline{M}_\mathrm{n}} \geq 1. \tag{2.8}$$

By definition, $\overline{M}_\mathrm{w}$ is never smaller than $\overline{M}_\mathrm{n}$ and the lowest possible value of $Đ$ is unity. In this case, the MMD only consists of molecules with the very same molar mass. However, in RP of synthetic polymer, $Đ = 1$ is impossible and more or less broad MMDs are always obtained.

2.3.2 Conventional radical polymerization versus reversible-deactivation radical polymerization

2.3.2.1 Conventional radical polymerization

In conventional RPs, the obtained $\overline{M}_\mathrm{n}$ values depend on the so-called kinetic chain length, ν, which is determined by the ratio of propagation and initiation[55] (or termination in case of a steady radical concentration):

$$\nu = \frac{k_\mathrm{p} \cdot [\mathrm{monomer}]}{2 \cdot \sqrt{f \cdot k_\mathrm{dec} \cdot k_\mathrm{t} \cdot [\mathrm{initiator}]}} \,. \tag{2.9}$$

It gives the average number of propagation steps of a macromolecule during its lifetime. When termination of macroradicals occurs exclusively via disproportionation, $\overline{M}_\mathrm{n} = \nu \cdot M_\mathrm{mon}$, with the molar mass of the monomer, M_mon. In case of combination, $\overline{M}_\mathrm{n} = 2 \cdot \nu \cdot M_\mathrm{mon}$. In contrast to RDRPs, $\overline{M}_\mathrm{n}$ values are normally rather high from an early state of polymerization. If effects that influence the rate coefficients are negligible (e. g., chain-length dependencies, viscosity), $\overline{M}_\mathrm{n}$ has a slightly decreasing trend with increasing monomer conversion, since [monomer] commonly decreases more quickly than $\sqrt{[\mathrm{initiator}]}$ throughout the polymerization. The obtained $Đ$ values depend on the termination mode. With ideal polymerization kinetics, macroradicals that completely combinate give $Đ \approx 1.5$, while complete disproportionation leads to $Đ \approx 2.0$.

2.3.2.2 Reversible-deactivation radical polymerization

In case of a hypothetically ideal (living)[56] RDRP without irreversible termination, as many chains exist as there are capping-agent (X) molecules. They are initially provided by *chain-transfer-agent* (CTA) molecules, which normally attach to the polymer chain (a detailed description will be given in the context of ITP). As monomer molecules are evenly consumed by living chains during polymerization, resulting $\overline{M}_\mathrm{n}$ values are given by

$$\overline{M}_\mathrm{n} = \frac{[\mathrm{monomer}]_0}{[\mathrm{CTA}]_0} \cdot M_\mathrm{mon} \cdot \alpha_\mathrm{mon} + M_\mathrm{CTA} \,, \tag{2.10}$$

with the initial concentrations of the monomer and the CTA, $[\mathrm{monomer}]_0$ and $[\mathrm{CTA}]_0$, respectively, the fractional monomer conversion, α_mon, and the molar mass of the CTA, M_CTA. Thus, a plot of $\overline{M}_\mathrm{n}$ versus monomer conversion should have a linear trend[7] with a slope of $[\mathrm{monomer}]_0 \cdot M_\mathrm{mon} / [\mathrm{CTA}]_0$ and an offset of M_CTA. MMDs can be much narrower and thus $Đ$ values much lower compared to conventional RPs. In the hypothetical case of a living polymerization, MMDs are Poisson-distributed[57] and

$$Đ = 1 + \frac{[\mathrm{CTA}]_0}{[\mathrm{monomer}]_0 \cdot \alpha_\mathrm{mon}} = 1 + \frac{M_\mathrm{mon}}{\overline{M}_\mathrm{n}} = 1 + \frac{1}{\overline{DP}_\mathrm{n}} \,, \tag{2.11}$$

with the number-average degree of polymerization, $\overline{DP}_\mathrm{n}$, which clarifies the naturally decreasing trend of $Đ$ as chains are growing. $Đ$ values normally obtained in well-controlled RDRPs are somewhat higher. Usually, the higher the activation–deactivation frequency of the living chains is, the lower $Đ$ is.[49] This will be explained in more detail in the context of ITP.

iodine-transfer polymerization (ITP)

(a) pre-equilibrium

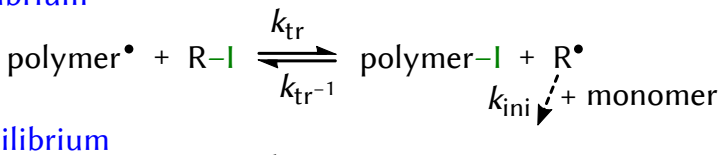

(b) main equilibrium

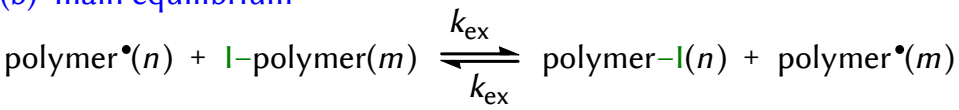

Scheme 2.5 (a) Pre-equilibrium and (b) main equilibrium in ITP with respective rate coefficients.

2.3.3 Determination via size-exclusion chromatography

While a few different methods exist to directly determine values such as $\overline{M}_n$ or $\overline{M}_w$ (e. g., osmometry, light scattering), the worldwide overwhelmingly used method to record *complete* MMDs of synthetic polymer is the *size-exclusion chromatography* (SEC, also known as gel-permeation chromatography, GPC).[48] It was also the method of choice to determine MMDs in the present thesis. Very briefly, SEC is a type of liquid column chromatography with a porous and swollen polymer network as stationary phase. Separation takes place according to different molecular sizes. SEC is a relative method and requires a calibration process, usually conducted with narrow-distribution polymer standards. The concept of SEC (i. e., experimental setup, separation principle, calibration process) will be explained more precisely in the context of band-broadening effects in SEC presented in Chapter 6 on page 139 in Part III of this thesis.

2.4 Iodine-transfer polymerization

2.4.1 Mechanism

A basic ITP system consists of (i) a monomer, (ii) an iodo CTA R–I, and (iii) a conventional initiator (source of polymer•).[16] At the beginning of the polymerization, in the *pre-equilibrium,* polymer• undergoes a reversible chain-transfer reaction with R–I giving polymer–I and R• (see Scheme 2.5a on the current page). R• can then react with monomer to (re)initiate new chains. If iodine transfer and subsequent (re)initiation are quick compared to conventional initiation and propagation, all chains start to grow at nearly

$$CN \approx C(O)OR > Br \approx Cl > F > CH_3 > H$$

Scheme 2.6 Impact of functional groups neighboring the C–I bond of an iodo CTA on the activity toward transfer of the iodine atom.[60]

(a) PE–I (secondary) with polySt (secondary)

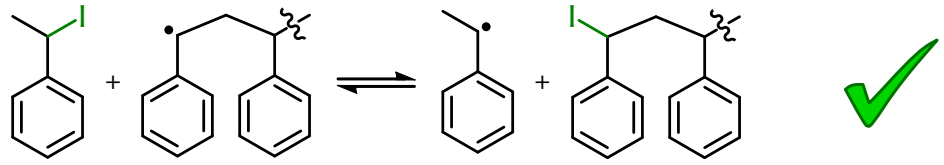

(b) PE–I (secondary) with polyMMA (tertiary)

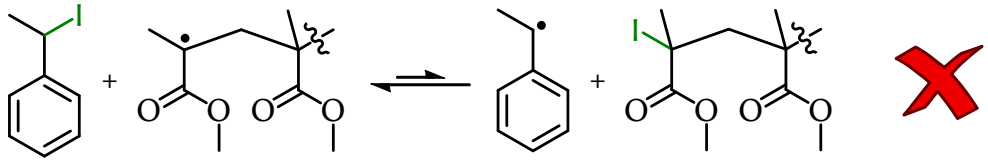

(c) CP–I (tertiary) with polyMMA (tertiary)

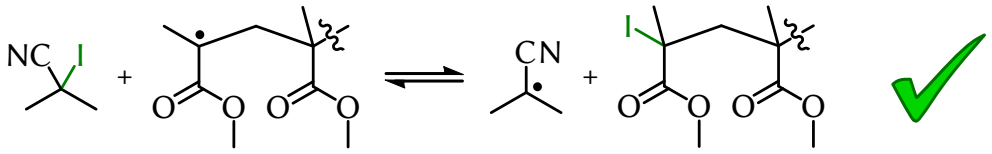

Scheme 2.7 (a) Phenylethyl iodide (PE–I) is a suitable CTA for the polymerization of St,[16] whereas (b) it is not for the polymerization of MMA.[16] (c) For MMA, the more highly activated cyanopropyl iodide (CP–I) can be used instead.[25]

the same time, resulting in good control of molar masses and narrow MMDs. Once R–I is mostly consumed, the *main equilibrium* and DT is predominant (Scheme 2.5b).[58,59]

2.4.2 Impact of the chain-transfer agent

Besides the (re)initiating behavior of R•, the controlled growth of molar masses in an ITP system strongly depends on the activity of R–I to transfer

its iodine atom to polymer$^\bullet$. In this regard, k_{tr} should be high compared to k_p of the polymer,[49] or in other words, the transfer constant

$$C_{tr} = \frac{k_{tr}}{k_p} \tag{2.12}$$

of the CTA should be high. This strongly depends on the structure of both the CTA and the polymer molecule. Generally, the less stable the C–I bond is in R–I and the more stable it is in polymer–I, the more readily the iodine atom is transferred from R–I to polymer$^\bullet$ and the higher is k_{tr}. Functional neighboring groups of the respective C–I bonds in R–I and polymer–I play an important role in this context. The more the resulting radical (R$^\bullet$ and polymer$^\bullet$, respectively) is stabilized, the less stable the C–I bond is. In Scheme 2.6 on the facing page, exemplary neighboring groups are presented in descending order regarding their impact on the activity of an iodo CTA to transfer its iodine atom.[60] In addition, the activity generally decreases for tertiary > secondary > primary C–I bonds.[61] Of course, R$^\bullet$ should not be too stable, otherwise, (re)initiation would be slow and pronounced rate retardation could be observed (referred to as degradative chain transfer).[62]

For a fast formation of iodine-capped polymer in the beginning of the polymerization, the pre-equilibrium constant $K_{tr/tr^{-1}} = k_{tr}/k_{tr^{-1}}$ should not be lower than unity. $K_{tr/tr^{-1}} > 1$ is preferred for fast (re)initiation, however, generally, $K_{tr/tr^{-1}} \approx 1$ is sufficient to achieve good molar-mass control.[8] The latter case is obtained when the radical functions in R$^\bullet$ and polymer$^\bullet$ resemble each other thus making the pre-equilibrium thermodynamically neutral. This effect is exemplarily illustrated in Scheme 2.7 on the preceding page. For ITPs of St, phenylethyl iodide (PE–I) is a suitable CTA as the phenylethyl radical, PE$^\bullet$, resembles the polystyryl radical, polySt$^\bullet$ (Scheme 2.7a).[16] However, PE–I is *not* a suitable CTA for the polymerization of MMA, since the tertiary poly(methyl methacrylic) radical, polyMMA$^\bullet$, is more stable than PE$^\bullet$ and thus the equilibrium shifted toward polyMMA$^\bullet$ (Scheme 2.7b).[16] For a successful ITP of MMA, the more active CTA cyanopropyl iodide (CP–I) is needed, generating the tertiary cyanopropyl radical, CP$^\bullet$ (Scheme 2.7c). In this context, CP$^\bullet$ is considered to resemble polyMMA$^\bullet$, since the respective radical functions are similarly stabilized by two methyl groups and one electron-withdrawing group—CN for CP$^\bullet$ and C(O)OMe for polyMMA$^\bullet$ (cf. Scheme 2.6 on the facing page).[25]

Normally, iodo CTAs are fairly unstable and tend to decompose during synthesis, isolation, or storage. While less activated CTAs such as PE–I can be applied with only minor experimental problems, the employment

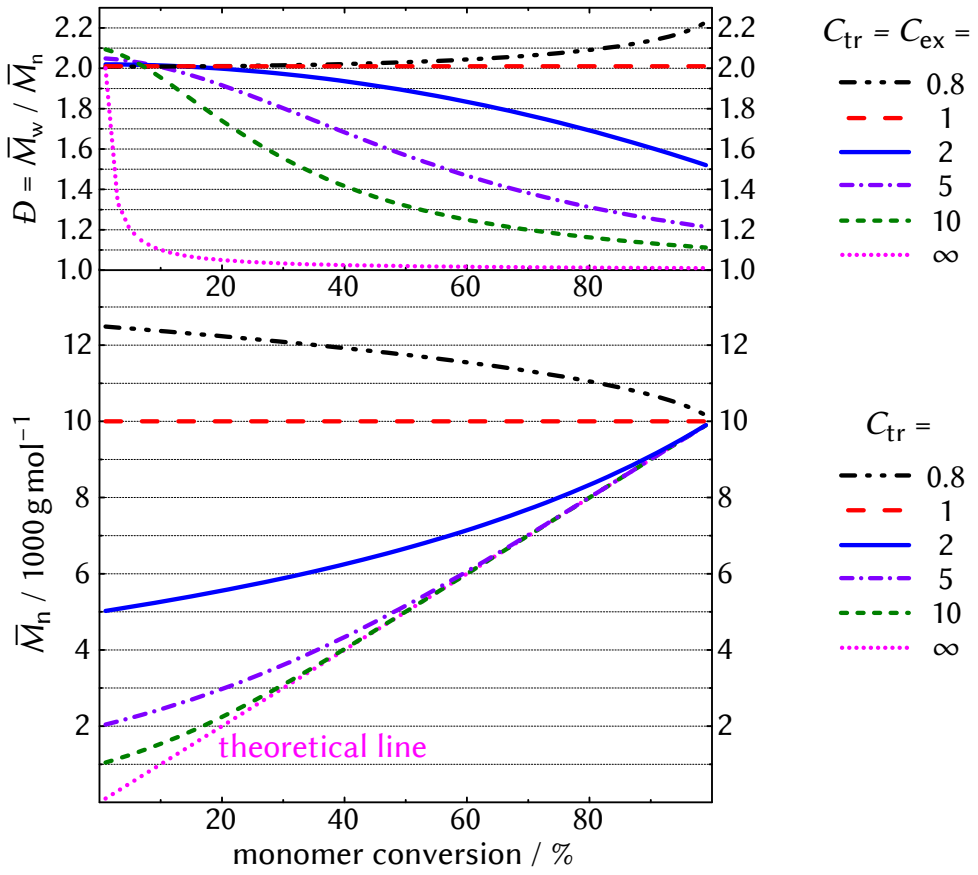

Figure 2.1 Calculated $\overline{M}_n$ values (Equation 2.13 on the facing page) for varying C_{tr} and calculated $Đ$ values (Equation 2.14 on the next page) for varying $C_{ex} = C_{tr}$ versus monomer conversion of polymer obtained from an ideal ITP with $[\text{monomer}]_0 / [\text{CTA}]_0 = 100$ and $M_{mon} = 100\,\text{g mol}^{-1}$.

of highly activated such as CP–I is much more challenging.[58,63] In this context, the *reverse iodine-transfer polymerization* (RITP) technique was developed to overcome this problem by an in-situ generation of highly activated CTAs prior to polymerization,[24,25] which will be explained in more detail at the beginning of Chapter 3 on page 29.

2.4.3 Kinetics

2.4.3.1 Molar-mass evolution

As already mentioned, the control of chain growth in ITP (and DT systems in general) depends on (i) fast (re)initiation and (ii) a high activation–

deactivation frequency of living chains, which is determined by (i) C_{tr} and (ii) C_{ex} ($= k_{ex}/k_p$). For the ideal case of no side-reactions and a negligible termination reaction, laws exist that predict the evolution of $\overline{M}_n$ and $Đ$ for given values of C_{tr} and C_{ex}. In this context, for the hypothetical case of $M_{CTA} = 0\,\mathrm{g\,mol^{-1}}$, $\overline{M}_n$ and $Đ$ can be calculated via [49,64,65]

$$\overline{M}_n = \frac{\alpha_{mon} \cdot [\mathrm{monomer}]_0 \cdot M_{mon}}{[\mathrm{CTA}]_0 \cdot \left(1 - [1 - \alpha_{mon}]^{C_{tr}}\right)} \tag{2.13}$$

and for the assumption $C_{ex} = C_{tr}$,

$$Đ = \frac{1 + \frac{[\mathrm{monomer}]_0}{[\mathrm{CTA}]_0} \cdot \left(2 + \frac{(2-\alpha_{mon}) \cdot (1-C_{ex})}{C_{ex}}\right)}{\frac{[\mathrm{monomer}]_0 \cdot \alpha_{mon}}{[\mathrm{CTA}]_0 \cdot \left(1-[1-\alpha_{mon}]^{C_{ex}}\right)}}. \tag{2.14}$$

As the equations are rather complex, the so-calculated $\overline{M}_n$ and $Đ$ values versus monomer conversion are illustrated for different values of C_{tr} and C_{ex} in Figure 2.1 on the facing page. For exemplary values of $[\mathrm{monomer}]_0/[\mathrm{CTA}]_0 = 100$ and $M_{mon} = 100\,\mathrm{g\,mol^{-1}}$, the observed trends will be discussed in the following.

Average molar masses

The evolution of $\overline{M}_n$ values mainly depends on the number of living chains in the system. The higher the number is, the shorter the chains are for a given monomer conversion. Therefore, $\overline{M}_n$ is only influenced by C_{tr}—which determines the rate of (re)initiation—and indeed independent of C_{ex}, which has no impact on the number of living chains. For the extreme case of full monomer conversion ($\alpha_{mon} = 1$), Equation 2.13 yields

$$\underset{\alpha_{mon}=1}{\overline{M}_n} = \frac{[\mathrm{monomer}]_0}{[\mathrm{CTA}]_0} \cdot M_{mon} \tag{2.15}$$

and $\overline{M}_n$ is independent of C_{tr}. While $\overline{M}_n$ values are thus similar at high monomer conversion, they especially differ at low monomer conversion. In this context, for $\alpha_{mon} \to 0$, $\overline{M}_n$ values are given by [67]

$$\lim_{\alpha_{mon}\to 0} \overline{M}_n = \frac{1}{C_{tr}} \cdot \frac{[\mathrm{monomer}]_0}{[\mathrm{CTA}]_0} \cdot M_{mon} = \frac{1}{C_{tr}} \cdot \underset{\alpha_{mon}=1}{\overline{M}_n}\,. \tag{2.16}$$

The lower C_{tr} is, the higher $\overline{M}_n$ is for low monomer conversion. For $C_{tr} < 1$, $\overline{M}_n$ even defies the naturally expected trend of increasing $\overline{M}_n$ for RDRPs.

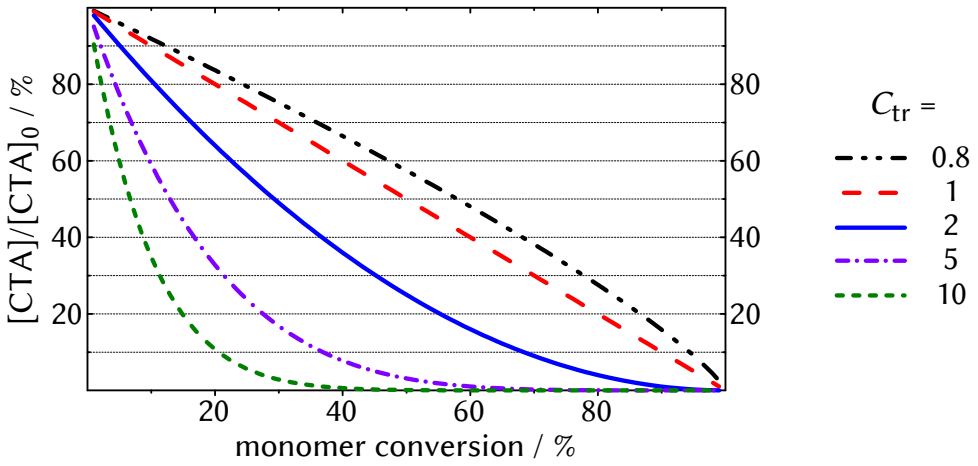

Figure 2.2 Calculated consumption of the CTA for different C_{tr} in DT polymerization as a function of monomer conversion. $[CTA]/[CTA]_0 = \exp(C_{tr} \cdot \ln(1 - \alpha_{mon}))$.[18,66]

Significantly high $\overline{M}_n$ values for low monomer conversion are sometimes referred to as *hybrid behavior* (hybrid between conventional-RP and RDRP behavior).[68] They are caused by the effect that for lower C_{tr} values, polymer$^\bullet$ undergoes more propagation steps before it is deactivated for the first time by the CTA. In addition, it takes longer until the CTA is effectively consumed, as can be seen in Figure 2.2.[18,66] Until that point, the number of living chains in the system is lower and thus $\overline{M}_n$ higher than theoretically expected.

The higher C_{tr} and the more quickly (re)initiation is, the more closely $\overline{M}_n$ values resemble the ideal trend for living polymerization, which is observed for $C_{tr} \to \infty$ (cf. Equation 2.10 on page 16):

$$\lim_{C_{tr} \to \infty} \overline{M}_n = \frac{[\text{monomer}]_0}{[\text{CTA}]_0} \cdot \alpha_{mon} \cdot M_{mon} \,. \tag{2.17}$$

Dispersities

Since the evolution of $Đ$ is much more complicated and affected by both C_{tr} and C_{ex}, it is analytically solved only for the assumption of $C_{ex} = C_{tr}$,[49,65] which corresponds to $K_{tr/tr^{-1}} = 1$. For all C_{ex}, $Đ \approx 2$ for low monomer

conversion, while according to Equation 2.14 on page 21, for full monomer conversion, they trend toward

$$\underset{\alpha_{\mathrm{mon}}=1}{Đ} = 1 + \frac{[\mathrm{CTA}]_0}{[\mathrm{monomer}]_0} + \frac{1}{C_{\mathrm{ex}}} \approx 1 + \frac{1}{C_{\mathrm{ex}}} \qquad ([\mathrm{monomer}]_0 \gg [\mathrm{CTA}]_0)\ . \tag{2.18}$$

While $Đ$ is generally higher for lower C_{ex}, for $C_{\mathrm{ex}} < 1$, $Đ$ again defies the expected decreasing trend for increasing monomer conversion. Similar to $\overline{M}_{\mathrm{n}}$, for $C_{\mathrm{ex}} \to \infty$, the theoretical trend of a living polymerization is obtained:

$$\lim_{C_{\mathrm{ex}}\to\infty} Đ = 1 + \frac{[\mathrm{CTA}]_0}{\alpha_{\mathrm{mon}} \cdot [\mathrm{monomer}]_0} \overset{\text{(Eq. 2.17)}}{=} 1 + \frac{1}{\overline{DP}_{\mathrm{n}}}\ . \tag{2.19}$$

For $C_{\mathrm{tr}} \neq C_{\mathrm{ex}}$, the evolution of $Đ$ is in fact less predictable and might be highly individual.

Typical ITP systems

As already mentioned, compared to a few other well-established RDRP methods, iodine transfer is only moderately fast and typical values of C_{tr} and C_{ex} are of the order of 10^0 [8,18] (against up to 10^2 for RAFT, for example[13]). For instance, C_{ex} was determined to be 3.6 for polySt (in bulk at 80 °C),[59] 2.2 for polyMA (in benzene at 70 °C),[24] and 2.6 for polyMMA (in toluene at 80 °C).[25] In this context, the experimentally obtained molar-mass evolutions in the respective literature studies indeed resemble the trends presented in Figure 2.1 on page 20. As a matter of course, several factors during polymerization (e. g., termination, side-reactions, varying rate coefficients) and analysis (e. g., band broadening in SEC, subjective data evaluation) might lead to a more or less pronounced deviation from the expected behavior of $\overline{M}_{\mathrm{n}}$ and $Đ$ when real polymerizations are conducted. Indeed, this should be generally kept in mind when MMD results are discussed. However, the presented trends in Figure 2.1 often serve as a strong basis for the kinetic interpretation of molar-mass evolution and development of well-controlled ITP systems. In fact, particularly $\overline{M}_{\mathrm{n}}$ is considered as rather robust and Equation 2.13 on page 21 and 2.16 on page 21 are frequently used for fitting experimental results to assess both C_{tr} and C_{ex} (via macromolecular CTAs and $C_{\mathrm{tr}} \approx C_{\mathrm{ex}}$) for specific CTA–polymer combinations.[23–25,69]

2.4.3.2 Polymerization rate

In ITP, transfer of the iodine atom between two species occurs directly and without the formation of a stable intermediate (as opposed to RAFT systems). The concentration of the CTA should therefore ideally have no direct impact on [polymer$^\bullet$] and thus R_p. Indeed, no significant difference was found between R_p of an ITP of St (with CTA) and of its analogous conventional RP system (without CTA) in the literature.[59] However, it should be emphasized that R_p can be affected indirectly via chain-length-dependent termination of polymer$^\bullet$.[70,71] In this context, higher CTA concentrations lead to generally lower molar masses, more pronounced termination, and thus lower R_p.

It should as well be mentioned that the trends for $\overline{M}_n$ and $Đ$ presented in Figure 2.1 on page 20 in fact only depend on monomer conversion and are *independent* of R_p. This is a unique feature of a system based on the DT mechanism and due to the fact that for DT, the crucial pseudo-first-order coefficient k_{act} (see Scheme 2.2 on page 12) can be expressed via

$$k_{act} = k_{ex} \cdot [\text{polymer}^\bullet] \tag{2.20}$$

(cf. Scheme 2.4a on page 14), which clarifies that k_{act} is proportional to [polymer$^\bullet$] and hence R_p (see Equation 2.4 on page 11).[49,72,73] This behavior is indeed not obtained for systems based on RT, in which k_{act} is not affected by [polymer$^\bullet$]:

$$k_{act} = k_a \, (\cdot [\text{A}]) \tag{2.21}$$

(cf. Scheme 2.3a on page 13). In this case, lower [polymer$^\bullet$] leads to less pronounced propagation compared to activation–deactivation processes and therefore generally results in higher molar-mass control.[49,73–75]

2.5 Reversible chain-transfer catalyzed polymerization

In 2007, Goto et al. presented a method to increase the molar-mass control of ITP systems while fully retaining their advantages regarding versatility and environmental sustainability.[26] It is based on the addition of low-molar-mass substances, which are proposed to introduce a reversible chain-transfer mechanism that enhances the activation–deactivation frequency of living chains.[27] As these substances are expected to act catalytically, the method was termed *reversible chain-transfer catalyzed polymerization* (RTCP), while

reversible chain-transfer catalyzed polymerization (RTCP)

(a) pre-equilibrium

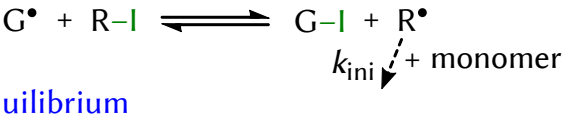

(b) main equilibrium

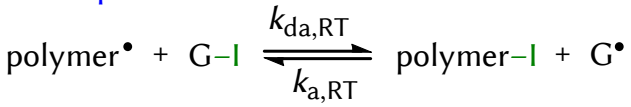

Scheme 2.8 (a) Pre-equilibrium and (b) main equilibrium in RTCP with the activating and deactivating catalyst species, G• and G–I, respectively.

the substances are called *catalysts*. To date, RTCP has been applied to homo- and (block-)co-polymerizations of styrenics and methacrylates[27,76], including systems in bulk, in organic solution (including supercritical CO_2),[77,78] and in emulsion.[79–81] The general mechanism and examples of employed catalysts are presented in the following.

2.5.1 Mechanism

Being based on ITP systems, RTCP systems consist of (i) monomer, (ii) the CTA R–I, (iii) a conventional initiator (source of polymer•), and (iv) the catalyst. The proposed mechanism is presented in Scheme 2.8. Like in ITP, it can be divided into (a) a pre-equilibrium and (b) a main equilibrium, in which an iodine atom is transferred between the catalyst (activating species: G•, deactivating species: G–I) and either (a) the CTA or (b) polymer. While G• should increase the formation of R• and thus (re)initiation of chains, G• should not (re)initiate new chains itself, otherwise, the catalyst would behave like a common CTA and be significantly consumed during polymerization. In this context, it should be emphasized that chain transfer of the catalysts is *superimposed* on the ITP mechanism and that DT is expected to still occur. However, in well-controlled RTCP systems, activation–deactivation via DT might not be significant, which will be discussed below.

2.5.2 Catalysts

As a crucial requisite of a suitable catalyst, the affinity of G• toward iodine should be high enough to allow frequent activation of polymer–I while on the other hand, G–I should still be able to readily give away its iodine

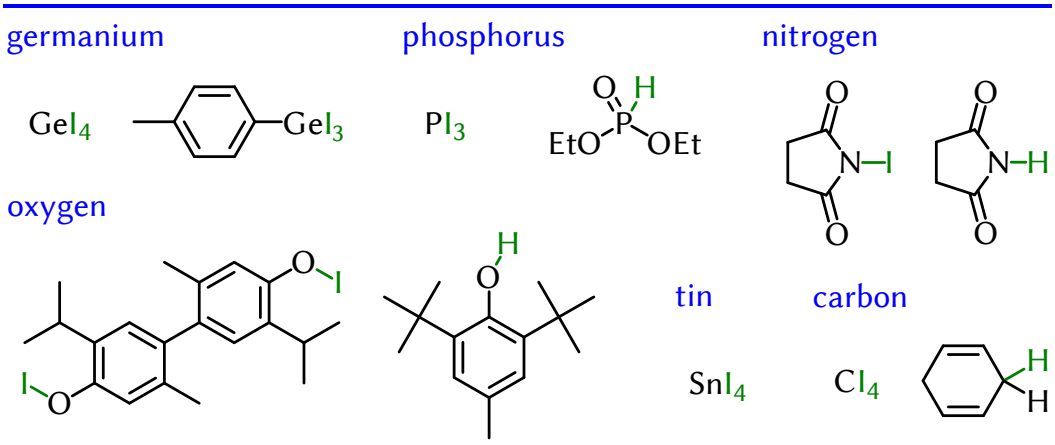

Figure 2.3 Exemplary catalysts used in RTCP added in the form of either the deactivating G–I or in the form of G–H, which yields the activating G$^\bullet$ after hydrogen-atom abstraction.

atom to allow frequent deactivation of polymer$^\bullet$. To date, several different compound classes have been applied as catalysts, including Ge-,[26,77] Sn-,[26] N-,[28,78–80,82] P-,[26,28,83,84] O-,[29] and C-centered[29] compounds. Examples are given in Figure 2.3. The catalysts can either be employed as deactivating G–I, i. e., already bearing an iodine atom, or in the form of G–H. In the latter case, the hydrogen atom can be abstracted by fragments of the conventional initiator for example, which in situ gives the activating G$^\bullet$.[26,28,29,83]

2.5.3 Kinetics

Catalyzed reversible chain-transfer versus DT

RTCP catalysts can be employed in rather low concentrations (down to about 1 mmol L^{-1}) and still significantly improve molar-mass control compared to the corresponding catalyst-free ITP system. In common RTCP systems, iodine transfer between polymer and catalyst molecules ($k_{\mathrm{da,RT}}$ and $k_{\mathrm{a,RT}}$ in Scheme 2.8b on the preceding page) was found to be about 10^2 to 10^3 times faster than between two polymer molecules (k_{ex} in Scheme 2.5b on page 17).[26,27,85] In this context, the addition of catalyst led to a systematical increase of the activation–deactivation frequency of living chains. For sufficiently high catalyst concentrations and well-controlled RTCP systems, DT is therefore expected to be negligible regarding its impact on molar-mass control.[85,86]

Rate retardation

In contrast to ITP systems, rate retardation was observed in all kinetic studies of RTCP systems.[26,27,85] It is ascribed to the irreversible cross-termination reaction between G$^\bullet$ and polymer$^\bullet$ (similar to cross-termination between the intermediate radical and polymer$^\bullet$ in RAFT polymerizations).[87] The extent of rate retardation was found to depend on the structure of both G$^\bullet$ and polymer$^\bullet$. Besides its adverse impact on R_p, cross-termination should lead to a slow but steady depletion of the catalyst,[86] which results in reduced activation and deactivation as polymerization proceeds. Guidelines were developed to overcome this problem by a repeated addition of the catalyst.[86]

CHAPTER 3

RITPs and RITP-based RTCPs of methyl methacrylate

ITP systems have been successfully applied to a wide range of monomers forming *secondary* propagating radicals (e. g., styrenics,[69] acrylates,[88] vinyl acetate[89]). While for an effective reversible deactivation of these polymer classes, the utilization of only moderately active CTAs is sufficient, monomers giving *tertiary* propagating radicals like methacrylates require highly activated CTAs, as it is illustrated in Scheme 2.7 on page 18. Unfortunately, for iodo CTAs, high activities regarding iodine transfer are inherently accompanied by weak C–I bonds, resulting in low stability and potential decomposition of the CTAs during synthesis, isolation, or storage.[58,63] To overcome this problem, Lacroix-Desmazes et al. invented the RITP in 2005,[24] in which a highly activated iodo CTA is produced in situ right before polymerization sets in. Details on the mechanism will be given in the following section. RITP was shown to allow for molar-mass control of methacrylates[25] and has already been used in several homo- and heterogeneous systems.[24,90,91] Because of its well-feasible procedure and low costs applying rather basic chemicals, RITP has even become popular for several of the above-mentioned secondary-radical polymers.[8,24,92,93]

In 2008, Goto et al. suggested that RITP systems of methacrylates can be adapted to RTCP as the addition of catalysts resulted in an improved chain-growth control.[27] As presented in Scheme 2.8 on page 25, in RTCP systems, iodine atoms are expected to be transferred between living chains and

catalyst molecules. Kinetic studies[26,27,85] demonstrated that the activation–deactivation frequency of living chains systematically increases when potential catalysts are added to ITPs of St and MMA. For all RTCP systems investigated in the literature so far, evolutions of $\overline{M}_n$ as a function of monomer conversion indicate that $\overline{M}_n$ is mainly determined by the stoichiometry of iodine (= iodo CTA) and not of the catalyst (see Equation 2.10 on page 16 or Figure 2.1 on page 20). This is in accordance with the mechanistic theory of RTCP and indicates that the capping agents of dormant chains are indeed iodine atoms. However, to the best of knowledge, no thorough end-group analysis of polymer produced by RTCP has yet been conducted to investigate the capping-agent species or a potential impact of the catalysts on chain-end functionality of the obtained polymer.

Electrospray-ionization mass-spectrometry (ESI-MS) is based on a rather soft ionization technique and offers great accuracy and high sensitivity. It is thus a powerful tool to investigate the structure of macromolecules.[94] Particularly the macromolecules' end-groups—which form during initiation and termination—straightforwardly offer information about the mechanism and kinetics of a polymerization process and are hence frequently used to study into both RDRP[95,96] and conventional RP systems.[97–99]

In the present chapter, ESI-MS was chosen as the ideal technique for end-group analysis of polymer produced via RITP and RITP-based RTCP systems. As the representative of the commonly employed methacrylate family, MMA was the monomer of choice. PolyMMA is indeed especially suitable for ESI-MS analysis as its numerous carboxyl functions are readily attached by ions, which leads to a high spectral signal-to-noise ratio (in contrast to polySt, for example). It should be noted that end-group analysis may not only give information about the nature of the capping agent in an RTCP. It can also clarify the impact of undesired side-reactions by the catalyst on the polymerization process. In this context, the activating catalyst species $G^{\bullet}$ might contribute to initiation or termination (= cross-termination with polymer$^{\bullet}$, cf. Section 2.5.3 on page 26). Both reactions would lead to an adverse depletion of the catalytic species and a continuously decreasing quality of chain-growth control during polymerization. In addition, information about the impact of catalysts on chain-end functionality is crucial when further processing of living polymer is planned.

RITPs of MMA were conducted and analyzed in comparison to RTCP systems using three different catalysts, namely (1) *N*-iodosuccinimide, NIS, as well as the *H*-phosphonic acid derivatives (PADs) (2) diethyl phosphonate, $(EtO)_2P(O)H$ and (3) 4,4,5,5-tetramethyl-1,3,2-dioxaphospholane 2-oxide,

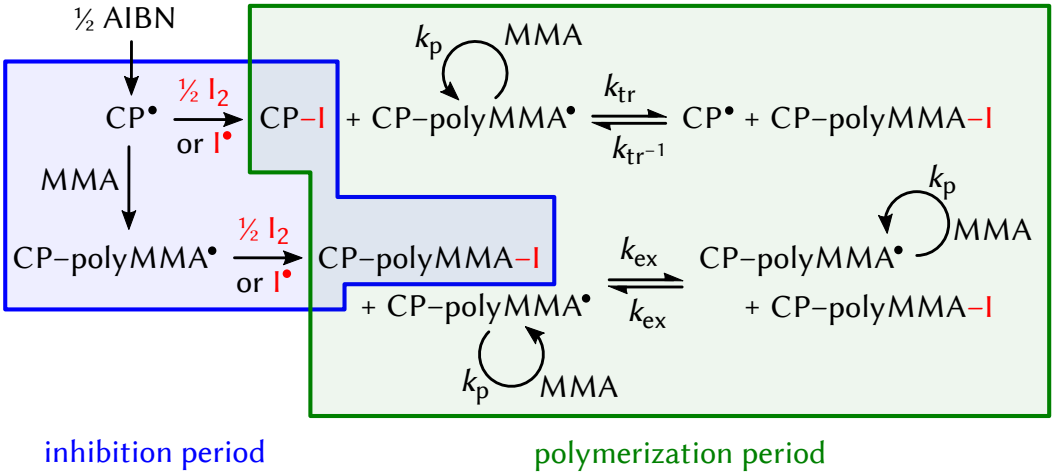

Scheme 3.1 Simplified RITP mechanism on the basis of a system with (i) MMA, (ii) molecular iodine (I_2), and (iii) AIBN. During the inhibition period, radicals almost exclusively react with free iodine (I_2 or $I^\bullet$) with almost no monomer conversion. When free iodine is consumed, the polymerization period starts according to a common ITP with the pre-equilibrium (top) and main equilibrium (bottom).[24,25]

PinP(O)H (for structural formulas see Figure 10.4 in the Experimental Section on page 220). While NIS and $(EtO)_2P(O)H$ are well-established catalysts for the investigated system,[27,28] the specially designed cyclic PinP(O)H has shown good activity in RTCPs of St in previous studies.[83] To assure practical relevance of the obtained results, polymerization conditions were chosen following literature recommendations.[27,28,82]

In addition to the analysis of RTCP systems, general aspects of the stability iodine end-capped polymer will be presented via ESI-MS. In this regard, the potential loss of functional iodine end-groups is important for iodine-mediated polymerizations in general, including ITPs, RITPs, RTCPs, and UV-initiated iodine-mediated polymerizations presented in Chapter 4.

Eventually, a method will be shown to overcome the fairly long inhibition periods prior to polymerization, which are an inherent feature of the investigated RITP systems, as will be explained in the following.

3.1 Basics & mechanism of RITP

A typical RITP system consists of (i) monomer, (ii) molecular iodine (I_2), and (iii) a conventional radical initiator. The RITP mechanism is based on

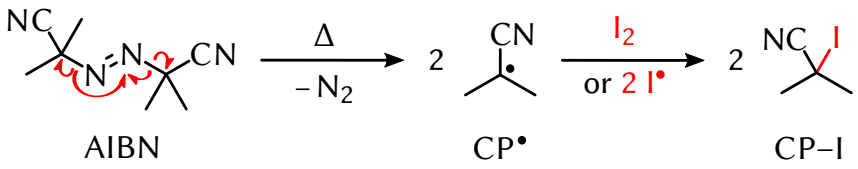

Scheme 3.2 Simplified decomposition of AIBN forming cyanopropyl radicals, CP•, and successive reaction with free iodine, which yields the CTA cyanopropyl iodide, CP–I.

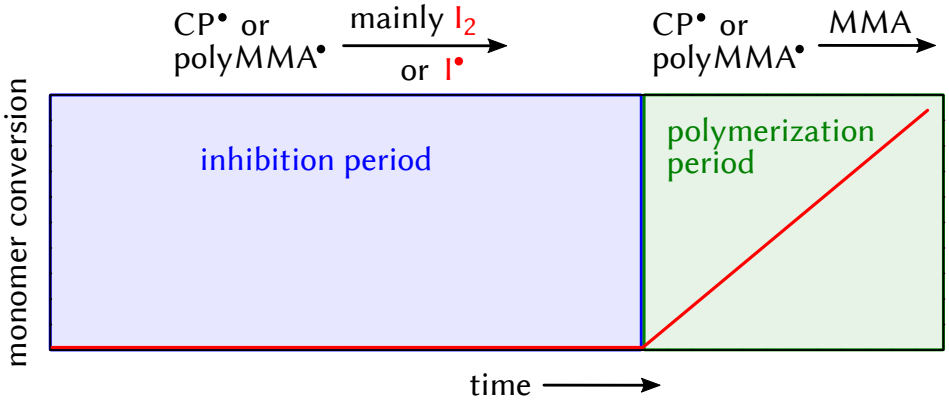

Figure 3.1 Schematic profile of monomer conversion versus time in an RITP system of MMA: during the inhibition period, radicals mainly react with free iodine; during the polymerization period, radicals react with MMA (cf. Scheme 3.1 on the previous page).

the fact that free iodine ($I^\bullet$ and I_2) is a very strong radical scavenger and inhibitor of RPs.[24,100,101] The reaction of carbon-centered radicals with free iodine is even faster than the diffusion-controlled self-termination of carbon-centered low-molar-mass radicals, which is ascribed to minor sterical hindrance and to the absence of spin effects.[102–104] As a consequence, almost no monomer conversion is observed in RITP as long as there still is free iodine present in the system. The simplified mechanism is illustrated in Scheme 3.1 on the preceding page. It will be explained based on the example of the here investigated system comprising (i) MMA, (ii) I_2, and (iii) 2,2′-azobis(2-methylpropionitrile) (AIBN). AIBN is the most frequently used initiator in RITP systems,[8,18] since it decomposes to give tertiary cyanopropyl radicals, CP•, which lead to the highly activated CTA cyanopropyl iodide, CP–I, after the reaction with free iodine (see Scheme 3.2). Mechanistically, during the first stage—the so-called *inhibition period*—CP• almost

Table 3.1 Initial concentrations of substances used for RITP (without catalyst (cat.)) and RTCPs of MMA in bulk at 80 °C.

entry[a]	$[MMA]_0$ / mol L^{-1}	$[I_2]_0$ / mol L^{-1}	$[AIBN]_0$ / mol L^{-1}	$[cat.]_0$ / mol L^{-1}	cat.
1 (□)	8.7	4.4×10^{-2}	8.7×10^{-2}	–	–
2 (⊙)	8.7	4.4×10^{-2}	8.7×10^{-2}	1.1×10^{-2}	NIS
3 (◈)	8.7	4.4×10^{-2}	8.7×10^{-2}	1.1×10^{-2}	$(EtO)_2P(O)H$
4 (△)	8.7	4.4×10^{-2}	8.7×10^{-2}	1.1×10^{-2}	PinP(O)H

[a] See Figure 3.2 on the next page and Figure 3.3 on page 38.

exclusively reacts with free iodine rather than to effectively initiate polymerization. In this regard, short oligomeric polyMMA chains are indeed formed as well[25] but promptly deactivated by free iodine (left box). At the end of the inhibition period, the system consists of (i) MMA, (ii) CP–I and oligomeric CP–polyMMA–I, as well as (iii) residual AIBN. During the *polymerization period,* the residual AIBN then initiates polymerization and the system behaves like a common ITP exhibiting a pre-equilibrium and a main equilibrium (right box). A typical profile of monomer conversion versus time is given in Figure 3.1 on the facing page.

3.2 Polymerization results of RITP-based RTCPs

RITP-based RTCPs of MMA in bulk were conducted at 80 °C employing I_2, AIBN, and either NIS, $(EtO)_2P(O)H$, or PinP(O)H as a catalyst. In comparison to these systems, polymerizations without a catalyst were conducted as well. A typical polymerization procedure is presented in the Experimental Section 10.4.1 on page 224. The initial concentration of I_2, $[I_2]_0$, was chosen to target a number-average degree of polymerization, $\overline{DP}_n$, of 100 for full monomer conversion, which corresponds to $\overline{M}_n$ of about 10 000 g mol^{-1}. According to the principles of RDRPs (cf. Section 2.3.2.2 on page 16), theoretical $\overline{M}_n$ values are given by

$$\overline{M}_{n,theo} = \frac{[MMA]_0 \cdot M_{MMA} \cdot \alpha_{mon}}{2 \cdot [I_2]_0} + M_{CP-I}\,, \tag{3.1}$$

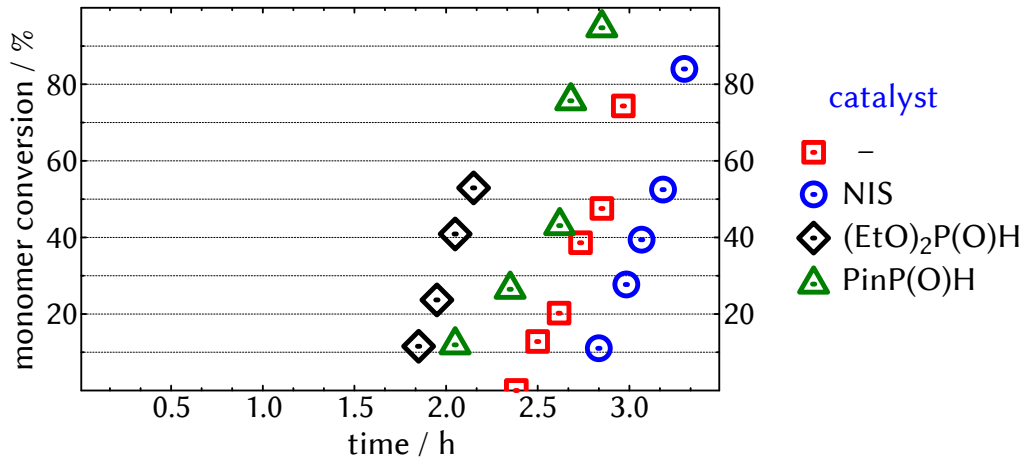

Figure 3.2 Monomer conversion as a function of time of the RITP and RTCP systems of MMA in bulk at 80 °C presented in Table 3.1 on the previous page.

with the molar mass of MMA and the CTA CP–I, M_{MMA} and M_{CP-I}, respectively, the initial concentration of MMA, $[MMA]_0$, and the fractional monomer conversion, α_{mon}. Note the prefactor of 2 for $[I_2]_0$ in consequence of *two* CP–I molecules being formed from *one* I_2 molecule. Initial catalyst concentrations are chosen following literature systems.[27,28] The respective polymerization systems including the applied initial concentrations are given in Table 3.1 on the previous page. It should be emphasized that to fully consume I_2, $[AIBN]_0$ has to be higher than $[I_2]_0$ (here, $[AIBN]_0 = 2 \cdot [I_2]_0$) since the initiator efficiency of AIBN, f, is distinctly lower than unity.[105]

3.2.1 Inhibition period and polymerization rate

Catalyst-free system

In Figure 3.2, values of monomer conversion as a function of time are given. First, the catalyst-free RITP system will be discussed. In compliance with the theory of RITP, a rather long inhibition period of about 2.4 h can be observed, in which no effective polymerization takes place. During this period, the solution has a characteristic reddish color caused by the dissolved I_2. (A more detailed description of the optical behavior of I_2 will be given in the context of the UV-initiated polymerization systems in Chapter 4.) At the end of the inhibition period, the reddish color fades, indicating complete consumption of I_2 and the beginning of the polymerization process. As a side note, this

Table 3.2 Experimentally obtained inhibition periods, t_{inh}, in RITPs of MMA in bulk at 80 °C for different values of $[I_2]_0$ and $[AIBN]_0$ and calculated efficiency values of AIBN, f.

$[I_2]_0$ / mol L^{-1}	$[AIBN]_0$ / mol L^{-1}	$[AIBN]_0/[I_2]_0$	t_{inh} / h [a]	f [b]
2.2×10^{-2}	4.4×10^{-2}	2.0	2.4	0.67
4.4×10^{-2}	8.7×10^{-2}	2.0	2.4	0.67
8.7×10^{-2}	1.7×10^{-1}	2.0	2.5	0.66

[a] Via extrapolation of monomer conversions below 40 % to a monomer conversion of 0 % (data not shown); [b] with Equation 3.4: $t_{inh,theo} = t_{inh}$ and $k_{dec} = 1.6 \times 10^{-4}$ s^{-1}.[106]

change in color allows to conveniently estimate the end of inhibition by a brief look at the polymerization mixture. While the inhibition period is long, polymerization is fast and reaches monomer conversions of 80 % within only about 40 min. This is a result of the combination of the relatively high polymerization temperature and high amount of AIBN in the system so as to keep inhibition short.

Theoretically, polymerization is inhibited as long as there is still free iodine in the system. Polymerization should start after the theoretical inhibition period, $t_{inh,theo}$, when AIBN has produced as many radicals as there are iodine atoms:

$$2 \cdot [I_2]_0 = 2 \cdot \left([AIBN]_0 - [AIBN]_{t_{inh,theo}} \right) \cdot f \,, \tag{3.2}$$

with [AIBN] at $t = t_{inh,theo}$, $[AIBN]_{t_{inh,theo}}$. In combination with the integrated rate law for the decomposition of AIBN

$$[AIBN]_{t_{inh,theo}} = [AIBN]_0 \cdot \exp(-k_{dec} \cdot t_{inh,theo}) \,, \tag{3.3}$$

this leads to

$$t_{inh,theo} = -\frac{\ln\left(1 - \frac{[I_2]_0}{[AIBN]_0 \cdot f}\right)}{k_{dec}} \,. \tag{3.4}$$

Equation 3.4 clarifies that $t_{inh,theo}$ does not depend on the absolute values of either $[I_2]_0$ or $[AIBN]_0$ but on the ratio $[I_2]_0/[AIBN]_0$. For the here obtained $t_{inh} = 2.4$ h (from linear extrapolation of monomer conversions below 40 % to a monomer conversion of 0 %) and $t_{inh,theo} = t_{inh}$, Equation 3.4 yields $f = 0.67$ for $k_{dec} = 1.6 \times 10^{-4}$ s^{-1} of AIBN at 80 °C.[106] This f value is in excellent agreement with literature results.[105,107] The correlation of t_{inh} and

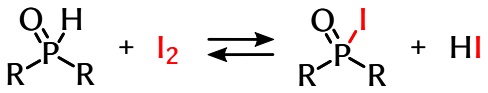

Scheme 3.3 Potential redox equilibrium between PADs and I_2.[108,109]

$[I_2]_0/[AIBN]_0$ is demonstrated by comparing RITP systems with the same values of $[I_2]_0/[AIBN]_0$ but different absolute values of $[I_2]_0$ and $[AIBN]_0$ (see Table 3.2 on the preceding page). All t_{inh} values are very similar, which also clarifies the robustness of t_{inh} (and thus f) for individual polymerization systems.

NIS system

Compared to the catalyst-free system, the polymerization rate is rather similar for the RTCP system with NIS. However, inhibition is slightly longer with $t_{inh} = 2.7$ h. Since a potential impact of NIS on the kinetics of AIBN (i. e., either k_{dec} or f) is unlikely, this is ascribed to the release of free iodine by NIS. It can be caused by either thermally induced homolytic N–I-bond cleavage or by reactions of NIS with other (radical) species. According to Equation 3.4 on the previous page, in order that $t_{inh} = 2.7$ h is obtained rather than $t_{inh} = 2.4$ h (as for the catalyst-free system), $[I_2]_0$ has to increase from 44 mmol L^{-1} to 46 mmol L^{-1}. Indeed, $[NIS]_0$ is high enough to cause this as the additional amount of I_2 is formed when about 40 % of NIS releases iodine during the inhibition period.

PAD systems

Compared to the catalyst-free and the NIS system, t_{inh} is distinctly *lower* when PADs are employed. This behavior was already observed for $(EtO)_2P(O)H$ in the literature.[28] It was ascribed to the reactivity of PADs toward I_2, undergoing a redox reaction to form the iodinated PAD and hydrogen iodide, potentially by establishing an equilibrium as presented in Scheme 3.3.[108,109] This consumes part of the inhibiting I_2 and lowers t_{inh}. The reaction is in fact favorable in the context of RTCP since the produced iodinated PAD corresponds to the deactivating species of the RTCP equilibrium, which is hence present from the very beginning of polymerization. Extrapolation to monomer conversions of 0 % gives $t_{inh} \approx 1.8$ h for both systems, resulting in a consumption of about 6 mmol L^{-1} of I_2 in comparison to the catalyst-free system according to Equation 3.4. This can indeed be achieved when about 50 % of the PADs effectively consume I_2. Slightly

longer t_{inh} for PinP(O)H might be a result of the redox equilibrium being slightly more shifted to the I_2 side compared to $(EtO)_2P(O)H$.

While the values of monomer conversion are somewhat scattered for the PinP(O)H system, the $(EtO)_2P(O)H$ system indicates that after inhibition, the polymerization rate is slightly higher compared to the catalyst-free system. In this context, monomer conversion of about 50 % is reached within 20 min for the $(EtO)_2P(O)H$ and within 30 min for the catalyst-free system. This can also be observed in literature studies[28] and is closely related to the effect of shorter inhibition, as the remaining [AIBN] is higher when less I_2 has to be consumed. The correlation between the polymerization rate and t_{inh} will again be addressed at a later stage.

3.2.2 Molar masses

In Figure 3.3 on the next page, values of $\overline{M}_n$ and dispersity, $Đ$ ($= \overline{M}_w/\overline{M}_n$; $\overline{M}_w$: weight-average molar mass) for the MMDs obtained from the discussed systems are given as a function of monomer conversion. For all systems, $\overline{M}_n$ values are very close to $\overline{M}_{n,theo}$ from an early stage, indicating good molar-mass control and fast (re)initiation of polymer chains. This even holds true for the catalyst-free system, which is remarkable for a polymerization controlled by degenerative chain transfer (DT) of iodine alone and in fact unaddressed in the corresponding literature studies. As already stated, from a kinetic point of view, low $\overline{M}_n$ values from an early stage indicate fast (re)initiation and a high C_{tr} value of the CTA (cf. Figure 2.1 on page 20). However, C_{tr} of CP–I is expected to be only slightly higher than unity since (i) C_{ex} for polyMMA was determined to be 2.6 for the here discussed system[25] while (ii) CP–I structurally resembles polyMMA–I, leading to $C_{tr} \approx C_{ex}$ (cf. Section 2.4.2 on page 18). $\overline{M}_n$ values should therefore be distinctly higher at low monomer conversions. A probable interpretation of this effect might be based on an inherent characteristic of the RITP mechanism. As mentioned above, during the inhibition period, not only CP–I is formed but oligomeric CP–polyMMA–I as well. This means that at the time polymerization effectively starts, a significant number of dormant chains already exists, which basically simulates the effect of fast (re)initiation of new chains. Indeed, in a related ITP of *n*-butyl methacrylate (BMA), for which the employed CTA CP–I was not produced in situ but was separately added to the monomer (so that no oligomers were present when polymerization effectively started), distinctly higher $\overline{M}_n$ values were obtained for low monomer conversion (see

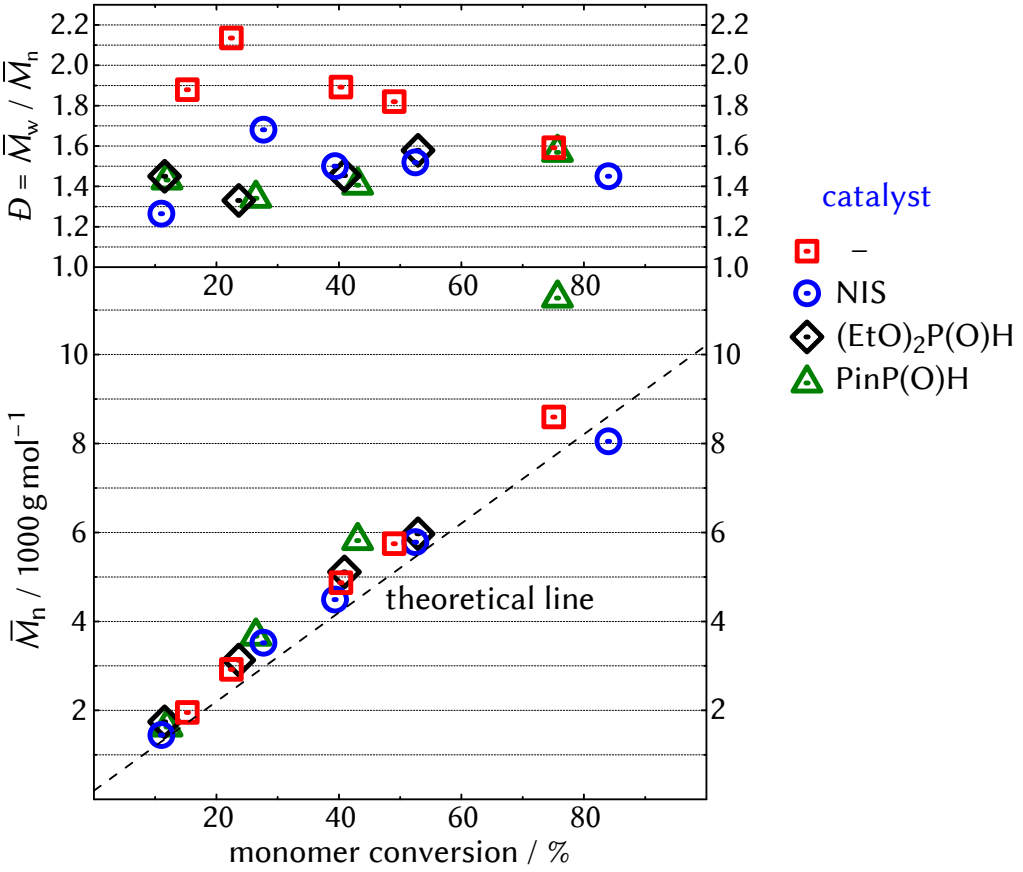

Figure 3.3 $\overline{M}_n$ and $Đ$ values as a function of monomer conversion of the RITP and RTCP systems of MMA in bulk at 80 °C presented in Table 3.1 on page 33.

Figure A.4 in the Appendix on page 232). This illustrates the only moderately fast (re)initiation behavior of CP–I alone in ITPs of methacrylates.

Throughout the polymerization, $\overline{M}_n$ values increase linearly for all systems. Although the effect is not expected to be strong, slightly (i) lower $\overline{M}_n$ values for NIS and slightly (ii) higher $\overline{M}_n$ values for PinP(O)H at high monomer conversion might indicate the (i) generation and (ii) consumption of iodine. This leads to either (i) more or (ii) less chains growing simultaneously. It should be stated that band-broadening (BB) effects during the SEC analysis of the polyMMA samples were estimated to be almost negligible for the obtained $\overline{M}_n$ values. As will be thoroughly explained in Part III of this thesis, BB was found to potentially lead to lower apparent $\overline{M}_n$ values compared to the true ones. Here, the extent of BB determined for the used

SEC setup (SEC setup 1, cf. Experimental Section 10.2.4 on page 223) results in a maximum downward deviation of the obtained $\overline{M}_n$ values from the true ones of only about 2 % (calculated via Equation 8.2, 8.8, 8.18, and 8.19 on pages 187–201).

$Đ$ values for the catalyst-free system are between 2.2 and 1.6, which is in good agreement with values from the literature.[25] $Đ$ values of the RTCP systems are distinctly lower, especially for low monomer conversion. This illustrates the positive impact of the catalysts on molar-mass control and indicates a higher activation–deactivation frequency of the living chains as proposed for RTCP.[26,85] In this context, PinP(O)H has a similar influence as the already established catalysts NIS and $(EtO)_2P(O)H$.

3.3 End-group analysis via ESI-MS

For each of the four discussed RITP-based systems, one representative polymer sample was analyzed via ESI-MS with special regard to identify polymer species by means of the detected chain end-groups. A typical ESI-MS experiment is described in the Experimental Section 10.2.1 on page 221. To clarify general aspects of ESI-MS analysis, the spectrum of the catalyst-free RITP system will be initially presented and discussed in more detail. It serves as a basis to assess the impact of the respective RTCP catalysts on the obtained polymeric species. It should be noted that end-group analysis via ESI-MS was also conducted for several polymeric products later in the present chapter as well as in the context of UV-initiated polymerization systems in Chapter 4. Information on the detected species will there be given concisely, while the results are of course based on the same thorough data evaluation as presented in the following.

3.3.1 Catalyst-free RITP system

Expected polymeric species

As the RITP mechanism (and RDRP mechanisms in general) does not replace but *superimposes* conventional RP, chains are partially expected that can be derived from conventional radical reactions (cf. Section 2.1 on page 9). After initiation by the conventional-initiator fragment $CP^{\bullet}$ (initiation: α-end-group) and successive propagation steps, irreversible termination and thus formation of dead polymer takes place by either disproportionation or combination (termination: ω-end-group) (see Scheme 3.4a on the following page).

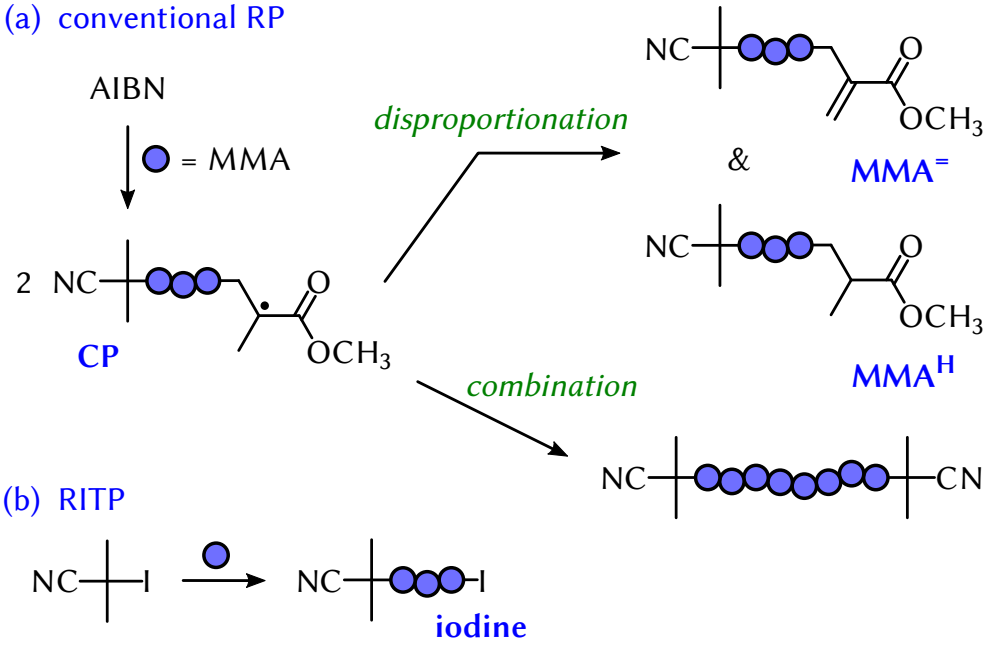

Scheme 3.4 Expected polymeric species and end-groups in an ideal RITP of MMA initiated by AIBN.

Disproportionation yields one chain with a terminal unsaturated ($MMA^{=}$) and one with a saturated MMA ω-end-group (MMA^{H}). Combination yields only one chain with a CP ω-end-group. For polyMMA, the ratio between disproportionation and combination is about 2 : 1.[98,110] In addition to that, the (R)ITP mechanism leads to dormant polymer chains with iodine as ω-end-group and the (re)initiating fragment of the CTA as α-end-group, which is CP and coincides with the fragment of the conventional initiator in this case (see Scheme 3.4b). In this context, although dead chains are inherently produced during polymerization, it is a feature of a well-controlled RDRP that they are massively outnumbered by dormant chains.

Detected polymeric species

The full spectrum and a spectrum of one monomeric repeating-unit from mass-to-charge ratio m/z = 900 to 1000 ($\Delta m/z = M_{\mathrm{MMA}} = 100\,\mathrm{g\,mol^{-1}}$) of a polyMMA sample of the RITP system ($\overline{M}_{\mathrm{n}} = 2000\,\mathrm{g\,mol^{-1}}$, $Đ = 1.88$, monomer conversion = 15 %) are presented in Figure 3.4 on the next page. It should be noted that the distribution in Figure 3.4a does not reflect the true MMD of the sample as ionization probabilities and thus signal intensities

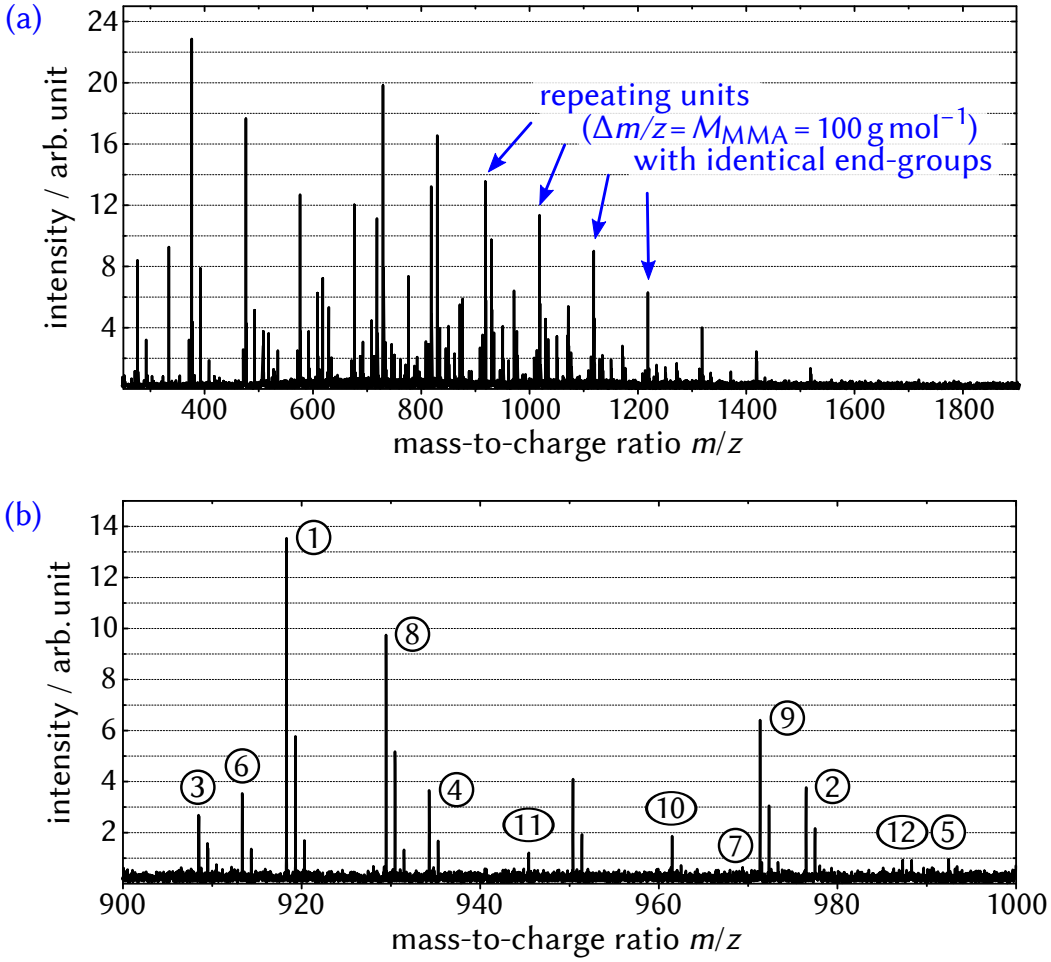

Figure 3.4 ESI-MS spectrum of a polyMMA sample ($\overline{M}_n$ = 2000 g mol^{-1}, $Đ$ = 1.88, monomer conversion = 15 %) obtained from the RITP system given in Table 3.1 on page 33 (entry 1): (a) full spectrum and (b) spectrum of one repeating unit between m/z = 900 and 1000 with peaks labeled according to Table 3.3 on the following page.

in ESI-MS strongly decrease for high molar masses of the macromolecules. Species were identified by means of m/z and further supported by the existence of species with more or less repeating units and by their characteristic isotope patterns. In this context, the natural abundances of ^{12}C (98.9 %) and ^{13}C (1.1 %)[111] lead to side peaks of isotopologues containing ^{13}C at $\Delta m/z$ = +1, +2, . . . , which can be seen in Figure 3.4b. The isotope patterns of the other elements can be regarded as negligible in this m/z area. While 37 different iodine isotopes from ^{108}I to ^{144}I are known, only ^{127}I is nonra-

Table 3.3 Polymeric species with the theoretical and the experimentally obtained m/z values, $(m/z)_{theo}$ and $(m/z)_{exp}$, respectively, and the relative intensities (rel. int.) from the ESI-MS spectrum in Figure 3.4b on the previous page.

No. [a]	α-end-group	ω-end-group [b]	mon. units [c]	ion	$(m/z)_{theo}$ [d]	$(m/z)_{exp}$ [d]	rel. int. / %
1	CP	iodine	7	Na^+	918.3	918.3	100
2	CP	lactone	7	Na^+	976.5	976.5	27
3	CP	OH	8	Na^+	908.5	908.5	19
4	CP	iodine	7	K^+	934.3	934.3	27
5	CP	lactone	7	K^+	992.5	992.5	6
6	CP	iodine	7	NH_4^+	913.4	913.4	25
7	CP	lactone	7	NH_4^+	971.5	971.5	5
8	2 × CP	2 × lactone	4	Na^+	929.5	929.5	73
9	2 × CP	lactone, iodine	5	Na^+	971.3	971.3	48
10	2 × CP	lactone, OH	6	Na^+	961.5	961.5	13
11	2 × CP	2 × lactone	4	K^+	945.4	945.4	8
12	2 × CP	lactone, iodine	5	K^+	987.3	987.3	6

[a] See Figure 3.4b on the preceding page; [b] transformations of iodine end-groups are given in Scheme 3.5 on the next page; [c] monomeric repeating-units; [d] for m/z = 900–1000.

dioactive and stable, so that iodine is a truly monoisotopic element and has no contribution to the observed isotope patterns as well.[111]

As a general comment, one should be aware that one and the same polymer species can lead to several different species obtained in an ESI-MS spectrum (with different m/z values), which is due to the following effects:

- Ionization by different (cat)ions, typically NH_4^+, Na^+, K^+, and H^+, depending on sample preparation and potentially added ionization agents.
- Ionization of two or more chains by one ion.
- Ionization by more than one ion, leading to $z = 2, 3, \ldots$. Conveniently, these species can be easily recognized as the differences between isotopologues or species with more or less repeating units depend on z and are thus smaller.

Indeed, all three effects were somehow observed in ESI-MS spectra analyzed within the present work.

In Table 3.3, the polymeric species are given for the labeled peaks in Figure 3.4b. Although a variety of different signals are obtained, including

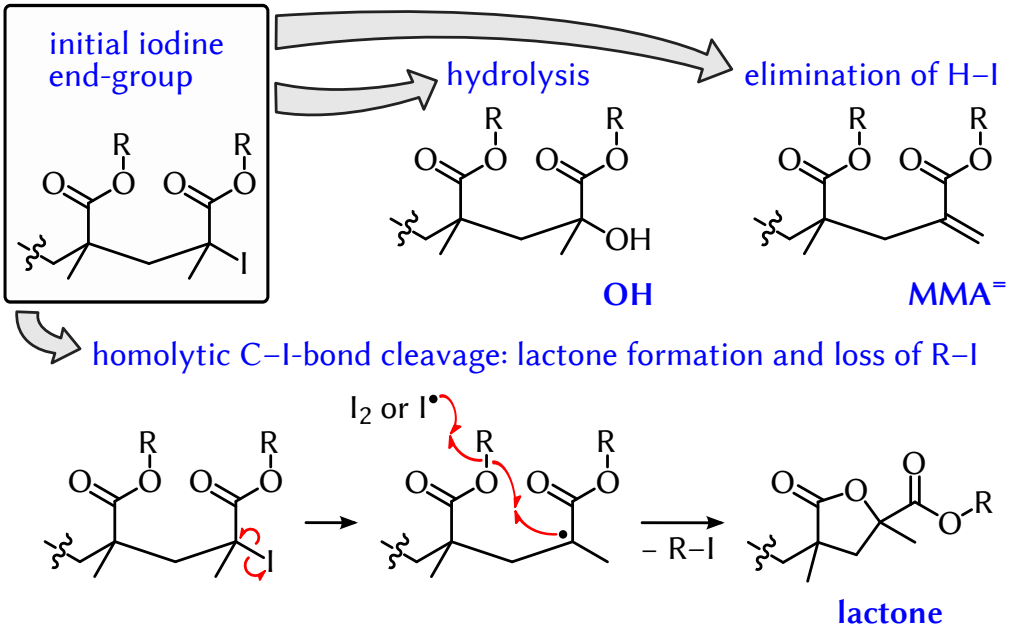

Scheme 3.5 Potential end-group transformations of iodine-capped poly(methacrylates) (R = CH_3 for polyMMA) according to literature studies.[24,25,93,112–115] The mechanism of lactone formation is inspired by Chiantore et al.[116,117] and not fully elucidated yet.

ionization by different cations and the occurrence of two chains being ionized by one ion (No. 8 to 12), only three different polymer species are detected. In agreement with the RITP mechanism, all chains are (re)initiated by CP•. Besides the expected ω-end-group iodine (highest intensity), additional end-groups are obtained that are typical for iodine-capped poly(methacrylates), namely OH and lactonic end-groups. As frequently described in the literature, halogen-(Hal-)capped polymer chains readily undergo characteristic end-group transformation upon both storage and analytical treatment, which is (i) hydrolysis,[93,112] (ii) H–Hal elimination,[24,25,93,112,114] and particularly for polymers of (meth)acrylates: (iii) formation of a lactonic structure in conjunction with the elimination of a haloalkane R–Hal[24,25,113–115] (Scheme 3.5). The structure of R–Hal is determined by the ester moiety (e. g., in case of polyMMA: R–Hal = H_3C–Hal; in case of poly(*n*-butyl acrylate): R–Hal = *n*Bu–Hal).[24] In this context, the mechanism of lactone formation has not been completely elucidated yet. A reasonable pathway is given in Scheme 3.5, which is inspired by Chiantore et al.,[116,117] who observed that a lactonic structure also forms upon oxidative degradation of (meth)acrylic

Table 3.4 Na^+-ionized species detected in ESI-MS of a polyMMA sample produced via RTCP with NIS (Table 3.1 on page 33, entry 2, $\overline{M}_n$ = 3500 g mol^{-1}, $Đ$ = 1.68, monomer conversion = 28 %) with the theoretical and the experimentally obtained m/z values, $(m/z)_{theo}$ and $(m/z)_{exp}$, respectively, and their relative intensities (rel. int.).

No.	α-end-group	ω-end-group [a]	mon. units [b]	$(m/z)_{theo}$ [c]	$(m/z)_{exp}$ [c]	rel. int. [d] / %
1	CP	iodine	7	918.3	918.3	64
2	CP	lactone	7	976.5	976.5	26
3	CP	OH	8	908.5	908.5	3
4	CP	$MMA^{=}$	8	990.5	990.5	3
5	CP	MMA^{H}	8	992.5	992.5	3
6	CP	CP	8	959.5	959.5	1

[a] Transformations of iodine end-groups are given in Scheme 3.5 on the preceding page; [b] monomeric repeating-units; [c] for m/z = 900–1000; [d] only the here given species are taken account of, sum = 100 %.

polymer. It should be noted that the reaction is estimated to be much slower than propagation; otherwise, lactonic end-groups would be observed for RPs of (meth)acrylates in general. All chain-end transformations are expected to happen mainly *after* polymerization, since (i) the evolution of $\overline{M}_n$ is very close to $\overline{M}_{n,theo}$ (corresponding to 100 % iodine end-groups, see Figure 3.3 on page 38) and (ii) the percentage of transformed end-groups always increases when samples are measured for a second time after a few days or weeks. The stability of iodine end-groups will be more deeply discussed at a later stage.

Peaks indicating dead polymer molecules are too low to be detected for the given signal-to-noise ratio in the presented spectrum. This is mainly ascribed to the fact that the polymer sample was taken at a rather low monomer conversion (15 %), for which the amount of dead chains from continuously occurring irreversible termination was still low. This clarifies that the (formerly) living chains strongly outnumber the dead ones at this point, which is in accordance with the concept of RITP.

3.3.2 RTCP systems

3.3.2.1 NIS system

In Table 3.4 on the preceding page, the detected species of a polyMMA sample of the RTCP system with NIS are presented ($\overline{M}_n$ = 3500 g mol^{-1}, $Đ$ = 1.68, monomer conversion = 28 %). For reasons of clarity, only species ionized with Na^+ are given (highest intensities of all cations). The results closely resemble the ones for the catalyst-free system. This fully supports the concept of RTCP with (i) the iodo CTA CP–I forming the (re)initiating species and (ii) the capping agent iodine. End-groups derived from fragments of the catalyst NIS could not be detected, indicating that contribution to either initiation or termination is very low, if at all existent. As described at the beginning of this chapter, minor contribution to initiation and termination is mandatory for a good catalyst since it would be consumed rather quickly otherwise. In this context, the fact that similar polymerization rates are obtained for the catalyst-free and the NIS system indicates low significance of rate-retarding cross-termination between the activating succinimidyl radical, NS$^\bullet$, and the propagating polyMMA radical, polyMMA$^\bullet$. This is supported by the absence of the corresponding termination species in the ESI-MS spectrum.

It should be stated that at first sight, the fact that the species formed during polymerization are not affected by the addition of a catalyst might not be a persuasive argument for the occurrence of an RTCP mechanism. However, as mentioned before, kinetic studies[26,27,85] demonstrated that the addition of suitable RTCP catalysts (such as NIS) to ITP systems systematically increases the rate of both reversible activation and deactivation of living chains.[26,27,85] This is also indicated by the molar-mass results obtained here and in other literature studies.[28,82] In this context, the ESI-MS results support the proposed "catalytic" behavior of RTCP catalysts. Similarly to the catalysts used in ATRPs, they transfer the capping agent (here: iodine) to the propagating chain without being part of the formed dormant species.

As opposed to the catalyst-free system, dead polymer chains with a reasonable ratio between disproportionation and combination are detected (No. 4 to 6). As indicated above, this is due to (i) a generally higher signal-to-noise ratio and (ii) the fact that here, the polymerization has proceeded much further with a monomer conversion almost twice as high (28 % versus 15 %). Still, (formerly) dormant chains strongly outnumber dead ones with a total percentage of 93 %. In this context, the application of NIS does not interfere

Table 3.5 Species detected in ESI-MS of polyMMA samples produced via RTCP with either $(EtO)_2P(O)H$ (Table 3.1 on page 33, entry 3) or PinP(O)H (entry 4) and their relative intensities (rel. int.).

No.	α-end-group	ω-end-group [a]	mon. units [b]	rel. int. / % [c] $(EtO)_2P(O)H$ [d]	rel. int. / % [c] PinP(O)H [e]
1	CP	iodine	8	19	11
2	CP	lactone	8	60	68
3	CP	OH	9	4	3
4	CP	$MMA^{=}$	9	4	2
5	CP	MMA^{H}	9	13	15
6	CP	CP	9	–	1

[a] Transformations of iodine end-groups are given in Scheme 3.5 on page 43; [b] monomeric repeating-units, for m/z = 1000–1100; [c] only the here given species are taken account of, respective sum = 100 %; [d] $\overline{M}_n$ = 3100 g mol^{-1}, $Đ$ = 1.33, monomer conversion = 24 %, ionized with NH_4^+; [e] $\overline{M}_n$ = 3700 g mol^{-1}, $Đ$ = 1.34, monomer conversion = 26 %, ionized with Na^+.

with the iodo chain-end functionalities, which is of high importance for potential further processing of the polymer.

3.3.2.2 PAD systems

In Table 3.5, the detected species of the polyMMA samples obtained from the $(EtO)_2P(O)H$ system ($\overline{M}_n$ = 3100 g mol^{-1}, $Đ$ = 1.33, monomer conversion = 24 %) and the PinP(O)H system ($\overline{M}_n$ = 3700 g mol^{-1}, $Đ$ = 1.34, monomer conversion = 26 %) are presented. For both systems, the species again resemble the ones detected for the NIS and the catalyst-free system. All chains are (re)initiated by $CP^{\bullet}$ and have ω-end-groups typically expected for an iodine-mediated system. As for the NIS system, no species were detected in neither of the two systems which indicate a contribution of the respective activating radical species or reasonable fragments to initiation or termination under the chosen polymerization conditions. Cross-termination is again expected to be low in both cases. All these findings are consistent with the principles of RTCP and indicate that both $(EtO)_2P(O)H$ and PinP(O)H are suitable catalysts in terms of this polymerization method.

As a striking effect, for both PAD systems, the relative intensities of the species with the ω-end-group MMA^{H} are rather high (13 % and 15 %, respectively). Since the intensities are much higher than for $MMA^{=}$, the

Table 3.6 Species detected in ESI-MS with relative intensities (rel. int.) of a polyMMA sample produced via RTCP with NIS 1 day after polymerization (cf. Table 3.4 on page 44) and after storing the sample for an additional month at ambient light and temperature.

No.	α-end-group	ω-end-group [a]	mon. units [b]	rel. int. / % [c] after 1 day	after 1 month
1	CP	iodine	7	64	3
2	CP	lactone	7	26	77
3	CP	OH	8	3	12
4	CP	$MMA^{=}$	8	3	3
5	CP	MMA^{H}	8	3	4
6	CP	CP	8	1	1

[a] Transformations of iodine end-groups are given in Scheme 3.5 on page 43; [b] monomeric repeating-units; [c] only the here given species are taken account of, respective sum = 100 %.

species are unlikely to stem from termination via disproportionation. As this effect is obtained for both PAD systems and for none of the investigated systems in this thesis containing *no* PADs, a contribution is highly probable. In this context, during polymerization, the propagating polyMMA$^{\bullet}$ chain might undergo a transfer reaction by abstracting the hydrogen atom from the weak P–H bond of the PAD. However, the high percentage of dead polymer chains at an early stage of the polymerization would arguably have an adverse impact on molar-mass control, whereas this cannot be gathered from the obtained $\overline{M}_n$ and $Đ$ values of the two systems (cf. Figure 3.3 on page 38, between 20 % and 30 % of monomer conversion). Another possible explanation might be a reaction of iodine-end-capped polyMMA with the PADs *after* polymerization and before ESI-MS analysis. In this context, through a slower nonradical process, PADs were indeed shown to react with iodoalkanes, potentially leaving saturated end-groups.[26,118] While this issue was not fully resolved within the here presented work, it is relevant when a high extent of end-group functionality is desired for further processing of the polymer. A prompt separation of the PADs from the polymeric product after polymerization might be necessary in that case.

3.3.3 Stability of iodine end-groups

As previously explained in Section 3.3.1 on page 39 and obtained for every analyzed polymer sample in the present thesis, Hal-end-capped polymer molecules are readily susceptible to undergo end-group transformation. In literature studies, when Hal-end-capped polymer is analyzed via MALDI-(matrix-assisted laser desorption/ionization-)MS, detected end-group transformation is often ascribed to the harsh ionization conditions. In this context, although both ESI and MALDI are commonly considered as *soft* ionization methods, MALDI is expected to be slightly harder than ESI, often leading to more pronounced end-group transformation, not only for Hal-end-capped polymer.[94,96] For example, when chlorine-end-capped polyMMA was analyzed via MALDI-MS, a slight amount of lactonic end-groups could only be detected for high laser powers, while transformation was completely prevented for low laser powers.[114] A comparative MALDI-MS study[115] demonstrated that bromine-end-capped polyMMA much more readily forms a lactonic end-group than chlorine-end-capped polyMMA. In this regard, the lactonic end-group also readily formed from bromine-end-capped polyMMA upon heat treatment, which (i) could then be detected via alternative methods such as NMR spectroscopy, while (ii) this behavior was much less significant for chlorine-end-capped polyMMA. This clarifies that (i) formation of the lactonic structure is not limited to the MS method and that (ii) chlorine-end-capped polymer is generally less prone to end-group transformation than bromine-end-capped polymer. The latter is ascribed to the weaker terminal C−Br bond in comparison to C−Cl. Consequently, as the terminal C−I bond is even weaker, end-group transformation is generally very pronounced for MALDI-MS analysis of iodine-end-capped polyMMA.[25] While it is barely addressed in the literature, the C−I bond is even expected to be so weak that in contrast to bromine- and chlorine-end-capped polymer, a significant end-group transformation should take place already during the storage of the polymer. It should in fact be noted that its labile tertiary C−I bond is the reason why the in situ generation of the CTA CP−I is applied in the first place. In the here presented work, even for the softer ESI-MS method, distinct transformation of iodine end-groups can be generally observed. Moreover, as stated above, without a single exception, for all polymer products analyzed in this thesis (polyMMA, polyBMA, polyBA), the percentage of iodine end-capped polymer chains was always lower and the percentage of transformed end-groups was always higher when a polymer sample was again measured after a few days or weeks. This effect was commonly ac-

companied by an apparent reddish coloring of the stored polymer over time, indicating the release of molecular I_2. As an example, the results for the RTCP system with NIS in Table 3.4 on page 44—which were obtained 1 d after polymerization—are compared to results of an ESI-MS analysis after storing the sample for an additional month at ambient light and temperature (see Table 3.6 on page 47). While the percentage of dead polymer is basically constant, most iodine end-groups are transformed into both lactonic and OH end-groups.

The extent of end-group transformation is expected to highly depend on the type of polymer, more precisely on the activity of the C–I bond. In this context, MALDI-MS analysis of iodine-end-capped polyMA (*secondary* C–I bond) showed distinctly less transformation.[24] This could be confirmed for a polyBA sample produced under RITP conditions similar to the ones employed for MMA. In this context, end-group transformation of below 1 % was observed via ESI-MS analysis 1 d after polymerization (data not shown). Here, it should also be stated that the addition of formic acid as ionizing agent turned out to be adverse as it promoted hydrolysis and led to a distinctly higher transformation of iodine into OH end-groups.

Chain-length-dependent end-group transformation

As another striking effect, it was observed that the detected extent of end-group transformation varies for different chain lengths. In Figure 3.5 on the next page, the relative intensities of the polyMMA species presented in Table 3.6 on page 47 are given as a function of monomeric repeating-units (~ chain lengths). It should be stated that the species are quantitatively compared as they are compared in Table 3.6. More precisely, for the abscissa value *monomeric repeating-unit* = 1 in Figure 3.5, the species of the iodine and the lactone series with monomeric repeating-unit = 1 are compared with the species of the OH, $MMA^{=}$, MMA^{H}, and CP series with monomeric repeating-unit = 2. For *monomeric repeating-unit* = 2, the species of the iodine and the lactone series with monomeric repeating-unit = 2 are compared with the species of the OH, $MMA^{=}$, MMA^{H}, and CP series with monomeric repeating-unit = 3, etc. Indeed, this leads to the fact that some of the compared species do not stem from macromolecules with the same chain length (e. g., when a lactonic end-group is formed, the process consumes two monomeric repeating-units; termination via combination leads to a higher chain length than via disproportionation). However, as the molar masses of the compared species and thus their ionization probability are more alike,

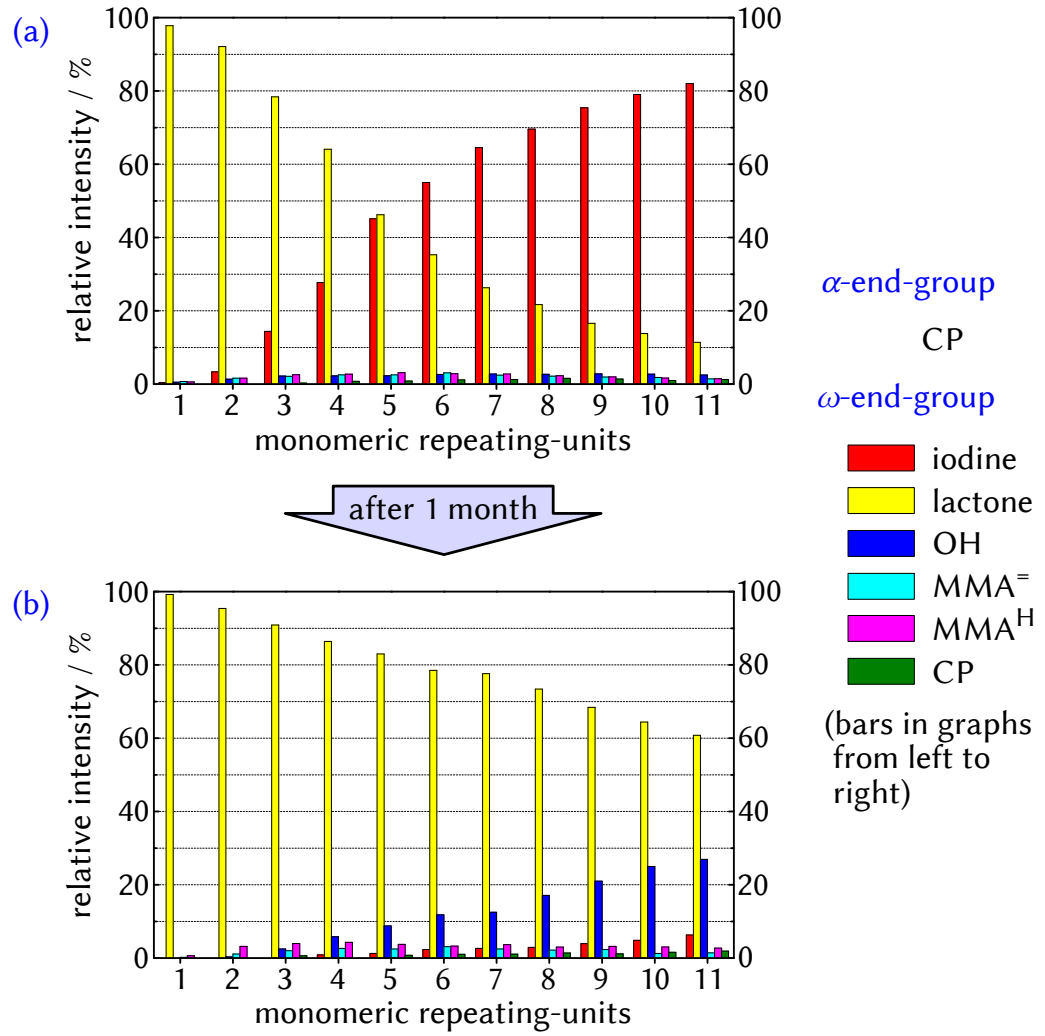

Figure 3.5 Relative intensities of polyMMA species from RTCP with NIS detected via ESI-MS as a function of monomeric repeating-units (a) 1 day and (b) 1 month after polymerization (cf. Table 3.6 on page 47).

the relative intensities arguably more closely represent the actual abundance of species in the polymer.

As a result, it can be observed that the amount of dead polymer is low irrespectively of the chain length. However, the transformation of iodine end-groups into lactonic end-groups shows a remarkable chain-length dependence. While the amount of iodine end-groups is lower and the amount of lactonic end-groups is higher after 1 month, it is evident that the percentage of lactonic end-groups decreases for higher chain lengths in both

cases. To the contrary, the percentage of iodine end-groups *increases* in both cases (at least slightly in Figure 3.5b). Indeed, this behavior of lactonic and iodine end-groups was obtained for every single polymer analyzed in the present chapter. This indicates that the transformation of iodine end-groups might be a chain-length-dependent process. While this effect still lacks a reliable interpretation at this point, potential reasons might be (i) chain-length-dependent reactivities of the terminal C–I bond and/or (ii) a chain-length-dependent intramolecular attack of the radical function, which could be due to a less flexible backbone of the polymer molecules and a more impeded reaction as chain lengths increase.

At the end of the day, the results clarify that working with iodine-end-capped polymer requires special awareness of potential transformation of living chains. In this context, the presented types of transformed end-groups and their respective formation mechanisms indicate that the polymer should be stored at a (i) low level of air humidity (cf. OH end-group) and (ii) under conditions preventing homolytic C–I-bond cleavage (cf. lactone end-group), i. e., low temperatures and low exposure to light. This is of particular importance when the iodine chain-end functionality shall be processed further, for example in chain-extension or coupling reactions. In this context, especially in case of poly(methacrylates), it is recommended preventing long storage times if possible.

3.4 Initiator cocktail in RITP

Although RITP systems offer a convenient way to apply highly active iodo CTAs, long inhibition periods in comparison to relatively short subsequent polymerization periods might be a serious drawback for some applications. According to Equation 3.4 on page 35, there are two basic strategies to shorten inhibition: (i) increasing the ratio between $[\mathrm{AIBN}]_0$ and $[\mathrm{I}_2]_0$, and (ii) increasing k_{dec}. The first option is rather straightforward and can be influenced by the employed amount of AIBN, while the amount of I_2 is often less adjustable since it determines the targeted $\overline{M}_{\mathrm{n}}$ values. For the second option, k_{dec} can be increased by either polymerizing at higher temperatures or by employing a more active radical initiator. Several structurally related azo initiators indeed exist that decompose more readily than AIBN.[105] While both strategies have been adopted in the literature,[24,25,28,90] they basically just increase the general production of radicals. As a result, significantly shorter inhibition leads to a significantly faster polymerization,

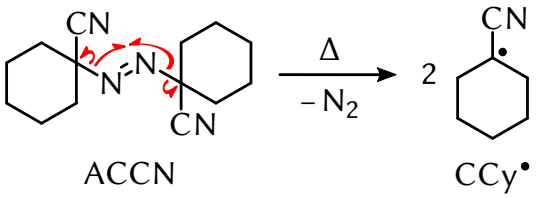

Scheme 3.6 Simplified decomposition of ACCN forming cyanocyclohexyl radicals, CCy•.

which might bear challenges in handling and monitoring the polymerization process. Under the conditions employed for the systems in Figure 3.2 on page 34—i. e., high $[I_2]_0$, relatively high k_p of MMA at 80 °C—it can in fact be regarded as an inherent feature of RITP that the polymerization period is significantly shorter than the inhibition period. As mentioned above, for the $(EtO)_2P(O)H$ system, reduced inhibition from t_{inh} = 2.4 h to 1.8 h leads to faster polymerization with 50 % of monomer conversion within only about 20 min (rather than 30 min for t_{inh} = 2.4 h). This illustrates that smooth polymerization can arguably only be observed when inhibition lasts several hours.

Initiator cocktail A solution to this dilemma will be presented in the following. It is based on the application of two different radical initiators rather than a single one. In this context, the two initiators are supposed to share tasks: (i) a rapidly decomposing initiator is mainly responsible for the consumption of I_2 and generation of the CTA, while (ii) a slowly decomposing initiator ideally takes up the baton after inhibition is over, allowing for a smooth radical flow and polymerization. This technique is inspired by Nguyen and Vana,[119] who managed to eliminate the induction period in a RAFT polymerization with the mediator dithiobenzoic acid by applying an initiator cocktail. The feasibility of this strategy for RITP will be demonstrated in the following on the exemplary basis of an initiator cocktail of AIBN (fast decomposition) and 1,1′-azobis(cyclohexanecarbonitrile) (ACCN, see Scheme 3.6) (slow decomposition).

3.4.1 Polymerization rate and inhibition time

The initiator cocktail was applied to RITP of MMA in bulk at 100 °C. $[I_2]_0$ was again chosen to target $\overline{DP}_n$ = 100 for full monomer conversion. The employed initial concentrations of the initiators might require slight tuning when their kinetics is only roughly known, while here, the well-characterized decomposition behavior of both AIBN and ACCN allowed for a straight-

Table 3.7 Initial concentrations of substances used RITP of MMA in bulk at 100 °C applying an initiator cocktail.

entry[a]	$[MMA]_0$ / mol L^{-1}	$[I_2]_0$ / mol L^{-1}	$[AIBN]_0$ / mol L^{-1}	$[ACCN]_0$ / mol L^{-1}
⬠	8.5	4.2×10^{-2}	5.2×10^{-2}	1.9×10^{-2}

[a] See Figure 3.6.

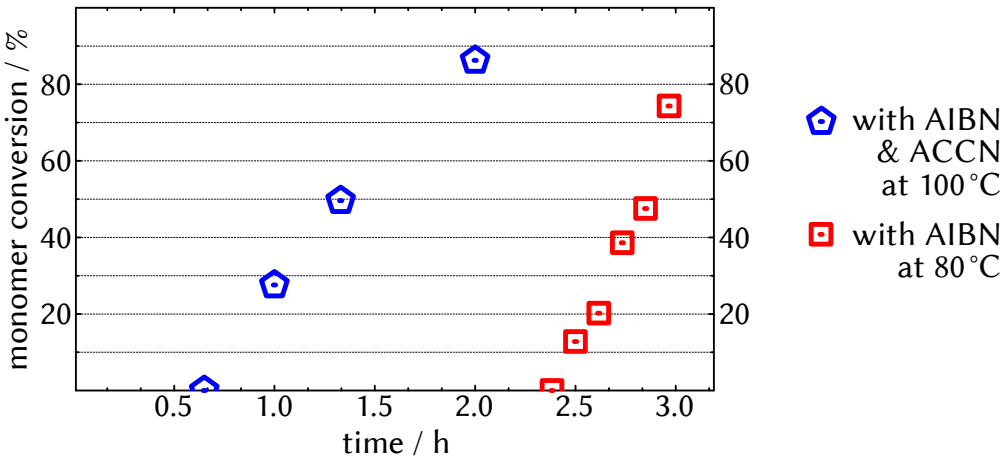

Figure 3.6 Monomer conversion as a function of time of the RITP of MMA in bulk at 100 °C applying an initiator cocktail (Table 3.7) in comparison to the RITP of MMA at 80 °C applying a single initiator presented in Figure 3.2 on page 34.

forward choice of $[AIBN]_0$ and $[ACCN]_0$. This will be more precisely discussed below. The initial concentrations of all substances are given in Table 3.7. In this context, at 100 °C, the fast initiator AIBN decomposes with $k_{dec}(AIBN) = 1.7 \times 10^{-3}\,s^{-1}$ [106] and the slow initiator ACCN with $k_{dec}(ACCN) = 1.4 \times 10^{-4}\,s^{-1}$ [106] about 12 times more slowly. Monomer conversion as a function of time is given in Figure 3.6 in comparison to the RITP system at 80 °C presented in Figure 3.2 on page 34. Inhibition is significantly reduced to about a quarter of the comparative system while still, polymerization proceeds quite smoothly with a rate about only half as high. Considering that the polymerization is conducted at 100 °C rather than 80 °C and that propagation of polyMMA is much faster ($k_p = 2000\,L\,mol^{-1}\,s^{-1}$ for 100 °C and $1300\,L\,mol^{-1}\,s^{-1}$ for 80 °C),[120] this demonstrates the signifi-

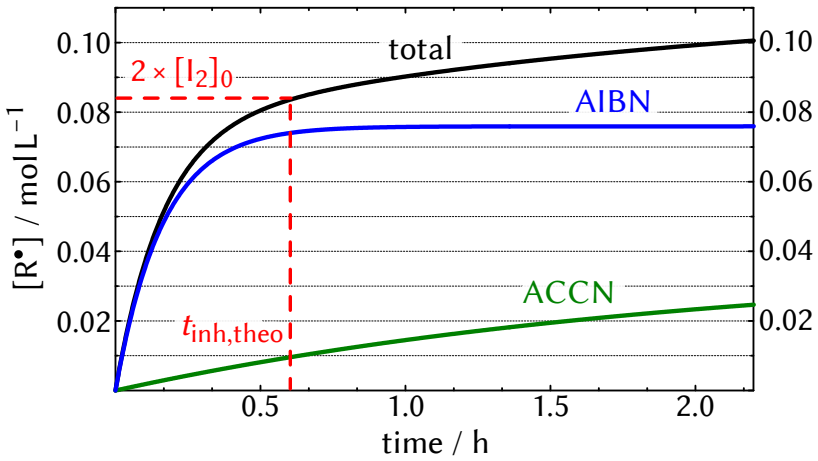

Figure 3.7 Concentration of produced radicals (Equation 3.5) versus time for (i) AIBN ($[\text{AIBN}]_0 = 5.2 \times 10^{-2}\,\text{mol}\,\text{L}^{-1}$, $k_{\text{dec}} = 1.7 \times 10^{-3}\,\text{s}^{-1}$,[106] $f = 0.73$[107]), (ii) ACCN ($[\text{ACCN}]_0 = 1.9 \times 10^{-2}\,\text{mol}\,\text{L}^{-1}$, $k_{\text{dec}} = 1.4 \times 10^{-4}\,\text{s}^{-1}$,[106] $f = 0.98$[121]), and (iii) the sum of both (total) for the polymerization presented in Figure 3.6 on the previous page. When $[\text{R}^\bullet] = 2 \times [\text{I}_2]_0$, inhibition is over and $t = t_{\text{inh,theo}}$.

cantly lower radical flow during polymerization, while the radical flow is clearly higher during the shorter inhibition period.

Radical flow

The interplay of the two initiators is clarified when the radical production of both is illustrated throughout polymerization. The concentration of radicals, $\text{R}^\bullet$, generated by an initiator is given by

$$[\text{R}^\bullet] = 2f \cdot [\text{initiator}]_0 \cdot (1 - \exp(-k_{\text{dec}} \cdot t)) \tag{3.5}$$

(cf. Section 2.1 on page 9). In Figure 3.7, $[\text{R}^\bullet]$ versus polymerization time is displayed for (i) AIBN alone, (ii) ACCN alone, and (iii) AIBN and ACCN combined for the conditions of the here presented system. In this context, the respective efficiencies of the initiators are $f(\text{AIBN}) = 0.73$[107] and $f(\text{ACCN}) = 0.98$.[121] The much higher radical production of AIBN compared to ACCN is evident. The indicated $t_{\text{inh,theo}}$ (time until $[\text{R}^\bullet] = 2 \times [\text{I}_2]_0$) is in good agreement with the experimental results.

In Figure 3.8 on the facing page, the radical flow—i. e., $[\text{R}^\bullet]$ generated per second (= first derivative of the data given in Figure 3.7)—is given for AIBN and ACCN. The plots clearly show how the two initiators are respectively

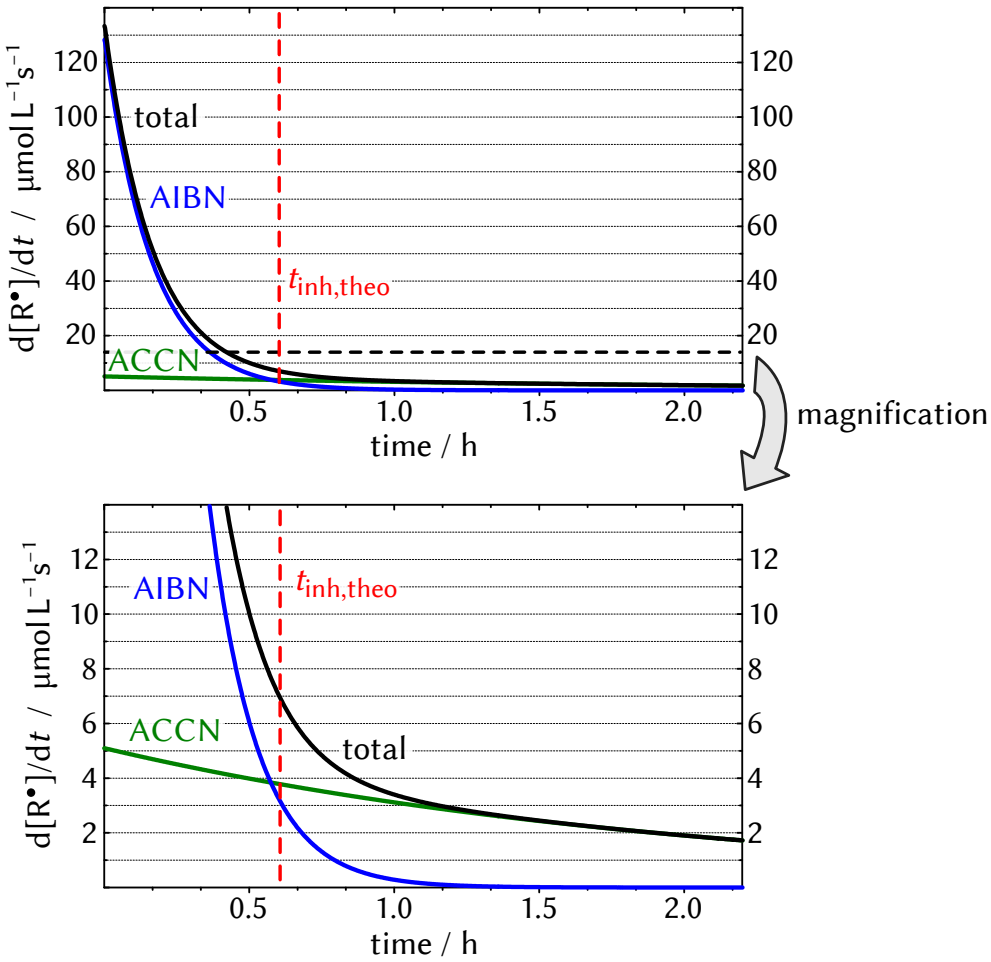

Figure 3.8 Radical flow d[R•]/dt during polymerization caused by (i) AIBN, (ii) ACCN, and (iii) both combined (total). The here given data corresponds to the first derivative of the data given in Figure 3.7 on the preceding page.

in charge during either inhibition or polymerization. During inhibition, R• mainly originates from the quickly decomposing AIBN. In this regard, decomposition is indeed so fast that only about 2 % of the initial AIBN is left after $t_{inh,theo}$. At this point, the low but consistent production of R• by ACCN exceeds the one by AIBN and smoothly takes over polymerization. After about 1 h, ACCN is almost exclusively in charge of generating R•, while AIBN is nearly completely decomposed. This illustrates an additional problem that might arise when a quickly decomposing initiator (like AIBN at 100 °C) is used alone: even if the amount of AIBN was high enough to

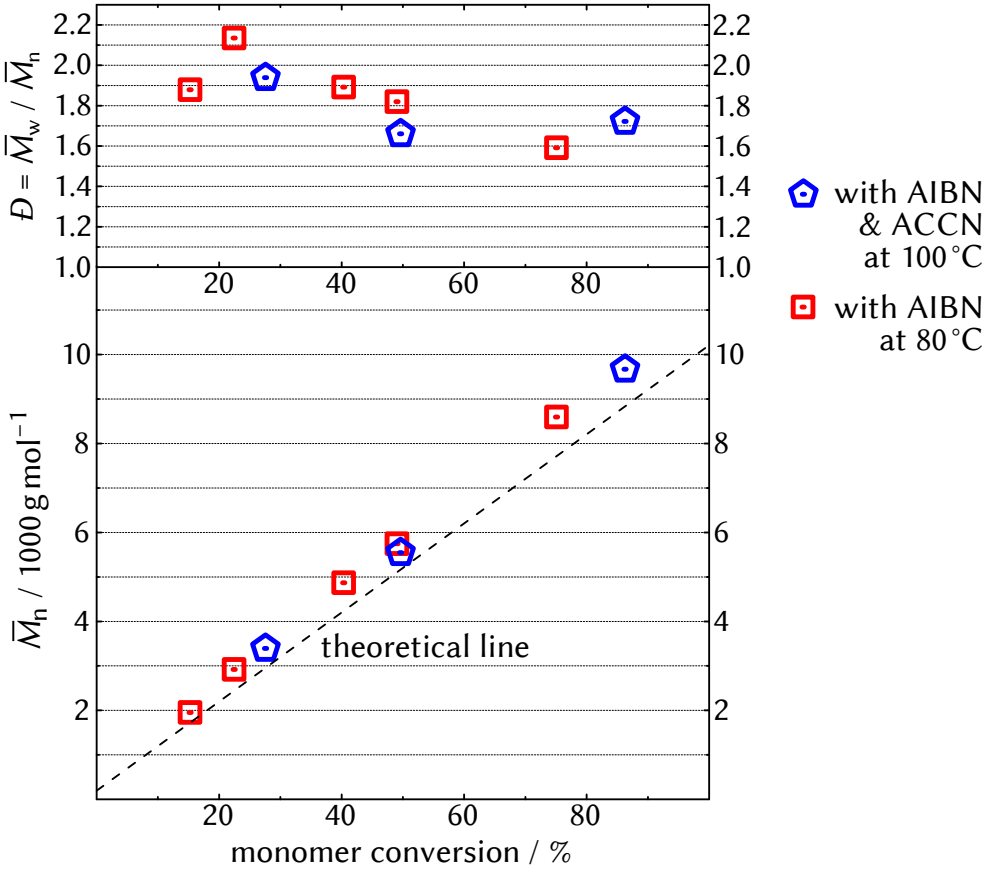

Figure 3.9 $\overline{M}_n$ and $Đ$ as a function of monomer conversion of the RITP of MMA in bulk at 100 °C employing a radical-initiator cocktail (Table 3.7 on page 53) in comparison to the RITP of MMA at 80 °C employing a single radical initiator presented in Figure 3.3 on page 38.

effectively consume all I_2, it generates a highly irregular radical flow and thus evolution of monomer conversion during polymerization.

3.4.2 Molar masses

In Figure 3.9, $\overline{M}_n$ and $Đ$ values of the MMDs obtained from the discussed systems are presented. $Đ$ values indicate similar molar-mass control compared to the system with just AIBN. In addition, $\overline{M}_n$ values are again very close to $\overline{M}_{n,theo}$ from an early stage, which clarifies that this characteristic feature of RITP caused by partial formation of oligomeric dormant chains (cf. Section 3.2.2 on page 37) also holds true for the cocktail system. The results show

Table 3.8 Na^+-ionized species detected in ESI-MS of a polyMMA sample produced via the initiator-cocktail–RITP system presented in Table 3.7 on page 53 ($\overline{M}_n$ = 3400 g mol^{-1}, $Đ$ = 1.94, monomer conversion = 28 %) with the theoretical and the experimentally obtained m/z values, $(m/z)_{theo}$ and $(m/z)_{exp}$, respectively, and their relative intensities (rel. int.).

No.	α-end-group	ω-end-group [a]	mon. units [b]	$(m/z)_{theo}$ [c]	$(m/z)_{exp}$ [c]	rel. int. [d] / %
1	CP	lactone	7	976.5	976.5	77
2	CP	iodine	7	918.3	918.3	5
3	CP	OH	8	908.5	908.5	3
4	CP	$MMA^=$	8	990.5	990.5	1
5	CP	MMA^H	8	992.5	992.5	2
6	CP	CP	8	959.5	959.5	1
7	CCy	lactone	6	916.5	916.5	8
8	CCy	iodine	7	958.3	958.3	3

[a] Transformations of iodine end-groups are given in Scheme 3.5 on page 43; [b] monomeric repeating-units; [c] for m/z = 900–1000; [d] only the here given species are taken account of, sum = 100 %.

that the system allows for significant shortening of inhibition and smooth polymerization while fully retaining the inherent molar-mass control of RITP.

3.4.3 End-group analysis

In Table 3.8, species detected in an ESI-MS analysis of a polyMMA sample obtained from the initiator-cocktail system are presented ($\overline{M}_n$ = 3400 g mol^{-1}, $Đ$ = 1.94, monomer conversion = 28 %). The results show ω-end-groups as expected from an iodine-mediated polymerization and previously discussed in this chapter. The obtained α-end-groups demonstrate the contribution of both AIBN and ACCN, while the proportion between chains initiated by CP$^\bullet$ and by CCy$^\bullet$ is in good agreement with the provided [R$^\bullet$] presented in Figure 3.7 on page 54. In this context, it should be emphasized that a small part of I_2 is indeed consumed by CCy$^\bullet$, thus forming the additional CTA CCy–I. However, as CCy$^\bullet$ is structurally related to CP$^\bullet$, it is expected that the (re)initiation behavior is rather similar.[28] This can also be gathered from the unaffected molar-mass evolution in Figure 3.9 on the facing

page. This clarifies that when an initiator-cocktail system is composed, *both* initiators should form sufficiently active iodo CTAs.

3.5 Concluding remarks

ESI-MS was shown to be a suitable method to study into mechanistic effects and end-group functionalities for RITPs and RITP-based RTCPs. While the RTCP systems with the catalysts NIS, $(EtO)_2P(O)H$, and PinP(O)H exhibit (i) improved chain-growth control, (ii) the obtained end-groups clearly identify iodine as reversible capping-agent, which supports the mechanistic principles of RTCP. In addition, no contribution of catalyst fragments to initiation or termination events could be found. Potential (re)initiation or cross-termination reactions are therefore expected to be minor for the investigated systems. The low extent of cross-termination and thus rate-retardation was further demonstrated by the rather similar polymerization rates compared to the catalyst-free system. In this context, rate retardation by NIS for the here presented MMA system is much less pronounced as in polymerizations of St.[85] There, the polymerization rate is distinctly reduced by about 40 % when comparable NIS concentrations are employed. Thus, the MMA systems beneficially improve chain-growth control without suffering from adverse rate retardation.

While the extent of end-group functionality is expected to be high during polymerization, pronounced iodine chain-end transformation is generally observed after polymerization. As described, this effect is especially pronounced for poly(methacrylates) with rather weak tertiary C–I bonds. When further processing of the polymer is desired, special experimental care (e. g., low humidity, low temperature, low exposure to light) has thus to be taken, while it is generally recommended to keep storage time as short as possible. A pronounced formation of saturated MMA^H end-groups was detected when the two PAD catalysts were employed. In this case, a prompt separation of the catalysts from the produced polymer might be necessary when further processing is planned.

Eventually, the adverse inhibition period of RITP systems could be effectively reduced by using an initiator cocktail with one quickly and one slowly decomposing radical initiator. This technique directly addressed one of the major drawbacks of RITP systems while fully retaining its advantageous convenient procedure to produce functionalized and well-defined polymer. In Figure 3.7 to 3.8 on pages 54–55, the general strategies are clarified that have

to be pursued when individual systems with different initiators under different conditions are composed. In this context, it should be stated that the approach of an initiator cocktail might be especially worthwhile for monomers with even higher k_p values than MMA at 80 °C. For example, under typical RITP conditions at 70 °C, methyl acrylate (k_p = 33 000 L mol^{-1} s^{-1} [122]) has to endure an inhibition period of not less than 12 h before high monomer conversions are reached within only 1 h.[24]

CHAPTER 4

UV-initiated iodine-mediated polymerizations

Scavenging iodine

Since the pioneering work of Otsu et al. on photoiniferters,[35,36] UV/vis radiation has been applied to several RDRP systems including NMP,[123] ATRP,[37,38,124] RAFT,[39,40] and organotellurium-mediated polymerization (TERP).[125,126] In contrast, examples of *iodine-mediated* photosystems are rare. The main reason for this can probably be assigned to the intrinsic chemical nature of iodine. Organoiodine compounds like polymer–I are well-known to be often very light-sensitive, and C–I bonds are readily cleaved homolytically to give polymer$^\bullet$ and I$^\bullet$. On the face of it, this reaction seems favorable, since it produces radicals needed for polymerization and even increases the activation rate of polymer–I toward the relatively slow activation via DT (cf. Paragraph Typical ITP systems on page 23).[16,18] However, when polymer$^\bullet$ undergoes irreversible self-termination, free iodine (I$^\bullet$ and I_2, the

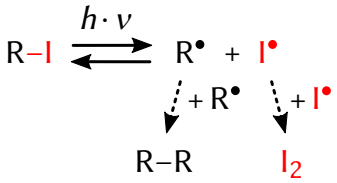

Scheme 4.1 Accumulation of free iodine caused by photoinduced homolytic C–I-bond cleavage of the organoiodine compound R–I and subsequent irreversible self-termination of R$^\bullet$.[42]

combination product of two $I^{\bullet}$) accumulates in the system (see Scheme 4.1 on the preceding page). While its scavenging behavior was clarified in the context of RITP in Chapter 3, as the concentration of free iodine increases, polymerization becomes slower until it stops eventually, indicated by the characteristic reddish color of I_2. Consequently, the few known literature systems pursue the approach of eliminating free iodine by an educated choice of the initiator, the reaction conditions, or additional reactants. For example, in polymerizations of vinyl acetate (VAc), methyl acrylate, styrene (St) and vinylidene fluoride, the dinuclear manganese complex $Mn_2(CO)_{10}$ served as the initiator.[41,127–129] Upon visible-light irradiation, $^{\bullet}Mn(CO)_5$ is formed, which does not initiate chains itself but abstracts iodine from the CTA R–I to give (re)initiating $R^{\bullet}$. Because of the strong I–Mn bond in $I–Mn(CO)_5$, reactions with R–I as well as with free iodine are expected to be irreversible, leading to consumption of iodine and a system mainly governed by DT. In a second system, Lacroix-Desmazes and co-workers showed that UV polymerization of VAc with a macrophotoiniferter R–I is possible even without the use of an initiator when proceeded in miniemulsion.[42] Accumulation of iodine is prevented by an equilibrium of I_2 solved in the organic and in the aqueous phase. In the aqueous phase, I_2 is converted into I_3^-, shifting the I_2 equilibrium and keeping the I_2 concentration in the organic phase low. In a third system, Goto and co-workers employed amines with a high reducing ability in visible-light-induced polymerizations of methacrylates with R–I[43] and without an initiator as well. Apart from promoting the activation of polymer–I,[130] these amines can either react with iodine to give organic salts[131] or they can undergo complex formation,[132] which drastically lowers the scavenging behavior of I_2.[133] Here, the control of chain growth is mainly attributed to the reversible complexation and contribution of DT is expected to be small. Notably, when the systems of (i) Lacroix-Desmazes et al. and (ii) Goto et al. were employed (i) not in emulsion but in bulk or (ii) without the use of amines, respectively, the results were the same: only very little monomer conversion and an accumulation of free iodine.

Conventional photoinitiator

Surprisingly, iodine-mediated systems with a conventional photoinitiator (initiating chains directly) have not been thoroughly investigated yet, even though a constant generation of $polymer^{\bullet}$ is of course an additional option to keep the concentration of free iodine low. This way, when just enough radicals are produced for the polymerization to proceed, one could even take

advantage of the incessant and ultrafast deactivation (= scavenging) reaction with free iodine. Therefore, in the present chapter, extensive studies on UV-initiated iodine-mediated polymerizations utilizing UV-responsive initiators will be presented. In this context, the application of UV initiators rather than visible-light initiators enables a much simpler handling and higher controllability of the systems, since unintentional polymerization through day- or artificial light can be kept at a low level. It should again be stated that here, the term *iodine-mediated* is used as a general term for a system based on reversible deactivation with iodine. It includes both (i) the common DT mechanism of ITP defined as *iodine transfer*[6] and (ii) the potential activation by photoinduced C−I-bond cleavage and deactivation by the reaction with free iodine, which can be classified as RT mechanism (cf. Scheme 2.3 and 2.4 on pages 13–14). In fact, the coexistence of DT and RT—the two general RDRP mechanisms—leads to special kinetic features of the investigated polymerization systems, which will be demonstrated in the course of this chapter. As it is one of the biggest advantages of photoinitiation, the focus was laid on polymerizations at room temperature. As monomers, BA, BMA, and St were employed as representatives of the three monomer classes of acrylates, methacrylates, and styrenics.

General polymerization conditions

Like for common ITPs, the investigated photosystems generally consisted of (i) monomer, (ii) an iodo CTA, and (iii) the conventional initiator. For selected systems, the impact of established RTCP catalysts on the polymerization behavior was tested as well. Polymerizations were mainly conducted at 22 °C, and UV irradiation was performed by an 8 W Hg-vapor lamp with an optical bandpass filter at a wavelength of $\lambda = 366\,\text{nm}$. A typical polymerization procedure is presented in the Experimental Section 10.4.2 on page 224. The choice of wavelength might be important for application because the investigated polymer classes were shown to be prone to statistical chain scission for irradiation below $\lambda = 320\,\text{nm}$.[134–137] No degradation could indeed be detected via SEC for all three polymer classes when respective toluene solutions were irradiated for several hours under polymerization conditions. Before the polymerization results will be presented, a brief insight into the optical behavior of molecular iodine will be provided.

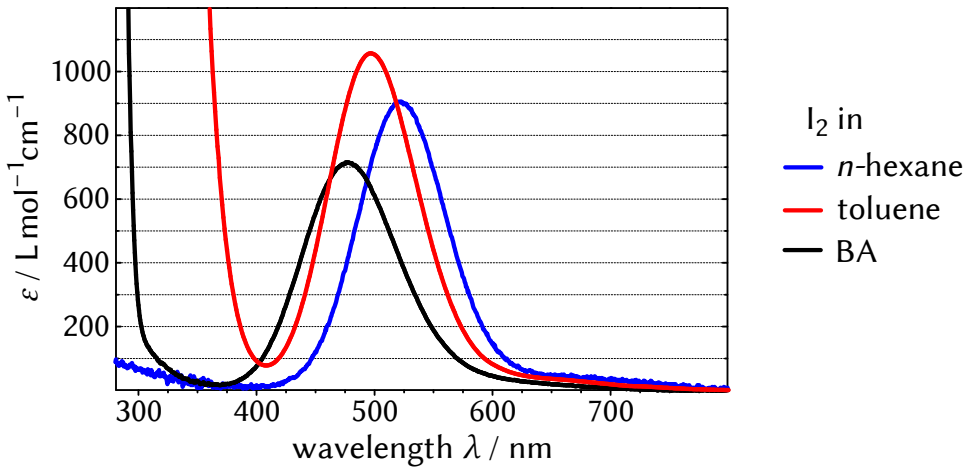

Figure 4.1 UV/vis spectra given as molar extinction coefficients ε of I_2 at room temperature in different solvents as indicated.

4.1 Optical behavior of iodine

Under standard conditions, elemental I_2 is an almost black solid with a metallic sheen. As it undergoes sublimation, the vapor displays its characteristic and indeed name-giving violet color (from Greek ἰοειδής, *ioeidēs,* meaning violet or purple). The color stems from an electronic HOMO–LUMO transition of the I_2 molecule, absorbing light at $\lambda_{max} \approx 520$ nm.[138] A remarkable effect is observed when I_2 is put into solution. In this case, a more or less strong deviation from its optical behavior can be observed, which is the result of a complex-formation between the Lewis-acidic I_2 and the potentially Lewis-basic solvent. With a higher strength of the formed complex, the absorption by I_2 shifts to lower λ. Whereas the genuine I_2-vapor absorption is barely affected by the nondonor solvent *n*-hexane ($\lambda_{max} = 522$ nm), the mentioned blue-shift of the signal can be observed for toluene ($\lambda_{max} = 497$ nm) and BA ($\lambda_{max} = 477$ nm) (see Figure 4.1), leading to less violet and redder solutions. Brownish orange solutions are obtained for even stronger donor solvents. Notably, the fairly high extinction coefficients allow for a convenient quantification of I_2 in solution via UV/vis spectroscopy, which was also exploited in the here presented work. In addition to the shift of the signal around 500 nm, a charge-transfer signal in the region from 230 nm to 400 nm (depending on the energy of the donor orbital) is normally observed.[139]

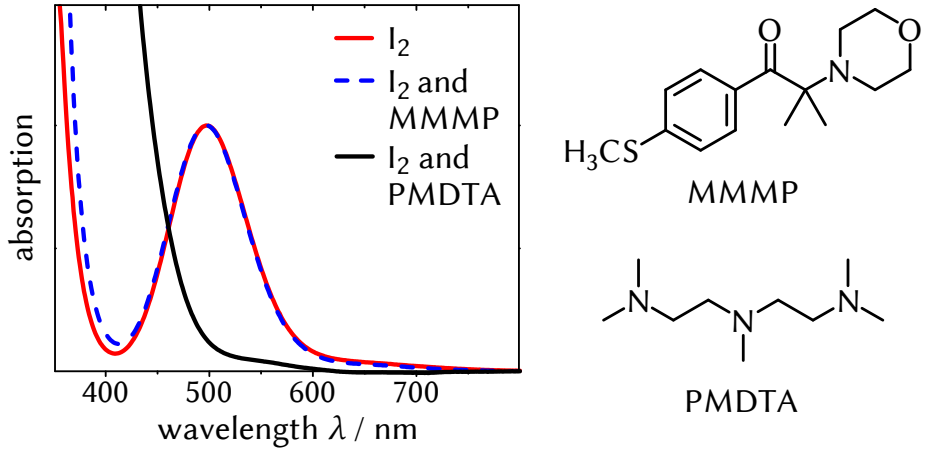

Figure 4.2 UV/vis spectra of toluene solutions of (i) I_2 (1.1 mmol L^{-1}, 1 equiv), (ii) after the addition of MMMP (8 equiv), and (iii) after the addition of PMDTA (8 equiv). In contrast to PMDTA, no alteration of the I_2 signal is observed after the addition of MMMP.

Table 4.1 Initial concentrations of substances used for UV-initiated iodine-mediated polymerization of BA with PE–I in bulk at 22 °C.

entry[a]	$[BA]_0$ / mol L^{-1}	$[PE-I]_0$ / mol L^{-1}	$[MMMP]_0$ / mol L^{-1}
◘	7.0	35×10^{-3}	10×10^{-3}

[a] See Figure 4.3 on page 67.

Although complexation of I_2 and thus the change of its energy states is obvious by Figure 4.1, literature studies showed that this moderately strong complexation has no significant impact on the crucial scavenging reactivity of I_2 toward carbon-centered radicals.[24,25,100] However, as mentioned in the context of the photopolymerization systems by Goto et al., for very strong electron donors such as amines, this might indeed be the case. In this regard, complexation heavily shifts the signal around 500 nm toward much lower λ.[132] An example for this effect will be presented below for *N,N,N′,N′,N″*-pentamethyldiethylenetriamine (PMDTA).

4.2 Polymerizations of *n*-butyl acrylate

4.2.1 Polymerizations with phenylethyl iodide

Photopolymerizations of BA in bulk were conducted at 22 °C using 2-methyl-4′-(methylthio)-2-morpholinopropiophenone (MMMP) as the UV initiator and phenylethyl iodide (PE–I) as the CTA. PE–I was already successfully employed in thermally initiated ITPs of BA in the literature.[58] MMMP has proven to be an excellent UV initiator of RP.[140–142] In addition, in contrast to above-mentioned highly reducing, aliphatic amines such as PMDTA,[132,143] its amino function shows no interaction with I_2 (see Figure 4.2 on the preceding page), which is mainly attributed to its electronic and bulky sterical environment. The solution was irradiated from a distance of 7 cm, which results in an intensity of about 4.5 mW cm^{-2}. The initial concentration of PE–I, $[PE\text{–}I]_0$, was chosen to target a number-average degree of polymerization, $\overline{DP}_n$, of 200 for full monomer conversion, which corresponds to a number-average molar mass, $\overline{M}_n$, of about 25 000 g mol^{-1}. According to the principles of RDRP, theoretical $\overline{M}_n$ values are given by

$$\overline{M}_{n,theo} = \frac{[BA]_0 \cdot M_{BA} \cdot \alpha_{mon}}{[PE\text{–}I]_0} + M_{PE\text{–}I} \,, \tag{4.1}$$

with the molar mass of BA and PE–I, M_{BA} and $M_{PE\text{–}I}$, respectively, the initial concentration of BA, $[BA]_0$, and the fractional monomer conversion, α_{mon}. All applied initial concentrations are given in Table 4.1 on the previous page.

4.2.1.1 Polymerization rate and inhibition

Monomer conversion versus time as well as $\overline{M}_n$ and $Đ$ values versus monomer conversion are given in Figure 4.3 on the facing page. Polymerization started after a short inhibition period of about 10 min and proceeded up to high monomer conversion within additional 30 min. During inhibition, the initially slightly yellow solution (caused by the color of PE–I)[16] turned into a more intense orange, while eventually, it decolorized right before polymerization set in. The change in color in combination with the observed inhibition indicates a temporary formation of I_2. As described in the context of Scheme 4.1 on page 61, after photoinduced homolytic C–I-bond cleavage occurs for PE–I (or polyBA–I), free iodine accumulates in the system.[42] Radicals consuming I_2 are incessantly formed by MMMP, while the formation of I_2 is more pronounced at the beginning and less pronounced toward

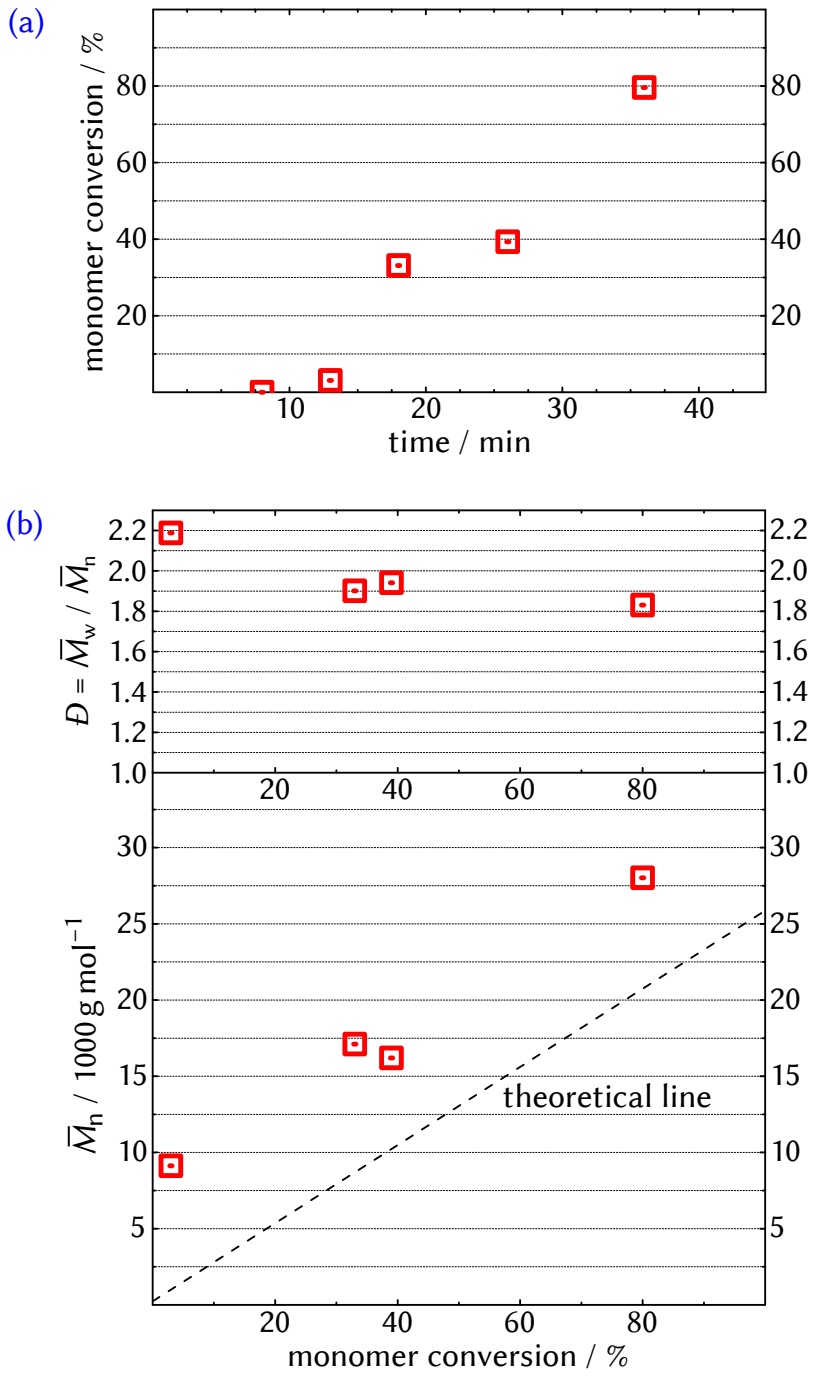

Figure 4.3 (a) Monomer conversion as a function of time and (b) $\overline{M}_n$ and $Đ$ as a function of monomer conversion of the UV-initiated iodine-mediated polymerization of BA with PE–I in bulk at 22 °C given in Table 4.1 on page 65.

the end of the inhibition period. Since PE–I is continuously consumed during inhibition and polyBA–I or iodine-capped fragments of MMMP are continuously formed, this indicates that C–I-bond cleavage is slightly more pronounced for PE–I than for the latter two species. Indeed, computational studies revealed a smaller calculated bond-dissociation energy for the styrene-like PE–I than for a corresponding acrylate-like molecule.[144] When $[\mathrm{MMMP}]_0$ was slightly reduced from $10 \times 10^{-3}\,\mathrm{mol\,L^{-1}}$ to $4 \times 10^{-3}\,\mathrm{mol\,L^{-1}}$ or lower, no monomer conversion could be obtained after several hours, while the reddish color of the solution continuously intensified. This demonstrates the highly competitive character between formation and consumption of I_2 during the early stage of polymerization.

4.2.1.2 Molar masses

$\overline{M}_n$ values increase linearly with an offset at low monomer conversion of about $10\,000\,\mathrm{g\,mol^{-1}}$, corresponding to about 40 % of $\overline{M}_{n,theo}$ for full monomer conversion. According to Equation 2.16 on page 21, this indicates $C_{tr} \approx 2.5$ for PE–I in the here presented BA system. Notably, this might appear as a rather rough estimation, since Equation 2.16 is only valid for ITP systems, i. e., *without* the existence of homolytic C–I-bond cleavage. However, very similar evolution of $\overline{M}_n$ and thus similar C_{tr} was obtained in the literature[58] for thermally initiated ITPs of BA with PE–I at 70 °C *in the absence of light.* In this context, it should be noted that the temperature dependence of molar-mass control and thus $\overline{M}_n$ evolution (i. e., of C_{tr} and C_{ex}) in ITP is expected to be small in this region—for example, C_{ex} for polySt increases from 4.0 at 60 °C to 4.9 at 22 °C.[59] Therefore, when $\overline{M}_n$ evolution of the DT-governed ITP system at 70 °C is similar to the here presented photosystem, the governing RDRP mechanism for the photosystem is expected to be DT as well and the impact of C–I-bond cleavage is hence expected to be minor. In addition, for thermally initiated ITPs of methyl acrylate (MA) at 70 °C, C_{ex} was determined to be 2.2.[24] Assuming that (i) the reactivities of polyMA and polyBA are similar and (ii) temperature dependence of C_{ex} is again small, $C_{ex} \approx 2.2$ can be roughly estimated for the here presented BA system at 22 °C as well.

The obtained $Đ$ values are slightly lower than 2.0 and decrease with increasing monomer conversion. This is expected for an ITP system with C_{tr} and C_{ex} slightly higher than unity (cf. Figure 2.1 on page 20) and further supports the low impact of C–I-bond cleavage for the presented system.

Table 4.2 Na^+-ionized species detected in ESI-MS of a polyBA sample produced via UV-initiated iodine-mediated polymerization with PE–I (Table 4.1 on page 65, $\overline{M}_n$ = 9100 g mol^{-1}, $Đ$ = 2.2, monomer conversion = 3 %) with the theoretical and the experimentally obtained m/z values, $(m/z)_{theo}$ and $(m/z)_{exp}$, respectively, and their relative intensities (rel. int.).

No.	α-end-group [a]	ω-end-group [b]	mon. units [c]	$(m/z)_{theo}$ [d]	$(m/z)_{exp}$ [d]	rel. int. [e] / %
1	PE	iodine	7	1151.6	1151.6	53
2	PE	OH	8	1169.7	1169.7	29
3	PE	PE	7	1129.7	1129.7	6
4	PE	BA^H	7	1153.7	1153.7	5
5	$MMMP^N$	iodine	7	1174.6	1174.6	4
6	$MMMP^S$	iodine	7	1197.5	1197.5	3

[a] $MMMP^N$, $MMMP^S$: MMMP end-groups (see Scheme 4.2); [b] BA^H: saturated BA end-group, OH: after hydrolysis, cf. Scheme 3.5 on page 43; [c] monomeric repeating-units; [d] for m/z = 1150–1278; [e] only the here given species are taken account of, sum = 100 %.

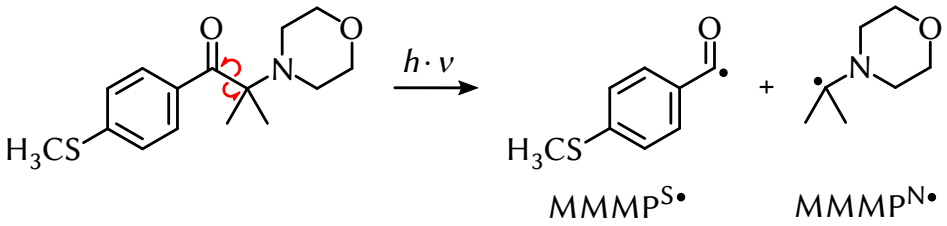

Scheme 4.2 Photochemically induced decomposition of MMMP.

Similar to the analysis of MMDs for the RITP-based systems in Chapter 3 (cf. Section 3.2.2 on page 37), the influence of band-broadening (BB) during SEC analysis on $\overline{M}_n$ was determined to be almost negligible. In this context, the maximum downward deviation of the obtained $\overline{M}_n$ values from the true ones is below 3 %. This also holds true for all following polymer samples with $\overline{M}_n$ < 50 000 g mol^{-1} investigated in the present chapter.

4.2.1.3 End-group analysis

End-group analysis of a polyBA sample of the presented system ($\overline{M}_n$ = 9100 g mol^{-1}, $Đ$ = 2.2, monomer conversion = 3 %) was performed via ESI-

MS. The detected polymeric species are given in Table 4.2 on the previous page within the range of one monomeric repeating-unit (M_{BA} = 128 g mol^{-1}). In accordance with the principles of RDRP, the majority of species was (re)initiated by PE$^{\bullet}$, while 7 % were initiated by fragments of the conventional initiator MMMP (see Scheme 4.2 on the preceding page). About 90 % of the chains are (formerly) living and capped with either iodine or OH (hydrolysis of iodine end-group, for potential transformations of iodine end-groups see Scheme 3.5 on page 43), while the rest is dead polymer produced by either irreversible combination (PE end-group) or hydrogen transfer (saturated BA end-group, BA^{H}).

Both molar-mass and end-group analysis clearly show that UV-initiated iodine-mediated polymerization is successfully performed and applicable for BA. The evolution of both $\overline{M}_n$ and $Đ$ indicates that molar-mass control is mainly governed by DT and that the impact of C–I-bond cleavage is small. Therefore, based on this system, several RTCP catalysts were tested toward their potential to increase iodine transfer, which will be presented in the next section. Indeed, whereas a variety of RTCP systems exist for styrenics and methacrylates, comments on acrylate systems have not been reported so far, which makes studying this system particularly worthwhile.

4.2.2 Polymerizations with phenylethyl iodide and RTCP catalysts

4.2.2.1 Employed catalysts

On the basis of the iodine-mediated system presented in the previous section, the two PADs $(EtO)_2P(O)H$ and $(BuO)_2P(O)H$, as well as NIS, GeI_4, and SnI_4 were tested regarding their impact on molar-mass control as well-established RTCP catalysts (for structural formulas see Figure 10.4 in the Experimental Section on page 220).[26,27] In this context, the addition of either GeI_4 or SnI_4 to the system of BA, MMMP, and PE–I led to a rapid precipitation of a white solid, which could be identified as the ammonium salt [MMMP–H]$^+$I$^-$ via crystallographic analysis (for crystal structure see Appendix A.1.1 on page 229). It was indeed shown in literature studies that the Lewis-acidic SnI_4 can undergo strong complexation with aliphatic amines under formation of hydrogen iodide, which can then protonate the amine under formation of the corresponding ammonium salt.[145,146] No polymerizations with GeI_4 or SnI_4 were therefore conducted in combination with MMMP. However, GeI_4

Table 4.3 Initial concentrations of substances used for UV-initiated iodine-mediated polymerizations of BA with PE–I in bulk at 22 °C with and without RTCP catalysts (cat.).

entry [a]	$[BA]_0$ / mol L^{-1}	$[PE-I]_0$ / mol L^{-1}	$[MMMP]_0$ / mol L^{-1}	$[cat.]_0$ / mol L^{-1}	cat.
1 (□) [b]	7.0	35×10^{-3}	10×10^{-3}	–	–
2 (◇)	7.0	35×10^{-3}	10×10^{-3}	30×10^{-3}	$(EtO)_2P(O)H$
3 (○)	7.0	35×10^{-3}	10×10^{-3}	30×10^{-3}	$(BuO)_2P(O)H$
4 (△)	7.0	35×10^{-3}	100×10^{-3}	4×10^{-3}	NIS

[a] See Figure 4.4 on the following page; [b] catalyst-free system discussed in the previous section.

and SnI_4 systems were investigated with a different UV initiator and will be presented at a later stage.

4.2.2.2 Polymerization results

The initial concentrations of the applied substances for the system without and the systems with catalysts are given in Table 4.3. Common catalyst concentrations were chosen according to literature systems.

Polymerization rate and inhibition

Monomer conversion versus time as well as $\overline{M}_n$ and $Đ$ values versus monomer conversion are given in Figure 4.4 on the following page. Distinctly different inhibition periods can be observed for the respective systems. The causes are expected to be similar to the RITP systems in Chapter 3 (Figure 3.2 on page 34). No inhibition or coloring is observed in case of the PADs, which is ascribed to their reactivity toward iodine (Scheme 3.3 on page 36), nipping formation of I_2 in the bud. The extent of this reaction is expected to be small, as it also generates hydrogen iodine, whereas no significant precipitation of $[MMMP-H]^+I^-$ could be observed. In contrast to the PAD systems, the rather long inhibition for NIS accompanied by a reddish coloring of the solution is ascribed to photoinduced N–I-bond cleavage and formation of free iodine. It should be noted that for the NIS system, $[MMMP]_0 = 100$ mmol L^{-1}, which is ten times higher than for the other systems; for $[MMMP]_0 = 10$ mmol L^{-1}, no monomer conversion was observed

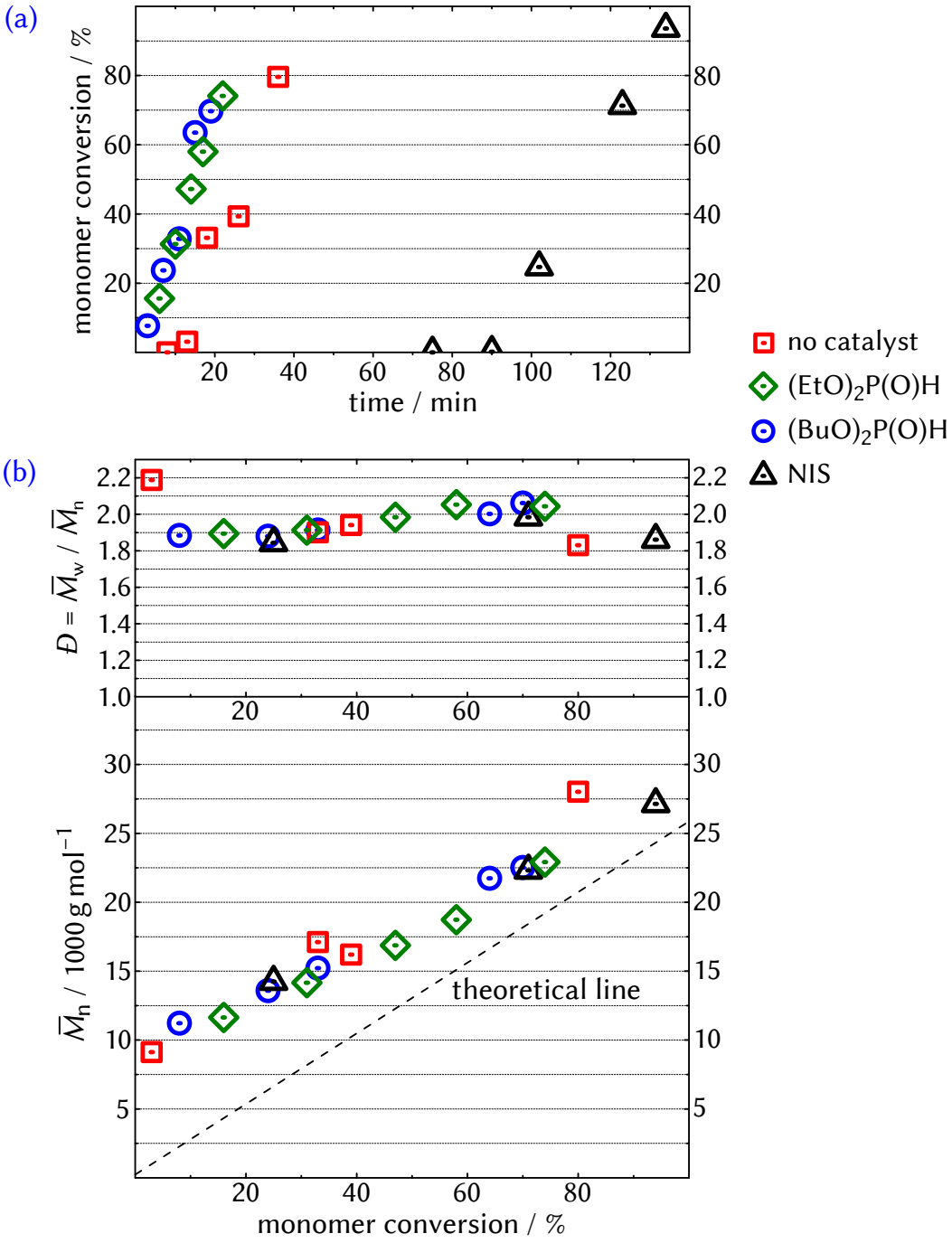

Figure 4.4 (a) Monomer conversion as a function of time and (b) $\overline{M}_n$ and $Đ$ as a function of monomer conversion of the UV-initiated iodine-mediated polymerizations of BA with PE–I in bulk at 22 °C with and without RTCP catalysts given in Table 4.3 on the previous page.

after several hours, while the reddish color of the solution continuously intensified.

Molar masses

For all catalysts, evolution of both $\overline{M}_n$ and $Đ$ values is remarkably congruent with the catalyst-free system. This indicates rather unambiguously that although the catalysts affect the inhibition behavior of the polymerization, the potential iodine transfer of the catalysts is not fast enough to have a significant impact on molar-mass control for the applied conditions. Despite (i) UV irradiation and (ii) the addition of catalysts, DT is therefore expected to still be the dominant activation–deactivation mechanism.

As mentioned above, the fairly high $\overline{M}_n$ values for low monomer conversion in combination with high $Đ$ values indicate only moderately fast (re)initiation by PE–I. In order to enhance (re)initiation and potentially increase molar-mass control, the more active cyanopropyl iodide (CP–I, cf. Scheme 2.7 on page 18) was applied in place of PE–I. As described in the context of RITP in Chapter 3, because of its weak C–I bond, CP–I is rather unstable and tends to decompose upon synthesis, isolation, or storage. Therefore, a semi-in-situ approach was followed to employ CP–I in a convenient way with only little experimental effort, which will be presented in the following.

4.2.3 Preparation of cyanopropyl iodide

The preparation of CP–I for the application in UV-initiated polymerizations was mainly inspired by (i) the synthesis of CP–I from I_2 and AIBN in benzene by Bałczewski and Mikołajczyk[147] and (ii) the in-situ generation of CP–I within the concept of RITP.[24] In this regard, CP–I was prepared from a solution of I_2 and AIBN in toluene heated to 100 °C (for details on the reaction procedure see Experimental Section 10.1.3.1 on page 218). In contrast to RITP, the formation of CP–I did not take place in the presence of monomer. That way, after CP–I was formed, it could be conveniently added to the monomer solution.

For a successful application of this technique, it is essential that (i) I_2 is completely consumed leading to (ii) the desired amount of CP–I with $[\text{CP–I}] = 2 \times [I_2]_0$ at the end of the reaction. The reaction occurs with a characteristic decoloration of the initially dark red solution. In Figure 4.5 on the next page, UV/vis spectra of the (diluted) reaction mixtures heated for

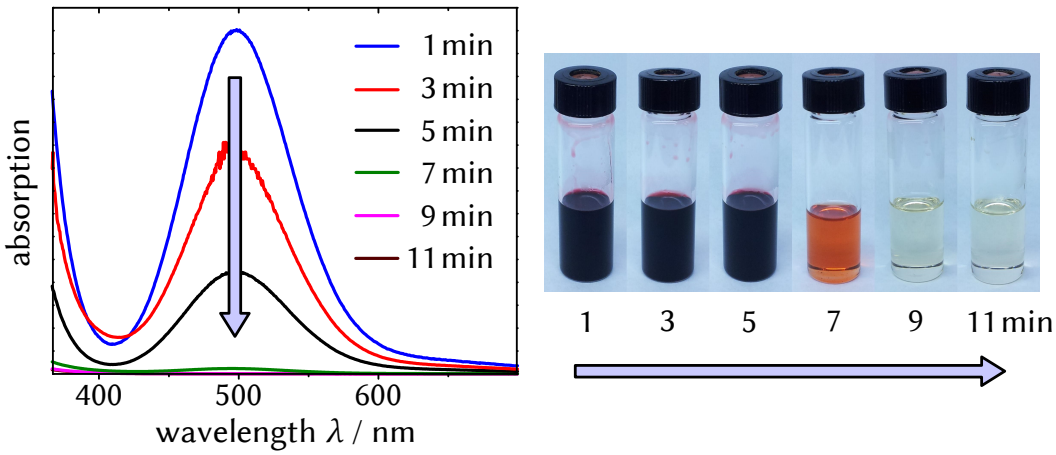

Figure 4.5 UV/vis spectra and photographs after indicated periods of time of the reaction of I_2 and AIBN in toluene at 100 °C yielding CP–I.

different periods of time as well as photographs of the respective mixtures are presented. For the here used $[I_2]_0$ and $[AIBN]_0$, the signal of I_2 (and the coloration) completely disappears after 9 min. (The strong coloration behavior of I_2 is indeed clarified by the sample at $t = 7$ min, for which $[I_2]$ is only about 1 mmol L^{-1}, while the solution is still intensely colored.) The formation of CP–I was investigated via ^{1}H-NMR spectroscopy. The relatively high concentrations (high ratio between [CP–I] and [toluene]) allowed for a comparison of the increasing signal of the six equivalent protons of CP–I at $\delta_{CP-I} \approx 2.1$ ppm with the signal of the methyl group of the *nondeuterated* toluene at $\delta_{Ph-CH_3} \approx 2.4$ ppm. CP–I formation as a function of time as well as an exemplary ^{1}H-NMR spectrum are given in Figure 4.6 on the facing page. Whereas the method potentially suffers from uncertainties for low [CP–I], the results correlate well with the UV/vis-spectroscopic results at longer reaction times, indicating full conversion of I_2 to CP–I, which is also described by Bałczewski and Mikołajczyk.[147] By knowing the concentration of CP–I in the toluene solution, the amount of solution was known to apply the desired $[CP-I]_0$ for polymerization.

By this technique, CP–I was not only employed in polymerizations of BA but also in polymerizations of BMA and St, which will be presented later. Although CP–I forms rather quickly, the reaction was generally proceeded for 60 min, during which no depletion of the formed CP–I could be detected via ^{1}H-NMR and UV/vis spectroscopy. This way, complete decomposition of AIBN was ensured, leaving over mainly CP–I and the inert byproduct

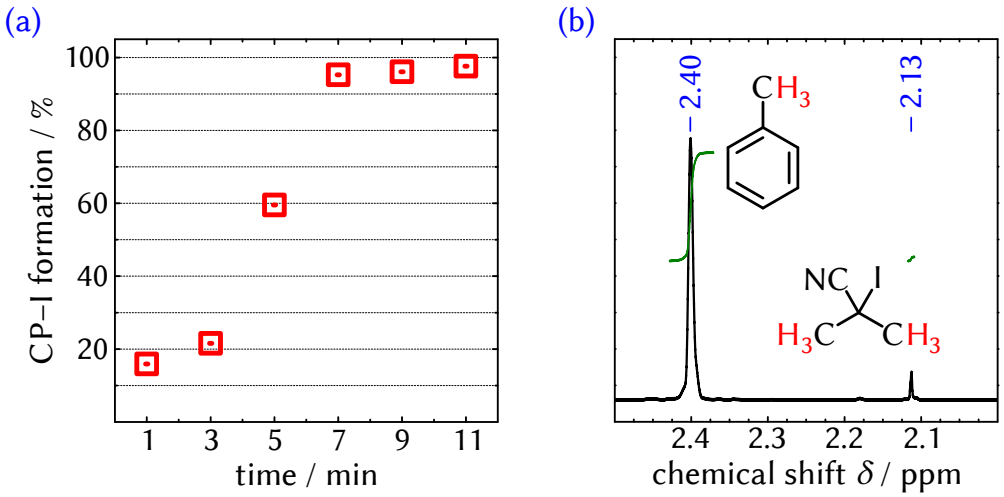

Figure 4.6 (a) CP–I formation (from I_2) versus time of the samples presented in Figure 4.5 on the facing page determined from ^{1}H-NMR signals of the solvent toluene and of CP–I. (b) Exemplary ^{1}H-NMR signals (in $CDCl_3$ at room temperature) of toluene and CP–I for t = 11 min.

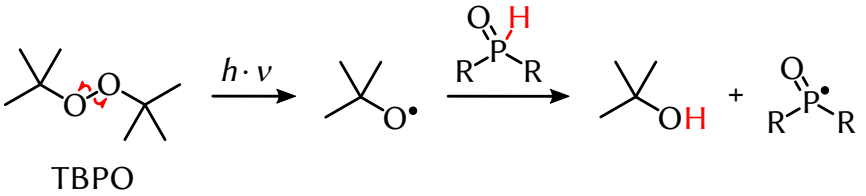

Scheme 4.3 Photochemically induced decomposition of TBPO and subsequent abstraction of a hydrogen atom from a PAD.[148]

CP–CP. However, for some applications, it might be beneficial to stop the reaction at an earlier time and to use the remaining AIBN as an additional source of radical formation, which will be presented at a later stage.

4.2.4 Polymerizations with cyanopropyl iodide

In the following, UV-initiated polymerizations of BA with CP–I will be described. In contrast to the polymerizations with PE–I, di-*tert*-butyl peroxide (TBPO) was used as the UV initiator instead of MMMP. TBPO was chosen with regard to a potential application of RTCP catalysts for this system, which will be presented at a later stage. Unlike MMMP, TBPO shows no reactivity toward GeI_4 and SnI_4. In addition, initiators giving oxygen-

Table 4.4 Initial concentrations of substances used for UV-initiated iodine-mediated polymerizations of BA with CP–I in toluene at 22 °C.

entry [a]	$[BA]_0$ / mol L^{-1}	$[CP–I]_0$ / mol L^{-1}	$[TBPO]_0$ / mol L^{-1}
1 [b]	5.6	28×10^{-3}	0.32
2 (□)	1.8	9×10^{-3}	0.32
3 (○)	1.8	9×10^{-3}	1.5
4 (△, ◇)	1.8	9×10^{-3}	0.32 [c]

[a] See Figure 4.7 on the next page; [b] no monomer conversion observed after several hours; [c] with 3×10^{-3} mol L^{-1} of AIBN from the CP–I solution.

centered fragments are frequently used in RTCPs with PADs,[26,27,83] since they readily abstract the hydrogen atom of the P–H bond, promoting the in-situ generation of the activating radical of the catalysts (see Scheme 4.3 on the previous page).[148,149] This behavior is especially pronounced for TBPO[148] and could be confirmed for the later employed PAD $(BuO)_2P(O)H$ by means of electron-paramagnetic-resonance (EPR) spectroscopy. By irradiating a mixture of TBPO and $(BuO)_2P(O)H$, the phosphorous-centered radical with a characteristic coupling constant $a_P = 695$ G[150] was detected (see Appendix A.1.2 on page 230), which was not the case for irradiation without TBPO.

Similar to the PE–I systems, $[CP–I]_0$ was chosen to target $\overline{DP}_n$ values of 200 for full monomer conversion. As TBPO is less active than MMMP at the irradiated wavelength, higher $[TBPO]_0$ were used while the distance of the UV lamp to the sample was reduced from 7 cm to 1 cm (corresponding to an intensity increase from about 4.5 mW cm^{-2} to 220 mW cm^{-2}). The development of an effective polymerization system with CP–I and TBPO required some fine tuning, which will be described in the following.

4.2.4.1 Monomer and initiator concentration

Polymerization rate and inhibition

In contrast to the PE–I systems, polymerizations of BA with CP–I and TBPO were not feasible in bulk. Exemplarily, for $[TBPO]_0 = 0.32$ mol L^{-1} (Table 4.4, entry 1), incessant formation of I_2 and no monomer conversion could be obtained after several hours. Here, the amount of the liquid TBPO and especially the amount of toluene from the CP–I solution leads to $[BA]_0 = 5.6$ mol L^{-1} in contrast to 7.0 mol L^{-1} in the case of PE–I. To

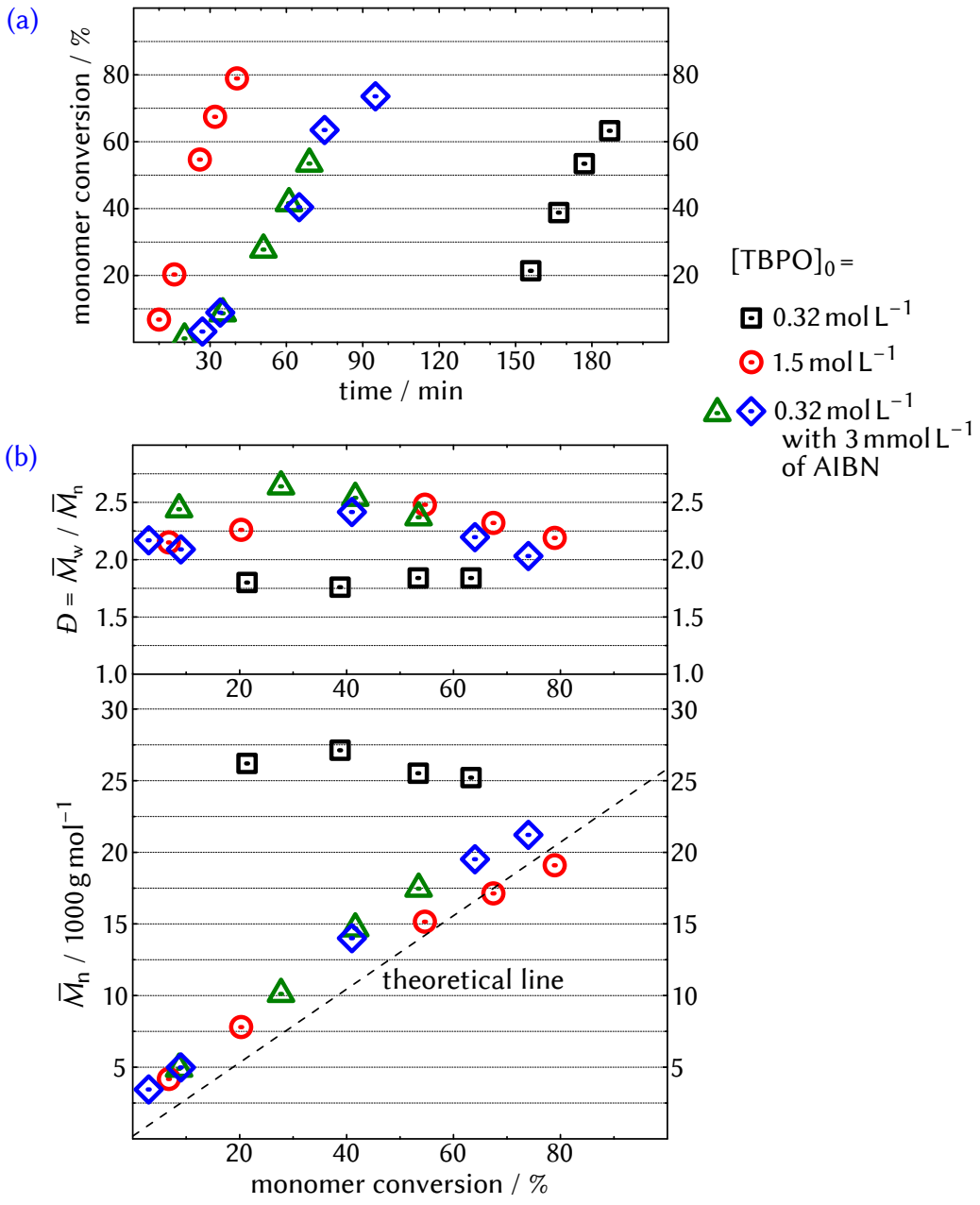

Figure 4.7 (a) Monomer conversion as a function of time and (b) $\overline{M}_n$ and $Đ$ as a function of monomer conversion of the UV-initiated iodine-mediated polymerizations of BA with CP–I in toluene at 22 °C given in Table 4.4 on the preceding page.

lower the potential amount of scavenging free iodine, $[CP{-}I]_0$ was reduced by increasing the amount of toluene, leading to solution polymerizations with $[BA]_0 = (200 \times [CP{-}I]_0 =) 1.8\,mol\,L^{-1}$ (entry 2). The resulting values of monomer conversion versus time are presented in Figure 4.7a on the previous page. The effect of free iodine is indeed reduced and polymerization occurs, however, inhibition is rather long and lasts about 2.5 h. To shorten inhibition, higher $[TBPO]_0$ can be used. In fact, for a five-fold $[TBPO]_0 = 1.5\,mol\,L^{-1}$, (entry 3), inhibition is very short and polymerization starts after about 10 min.

Support for TBPO

Although short inhibition is obtained, the rather high amount of TBPO might be a downside for some applications. In fact, when $[TBPO]_0 = 1.5\,mol\,L^{-1}$, TBPO constitutes no less than 30 % of the volume of the polymerization mixture. To allow for lower $[TBPO]_0$, the approach was followed to support radical formation by utilizing an additional initiator. In this regard, advantage was taken from the preparation procedure of CP–I described in Section 4.2.3 on page 73. As stated, the reaction was generally run for 60 min to achieve full decomposition of AIBN. Since AIBN does not only decompose upon heat but also upon UV irradiation, the approach was to stop the reaction earlier to benefit from the remaining AIBN in the CP–I solution as an additional source of radicals. The reaction was stopped after 15 min by a rapid temperature drop, leaving about 20 % of the initial amount of AIBN, which corresponds to $[AIBN]_0$ of about $3 \times 10^{-3}\,mol\,L^{-1}$ in the polymerization mixture. This simple method led to an effective support for TBPO and much shorter inhibition compared to the AIBN-free system with $[TBPO]_0 = 0.32\,mol\,L^{-1}$, as shown for two independently conducted polymerizations in Figure 4.7a (entry 4 in Table 4.4). The apparent high reproducibility of the method was additionally evident from numerous other polymerizations, some of which will be discussed in the further course of this chapter. For systems without TBPO and just AIBN, continuous formation of I_2 and no polymerization was obtained after several hours, so that TBPO can indeed be regarded as the main driving force of the polymerization.

Molar masses

$\overline{M}_n$ and $Đ$ values as a function of time for the discussed systems are presented in Figure 4.7b. Two fundamentally different behaviors of molar-mass

Table 4.5 NH_4^+-ionized species detected in ESI-MS of a polyBA sample produced via UV-initiated iodine-mediated polymerization with CP–I (Table 4.4 on page 76, entry 4, $\overline{M}_n$ = 3400 g mol^{-1}, $Đ$ = 2.1, monomer conversion = 9 %) with the theoretical and the experimentally obtained m/z values, $(m/z)_{theo}$ and $(m/z)_{exp}$, respectively, and their relative intensities (rel. int.).

No.	α-end-group [a]	ω-end-group [b]	mon. units [c]	$(m/z)_{theo}$ [d]	$(m/z)_{exp}$ [d]	rel. int. [e] / %
1	CP	iodine	5	853.4	853.4	93
2	CP	OH	6	871.6	871.6	< 1
3	CP	CP	6	922.6	922.6	1
4	CP	$BA^{=}$	5	853.6	853.6	1
5	CP	BA^{H}	5	855.6	855.6	2
6	*t*BuO	iodine	5	858.4	858.4	1
7	Bn	iodine	5	876.4	876.4	2

[a] *t*BuO, Bn: See Scheme 4.4 on the following page; [b] transformations of iodine end-groups are given in Scheme 3.5 on page 43; [c] monomeric repeating-units; [d] for m/z = 830–958; [e] only the here given species are taken account of, sum = 100 %.

evolution can be observed, which seem to mainly depend on the duration of inhibition. For the long-inhibition system, $\overline{M}_n$ is high from an early state of polymerization, indicating rather slow (re)initiation. For all short-inhibition systems, $\overline{M}_n$ values are close to $\overline{M}_{n,theo}$ throughout polymerization. They are also lower than for the PE–I system (cf. Figure 4.3 on page 67), especially at low monomer conversion. This illustrates the desired faster (re)initiation by CP–I for short inhibition, which is adversely affected when inhibition is long, which will be further clarified at a later stage in this chapter.

$Đ$ values seem to be slightly contradictory to the discussed $\overline{M}_n$ evolution. While $Đ \approx 1.8$ for slow (re)initiation, higher values are generally observed for the systems with fast (re)initiation. Thus, whereas molar-mass control is clearly higher in the latter systems and $\overline{M}_n$ values close to $\overline{M}_{n,theo}$ are obtained throughout polymerization, $Đ$ values indicate a less uniform chain growth. This discrepancy will also be thoroughly discussed at a later stage.

4.2.4.2 End-group analysis

End-group analysis of a polyBA sample of the system with short inhibition and $[TBPO]_0$ = 0.32 mol L^{-1} (Table 4.4 on page 76, entry 4, $\overline{M}_n$ =

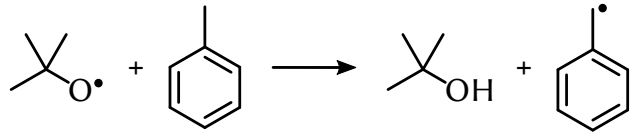

*t*BuO• Bn•

Scheme 4.4 Two initiating species: the *tert*-butoxy radical, *t*BuO• (fragment of TBPO), and the benzyl radical, Bn•, after hydrogen-atom abstraction from the solvent toluene by *t*BuO•.

3400 g mol^{-1}, $Đ$ = 2.1, monomer conversion = 9 %) was performed via ESI-MS. The detected polymeric species are given in Table 4.5 on the previous page. According to RDRP, most of the species are (re)initiated by CP•. Chains conventionally initiated by the *tert*-butoxy radical, *t*BuO• (TBPO fragment) and by the benzyl radical, Bn•, are minor. In this context, Bn• is formed via hydrogen-atom abstraction from the solvent toluene by *t*BuO• (see Scheme 4.4). The amount of dead chains by either irreversible combination (CP) or transfer (BA^{H}) is small and in total, about 97 % of the chains have (or formerly had) an iodine end-group. This clarifies the very high end-group functionality for the presented system.

4.2.4.3 Intermittent irradiation

To illustrate the sensitivity toward UV irradiation, the system was irradiated intermittently with alternating periods of irradiation (15 min) and no irradiation (dark periods, 10 min) after an initial irradiation period of 50 min. Figure 4.8a on the next page shows the evolution of monomer conversion in comparison to continuous irradiation. No polymerization is observed during the dark periods, and polymerization rates are very similar to the continuous system during periods of irradiation. The obtained SEC traces in Figure 4.8b show MMDs before and after the respective dark periods, during which no shift or change in any way is observed. The evolution of $\overline{M}_n$ and $Đ$ in Figure 4.9 on page 82 reveals almost no difference to the continuous system. This makes clear that the system is explicitly dormant with no active sites during the dark periods, while after the dark periods, chain-extended polymer is again formed. This illustrates the high potential as a photoswitchable "on–off" system.

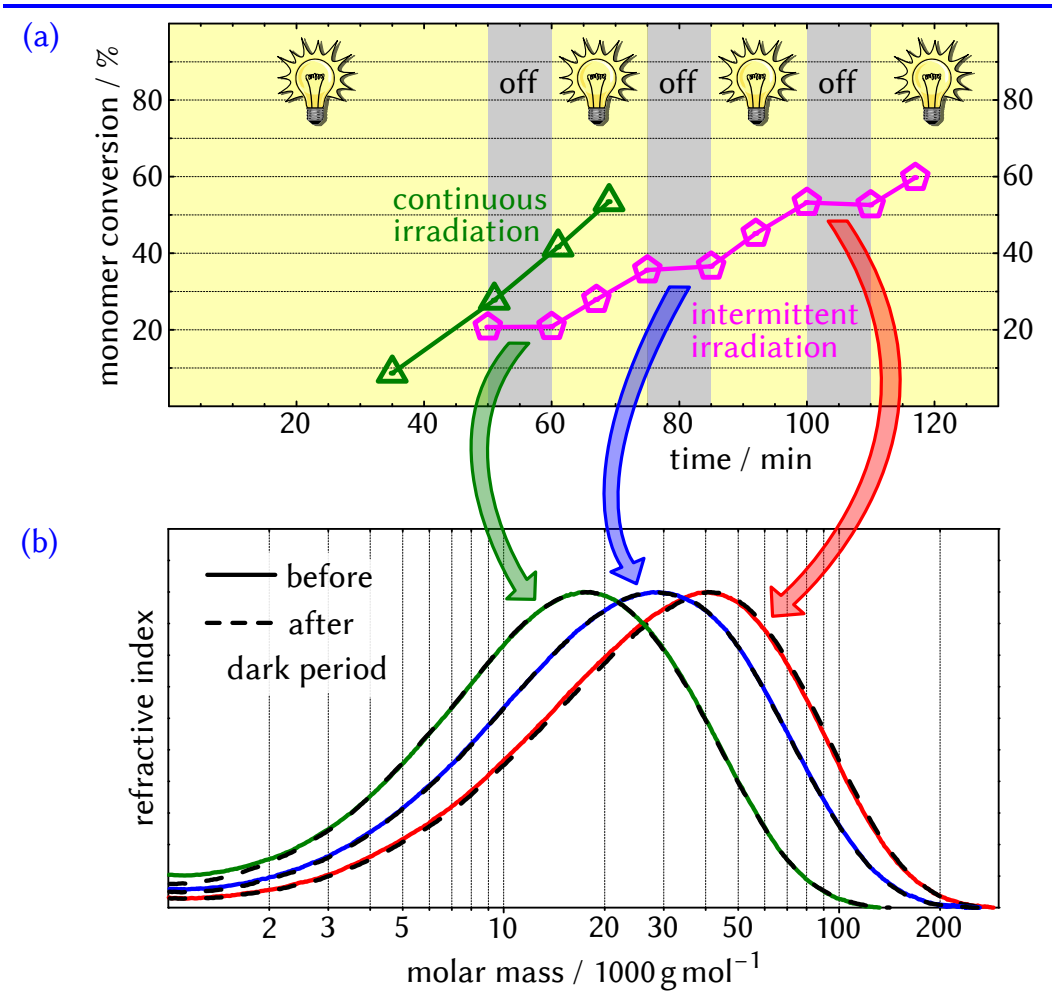

Figure 4.8 (a) Monomer conversion as a function of time of the UV-initiated iodine-mediated polymerization of BA with CP–I in toluene at 22 °C presented in Table 4.4 on page 76 (entry 4) for continuous and intermittent irradiation and (b) MMDs (SEC traces, all normalized to the same maximum intensity) of polymer samples taken before and after the respective periods of no irradiation (dark periods).

4.2.5 Impact of inhibition in polymerizations with cyanopropyl iodide

As presented in Figure 4.7 on page 77, the duration of inhibition has a significant impact on the evolution of $\overline{M}_n$ values. While in case of *short* inhibition, (re)initiation by CP–I is fast, in case of *long* inhibition, (re)initiation is much slower. From a mechanistic point of view, one of the major effects during

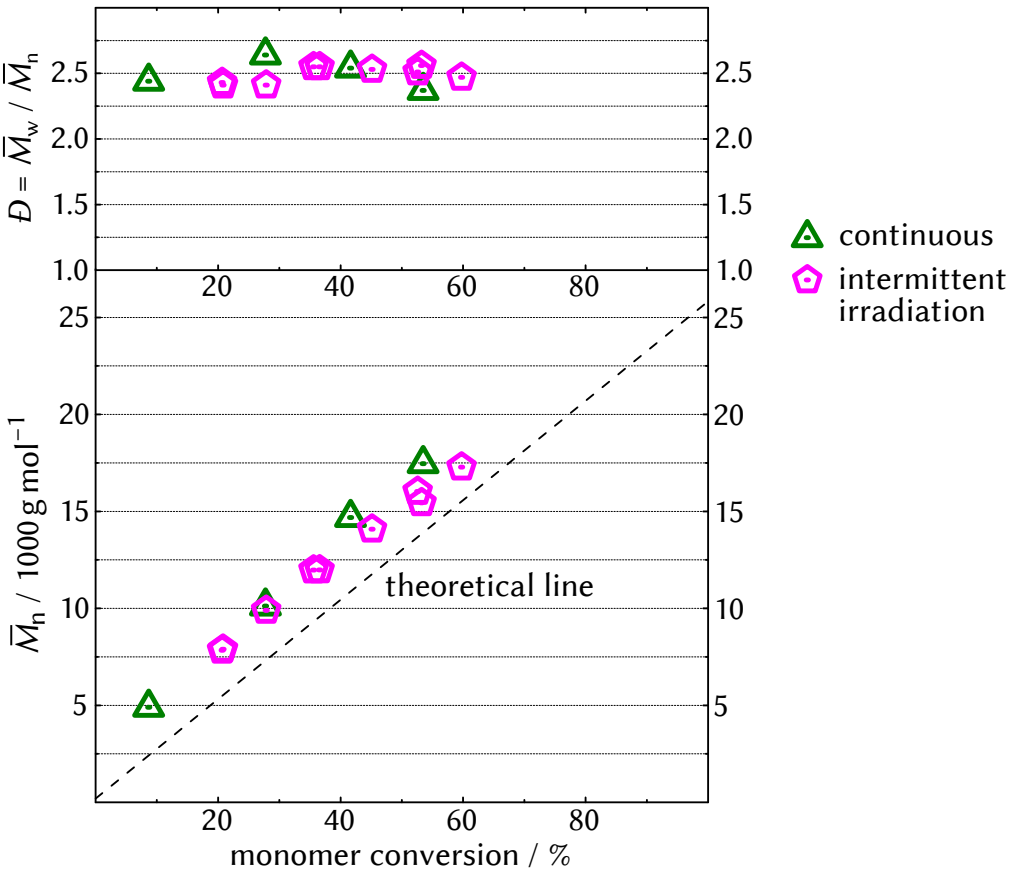

Figure 4.9 $\overline{M}_n$ and $Đ$ as a function of monomer conversion of the UV-initiated iodine-mediated polymerizations of BA with CP–I in toluene at 22 °C for continuous and intermittent irradiation presented in Figure 4.8 on the preceding page.

inhibition is the continuous decomposition of CP–I and formation of I_2. Therefore, as a rather straightforward interpretation, it is expected that for longer inhibition, less CP–I is present at the time inhibition is over and polymerization sets in.

Model polymerization

This effect was investigated by means of a model system, in which full decomposition of CP–I was simulated. For this, a polymerization was conducted under the common conditions, but directly employing I_2 rather than CP–I. The initial concentrations of the substances are given in Table 4.6 on page 84. In this context, $[I_2]_0$ equals $1/2 \times [CP–I]_0$ of the CP–I systems, while

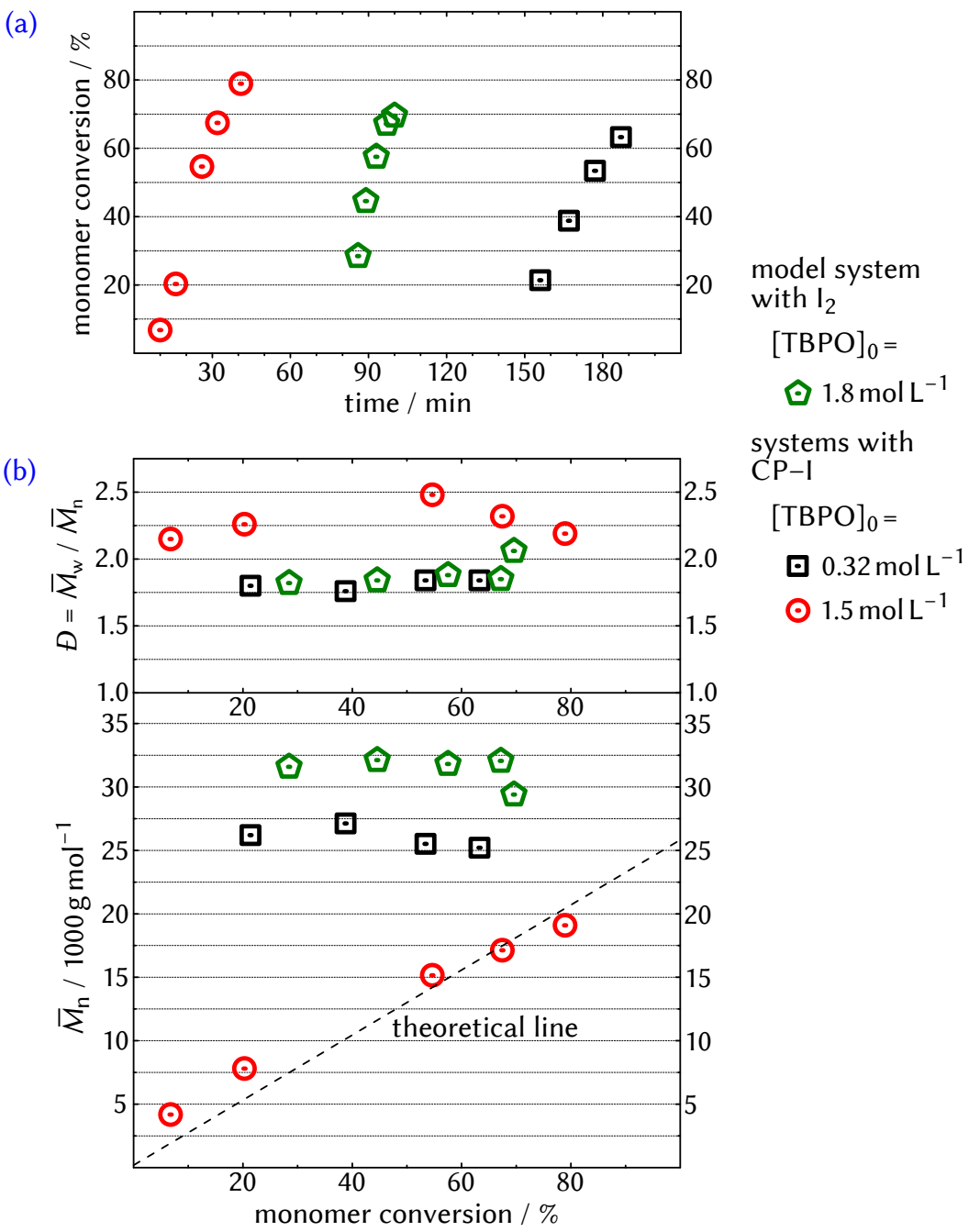

Figure 4.10 (a) Monomer conversion as a function of time and (b) $\overline{M}_n$ and $Đ$ as a function of monomer conversion of UV-initiated iodine-mediated polymerizations of BA in toluene at 22 °C: model system with I_2 (Table 4.6 on the next page) and regular systems with CP–I with short (Table 4.4 on page 76, entry 3) or long inhibition (entry 2).

Table 4.6 Initial concentrations of substances used to simulate full decomposition of CP–I in a UV-initiated iodine-mediated polymerization of BA in toluene at 22 °C.

entry [a]	$[BA]_0$ / mol L^{-1}	$[I_2]_0$ / mol L^{-1}	$[TBPO]_0$ / mol L^{-1}
⬠	1.8	4.5×10^{-3}	1.8

[a] See Figure 4.10 on the preceding page.

Table 4.7 NH_4^+-ionized species detected in ESI-MS of a polyBA sample obtained from the model system simulating full decomposition of CP–I (Table 4.6, $\overline{M}_n$ = 32 000 g mol^{-1}, $Đ$ = 1.82, monomer conversion = 28 %) with the theoretical and the experimentally obtained m/z values, $(m/z)_{theo}$ and $(m/z)_{exp}$, respectively, and their relative intensities (rel. int.).

No.	α-end-group [a]	ω-end-group [b]	mon. units [c]	$(m/z)_{theo}$ [d]	$(m/z)_{exp}$ [d]	rel. int. [e] / %
1	Bn	iodine	4	748.3	748.3	23
2	Bn	OH	5	766.5	766.5	9
3	Bn	BA$^=$	4	748.5	748.5	16
4	Bn	BA^H	4	750.5	750.5	19
5	Bn	Bn	4	712.5	712.5	28
6	Bn	*t*BuO	5	822.6	822.6	2
7	*t*BuO	iodine	4	730.3	730.3	1
8	*t*BuO	BA$^=$	4	730.5	730.5	1
9	*t*BuO	BA^H	4	732.5	732.5	1

[a] *t*BuO, Bn: See Scheme 4.4 on page 80; [b] transformations of iodine end-groups are given in Scheme 3.5 on page 43; [c] monomeric repeating-units; [d] for m/z = 700–828; [e] only the here given species are taken account of, sum = 100 %.

high $[TBPO]_0$ is needed so as to achieve reasonably low inhibition times. Monomer conversion versus time as well as $\overline{M}_n$ and $Đ$ versus monomer conversion are presented in Figure 4.10 on the preceding page in comparison to the CP–I systems for long and short inhibition, respectively. Indeed, molar-mass evolution of the model system shows strong resemblance to the CP–I system with long inhibition: while $Đ$ values are mainly about 1.8, $\overline{M}_n$ values are constantly high throughout polymerization. This supports that the major effect of long inhibition is indeed decomposition of CP–I and formation of I_2.

End-group analysis via ESI-MS was conducted for a polyBA sample of the model system ($\overline{M}_n$ = 32 000 g mol^{-1}, $Đ$ = 1.82, monomer conversion = 28 %). The detected polymeric species are given in Table 4.7 on the preceding page. As the most striking result, the majority of species is (re)initiated by Bn$^\bullet$. In the context of iodine-mediated polymerization, this indicates the formation of Bn–I during the inhibition period, which then constitutes the iodo CTA at the beginning of the polymerization. As presented in Scheme 4.4 on page 80, Bn$^\bullet$ is generated from the reaction of *t*BuO$^\bullet$ with the solvent toluene. When Bn$^\bullet$ subsequently reacts with I_2, it generates the rather stable Bn–I. In accordance with the fact that Bn–I is expected to be a much less active CTA for iodine-mediated polymerization compared to PE–I or CP–I (primary C–I bond versus secondary or tertiary C–I bond), (re)initiation is slow and $\overline{M}_n$ values are high from the very beginning. In this context, the evolution of $\overline{M}_n$ indicates $C_{tr} < 1$ for Bn–I (cf. Figure 2.1 on page 20). As an additional consequence of slow (re)initiation, a high percentage of dead polymer is detected via ESI-MS.

Slightly lower $\overline{M}_n$ values of the long-inhibition system with CP–I in comparison to the model system indicate that a small amount of CP–I survives decomposition during inhibition and takes part in (re)initiation. In this context, it should also be noted that the reaction of Bn$^\bullet$ with CP–I to give Bn–I and CP$^\bullet$ is expected to be fast (iodine transfer from tertiary to primary carbon atom). Part of the depletion of CP–I and generation of Bn–I might thus also take place without the detour over I_2 formation. As a general comment, the presented results clarify that in order to obtain good control of chain growth along with high end-group functionality for polyBA by CP–I, it is essential to keep inhibition short.

4.2.6 Fast (re)initiation and high dispersities: kinetic simulations

While short inhibition and fast (re)initiation by CP–I leads to a high control of $\overline{M}_n$, the obtained high $Đ$ values seem rather counterintuitive. This especially applies when the results for long inhibition are factored in, which show significantly lower $Đ$ values although slow (re)initiation is observed. In order to shine light on this effect and to get a deeper insight into the kinetics of the presented systems, kinetic simulations were conducted, which will be presented in the following.

In slight anticipation, the discussed effect indeed strongly depends on the (re)initiating behavior of the CTA. In addition, it is particularly significant

for polymerizations with a rather low activation–deactivation frequency of living chains during the main equilibrium, which is normally the case for iodine-mediated polymerizations. Before the simulation results will be presented, a concise description of the used simulation model will be given in the following.

4.2.6.1 Details of kinetic simulations

Kinetic simulations were performed by using the program package Predici©.[151–153] For details on a general simulation procedure see Experimental Section 10.3 on page 224. The investigated iodine-mediated polymerization systems of BA at 22 °C served as a basis for the here presented simulation model (e. g., substances, initial concentrations, reaction rate coefficients). In this context, the impact of the variation of crucial rate coefficients on the outcome of polymerization will be presented by means of the resulting simulated MMDs.

Simulation model

Before the simulation model will be presented, it should be stated that two reactions were not considered although they are expected to occur under to here given conditions, namely (i) intramolecular chain transfer to polymer (so-called *backbiting*)[154] and (ii) homolytic C–I-bond cleavage. Both reactions were omitted in order to keep the simulation model simple and to emphasize the general relevance of the obtained results for systems based on DT. This will be clarified in the course of the present section.

The implemented reactions and the respective rate coefficients are presented in Scheme 4.5 on the next page and Table 4.8 on page 88. Scheme 4.5a shows the conventional RP mechanism, including (Reaction I) the decomposition of the initiator (with the rate coefficient k_{dec}), (II) the initiation of chain growth (k_{ini}), the (III) subsequent propagation (k_p), and (IV) the eventual irreversible termination reaction (k_t). The k_p value is taken from the literature[157] while the frequently used assumption $k_{ini} = 10 \times k_p$ is motivated by studies into chain-length dependencies of k_p in the oligomeric chain-length regimes[155] and by experimental and theoretical studies into small-radical chemistry.[156] For k_t, chain-length-dependent values with two different chain-length regimes[159] are taken from the literature.[158] The k_{dec} value was chosen to roughly match the experimentally obtained poly-

(a) conventional radical polymerization

radical formation & initiation

(I) $\mathrm{TBPO} \xrightarrow{k_{dec}} \mathrm{In}^{\bullet} + \mathrm{In}^{\bullet}$

(II) $\mathrm{In}^{\bullet} + \mathrm{BA} \xrightarrow{k_{ini}} \mathrm{polyBA}^{\bullet}(1)$

propagation

(III) $\mathrm{polyBA}^{\bullet}(i) + \mathrm{BA} \xrightarrow{k_p} \mathrm{polyBA}^{\bullet}(i+1)$

irreversible termination

(IV) $\mathrm{polyBA}^{\bullet}(i) + \mathrm{polyBA}^{\bullet}(j) \xrightarrow[= k_t(i,i);\ i \approx j]{k_t} \mathrm{polyBA}_{dead}(i+j)$

(b) iodine-transfer polymerization

pre-equilibrium degenerative chain-transfer

(V) $\mathrm{polyBA}^{\bullet}(i) + \mathrm{R{-}I} \xrightarrow{k_{tr}} \mathrm{polyBA{-}I}(i) + \mathrm{R}^{\bullet}$

(VI) $\mathrm{polyBA{-}I}(i) + \mathrm{R}^{\bullet} \xrightarrow{k_{tr^{-1}}} \mathrm{polyBA}^{\bullet}(i) + \mathrm{R{-}I}$

reinitiation

(VII) $\mathrm{R}^{\bullet} + \mathrm{BA} \xrightarrow{k_{ini}} \mathrm{polyBA}^{\bullet}(1)$

main equilibrium degenerative chain-transfer

(VIII) $\mathrm{polyBA}^{\bullet}(i) + \mathrm{polyBA{-}I}(j) \xrightarrow{k_{ex}} \mathrm{polyBA{-}I}(i) + \mathrm{polyBA}^{\bullet}(j)$

Scheme 4.5 Reactions and corresponding rate coefficients implemented for the simulations of iodine-mediated polymerizations of BA in toluene at 22 °C (for the values of the coefficients see Table 4.8 on the following page).

merization rates, however, sensitivity of the resulting MMDs to k_{dec} was low and variation over a wide value range had no significant impact.

When the CTA R–I is added to the system, the conventional reactions are superimposed by DT. Here, Reactions V (k_{tr}) and VI ($k_{tr^{-1}}$) represent the pre-equilibrium of ITP, while (VII) the formed $\mathrm{R}^{\bullet}$ can also (re)initiate new chains (similar to Reaction II). The main equilibrium is given by Reaction VIII and k_{ex}. The k_{ex} value is taken from a literature ITP system of BA, for which $C_{ex} = k_{ex}/k_p = 2.2$ was determined in benzene at 70 °C.[24] As mentioned above, temperature dependence of C_{ex} is expected to be small[59] and $C_{ex} = 2.2$ chosen for simulation system at 22 °C as well, resulting in the presented

Table 4.8 Kinetic parameters for the simulations of iodine-mediated polymerizations of BA in toluene at 22 °C (see Scheme 4.5 on the preceding page for the respective reactions).

coefficient	value	reference
k_{dec}	$2.0 \times 10^{-8}\,s^{-1}$	–
k_{ini}	$1.5 \times 10^{5}\,L\,mol^{-1}\,s^{-1} = 10 \times k_p$	155–157
k_p	$1.5 \times 10^{4}\,L\,mol^{-1}\,s^{-1}$	157
k_t	$4.6 \times 10^{8} \cdot i^{-0.85}\,L\,mol^{-1}\,s^{-1}$ $(i \leq 30)$ $5.4 \times 10^{7} \cdot i^{-0.22}\,L\,mol^{-1}\,s^{-1}$ $(i > 30)$	158
ϕ	0.35, 1, 10, 20	–
k_{tr}	$\phi \cdot k_{ex}$	–
$k_{tr^{-1}}$	k_{ex}/ϕ	–
k_{ex}	$3.3 \times 10^{4}\,L\,mol^{-1}\,s^{-1}$	24,157
$[BA]_0$	$1.8\,mol\,L^{-1}$	–
$[R{-}I]_0$	$9 \times 10^{-3}\,mol\,L^{-1}$	–
$[TBPO]_0$	$3.2 \times 10^{-1}\,mol\,L^{-1}$	–

k_{ex} value. The rate coefficients k_{tr} and $k_{tr^{-1}}$ (or the corresponding transfer constants C_{tr} and $C_{tr^{-1}}$) can be regarded as crucial parameters to define the activity of R–I toward iodine transfer and thus (re)initiation. Therefore, to simulate the impact of different (re)initiation behaviors, k_{tr} and $k_{tr^{-1}}$ were varied. When R–I has a higher activity than polyBA–I (such as CP–I), then $k_{tr} > k_{ex}$. Naturally, this leads to a less favored back-reaction and $k_{tr^{-1}} < k_{ex}$. The relation $k_{tr} > k_{ex} > k_{tr^{-1}}$ (or $k_{tr} < k_{ex} < k_{tr^{-1}}$ for a less activated R–I such as Bn–I) was already successfully applied in kinetic simulations of ITP systems in the literature.[160] There, as a reasonable assumption and without further kinetic detail, the following relation was used:

$$\frac{k_{tr}}{k_{ex}} = \frac{k_{ex}}{k_{tr^{-1}}} = \phi = \frac{C_{tr}}{C_{ex}} = \frac{C_{ex}}{C_{tr^{-1}}}\,. \tag{4.2}$$

In this context, ϕ (> 0) is a variable parameter, while for $\phi = 1$, $k_{tr} = k_{ex} = k_{tr^{-1}}$ and R–I is a chemical mimic of polyBA–I. As an example, for the CTAs already mentioned in this chapter, it can be expected that for CP–I, $\phi > 1$, for PE–I, $\phi \approx 1$, and for Bn–I, $\phi < 1$ in ITPs of BA. The initial concentrations of the reagents presented in Table 4.8 are chosen according to the experimentally investigated CP–I systems.

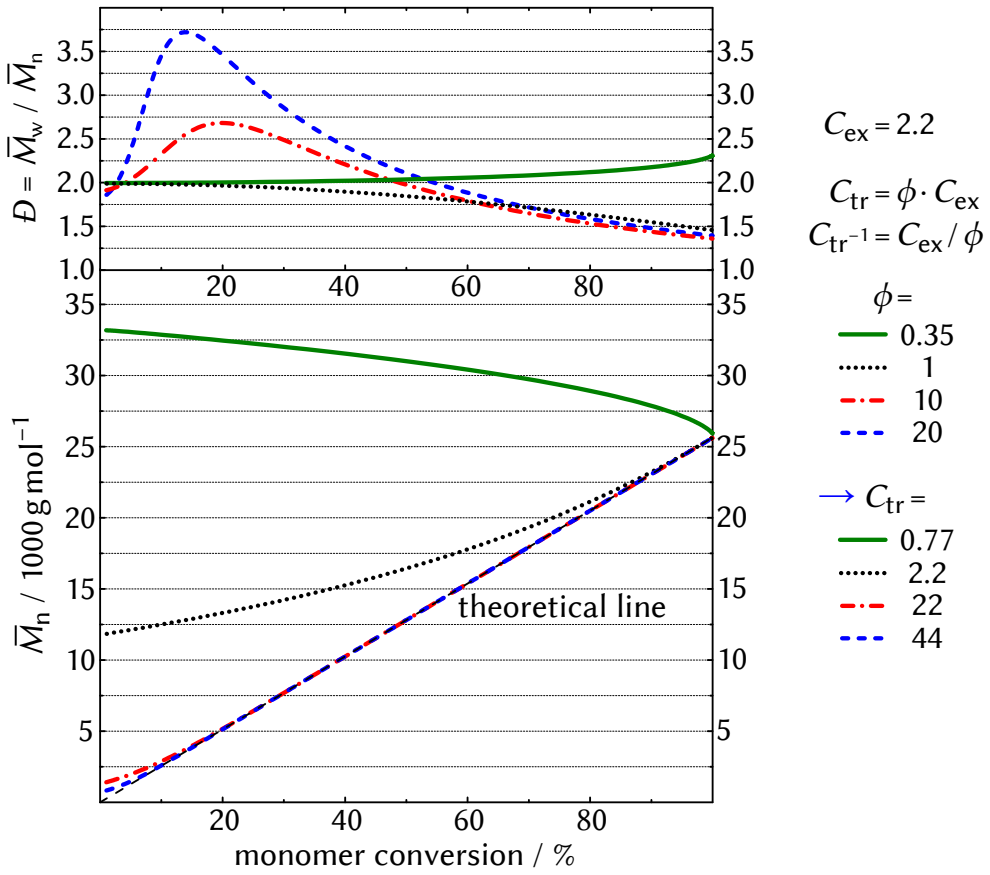

Figure 4.11 Simulated $\overline{M}_n$ and $Đ$ as a function of monomer conversion for iodine-mediated polymerizations of BA at 22 °C for different values of ϕ as indicated (for simulation model see Scheme 4.5 on page 87 and Table 4.8 on the facing page).

4.2.6.2 Fast and slow (re)initiation

To assess the impact of (re)initiation, simulations were conducted for ϕ = 0.35, 1, 10, and 20, while all other rate coefficients and the initial concentrations of all reagents remained constant. In this context, ϕ values were chosen since the obtained simulation results roughly match the discussed experimental ones, which will be presented below. In addition, the values are in the same region as for similar ITP simulation systems in the literature.[160] However, it should be emphasized that the presented simulations are mainly supposed to qualitatively express the experimentally observed effects and support the proposed mechanistic cause rather than being an exact quantitative mimic. The resulting simulated $\overline{M}_n$ and $Đ$ values as a

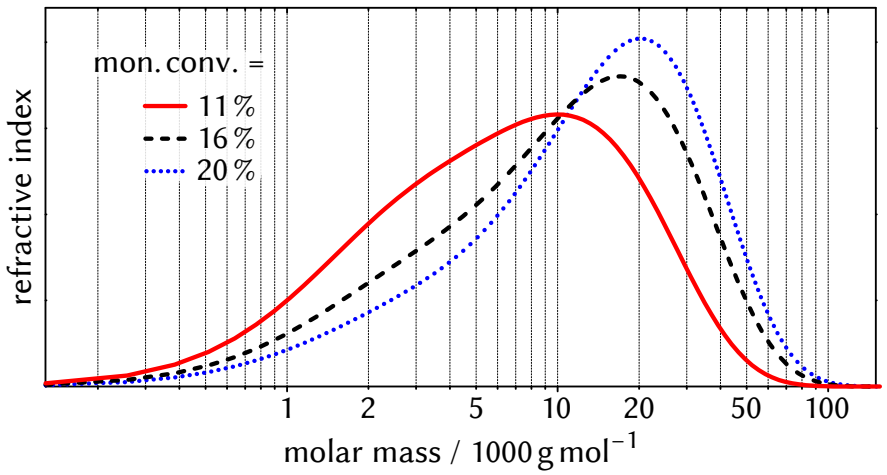

Figure 4.12 Simulated MMDs (SEC traces, all normalized to the same area) of the system with $\phi = 20$ presented in Figure 4.11 on the preceding page for different monomer conversions (mon. conv.) as indicated.

function of monomer conversion are presented in Figure 4.11 on the previous page. For all ϕ, $\overline{M}_n$ obeys the trend that is determined by the respective C_{tr} value (cf. Figure 2.1 on page 20), with decreasing $\overline{M}_n$ for $C_{tr} < 1$ and increasing $\overline{M}_n$ for $C_{tr} > 1$, while $\overline{M}_n$ is closer to $\overline{M}_{n,theo}$ for higher C_{tr}. In this context, for $\phi = 0.35$, $\overline{M}_n$ evolution resembles the experimentally obtained values for Bn–I (cf. Figure 4.10 on page 83), while for $\phi = 1$, $\overline{M}_n$ values resemble the values for PE–I (cf. Figure 4.3 on page 67).

For $\phi = 0.35$ and 1, $Đ$ values are generally close to 2, while they slightly increase for $\phi = 0.35$ and slightly decrease for $\phi = 1$ with increasing monomer conversion. When ϕ is set to either 10 or 20, a remarkable observation similar to the experiments can be made. While $\overline{M}_n$ values are closer to $\overline{M}_{n,theo}$ for higher ϕ, $Đ$ values show a distinct increase at the beginning of the polymerization. In this context, higher $Đ$ values are obtained for higher ϕ and thus faster (re)initiation. A deeper insight into the underlying effect for these trends can be gained by means of the corresponding MMDs, which will be presented in the following. As a side note, considering the pre-equilibrium, the simulation results exclusively depend on the forward reaction and C_{tr}, while the extent of back-reaction is negligible as unaltered results were obtained for $C_{tr^{-1}} = 0$ in every single case.

4.2.6.3 Molar-mass distributions

For the most pronounced case of high $Đ$ values with $\phi = 20$, MMDs were simulated close to the maximum $Đ$ values for monomer conversions of 11 %, 16 %, and 20 %. They are presented in Figure 4.12 on the preceding page and reveal the structural cause of the high $Đ$ values. A pronounced shoulder at the low-molar-mass side is obtained for each MMD, while the intensity of the shoulder decreases for higher monomer conversion. Mechanistically, this can be explained by the fact that for high ϕ and fast (re)initiation, polyBA$^\bullet$ is generally deactivated much faster by R−I than by polyBA−I. In this context, deactivation by R−I occurs mainly at the beginning of the polymerization (pre-equilibrium) and deactivation by polyBA−I mainly at a later stage (main equilibrium). When $k_{tr} > k_{ex}$ and deactivation by R−I is faster than by polyBA−I, the average number of propagation steps until polyBA$^\bullet$ is deactivated is smaller in the pre-equilibrium than it is in the main equilibrium. As a hypothetical mathematical example, if initially generated polyBA$^\bullet$ undergoes 10 propagation steps before being deactivated by R−I in the pre-equilibrium and then undergoes 100 additional propagation steps before being deactivated for a second time by polyBA−I in the main equilibrium, the difference in chain lengths on the typical logarithmic scale (cf. Figure 4.12) is

$$\log_{10}(100 + 10) - \log_{10}(10) = 1.04 \,. \tag{4.3}$$

If deactivation by R−I in the pre-equilibrium was much slower and polyBA$^\bullet$ would undergo 50 propagation steps before being deactivated for the first time, the difference would be

$$\log_{10}(100 + 50) - \log_{10}(50) = 0.48 \,. \tag{4.4}$$

This clarifies that the faster the deactivation (= (re)initiation) by R−I is compared to the one by polyBA−I, the more pronounced the obtained shoulder is. This can be further supported when the simulated MMDs in Figure 4.12 are divided according to different stages of deactivation, which will be presented in the following.

Peak of the first deactivation

To illustrate the effect of fast deactivation by R−I, an additional dormant polymer species, polyBA−I(FD), is implemented in the simulation model. It replaces the common polyBA−I species when initially generated polyBA$^\bullet$ is

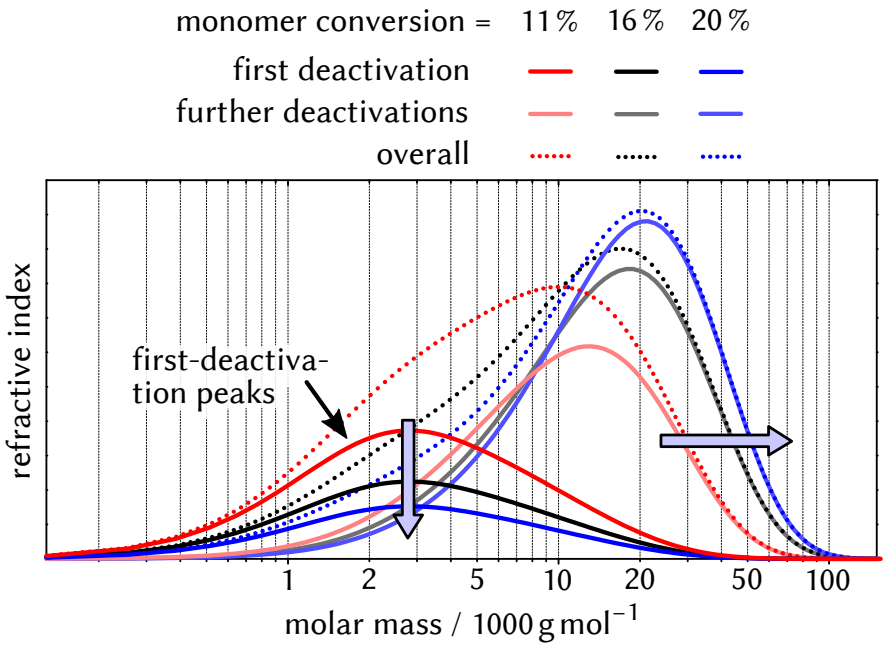

Figure 4.13 Simulated overall MMDs of the system with $\phi = 20$ presented in Figure 4.12 on page 90 being divided into distinct MMDs for polyBA–I being deactivated for the first time (denoted as polyBA–I(FD) in the text) and for polyBA–I of further deactivation steps.

(i) deactivated for the first time during its long lifetime (FD: first deactivation) while (ii) this deactivation is caused by R–I rather than polyBA–I (theoretically, polyBA$^\bullet$ can also be deactivated by polyBA–I at the beginning of the polymerization, although chances are much lower). When polyBA–I(FD) is then reactivated and deactivated for a second time, it is irreversibly transformed into the common polyBA–I species. In this context, it should be noted that naturally, polyBA–I(FD) is chemically identical to polyBA–I, which makes it impossible to distinguish between the two species experimentally. Simulations are therefore an ideal tool to study into such mechanistic effects. In Figure 4.13, the MMDs of Figure 4.12 are divided into polyBA–I(FD) and polyBA–I, while dead polyBA is not significant at this stage of polymerization. It is evident that the shouldering is due to the FD peak formed at the beginning of the polymerization. For higher monomer conversion, the FD peak is consumed while the distribution of polyBA–I continuously shifts toward higher molar masses, which eventually results in decreasing $Đ$ values (cf. Figure 4.11 on page 89).

Table 4.9 Initial concentrations of substances used for UV-initiated iodine-mediated polymerization of BA with CP−I in bulk at 22 °C.

entry [a]	$[BA]_0$ / mol L^{-1}	$[CP-I]_0$ / mol L^{-1}	$[MMMP]_0$ / mol L^{-1}
◘	6.8	34×10^{-3}	10×10^{-3}

[a] See Figure 4.14 on the following page.

4.2.6.4 Experimentally obtained molar-mass distributions

In contrast to the presented simulated MMDs for $\phi = 20$, shouldering is not perceptible for the experimentally obtained MMDs in Figure 4.8 on page 81. This is mainly ascribed to (i) BB during the SEC experiment smoothening the MMD curves and (ii) experimental $Đ$ values being smaller than the simulated ones in the first place ($Đ \approx 2.5$ versus $Đ > 3.5$). However, when polymerizations of BA with CP−I are conducted in bulk (rather than in solution), high $Đ$ values and a pronounced low-molar-mass shoulder can indeed be observed. In this context, bulk polymerizations were conducted with MMMP similar to the PE−I system described in Section 4.2.1 on page 66. High $[BA]_0$ were achieved by using a more highly concentrated CP−I solution (compared to the one used for solution polymerizations) by applying higher $[I_2]_0$ and $[AIBN]_0$ for the reaction in toluene (for further detail on the employed concentrations see Experimental Section 10.1.3.1 on page 218). The initial concentrations for the polymerization system are presented in Table 4.9. The resulting molar-mass evolution versus monomer conversion is given in Figure 4.14 on the next page. As for the solution polymerizations with CP−I, $\overline{M}_n$ values are close to $\overline{M}_{n,theo}$ throughout polymerization, whereas $Đ$ values are high with a maximum at almost 4.0. The respective MMDs are presented in Figure 4.15 on page 95. Low-molar-mass shouldering can be observed, especially for low monomer conversion, supporting the significance of fast (re)initiation for the here conducted polymerizations. In this regard, more pronounced shouldering compared to the systems in solution might be assigned to the fact that here, even slight formation of Bn−I is completely prevented (no TBPO, far less toluene) and (re)initiation is expected to occur exclusively via CP−I. This effect can also be observed in the context of RTCP systems, which will be discussed at a later stage.

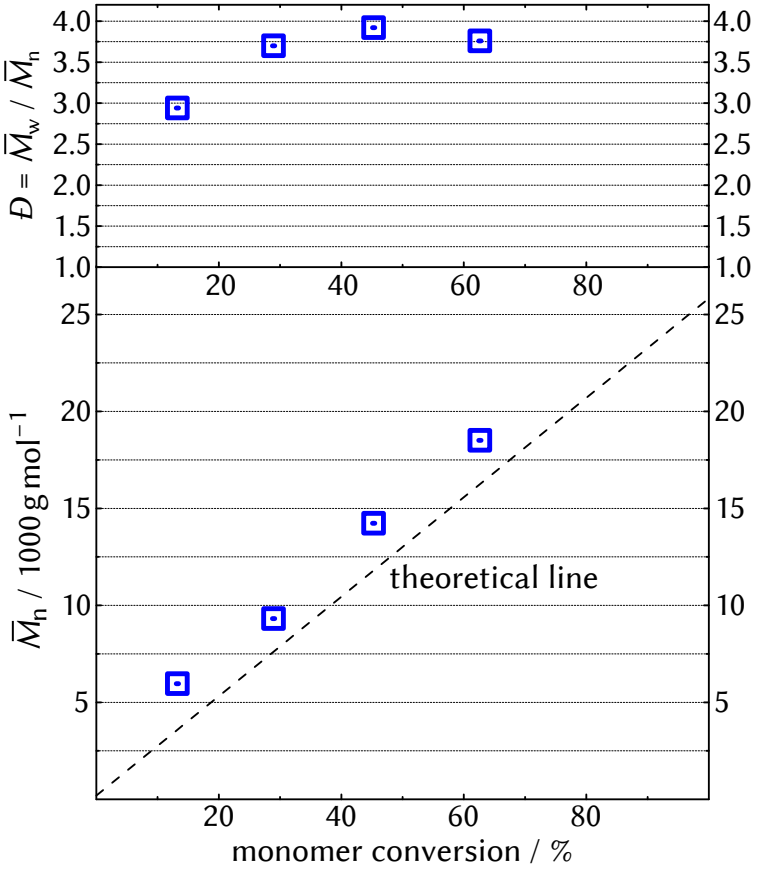

Figure 4.14 $\overline{M}_n$ and $Đ$ as a function of monomer conversion of the UV-initiated iodine-mediated polymerization of BA with CP–I in bulk at 22 °C given in Table 4.9 on the preceding page.

4.2.6.5 General significance for degenerative chain-transfer

It should be emphasized that the presented simulations are based on a rather simple model which superimposes the reactions of a conventional RP with the classic DT mechanism and reasonable reaction rate coefficients. The given results should therefore be valid for DT systems in general, in case chains are more quickly deactivated in the pre-equilibrium than in the main equilibrium. While this effect is clearly significant for the here conducted polymerizations of BA with CP–I, to the best of knowledge, no ITPs of acrylates with highly active CTAs such as CP–I have been reported so far. However, there are examples of acrylate polymerizations using highly active CTAs with a (re)initiating CP group for other DT-based polymerization techniques such as RAFT polymerization[161,162] or TERP.[163] Notwithstanding

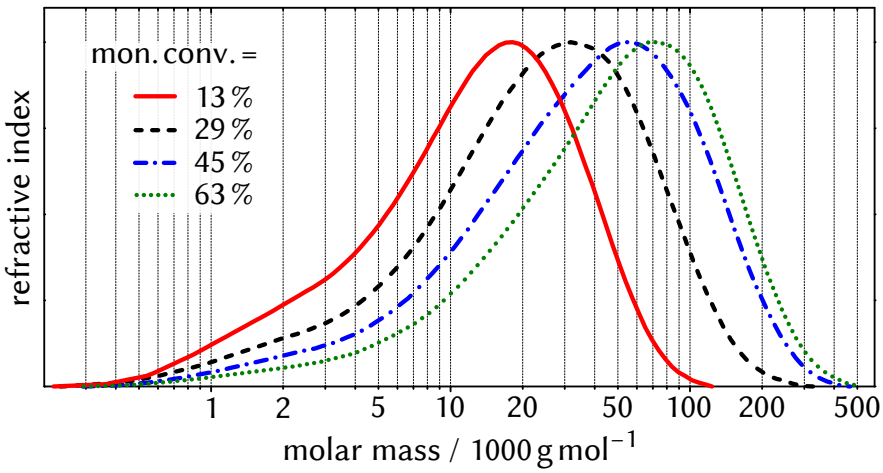

Figure 4.15 Experimentally obtained MMDs (SEC traces, all normalized to the same maximum intensity) of the system presented in Figure 4.14 on the facing page for different monomer conversions (mon. conv.) as indicated.

this, uncommonly high $Đ$ values are never reported and narrow MMDs are generally obtained for these systems. Kinetically, one major difference between RAFT and TERP systems on the one hand and ITP systems on the other is that for most polymer types, the activation–deactivation frequency in the main equilibrium ($\sim C_{ex}$) is much higher for RAFT or TERP (depending on the exact type CTA) compared to ITP[13,18,164] (e. g., in a representative TERP of methyl acrylate, $C_{ex} = 19$).[165] This makes it worthwhile to study into the impact of C_{ex} on the observed effect. In Figure 4.16 on the next page, the simulation results for $\overline{M}_n$ and $Đ$ with $\phi = 20$ and $C_{ex} = 2.2$ are compared to results for a faster and slower main equilibrium with $C_{ex} = 22$ and 0.8, respectively. While for all C_{ex}, $\overline{M}_n$ values are very close to $\overline{M}_{n,theo}$, higher C_{ex} values lead to a remarkably less pronounced maximum of $Đ$, which is also heavily shifted toward lower monomer conversion. $Đ < 2.0$ is already obtained at 8 % of monomer conversion and drastically decreases throughout polymerization, so that the observed effect of fast (re)initiation barely interferes with the trends normally expected for an effective RDRP. A less pronounced effect for higher C_{ex} values is indeed reasonable, since then, the FD peak and thus the MMD shoulder is consumed much faster during the polymerization process. For a slower main equilibrium and $C_{ex} = 0.8$, the FD peak is only slowly consumed and MMDs with $Đ > 2.0$ are obtained for almost the entire polymerization.

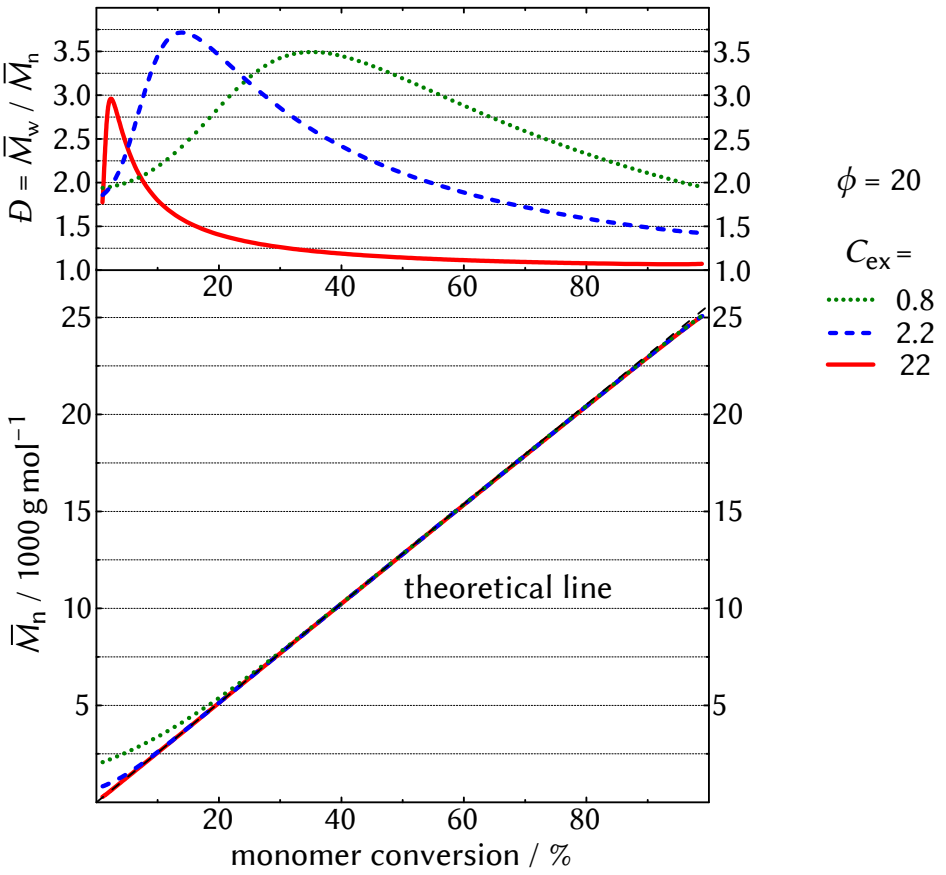

Figure 4.16 Simulated $\overline{M}_n$ and $Đ$ as a function of monomer conversion for iodine-mediated polymerizations of BA at 22 °C for different values of C_{ex} as indicated (for simulation model see Scheme 4.5 on page 87 and Table 4.8 on page 88).

The presented results clarify that shouldering should be generally observed for DT-based RDRPs with $C_{tr} > C_{ex}$. However, the effect is especially pronounced for systems with a rather low activation–deactivation frequency in the main equilibrium. Therefore, in contrast to other DT techniques such as RAFT polymerization or TERP, it is expected to be particularly important for ITP systems, which normally feature rather low C_{ex} and only moderately high molar-mass control.

In the final part of this section about polymerizations of BA, the application of RTCP catalysts for the developed system in toluene with CP–I (Table 4.4 on page 76, entry 4) will be presented. The investigation of these systems is especially worthwhile since a superimposed RTCP mechanism might

Table 4.10 Initial concentrations of substances used for UV-initiated iodine-mediated polymerizations of BA with CP–I in toluene at 22 °C with RTCP catalysts (cat.).

entry [a]	$[BA]_0$ / mol L^{-1}	$[CP–I]_0$ / mol L^{-1}	$[TBPO]_0$ [b] / mol L^{-1}	$[cat.]_0$ / mol L^{-1}	cat.
1 (□)	1.8	9×10^{-3}	0.32	5×10^{-3}	$(BuO)_2P(O)H$
2 (◇)	1.8	9×10^{-3}	0.32	5×10^{-3}	PinP(O)H
3 (△)	1.8	9×10^{-3}	3.7	1×10^{-3}	NIS
4 (⬠)	1.8	9×10^{-3}	3.7	1×10^{-3}	GeI_4
5 (◁)	1.8	9×10^{-3}	3.7	1×10^{-3}	SnI_4
6 (○)	1.8	9×10^{-3}	1.3	5×10^{-3}	BHT
7 (▷)	1.8	9×10^{-3}	0.64	10×10^{-3}	xanthene

[a] See Figure 4.17 on the following page; [b] with 3×10^{-3} mol L^{-1} of AIBN from the CP–I solution.

generally enhance the activation–deactivation frequency of living chains in both the pre- and the main equilibrium. In the context of Figure 4.16 on the preceding page, this would lead to a less pronounced effect of fast (re)initiation and a high control of chain growth.

4.2.7 Polymerizations with cyanopropyl iodide and RTCP catalysts

4.2.7.1 Employed catalyst systems

The applied RTCP catalysts included the two PADs $(BuO)_2P(O)H$ and PinP(O)H, as well as NIS, GeI_4, and SnI_4. In addition, 3,5-di-*tert*-butyl-hydroxytoluene (BHT) as a representative oxygen-centered and xanthene as a representative carbon-centered catalyst were employed, which both already showed a positive impact on chain-growth control in literature RTCPs[29] (for structural formulas see Figure 10.4 in the Experimental Section on page 220). The initial concentrations of the substances applied in the respective systems are given in Table 4.10. For each catalyst, various $[TBPO]_0$ were tested in order to (i) keep the amount of TBPO low and to (ii) still obtain rather short inhibition to ensure only little decomposition of CP–I. In this context, high $[TBPO]_0$ was needed for the iodo catalysts—i. e., NIS, GeI_4, and SnI_4—as a pronounced I_2 formation and no polymerization

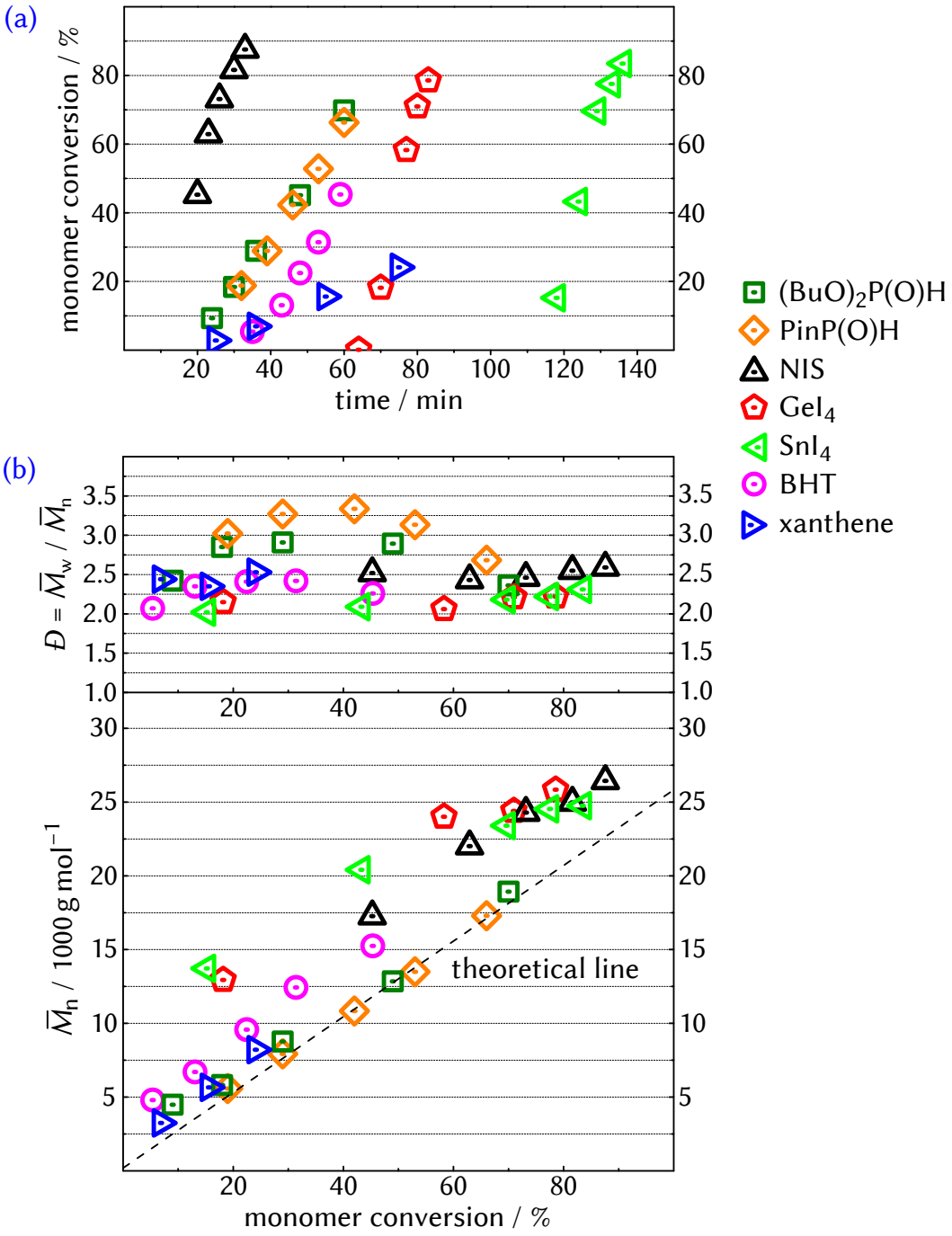

Figure 4.17 (a) Monomer conversion as a function of time and (b) $\overline{M}_n$ and $Đ$ as a function of monomer conversion of UV-initiated iodine-mediated polymerizations of BA with CP–I in toluene at 22 °C with RTCP catalysts given in Table 4.10 on the preceding page.

was observed otherwise. While this effect was already discussed for NIS in case of the PE–I system, a similar effect was found for both GeI_4 and SnI_4. In literature studies, SnI_4 was shown to decompose upon near-UV irradiation to form elemental Sn and 2 I_2.[166,167] A model experiment of SnI_4 in toluene revealed that decomposition is also significant under the conditions used for the presented photopolymerizations (see Appendix A.1.3 on page 230). However, only about 10 % of SnI_4 decomposed within 2.5 h, so that most of the initially employed SnI_4 is expected to be still present at the end of the obtained inhibition period of about 2 h, which will be presented below. The use of the oxygen-centered BHT also required higher $[TBPO]_0$, which is assigned to its radical-scavenging nature through the transfer of the hydroxyl group's hydrogen atom giving a highly stabilized phenoxy radical. Catalyst concentrations were again chosen according to literature recommendations,[26,27,29] while slightly lower concentrations were used for the iodo catalyst so as to keep I_2 formation low.

4.2.7.2 Polymerization rates and molar-mass evolution

Monomer conversion versus time as well as $\overline{M}_n$ and $Đ$ values versus monomer conversion are given in Figure 4.17 on the facing page. Almost all systems have a rather short inhibition period of below 30 min. The only exceptions are the systems with GeI_4 (60 min) and SnI_4 (110 min), although the concentration of (i) TBPO is rather high and of (ii) the respective catalyst is rather low in these cases. Comparing all three iodo catalysts, inhibition and thus release of I_2 is more pronounced in the order of SnI_4 > GeI_4 > NIS. The lowest $[TBPO]_0$ values were needed for the PAD systems, which is due to the frequently mentioned reactivity of the PADs toward I_2. Slightly higher $[TBPO]_0$ was used for xanthene, which showed a distinctly lower polymerization rate than all other systems. This indicates a retarding impact of xanthene on polymerization, however, this effect was not further investigated in the present work.

Having the longest inhibition period, the GeI_4 and the SnI_4 systems also show (i) the most pronounced difference between $\overline{M}_n$ and $\overline{M}_{n,theo}$ as well as (ii) the lowest $Đ$ values. With regard to the discussed depletion of CP–I and formation of Bn–I, these effects are in accordance with the presented catalyst-free polymerizations as well as the presented kinetic simulations. The opposite effect is observed for the PAD systems, for which (i) $\overline{M}_n$ values are the closest to $\overline{M}_{n,theo}$, while (ii) the $Đ$ values are the highest. In this context, the consumption of I_2 by the PADs impedes the formation of Bn–I.

In addition, as the PAD systems are the ones with the lowest $[TBPO]_0$, the amount of $Bn^\bullet$ generated during the rather short inhibition period is expected to be the lowest of all systems in the first place. To put it simply, the remaining catalyst systems tend to be in between these two extreme cases of faster and slower (re)initiation. Notably, when lower $[TBPO]_0$ were chosen and longer inhibition was obtained for particular systems, molar-mass evolution always bore closer resemblance to the case of slow (re)initiation (data not shown).

The results clearly show that all catalysts indeed have a respective impact on molar-mass control during polymerization. However, this impact is expected to be mainly caused by the individual tendencies of the catalysts to consume or release I_2, or to scavenge radicals, leading to faster or slower (re)initiation, as was already shown for the catalyst-free system. Under the here used conditions, the contribution of a potential RTCP mechanism that significantly increases the activation–deactivation frequency of living chains is expected to be minor. A further tweaking of the developed photosystem was thus not feasible.

4.2.8 Conclusions on BA polymerizations

As a straightforward statement, the presented results show that iodine-mediated photopolymerization is highly feasible and the accumulation of I_2 can be easily countered with a conventional radical initiator. It was shown that polymerizations can be conducted at room temperature without the need of a heating device. Polymer with a high chain-end functionality is obtained and the sensitivity toward UV irradiation illustrates the applicability as highly adjustable and photoswitchable "on–off" systems.

A semi-in-situ approach offered a convenient way to utilize the activated CTA CP–I so as to achieve fast (re)initiation. Kinetic simulations and mechanistic considerations revealed a peculiar effect of fast (re)initiation for DT systems with a rather slow main equilibrium, as it is normally the case for ITP systems. In this context, the impact of the CTA on molar-mass evolution is unambiguously illustrated by the PE–I system in Figure 4.3 on page 67 and the CP–I system in Figure 4.14 on page 94, which were indeed identical despite of the used CTA. As a general comment, the presented issue serves as a good example that considering complete MMDs rather than their reducing $\overline{M}_n$ and $Đ$ values can be a great help when polymerization results are interpreted.

Potential RTCP catalysts were shown to mainly have an impact on the inhibition period or the rate of polymerization. While the impact on inhibition led to an indirect influence on molar-mass evolution, direct effects on the crucial activation–deactivation process of living chains via the RTCP mechanism are expected to be minor. This indicates that potential iodine transfer of the employed catalysts is too slow to effectively control chain growth of rather quickly propagating poly(acrylates) under the here investigated conditions. The mentioned *indirect* impact on molar-mass evolution also demonstrates that knowing the characteristics of the original system well is the key to estimate the impact of potential additives, as misinterpretations may easily occur. While the focus of the present work was laid on polymerizations at *room temperature,* it should be stated that a higher activity of the catalysts might be obtained at higher temperatures. Indeed, kinetic investigations of RTCPs of St in the literature indicate that chain-growth control decreases for lower polymerization temperatures.[85]

For all polymerizations, the impact of a superimposed RT mechanism is expected to be small and activation–deactivation mainly achieved via DT. This might be due to the fact that the secondary C–I bond of polyBA–I is not labile enough to lead to a sufficient extent of C–I bond cleavage. In this context, the investigation of polymer forming a tertiary C–I bond such as poly(methacrylates) seems especially worthwhile. Polymerizations of BMA were thus studied similar to polymerizations of BA and will be presented in the next section.

4.3 Polymerizations of *n*-butyl methacrylate

UV-initiated iodine-mediated polymerizations of BMA were conducted similarly to the ones of BA. The identical experimental setup was chosen while the distance of the polymerization mixture to the lamp was 7 cm if not stated differently. Polymerizations were mainly conducted in bulk with MMMP as photoinitiator. In this section, the focus will be laid on the impact of C–I-bond cleavage and the significance of a potential RT mechanism. In the following, the general BMA system and the impact of the used CTA will be presented. As for the polymerization shown in Figure 4.14 on page 94, CP–I was used via the semi-in-situ preparation for high concentrations of AIBN and I_2.

4.3.1 Impact of the chain-transfer agent

Polymerizations of BMA in bulk were conducted at 22 °C using MMMP as the UV initiator and either PE–I or CP–I as the CTA. The initial CTA concentration, $[CTA]_0$, was chosen to target $\overline{DP}_n = 200$ for full monomer conversion, which corresponds to $\overline{M}_n \approx 30\,000\,\mathrm{g\,mol^{-1}}$. In Table 4.11, the initial concentrations are given for the PE–I (entry 1) and for the CP–I system (entry 2).

Polymerization rate and molar-mass evolution

The resulting values of monomer conversion versus time as well as $\overline{M}_n$ and $Đ$ versus monomer conversion are given in Figure 4.18 on the next page (continuous irradiation). High $Đ$ values at about 2.5 and $\overline{M}_n$ values distinctly higher than $\overline{M}_{n,theo}$ illustrate slow (re)initiation of PE–I and a C_{tr} value lower than unity. This validates the poor ability of PE–I to control growth

Table 4.11 Initial concentrations of substances used for UV-initiated iodine-mediated polymerizations of BMA in bulk at 22 °C with different CTAs.

entry[a]	$[BMA]_0$ / mol L^{-1}	CTA	$[CTA]_0$ / mol L^{-1}	$[MMMP]_0$ / mol L^{-1}
1 (⊙)	6.2	PE–I	31×10^{-3}	50×10^{-3}
2 (⊡)	6.2	CP–I	31×10^{-3}	50×10^{-3}

[a] See Figure 4.18 on the facing page.

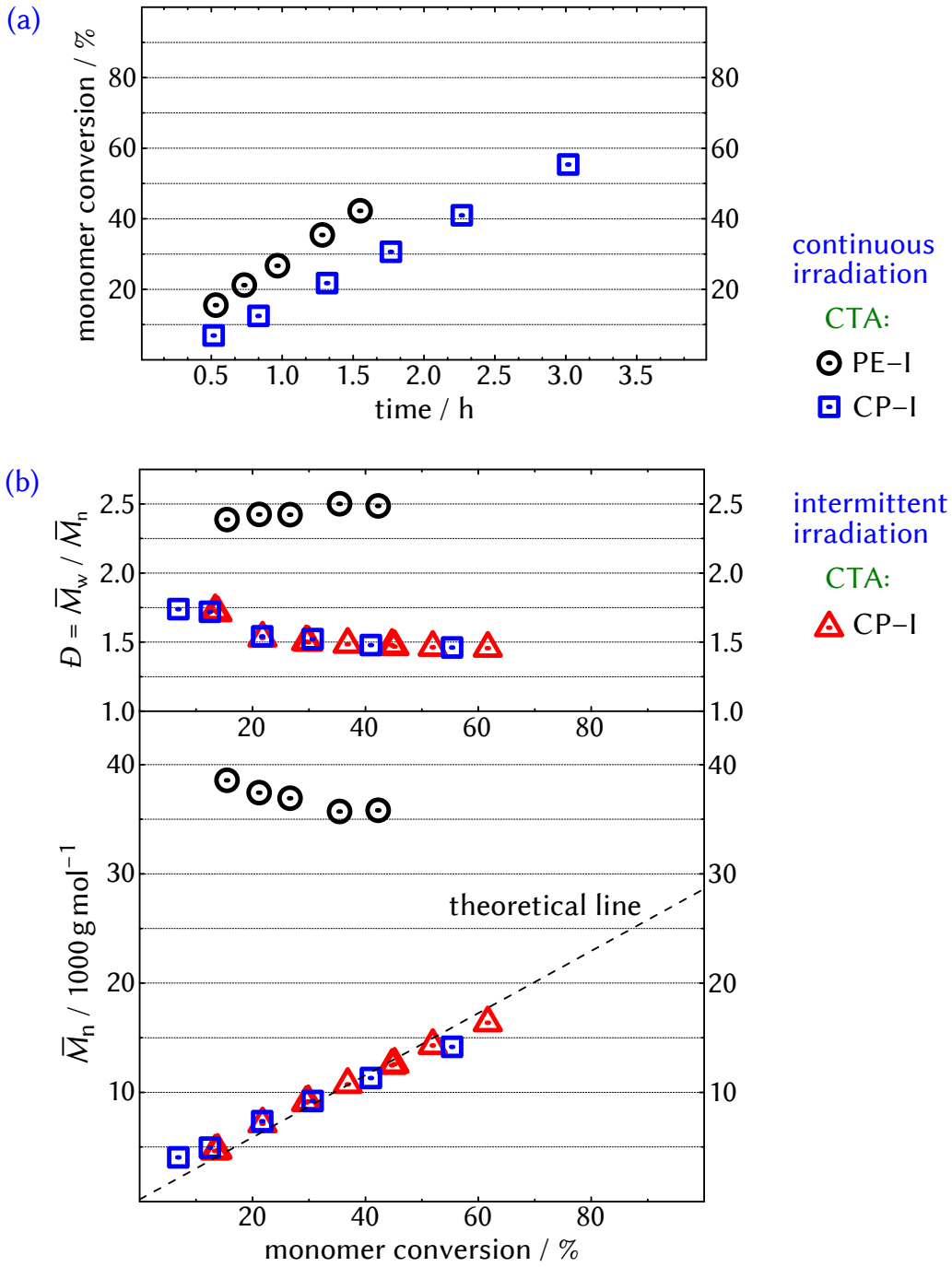

Figure 4.18 (a) Monomer conversion as a function of time (for data of intermittent irradiation see Figure 4.19 on page 106) and (b) $\overline{M}_n$ and $Đ$ as a function of monomer conversion of the UV-initiated iodine-mediated polymerizations of BMA in bulk at 22 °C with different CTAs given in Table 4.11 on the facing page.

of polymethacrylates in thermally initiated systems[16] (cf. Scheme 2.7 on page 18) also for the present photosystem. In this context, comparison to the BA system with PE–I in Figure 4.3 on page 67 clearly illustrates the difference of polymethacrylates (tertiary propagating radical) and polyacrylates (secondary propagating radical) in this context. For CP–I, (re)initiation is quick, causing low $\overline{M}_n$ values from an early stage, which are close to $\overline{M}_{n,theo}$ throughout the polymerization. The slight downward deviation for high monomer conversion is ascribed to formation of dead polymer and the incessant initiation of new chains by MMMP, which is more significant for slowly propagating monomers such as BMA, especially at low temperatures. $Đ$ values are much smaller (< 1.5 for monomer conversion > 40 %), which demonstrates the enhanced control of chain growth. In both the PE–I and the CP–I system, fairly high monomer conversion is reached within only a few hours. It should be noted that pronounced viscosity impeded sample taking via syringe for monomer conversion higher than 70 %. Slightly lower polymerization rates for CP–I are potentially due to chain-length-dependent termination of the growing macroradical,[70,71] which is more pronounced for lower molar masses, which is the case with CP–I. Pronounced inhibition is not observed and indeed less expected since polyBMA–I and CP–I should be similarly prone to C–I-bond cleavage. Hence, if radical production by MMMP would not be high enough to overcome formation of I_2 by CP–I, it would not be high enough for the incessant I_2 formation by polyBMA–I as well and polymerization would be completely inhibited. This behavior will be clarified at a later stage, when lower concentrations of MMMP will be applied.

4.3.2 End-group analysis

End-group analysis via ESI-MS was performed of a polyBMA sample of the CP–I system ($\overline{M}_n$ = 4900 g mol^{-1}, $Đ$ = 1.72, monomer conversion = 12 %). The detected polymeric species are given in Table 4.12 on the next page within the range of one monomeric repeating-unit (M_{BMA} = 142 g mol^{-1}). All species were (re)initiated by CP$^\bullet$, while the amount of conventional initiation by fragments of MMMP was too low for detection, which clarifies the high activity of CP–I. Dormant chains (iodine end-group) or formerly dormant chains (OH or lactone end-group) are present to an extent of 94 %. The abundance of dead polymer caused by irreversible termination via disproportionation (unsaturated and saturated BMA end-group, BMA$^=$ and BMA^H,

Table 4.12 Na^+-ionized species detected in ESI-MS of a polyBMA sample produced via UV-initiated iodine-mediated polymerization with CP–I (Table 4.11 on page 102, entry 2, $\overline{M}_n$ = 4900 g mol^{-1}, $Đ$ = 1.72, monomer conversion = 12 %) with the theoretical and the experimentally obtained m/z values, $(m/z)_{theo}$ and $(m/z)_{exp}$, respectively, and their relative intensities (rel. int.).

No.	α-end-group	ω-end-group [a]	mon. units [b]	$(m/z)_{theo}$ [c]	$(m/z)_{exp}$ [c]	rel. int. [d] / %
1	CP	OH	5	818.5	818.6	69
2	CP	iodine	5	928.4	928.5	19
3	CP	lactone	4	886.6	886.6	6
4	CP	$BMA^=$	5	942.6	942.6	3
5	CP	BMA^H	5	944.6	944.6	2
6	CP	CP	5	869.6	869.6	1

[a] Transformations of iodine end-groups are given in Scheme 3.5 on page 43, $BMA^=$ and BMA^H: unsaturated and saturated BMA end-group, respectively; [b] monomeric repeating-units; [c] for m/z = 810–952; [d] only the here given species are taken account of, sum = 100 %.

respectively) or combination (CP end-group)[98,110] is small. This clarifies the high extent of end-group functionality during the polymerization.

4.3.3 Intermittent irradiation

Similar to the developed photosystem of BA, the here presented CP–I system was irradiated intermittently with alternating periods of irradiation (50 min) and no irradiation (25 min). Figure 4.19a on the following page shows the evolution of monomer conversion in comparison to continuous irradiation. No polymerization is again observed during the dark periods while polymerization rates are very similar to the continuous system during irradiation. The MMDs obtained before and after the respective dark periods (Figure 4.19b, SEC traces) show no shift or change in any way. Molar-mass evolution in Figure 4.18b on page 103 reveals almost no difference to the continuous system. As for the BA polymerizations, this illustrates the high potential as a photoswitchable "on–off" system.

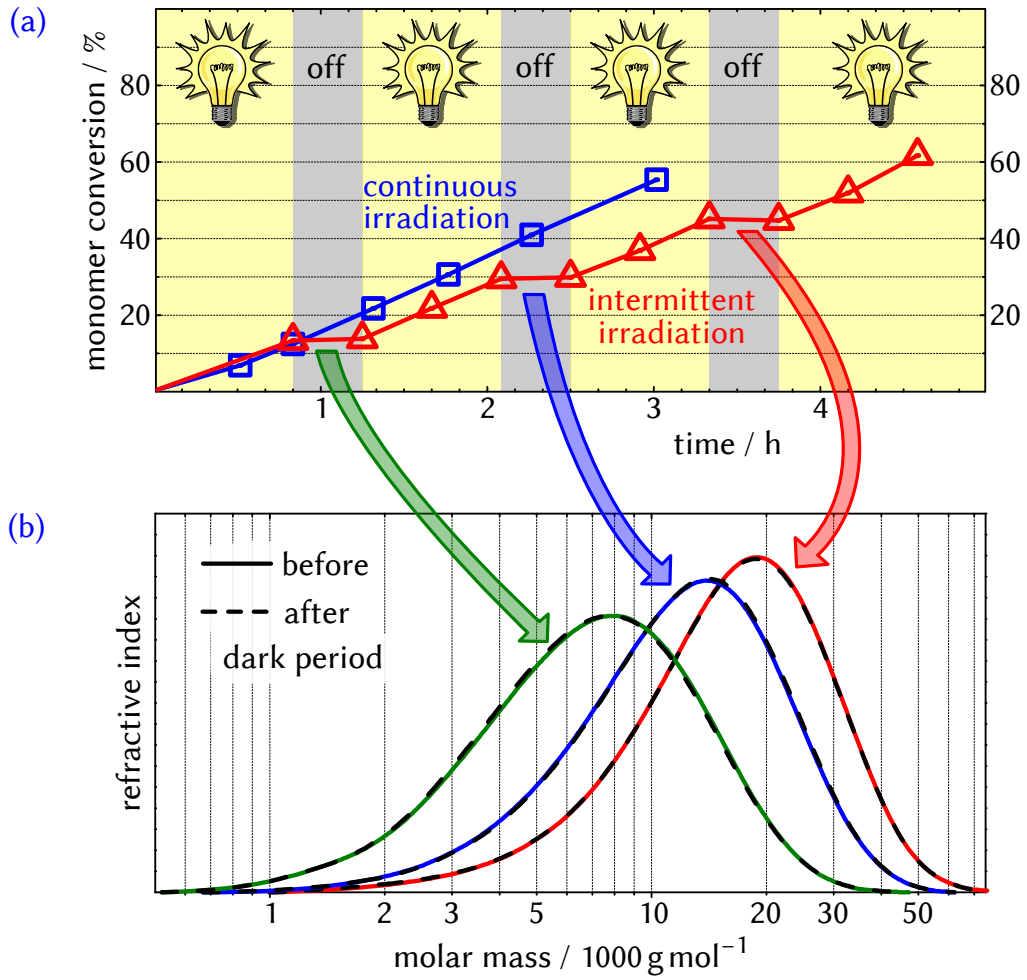

Figure 4.19 (a) Monomer conversion as a function of time of the UV-initiated iodine-mediated polymerization of BMA with CP–I in bulk at 22 °C presented in Table 4.11 on page 102 (entry 2) for continuous and intermittent irradiation and (b) MMDs (SEC traces) of polymer samples taken before and after the respective dark periods.

4.3.4 Impact of the initiator concentration

The impact of $[MMMP]_0$ on the polymerization behavior was studied. In this context, based on the discussed CP–I system, polymerizations were conducted for $[MMMP]_0$ lower than the used 50 mmol L^{-1}. The resulting values of monomer conversion versus time as well as of $\overline{M}_n$ and $Đ$ versus monomer conversion are shown in Figure 4.20 on the facing page and Figure 4.21 on page 108, respectively. In accordance with the above-mentioned

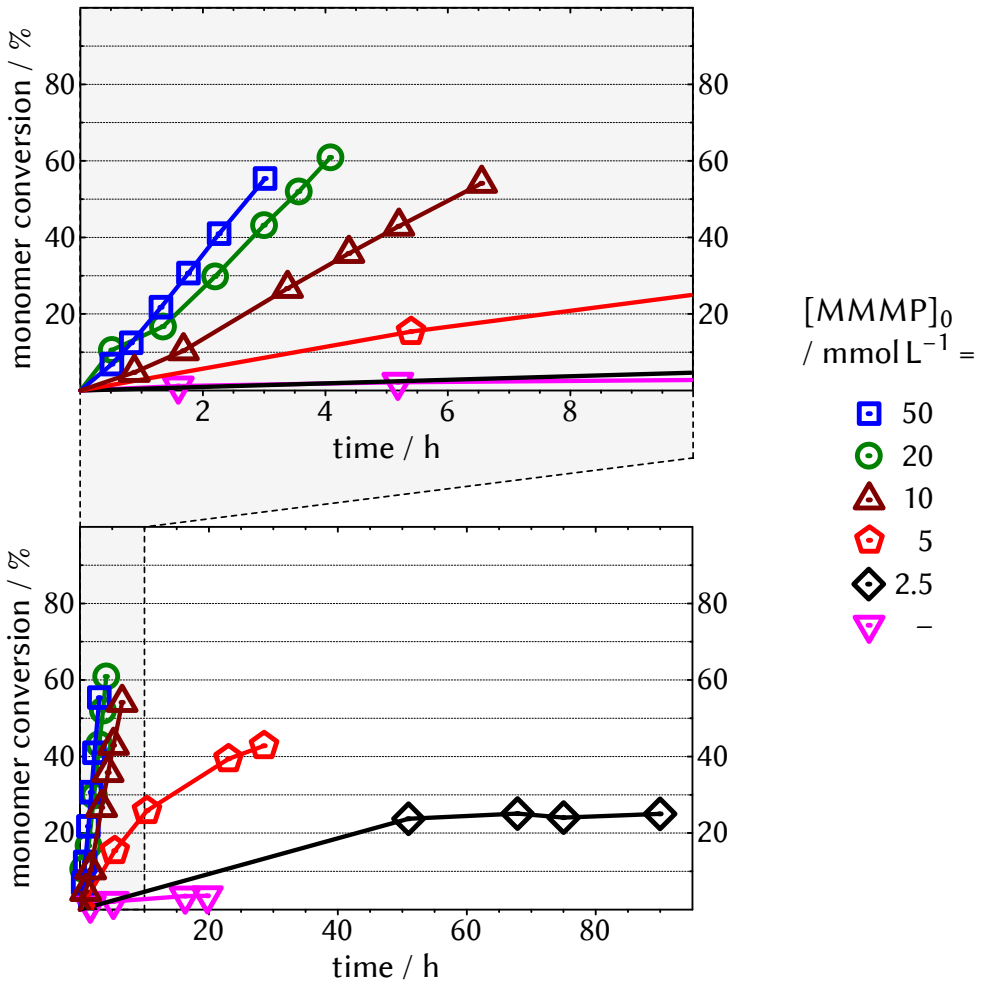

Figure 4.20 Monomer conversion as a function of time (for reasons of clarity with two different scalings) for different $[MMMP]_0$ of UV-initiated iodine-mediated polymerizations of BMA in bulk at 22 °C (based on entry 2 in Table 4.11 on page 102).

similar reactivities of CP–I and polyBMA–I toward C–I-bond cleavage, no pronounced inhibition period is observed even for lower $[MMMP]_0$. However, as $[MMMP]_0$ decreases, polymerization rates reasonably decrease as well. In case of $[MMMP]_0 = 2.5\,\text{mmol}\,\text{L}^{-1}$, radical generation is too low to complete polymerization, which stops early at 25 % of monomer conversion, accompanied by an emerging reddish color of inhibiting I_2. Without MMMP, the system only reaches 4 % of monomer conversion (via $CP^\bullet$) after 20 h. $\overline{M}_n$ values are again close to $\overline{M}_{n,theo}$ and almost independent of $[MMMP]_0$. In contrast, $Đ$ is significantly smaller for low $[MMMP]_0$, de-

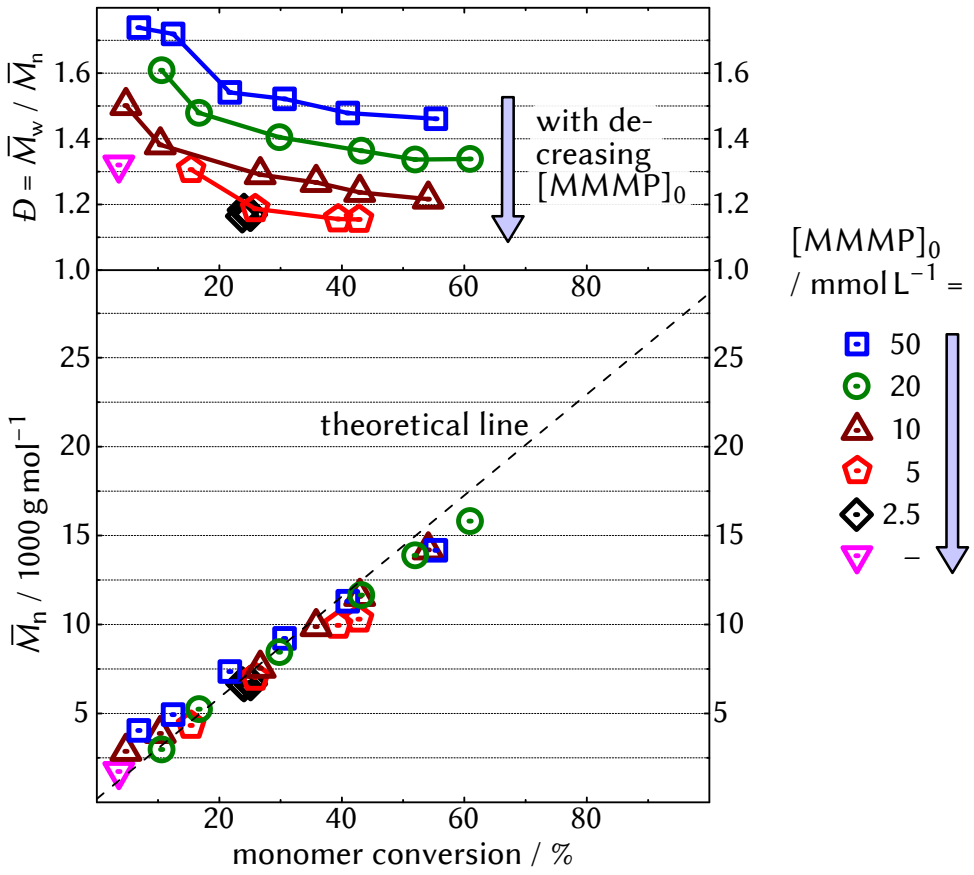

Figure 4.21 $\overline{M}_n$ and $Đ$ as a function of monomer conversion of the polymerizations presented in Figure 4.20 on the previous page.

creasing from 1.48 (50 mmol L^{-1}) to 1.15 (5 mmol L^{-1}) at 40 % of monomer conversion, while comparable thermally initiated ITP systems give $Đ > 1.6$ at that point.[25] This is remarkable not only because of the high extent of chain-growth control for an iodine-mediated system but also because of the fact that $\overline{M}_n$ and $Đ$ versus monomer conversion should be more or less independent of the initiator concentration (and polymerization rate) in systems governed by DT alone, if radical termination in not overwhelmingly pronounced.[18,49,64,65] Indeed, this is not the case for RT-based systems, which have shown to feature improved molar-mass control for lower polymerization rates under ideal polymerization conditions.[72–74,168] This effect was briefly discussed in Section 2.4.3.2 on page 24. Thus, the here observed impact of [MMMP]$_0$ indicates the existence of a significant RT mechanism

activation reactions of polymer–I

DT: (a) $\text{polymer–I} + \text{polymer}^\bullet \xrightarrow{k_{ex}} \text{polymer}^\bullet + \text{polymer–I}$

RT: (b) $\text{polymer–I} \xrightarrow{k_{hc}} \text{polymer}^\bullet + \text{I}^\bullet$

deactivation reactions of polymer$^\bullet$

DT: (c) $\text{polymer}^\bullet + \text{polymer–I} \xrightarrow{k_{ex}} \text{polymer–I} + \text{polymer}^\bullet$

RT: (d) $\text{polymer}^\bullet + \text{I}^\bullet \text{ (or } \text{I}_2\text{)} \xrightarrow{k_{iod}} \text{polymer–I (+ I}^\bullet\text{)}$

Scheme 4.6 Activation and deactivation reactions of living chains via DT and RT with respective rate coefficients.

introduced by homolytic C–I-bond cleavage, which will be more deeply discussed in the following.

Scheme 4.6 shows the general activation and deactivation reactions for living chains in the present system, which potentially occur either via DT or RT. The rate coefficients of the homolytic cleavage reaction, k_{hc}, and of the reversible termination reaction with free iodine, k_{iod}, correspond to k_a and k_{da} in Scheme 2.3 on page 13, respectively. The pseudo-first-order activation and deactivation rate coefficients k_{act} and k_{deact} (Scheme 2.2 on page 12) are given by

$$k_{act} = \underbrace{k_{ex} \cdot [\text{polymer}^\bullet]}_{\text{DT}} + \underbrace{k_{hc}}_{\text{RT}} \quad \text{and} \tag{4.5}$$

$$k_{deact} = \underbrace{k_{ex} \cdot [\text{polymer–I}]}_{\text{DT}} + \underbrace{k_{iod} \cdot ([\text{I}^\bullet] + [\text{I}_2])}_{\text{RT}} \,. \tag{4.6}$$

When more MMMP is used, [polymer$^\bullet$] is higher. According to Scheme 4.6d, this leads to a lower concentration of free iodine, what directly deacreases the crucial deactivation rate (Equation 4.6).[49] Estimation of k_{deact} would be possible if both [I$^\bullet$] and [I_2] during polymerization were known; however, concentrations were too low to be detected via UV/vis spectroscopy. In a typical ITP system, k_{ex} is of the order of 10^2–10^3 L mol^{-1} s^{-1},[8,18] while [polymer–I] is determined by $[CTA]_0$ and about 10^{-2} mol L^{-1}. Therefore, to hypothetically double k_{deact} in comparison to sole DT (which is the case for equal contributions of DT and RT), when k_{iod} is about 10^{10} L mol^{-1} s^{-1},[102–104] the sum of [I$^\bullet$] and [I_2] has to be in the region of 10^{-10}–10^{-9} mol L^{-1}. This demon-

Table 4.13 UV-initiated iodine-mediated polymerizations at 22 °C not shown in any figure for different monomers (mon.) and initiators (ini.). Exemplary data are given for the highest monomer conversion (mon. conv.).

entry	mon.	ini.	$[\text{mon.}]_0/[\text{ini.}]_0/[\text{CP–I}]_0$ / mmol L^{-1}	mon. conv. / %	$\overline{M}_n$ ($\overline{M}_{n,theo}$) / g mol^{-1}	$Đ$
1	MMA	MMMP	9000 (bulk)/20/45	53 [a]	8300 (10 800)	1.26
2	BMA	AIBN	6200 (bulk)/100/31	75 [b]	17 000 (21 300)	1.34
3	BMA	MMMP	4000 (in toluene)/10/20	92 [c]	22 100 (26 200)	1.36

[a] after 11.1 h; [b] after 9.5 h; [c] after 21.8 h.

strates that free iodine can have a significant impact on chain-growth control even in the ppb or ppt regime and also gives a possible explanation why no signals could be detected even by the rather sensitive UV/vis-spectroscopic method. In order to further shine light on the observed effects for different $[\text{MMMP}]_0$ and to get a deeper insight into the kinetics of the present system, kinetic simulations were performed and will be presented in the following section.

As a side note, the photosystems are not limited to the employment of BMA and MMMP, and polymerizations of MMA (Table 4.13, entry 1) and the use of AIBN (entry 2) lead to similar results. In this context, solution polymerization of BMA in toluene is also viable (entry 3). There, lower viscosities compared to bulk systems even allow for sample taking at higher monomer conversion.

4.3.5 Simulations and kinetic considerations

Similar to the kinetic simulations for polymerizations of BA in Section 4.2.6 on page 85, the here presented simulations were conducted with the program package Predici©. In this context, the polymerization systems in Figure 4.21 on page 108 with $[\text{MMMP}]_0$ = 10, 20, and 50 mmol L^{-1} served as a basis for the choice of initial concentrations and the later determination of reaction-rate coefficients. Before the results will be discussed, the simulation model will be concisely presented in the following.

4.3.5.1 Simulation details

The implemented reactions and their respective rate coefficients are given in Scheme 4.7 on the facing page and Table 4.14 on page 112. As for the simulations of BA polymerization, Scheme 4.7a shows the reactions present

(a) conventional radical polymerization

radical formation & initiation

$$\text{(I)}\quad \text{MMMP} \xrightarrow{k_{dec}} \text{In}^\bullet + \text{In}^\bullet$$

$$\text{(II)}\quad \text{In}^\bullet + \text{BMA} \xrightarrow{k_{ini}} \text{polyBMA}^\bullet(1)$$

propagation

$$\text{(III)}\quad \text{polyBMA}^\bullet(i) + \text{BMA} \xrightarrow{k_p} \text{polyBMA}^\bullet(i+1)$$

irreversible termination

$$\text{(IV)}\quad \begin{matrix}\text{polyBMA}^\bullet(i)\\ +\ \text{polyBMA}^\bullet(j)\end{matrix} \xrightarrow[=k_t(i,i);\ i\approx j]{k_t} \begin{matrix}\delta_t \times \text{polyBMA}_{dead}(i)\\ +\ \text{polyBMA}_{dead}(j)\\ \&\\ (1-\delta_t) \times \text{polyBMA}_{dead}(i+j)\end{matrix}$$

(b) iodine-transfer polymerization (without irradiation)

pre-equilibrium degenerative chain-transfer

$$\text{(V)}\quad \text{polyBMA}^\bullet(i) + \text{CP–I} \xrightarrow{k_{ex}} \text{polyBMA–I}(i) + \text{CP}^\bullet$$

$$\text{(VI)}\quad \text{polyBMA–I}(i) + \text{CP}^\bullet \xrightarrow{k_{ex}} \text{polyBMA}^\bullet(i) + \text{CP–I}$$

reinitiation

$$\text{(VII)}\quad \text{CP}^\bullet + \text{BMA} \xrightarrow{k_{ini}} \text{polyBMA}^\bullet(1)$$

main equilibrium degenerative chain-transfer

$$\text{(VIII)}\quad \begin{matrix}\text{polyBMA}^\bullet(i)\\ +\ \text{polyBMA–I}(j)\end{matrix} \xrightarrow{k_{ex}} \begin{matrix}\text{polyBMA–I}(i)\\ +\ \text{polyBMA}^\bullet(j)\end{matrix}$$

(c) irradiated iodine-mediated polymerization

homolytic C–I-bond cleavage

$$\text{(IX)}\quad \text{CP–I} \xrightarrow{k_{hc}} \text{CP}^\bullet + \text{I}^\bullet$$

$$\text{(X)}\quad \text{polyBMA–I}(i) \xrightarrow{k_{hc}} \text{polyBMA}^\bullet(i) + \text{I}^\bullet$$

combination

$$\text{(XI)}\quad \text{I}^\bullet + \text{I}^\bullet \xrightarrow{k_{iod}} \text{I}_2$$

reversible termination

$$\text{(XII)}\quad \text{polyBMA}^\bullet(i) + \text{I}^\bullet \xrightarrow{k_{iod}} \text{polyBMA–I}(i)$$

$$\text{(XIII)}\quad \text{polyBMA}^\bullet(i) + \text{I}_2 \xrightarrow{k_{iod}} \text{polyBMA–I}(i) + \text{I}^\bullet$$

Scheme 4.7 Reactions and corresponding rate coefficients implemented for the simulations of UV-initiated iodine-mediated polymerizations of BMA in bulk at 22 °C (for the values of the coefficients see Table 4.14 on the next page).

Table 4.14 Kinetic parameters for the simulations of UV-initiated iodine-mediated polymerization of BMA in bulk at 22 °C (see Scheme 4.7 on the previous page for the respective reactions).

coefficient	value	reference
k_{dec}	$1.0 \times 10^{-5}\,s^{-1}$	–
k_{ini}	$3370\,L\,mol^{-1}\,s^{-1} = 10 \times k_p$	155,156,169
k_p	$337\,L\,mol^{-1}\,s^{-1}$	169
k_t	$1.8 \times 10^8 \cdot i^{-0.65}\,L\,mol^{-1}\,s^{-1}$ $(i \leq 50)$ $3.1 \times 10^7 \cdot i^{-0.20}\,L\,mol^{-1}\,s^{-1}$ $(i > 50)$	141
δ_t	0.6	98,110
k_{ex}	$1.2 \times 10^3\,L\,mol^{-1}\,s^{-1}$	–
k_{hc}	$4.0 \times 10^{-4}\,s^{-1}$	–
k_{iod}	$10^{10}\,L\,mol^{-1}\,s^{-1}$	102–104
$[BMA]_0$	$6.2\,mol\,L^{-1}$	–
$[CP{-}I]_0$	$31 \times 10^{-3}\,mol\,L^{-1}$	–
$[MMMP]_0$	10, 20, or $50 \times 10^{-3}\,mol\,L^{-1}$	–

in a (conventional) radical polymerization system. The k_p value is taken from the literature,[169] while again, $k_{ini} = 10 \times k_p$.[155,156] The chain-length-dependent k_t value is taken from the literature as well,[141] while δ_t gives the fraction of termination via disproportionation and $1 - \delta_t$ via combination (cf. Equation 2.2 on page 10).[98,110] Database values of k_{dec} do not exist, since it is highly influenced by characteristics of the individual photosystem (e. g., competing reagent absorption, light intensity and scattering, quantum efficiency).[170] Therefore, it was obtained by modeling the evolution of monomer conversion versus time in the low-conversion regime (< 20 %) for the three different $[MMMP]_0$ values.

As described for BA, the conventional reactions are superimposed by the common reactions for the DT mechanism when CP–I is added to the system (Scheme 4.7b). In this context, all three iodine-transfer reactions (Reaction V, VI, and VIII) are expressed via a single rate coefficient, k_{ex}, because in all three reactions, the iodine atom is exchanged between two methacrylic-type radicals (cf. Scheme 2.7 on page 18). The k_{ex} value was determined via the exchange constant C_{ex} $(= k_{ex}/k_p)$ by modeling experimentally obtained $\overline{M}_n$ values of a polymerization of BMA with CP–I and AIBN in the absence of light (and therefore RT) at 60 °C with Predici© simulations (see Appendix A.2.1 on page 231). As shown in Section 2.4.3.1 on page 20, in DT,

$\overline{M}_n$ values are crucially influenced by the CTA's transfer constant C_{tr} (= C_{ex} in this case), thus making them frequently used for its calculation.[18,64,65] C_{ex} was estimated to be 3.6, being in good agreement with other ITP systems normally showing values slightly higher than unity[8] (e. g., C_{ex} = 2.6 for MMA in solution at 80 °C).[25] As mentioned above, temperature dependence of C_{ex} is expected to be small[59] and therefore, C_{ex} = 3.6 was also chosen for the simulation system at 22 °C, resulting in the presented k_{ex} value.

When the system is now irradiated, homolytic C–I-bond cleavage of (IX) CP–I and (X) polyBMA–I occurs. Because of the above-mentioned chemical similarity of the resulting radicals, both reaction rates are described with the same coefficient, k_{hc}. Like k_{dec}, k_{hc} highly depends on the characteristics of the individual system. To get an idea about the order of magnitude of k_{hc}, a model solution of CP–I in toluene saturated with air was irradiated. Under these conditions, CP–I decomposes to form CP$^\bullet$ and I_2, while the back reaction is suppressed because CP$^\bullet$ reacts much more likely with the present scavenging oxygen than with free iodine, especially for small iodine concentrations. The accumulation of I_2 was then quantified via UV/vis spectroscopy, from which k_{hc} could be calculated (see Appendix A.2.2 on page 232). The resulting k_{hc} value was $1.8 \times 10^{-4}\,s^{-1}$, whereas the value eventually used to better match experimental results is slightly higher. The residual reactions represent (XI) reversible self-termination of I$^\bullet$ and reversible termination of polyBMA$^\bullet$ with either (XII) I$^\bullet$ or (XIII) I_2, which are all supposed to be very fast ($\approx 10^{10}\,L\,mol^{-1}\,s^{-1}$),[102–104] as frequently stated above.

4.3.5.2 Simulation results

Comparison with experimental results

Simulations were conducted for $[MMMP]_0$ = 10, 20, and 50 mmol L^{-1}, while initial concentrations of all other reagents and all rate coefficients remained constant. Simulation results in comparison to the experimental ones are shown in Figure 4.22 on the next page. The simulated $\overline{M}_n$ values show similar trends with a slight downward deviation from $\overline{M}_{n,theo}$ for high monomer conversion, which is more pronounced for higher $[MMMP]_0$, thus supporting that this effect is mainly caused by irreversible termination and continuous conventional initiation (indeed, no downward deviation was observed for the hypothetical case of k_t = 0; data not shown). For low monomer conversion, $\overline{M}_n$ is slightly closer to $\overline{M}_{n,theo}$ when $[MMMP]_0$ is low,

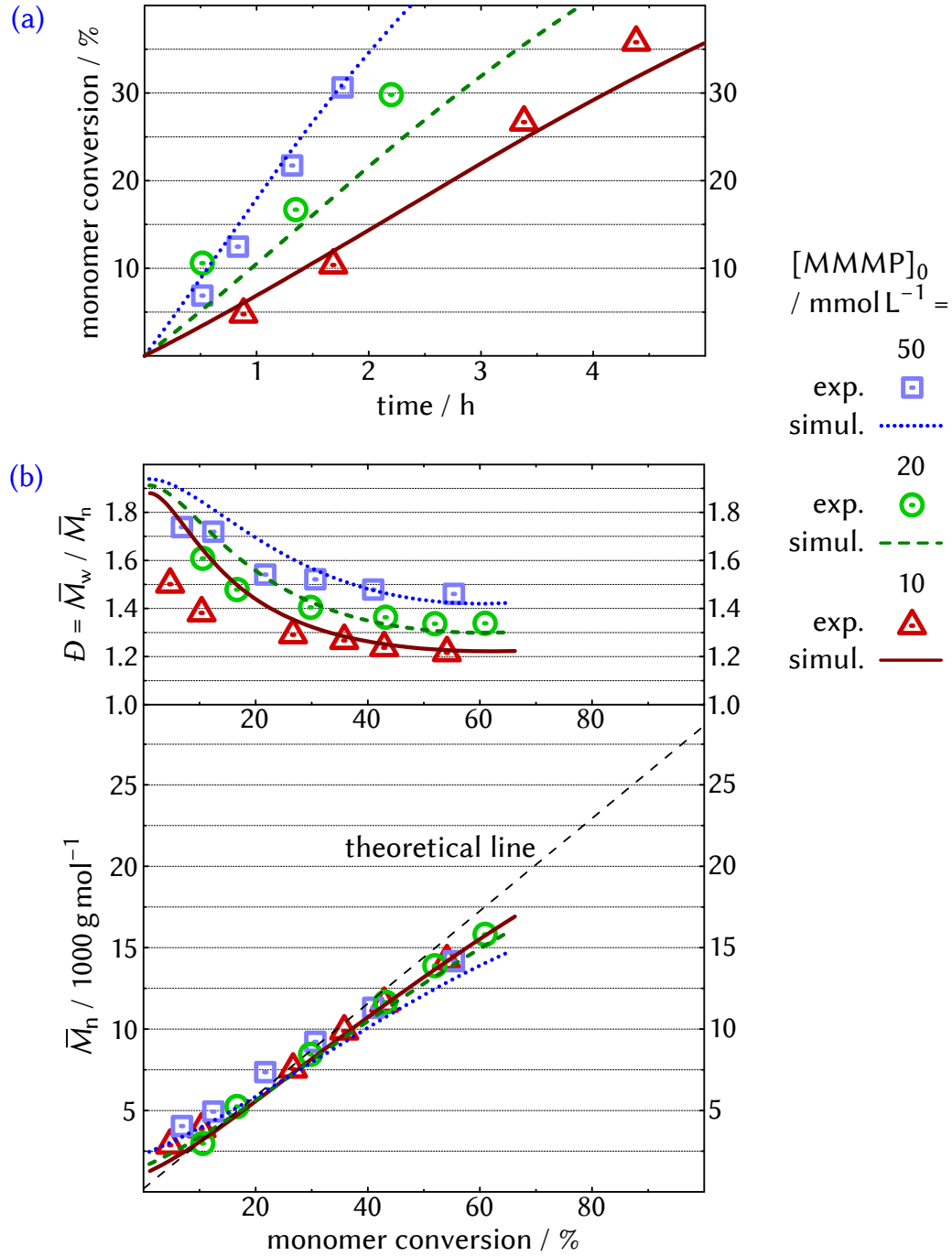

Figure 4.22 (a) Simulated monomer conversion as a function of time and (b) simulated $\overline{M}_n$ and $Đ$ values as a function of monomer conversion of UV-initiated iodine-mediated polymerizations of BMA in bulk at 22 °C for different $[MMMP]_0$ as indicated in comparison to the respective experimental results (for simulation model see Scheme 4.7 on page 111 and Table 4.14 on page 112).

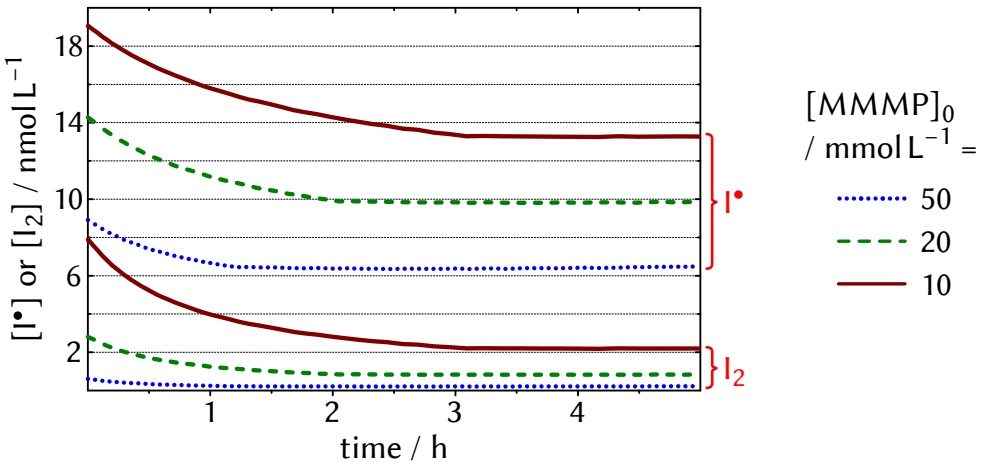

Figure 4.23 Simulated concentrations of free iodine ($I^\bullet + I_2$) versus time of the simulations shown in Figure 4.22 on the preceding page for different $[MMMP]_0$ as indicated.

which already indicates higher control of chain growth at an early state. Simulated $Đ$ values confirm the experimental finding of narrower MMDs for low $[MMMP]_0$. In this context, the simulations display the extent of decrease very closely. Evolution of monomer conversion versus time agrees well with the experiments, leading to reliable values of [polyBMA•], which are crucial for the amount of free iodine in the system, as already discussed. It should again be noted that the excellent match of the experimental results is achieved by a simple simulation model consisting of long-known reaction steps and reasonable rate coefficients. In addition, the experimental trends can be reproduced by just varying $[MMMP]_0$ and leaving the rest of the model unchanged, thus supporting the validity of the simulation system.

Reversible termination with free iodine

Simulated concentrations of $I^\bullet$ and I_2 throughout the polymerizations are given in Figure 4.23. Both $[I^\bullet]$ and $[I_2]$ are in the nanomolar region and become stationary after a medium period of time, clarifying the RT equilibrium between the continuous consumption of free iodine by polyBMA• and the incessant release of free iodine by C−I-bond cleavage. The initially higher iodine concentrations are assigned to chain-length-dependent k_t, leading to lower [polyBMA•] at the beginning of the polymerization, when chains are still short. Exact simulated values of $[I^\bullet] + [I_2]$ and [polyBMA•] are given in

Table 4.15 Simulated concentrations of polyBMA$^\bullet$ and free iodine ($I^\bullet + I_2$) and calculated overall k_{deact} values (k_{deact}(DT+RT)) and k_{deact} by DT only (k_{deact}(DT)) for the systems with given $[MMMP]_0$ at low and high monomer conversion (mon. conv.).

$[MMMP]_0$ / mmol L^{-1}	mon. conv. [a]	[polyBMA$^\bullet$] / nmol L^{-1}	$[I^\bullet] + [I_2]$ / nmol L^{-1}	k_{deact}(DT+RT) [b] / s^{-1}	k_{deact}(DT+RT) / k_{deact}(DT) [b]
50	low	130.2	9.5	132.5	3.5
50	high	188.9	6.7	104.5	2.8
20	low	72.4	17.0	207.7	5.5
20	high	115.5	10.7	144.6	3.8
10	low	46.0	26.8	305.7	8.1
10	high	80.2	15.4	192.1	5.1

[a] Low for $t = 0$ h, high for $t = 5$ h; [b] via Equation 4.6 on page 109.

Table 4.15. The higher [polyBMA$^\bullet$] is, the lower is $[I^\bullet] + [I_2]$, while the RT equilibrium between dormant and active chains,

$$k_{hc} \cdot [\text{polyBMA}{-}I] = k_{iod} \cdot [\text{polyBMA}^\bullet] \cdot ([I^\bullet] + [I_2]) \ , \qquad (4.7)$$

is validated for every $[MMMP]_0$ at low and high conversion by the RT-equilibrium constant

$$K_{RT} = \frac{k_{hc}}{k_{iod}} = \frac{[\text{polyBMA}^\bullet] \cdot \left([I^\bullet] + [I_2]\right)}{[\text{polyBMA}{-}I]} = 4 \times 10^{-14} \, \text{mol L}^{-1} \ , \qquad (4.8)$$

with $[\text{polyBMA}{-}I] = [\text{CP}{-}I]_0 = 31$ mmol L^{-1}. Via Equation 4.6 on page 109, overall k_{deact} values, k_{deact}(DT+RT), were calculated for each case. They were compared to k_{deact} values for sole DT, k_{deact}(DT), via the ratio k_{deact}(DT+RT)/k_{deact}(DT), which is a measure of how much faster the overall deactivation is compared to the system without RT. In this context, values vary from a 2.8-fold deactivation (high $[MMMP]_0$, high conversion) to an 8.1-fold deactivation (low $[MMMP]_0$, low conversion). In other words, in the latter case, polyBMA$^\bullet$ is deactivated by free iodine rather than by polyBMA–I in 7 out of 8 times. Hypothetically, in order for polyBMA–I (or CP–I) to lead to an 8.1-fold higher k_{deact} via the DT mechanism alone, C_{ex} had to increase to about 29 (e. g., $C_{tr} \approx 25$ for 2-(2′-cyanopropyl)dithiobenzoate in a representative RAFT polymerization of MMA at 60 °C).[171] This illustrates why considerably improved control of chain growth is observed in the conducted photopolymerizations. In addition, especially compared

to the conventional DT-based ITP system. It is a matter of course that for $[MMMP]_0 < 10\,mmol\,L^{-1}$ and hence lower polymerization rates, k_{deact} would be even higher.

4.3.5.3 Polymerization rate versus molar-mass control

As pointed out by both experiments and simulations, the counterplay between [polyBMA$^\bullet$] and molar-mass control is evident. As the polymerization rate increases, molar-mass control decreases. On the other hand, high control is achieved for low [polyBMA$^\bullet$] and slow polymerization. In this context, the natural limit is reached when the extent of radical formation is too low to overcome the incessant formation of I_2, as can be seen for $[MMMP]_0 = 2.5\,mmol\,L^{-1}$ in Figure 4.20 on page 107. No deviation from this relationship between polymerization rate and molar-mass control could be observed when the potential RTCP catalysts $(EtO)_2P(O)H$ and NIS were added to the system with $[MMMP]_0 = 50\,mmol\,L^{-1}$ (data not shown). The addition of $(EtO)_2P(O)H$ gave polymerization rates and molar-mass evolution very similar to the catalyst-free system. For the iodo catalyst NIS, inhibition was observed which was followed by a slightly lower polymerization rate in comparison to the catalyst-free system, which led to slightly lower $Đ$ values. These results indicate that for the presented polymerization conditions, a potential impact of RTCP catalysts on molar-mass control is mainly due to influencing [polyBMA$^\bullet$] rather than by a superimposed RTCP mechanism.

Naturally, the requirements imposed on RDRPs are not only to maximize control of molar masses. Often, high polymerization rates are desired as well—especially from an economical point of view. Therefore, when applying the presented photosystem, a reasonable compromise can be individually made between the intended control and the intended rate of polymerization, depending on its purpose. In this context, a way to obtain faster polymerization without suffering from lower control of chain growth will be pointed out in the next section.

4.3.6 Impact of irradiation

To experimentally clarify the influence of C−I-bond cleavage and RT, a system was investigated which is able to produce polymer even in the absence of irradiation. For this, polymerizations of BMA with CP−I and the conventional initiator AIBN were conducted (i) at 60 °C in the dark and (ii) at 60 °C

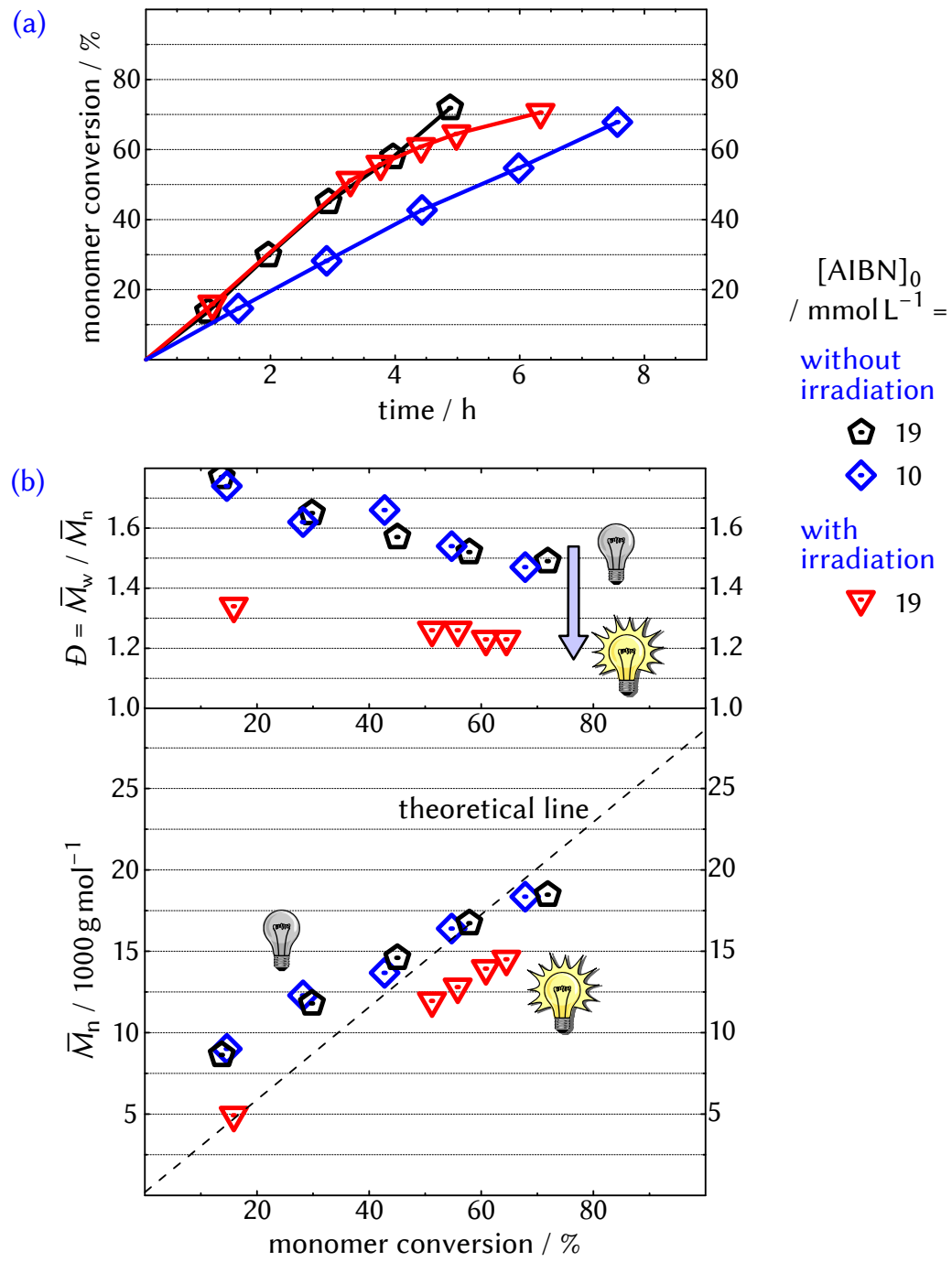

Figure 4.24 (a) Monomer conversion as a function of time and (b) $\overline{M}_n$ and $Đ$ as a function of monomer conversion of iodine-mediated polymerizations of BMA in bulk at 60 °C with and without UV irradiation (see Table 4.16 on the next page, entries 1 to 3).

Table 4.16 Initial concentrations of substances used for iodine-mediated polymerizations of BMA in bulk at 60 °C with and without UV irradiation.

entry	$[BMA]_0$ / mol L^{-1}	$[CP{-}I]_0$ / mol L^{-1}	ini.[a]	$[ini.]_0$ / mol L^{-1}	irradiation
1 (⬠)[b]	5.9	30×10^{-3}	AIBN	19×10^{-3}	no
2 (◇)[b]	5.9	30×10^{-3}	AIBN	10×10^{-3}	no
3 (▽)[b]	5.9	30×10^{-3}	AIBN	19×10^{-3}	yes
4[c]	5.9	30×10^{-3}	MMMP	10×10^{-3}	yes

[a] Initiator; [b] see Figure 4.24 on the preceding page; [c] exemplary sample for highest monomer conversion = 67 % after t = 9.7 h: $\overline{M}_n$ = 16 200 g mol^{-1} ($\overline{M}_{n,theo}$ = 19 000 g mol^{-1}), $Đ$ = 1.20.

while irradiated with UV light (see Table 4.16, entries 1 to 3). In this context, it should be stated that potential thermally initiated C–I-bond cleavage can indeed be ruled out here as no formation of I_2 could be detected when a solution of CP–I in toluene was heated at 85 °C for 2 h inside a UV/vis spectrometer (data not shown). The results of the polymerizations are given in Figure 4.24 on the preceding page. For the two polymerizations without irradiation, $Đ$ values are mainly over 1.5, while $\overline{M}_n$ values are much higher than $\overline{M}_{n,theo}$ at low monomer conversion, which is expected for a system solely governed by DT and in close agreement with comparable systems from the literature.[25] The polymerization rates of the two systems are similar to the UV systems in Figure 4.21 on page 108 for $[MMMP]_0$ = 10 and 20 mmol L^{-1}. However, without irradiation, the different polymerization rates do not have a significant impact on both $Đ$ and $\overline{M}_n$, according to the principles of DT.[49,64,65] When the system is additionally irradiated, $Đ$ is remarkably lower throughout the polymerization and values of about 1.2 are reached for high conversion. Furthermore, $\overline{M}_n$ is very close to $\overline{M}_{n,theo}$ at low monomer conversion, indicating promoted activation of CP–I by C–I-bond cleavage. Conveniently, the boost in controlling chain growth is achieved retaining the fairly high polymerization rate of the nonirradiated system. This shows that elevated temperatures might be an option to accelerate polymerization and still have rather high control of chain growth (considering that the polymerization rate is almost as high as for the system with $[MMMP]_0$ = 50 mmol L^{-1} in Figure 4.21 on page 108, which only gives $Đ > 1.4$).

Table 4.17 Initial concentrations of substances used for UV-initiated iodine-mediated polymerizations of BMA in bulk at 22 °C for different $[CP{-}I]_0$ and therefore $\overline{DP}_{n,target}$.

entry[a]	$[BMA]_0$ / mol L^{-1}	$[CP{-}I]_0$ / mol L^{-1}	$[MMMP]_0$ / mol L^{-1}	$\overline{DP}_{n,target}$
1 (□)	6.2	62×10^{-3}	40×10^{-3}	100
2 (○)	6.2	21×10^{-3}	7.5×10^{-3}	300
3 (△)	6.2	12×10^{-3}	4.0×10^{-3}	500
4 (⬠)	6.2	6.2×10^{-3}	2.5×10^{-3}	1000
5 (◇)	6.2	3.1×10^{-3}	1.5×10^{-3}	2000

[a] See Figure 4.25 on the next page.

The results show that UV irradiation can be applied as boost to conventional ITP systems without changing any of the conditions or substances employed. On the other hand, it makes clear that special experimental care has to be taken when studying into the kinetics of ITP systems or the impact of additional reactants on the control of chain growth. Ideally, these studies are carried out in the dark so that the results do not depend on the type of ambient light or time of the day, for example. Of course, polymerization at 60 °C can also be conducted using the solely photosensitive initiator MMMP (see Table 4.16 on the preceding page, entry 4), retaining the advantages of a photoswitchable system.

4.3.7 Toward higher molar masses

The potential to synthesize high-molar-mass polymer with the presented method was tested as well. Photopolymerizations at 22 °C were conducted for different $[CP{-}I]_0$, targeting $\overline{DP}_n$ values from $\overline{DP}_{n,target} = 100$ to 2000 for full monomer conversion (corresponding to $\overline{M}_n$ values from 14 000 to 280 000 g mol^{-1}). $[MMMP]_0$ was adjusted for each system so as to obtain similar polymerization rates. For example, $[MMMP]_0 = 1.5$ mmol L^{-1} leads to smooth polymerization in case of $\overline{DP}_{n,target} = 2000$, whereas almost no conversion is observed for $\overline{DP}_{n,target} = 100$, which can be ascribed to a combination of the higher amount of CP–I (and potential free iodine) and the more pronounced chain-length-dependent termination. The polymerization systems are given in Table 4.17 and the results are shown in Figure 4.25 on the next page. Again, $\overline{M}_n$ values are (slightly) lower than the respective $\overline{M}_{n,theo}$

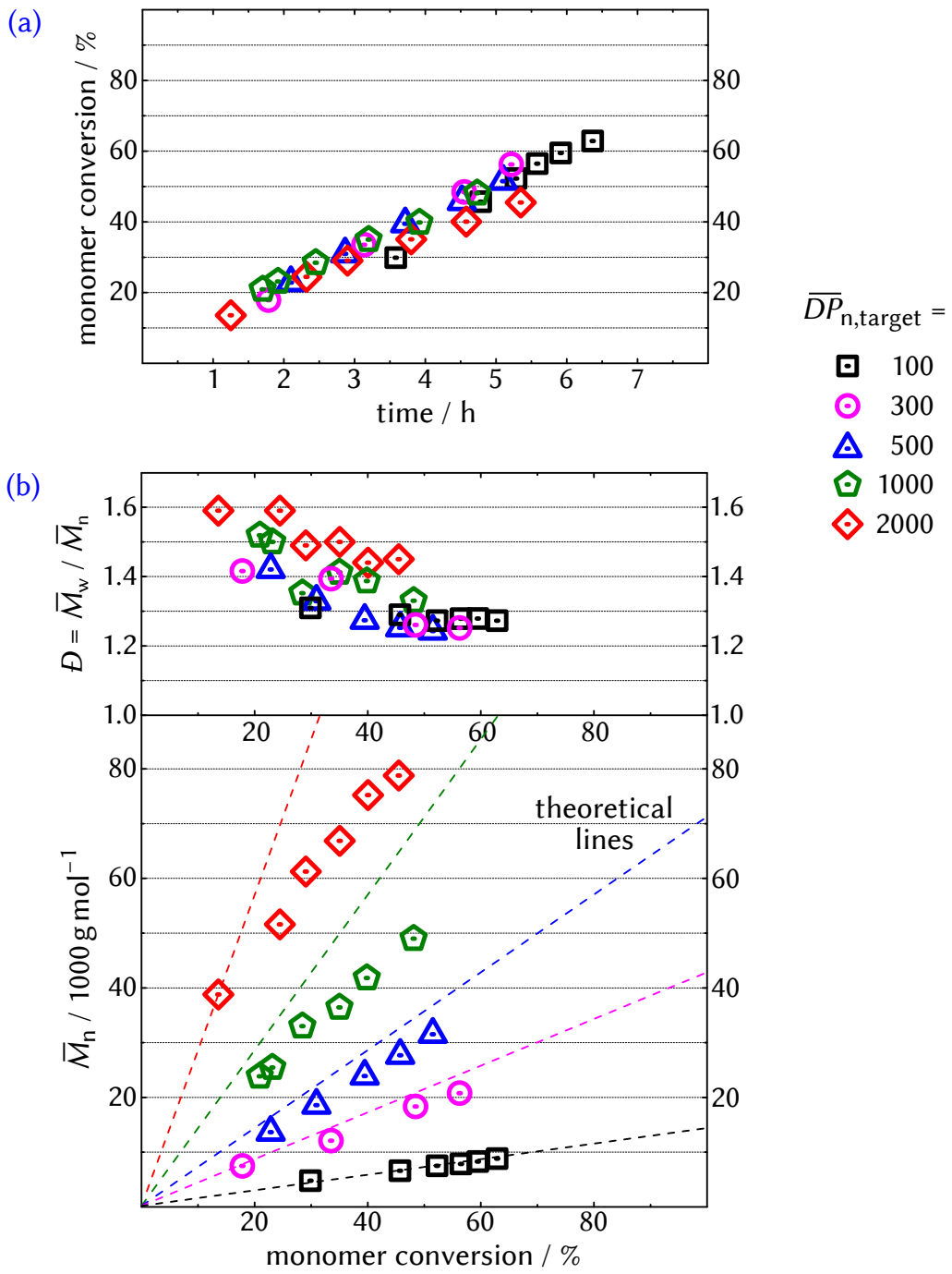

Figure 4.25 (a) Monomer conversion as a function of time and (b) $\overline{M}_n$ and $Đ$ as a function of monomer conversion of UV-initiated iodine-mediated polymerizations of BMA in bulk at 22 °C for different $[CP-I]_0$ and therefore $\overline{DP}_{n,target}$ (see Table 4.17 on the preceding page).

values. For the highest molar masses ($\overline{DP}_{\mathrm{n,target}} = 2000$), BB during SEC analysis is indeed expected to significantly participate in this effect. In this context, for $\overline{M}_{\mathrm{n}} > 60\,000\ \mathrm{g\,mol^{-1}}$, downward deviations of the experimentally obtained $\overline{M}_{\mathrm{n}}$ values from the true ones can be estimated to be about 7 %. Generally narrow MMDs are obtained, while for $\overline{DP}_{\mathrm{n,target}} = 2000$, $Đ$ values start to be significantly higher from an early stage. However, still $Đ < 1.5$ is obtained for $\overline{M}_{\mathrm{n}} > 60\,000\ \mathrm{g\,mol^{-1}}$ and monomer conversion > 30 %, showing the potential of this method to reach fairly high molar masses retaining good control. It is expected that the systems can be individually tweaked by using even lower $[\mathrm{MMMP}]_0$ according to Figure 4.22 on page 114.

4.3.8 Conclusions on BMA polymerizations

Similar to BA, iodine-mediated photopolymerizations of BMA were shown to be highly feasible by the straightforward utilization of a conventional UV initiator. In this regard, the incessant formation of I_2 is indeed higher for BMA as C–I-bond cleavage is more pronounced for the tertiary C–I bond in polyBMA–I than for the secondary one in polyBA–I.[144] In fact, it is often shied away from this effect by conducting polymerizations in the dark as significant formation of I_2 is generally related to a quick inhibition of polymerization. However, if I_2 formation is kept in check, pronounced C–I-bond cleavage is actually one of the major advantages of the system. As it was presented by both experiments and kinetic simulations, it led to a significant introduction of RT, which superimposes the classic DT mechanism of ITP systems. As the initiator concentration was reduced, polymerization rates decreased, RT became more pronounced, and chain growth was more controlled.

Notably, when the initiator concentration was reduced in case of BA, only longer inhibition or even no polymerization at all was observed, while polymerization was almost equally fast once inhibition was over. Considering that (i) C–I-bond cleavage is less pronounced for polyBA–I and (ii) propagation of polyBA$^{\bullet}$ is much faster, the crucial number of additional activation steps[49] of the dormant chains via RT is expected to be much lower compared to polyBMA–I throughout the polymerization process. This clarifies that UV irradiation is indeed highly applicable for iodine-mediated polymerizations of *meth*acrylates. In this context, the BMA system not only offers the general advantages of UV irradiation such as convenient control of radical flow or the potential to polymerize at low temperature without the need of a heating device. Here, UV irradiation even *significantly* increases

the crucial activation–deactivation frequency of living chains, resulting in higher control of chain growth. It should be noted that (i) this cannot be obtained for ITPs without irradiation and that (ii) for many other RDRP techniques, the activation–deactivation behavior of living chains is not affected at all by UV irradiation. Even worse, as some capping agents or CTAs might irreversibly decompose upon UV irradiation, it is sometimes highly undesired.[34] In this context, UV irradiation of ITP systems directly addresses arguably one of their major flaws, namely low molar-mass control, while fully retaining their numerous advantages.

4.4 Polymerizations of styrene

In the last part of the present chapter, UV-initiated iodine-mediated polymerizations of St will be briefly discussed. In contrast to polymerizations of BA and BMA, for which well-controlled molar-mass evolution was conveniently obtained for systems at room temperature, inherent problems arise for the slowly propagating St. This will be exemplarily demonstrated in the following.

4.4.1 Slow propagation

Compared to other monomer classes such as acrylates and methacrylates, radical propagation of St is rather slow. As the activation energy of the propagation reaction is relatively high for St, this holds especially true at low temperatures. For example, at 22 °C, the k_p value of St is 75 L mol^{-1} s^{-1},[172] of BMA is 336 L mol^{-1} s^{-1},[169] and of BA is 15 000 L mol^{-1} s^{-1}.[157] In combination with the fact that termination of polySt radicals, polySt$^\bullet$, is fast and k_t is high, this generally leads to low polymerization rates (cf. Equation 2.4 on page 11). As a matter of course, higher initiator concentrations can compensate for this effect and fast polymerization of St is feasible even at room temperature. However, this reveals the real issue for polymerizations of St at room temperature. While higher polymerization rates can be obtained for higher concentrations of initiator and thus polySt$^\bullet$, this leads to more pronounced termination ($\sim$ [polySt$^\bullet$]^2) compared to propagation ($\sim$ [polySt$^\bullet$]) and thus shorter chain lengths (cf. Equation 2.9 on page 15). While this trend is generally obtained for all monomer classes in RP, formation of *very short* chains is especially pronounced for low k_p and high k_t values, such as for St at room temperature.

Since the ITP mechanism does not replace but superimposes the conventional RP mechanism, this issue also exists for the here presented systems. In other words, for slow propagation and fast termination, the percentage of chains incessantly generated by the conventional initiator and the incessant formation of dead chains during the polymerization is higher, which results in low molar masses and a strong downward deviation of $\overline{M}_n$ from $\overline{M}_{n,theo}$. This effect was indeed proven to be very significant for the here investigated polymerizations of St at room temperature, which will be exemplarily shown in the following.

Table 4.18 Initial concentrations of substances used for UV-initiated iodine-mediated polymerizations of St with CP–I in bulk at 22 °C.

entry [a]	$[St]_0$ / mol L^{-1}	$[CP–I]_0$ / mol L^{-1}	$[MMMP]_0$ / mol L^{-1}
1 (⊡)	8.4	42×10^{-3}	50×10^{-3}
2 (⊙)	8.4	42×10^{-3}	250×10^{-3}

[a] See Figure 4.26 on the next page.

4.4.2 Polymerization results

Polymerizations of St in bulk were conducted at 22 °C using MMMP as the UV initiator and CP–I (high-concentration approach, as for BMA) as the CTA. The experimental setup was identical to the polymerizations of BA and BMA, while the distance of the polymerization mixture to the lamp was 7 cm. $[CP–I]_0$ was chosen to target $\overline{DP}_n = 200$ for full monomer conversion, which corresponds to $\overline{M}_n \approx 20\,000$ g mol^{-1}. In Table 4.18, the initial concentrations are given for slow ($[MMMP]_0 = 50$ mmol L^{-1}, entry 1) and rather fast polymerization ($[MMMP]_0 = 250$ mmol L^{-1}, entry 2).

Polymerization rate and molar-mass evolution

The resulting values of monomer conversion versus time as well as $\overline{M}_n$ and $Đ$ versus monomer conversion are given in Figure 4.26 on the next page. In this context, results of kinetic simulations are presented as well, which will be discussed below. For $[MMMP]_0 = 50$ mmol L^{-1}, polymerization is slow with 20 % of monomer conversion after almost 40 h. For $[MMMP]_0 = 250$ mmol L^{-1}, polymerization is faster with over 60 % of monomer conversion after almost 30 h. $\overline{M}_n$ values of both systems are close to $\overline{M}_{n,theo}$ at the beginning of the polymerization, indicating fast (re)initiation by CP–I. As polymerization proceeds, the above-mentioned effects of St polymerization at low temperature are clearly reflected in the obtained $\overline{M}_n$ values. Whereas for slow polymerization, $\overline{M}_n$ values close to $\overline{M}_{n,theo}$ are obtained, faster polymerization leads to a pronounced downward deviation from $\overline{M}_{n,theo}$. MMDs of both systems are rather broad with $Đ$ values slightly higher than 2.0. To demonstrate that the individual evolution of $\overline{M}_n$ values can be explained by the incessant formation of dead chains, kinetic simulations were conducted and will be presented in the following. In this context, the correlation between polymerization rate and $\overline{M}_n$ evolution is illustrated for the here presented polymerizations of St at 22 °C.

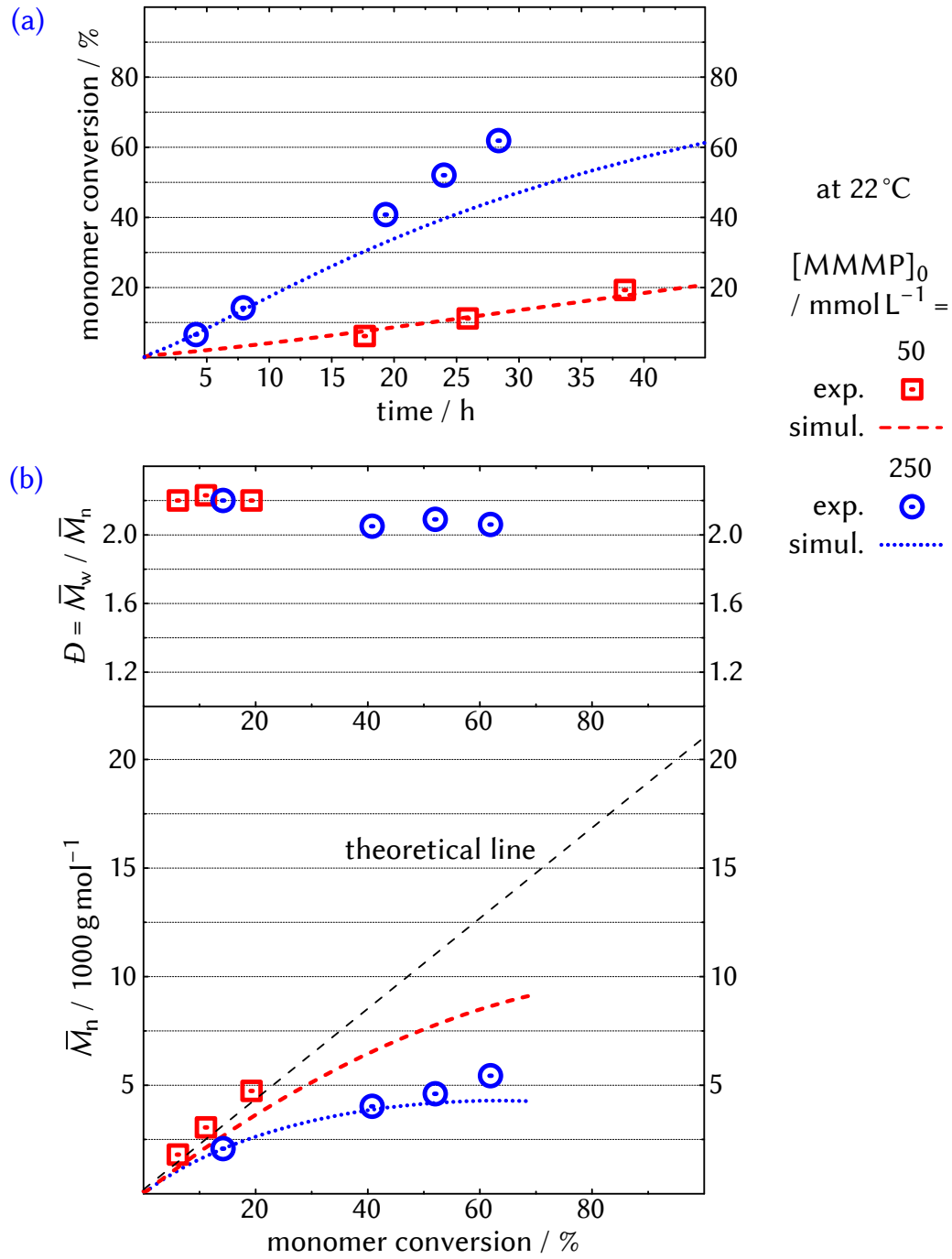

Figure 4.26 (a) Experimentally obtained (exp.) monomer conversion as a function of time and (b) $\overline{M}_n$ and $Đ$ as a function of monomer conversion of the UV-initiated iodine-mediated polymerizations of St with CP–I in bulk at 22 °C given in Table 4.18 on the preceding page in comparison to simulation (simul.) results (for simulation model see Scheme 4.8 on the next page and Table 4.19 on page 128).

(a) conventional radical polymerization

radical formation & initiation

(I) $\mathrm{MMMP} \xrightarrow{k_{dec}} \mathrm{In}^{\bullet} + \mathrm{In}^{\bullet}$

(II) $\mathrm{In}^{\bullet} + \mathrm{St} \xrightarrow{k_{ini}} \mathrm{polySt}^{\bullet}(1)$

propagation

(III) $\mathrm{polySt}^{\bullet}(i) + \mathrm{St} \xrightarrow{k_p} \mathrm{polySt}^{\bullet}(i+1)$

irreversible termination

(IV) $\mathrm{polySt}^{\bullet}(i) + \mathrm{polySt}^{\bullet}(j) \xrightarrow[= k_t(i,i);\ i \approx j]{k_t} \mathrm{polySt}_{dead}(i+j)$

(b) iodine-transfer polymerization

pre-equilibrium degenerative chain-transfer

(V) $\mathrm{polySt}^{\bullet}(i) + \mathrm{R{-}I} \xrightarrow{k_{ex}} \mathrm{polySt{-}I}(i) + \mathrm{R}^{\bullet}$

(VI) $\mathrm{polySt{-}I}(i) + \mathrm{R}^{\bullet} \xrightarrow{k_{ex}} \mathrm{polySt}^{\bullet}(i) + \mathrm{R{-}I}$

reinitiation

(VII) $\mathrm{R}^{\bullet} + \mathrm{St} \xrightarrow{k_{ini}} \mathrm{polySt}^{\bullet}(1)$

main equilibrium degenerative chain-transfer

(VIII) $\mathrm{polySt}^{\bullet}(i) + \mathrm{polySt{-}I}(j) \xrightarrow{k_{ex}} \mathrm{polySt{-}I}(i) + \mathrm{polySt}^{\bullet}(j)$

Scheme 4.8 Reactions and corresponding rate coefficients implemented for the simulations of iodine-mediated polymerizations of St in bulk at 22 °C (for the values of the coefficients see Table 4.19 on the following page).

4.4.3 Kinetic simulations

Similar to the previous sections, the here presented kinetic simulations were conducted with the program package Predici©. In this context, the two polymerization systems in Figure 4.26 on the facing page served as a basis for the simulation model. Before the results will be discussed, the simulation model will be concisely presented in the following.

Table 4.19 Kinetic parameters for the simulations of iodine-mediated polymerizations of St in bulk at 22 °C (see Scheme 4.8 on the preceding page for the respective reactions).

coefficient	value	reference
k_{dec} [a]	$8.5 \times 10^{-7}\,s^{-1}$	–
k_{dec} [b]	$2.5 \times 10^{-6}\,s^{-1}$	–
k_{ini}	$750\,L\,mol^{-1}\,s^{-1} = 10 \times k_p$	155,156,172
k_p	$75\,L\,mol^{-1}\,s^{-1}$	172
k_t	$4.5 \times 10^8 \cdot i^{-0.51}\,L\,mol^{-1}\,s^{-1}$ $(i \leq 30)$	173
	$1.4 \times 10^8 \cdot i^{-0.16}\,L\,mol^{-1}\,s^{-1}$ $(i > 30)$	
k_{ex}	$7.5 \times 10^4\,L\,mol^{-1}\,s^{-1} = 1000 \times k_p$	–
$[St]_0$	$8.4\,mol\,L^{-1}$	–
$[R{-}I]_0$	$42 \times 10^{-3}\,mol\,L^{-1}$	–
$[MMMP]_0$	50 or $250 \times 10^{-3}\,mol\,L^{-1}$	–

[a] For $[MMMP] = 50 \times 10^{-3}\,mol\,L^{-1}$; [b] for $[MMMP] = 250 \times 10^{-3}\,mol\,L^{-1}$.

4.4.3.1 Simulation details

The implemented reactions and their respective rate coefficients are given in Scheme 4.8 on the previous page and Table 4.19. In order to keep the model simple, C–I-bond cleavage and thus RT was omitted. As the applied reactions were already discussed in detail in case of BA and BMA, only the used rate coefficients will be explained at this point. Values of k_p [172] (with $k_{ini} = 10 \times k_p$)[155,156] and k_t [173] were taken from the literature. As for the simulations of BMA, values of k_{dec} were individually determined for both systems by modeling the evolution of monomer conversion versus time in the low-conversion regime (< 20 %). In this context, it should be noted that this led to slightly different k_{dec} values for $[MMMP]_0 = 50\,mmol\,L^{-1}$ and $250\,mmol\,L^{-1}$, which might be due to nonlinear concentration effects, which are indeed frequently observed in photosystems.[170]

To further simplify the model, for all reactions involving iodine transfer (in both the pre- and the main equilibrium), the same rate coefficient was used, which was hypothetically set to $k_{ex} = 1000 \times k_p$ ($C_{ex} = 1000$). Although different reactivities of CP–I (= R–I) and polySt–I are expected in the pre- and in the main equilibrium, (i) (re)initiation and thus Reaction V is indeed fast (see experimentally obtained $\overline{M}_n$ values) while (ii) the very high $C_{ex} = 1000$ shall emphasize that the obtained impact on $\overline{M}_n$ does not

Table 4.20 Initial concentrations of substances used for UV-initiated iodine-mediated polymerizations of St in bulk at 60 °C with either PE–I or CP–I.

entry [a]	$[St]_0$ / mol L^{-1}	CTA	$[CTA]_0$ / mol L^{-1}	$[MMMP]_0$ / mol L^{-1}
1 (◇)	8.3	PE–I	42×10^{-3}	50×10^{-3}
2 (△)	8.1	CP–I	41×10^{-3}	50×10^{-3}

[a] See Figure 4.27 on the following page.

depend on potentially low molar-mass control but is inherently present for St polymerizations at room temperature, even for very well controlled polymerizations.

4.4.3.2 Simulations results

The obtained simulation results for monomer conversion versus time (as described above, by modeling experimental monomer conversion below 20 %) and the corresponding $\overline{M}_n$ evolution versus monomer conversion are presented in Figure 4.26 on page 126. To put it simply, while the polymerization rates are well-expressed by the simulations (higher experimental values for higher monomer conversion are ascribed to viscosity effects accelerating polymerization), the resulting $\overline{M}_n$ values clearly reflect the downward deviation from $\overline{M}_{n,theo}$. This demonstrates that the obtained low molar masses are indeed caused by the inherently high extent of dead polymer formed during St polymerizations at 22 °C. In addition, it clarifies that inconveniently long polymerization times have to be chosen when good molar-mass control of polySt is desired.

While thorough investigations of UV-initiated polymerizations at *elevated* temperatures were not within the scope of the present work, additional heating is of course a strategy both to increase the polymerization rate and to obtain higher molar masses. Brief examples will be presented in the following.

4.4.4 Elevated temperatures

UV-initiated polymerizations were conducted at 60 °C for both PE–I and CP–I as the CTA. Initial concentrations are given in Table 4.20 and the corresponding polymerization results are presented in Figure 4.27 on the

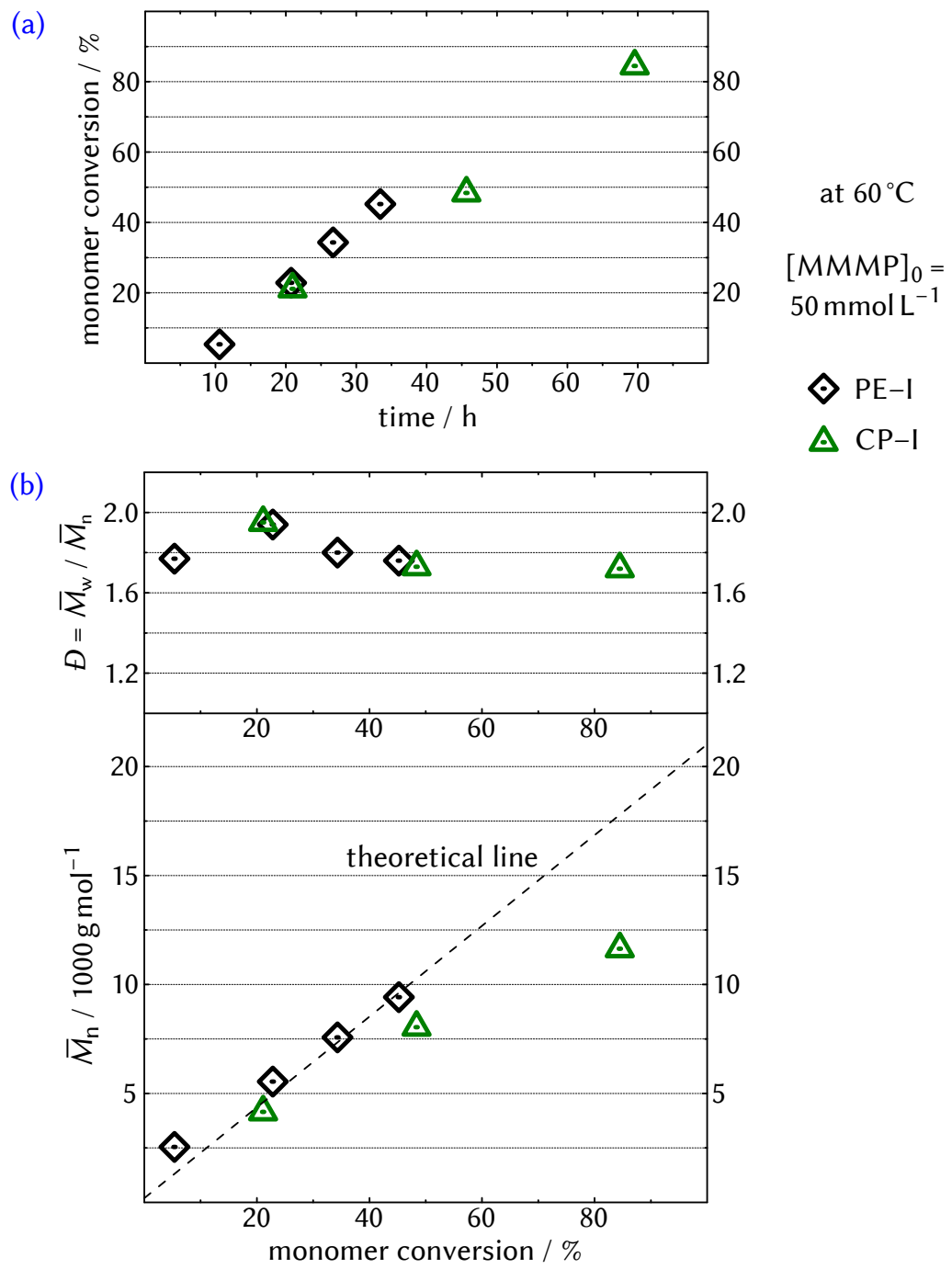

Figure 4.27 (a) Monomer conversion as a function of time and (b) $\overline{M}_n$ and $Đ$ as a function of monomer conversion of the UV-initiated iodine-mediated polymerizations of St in bulk at 60 °C given in Table 4.20 on the preceding page.

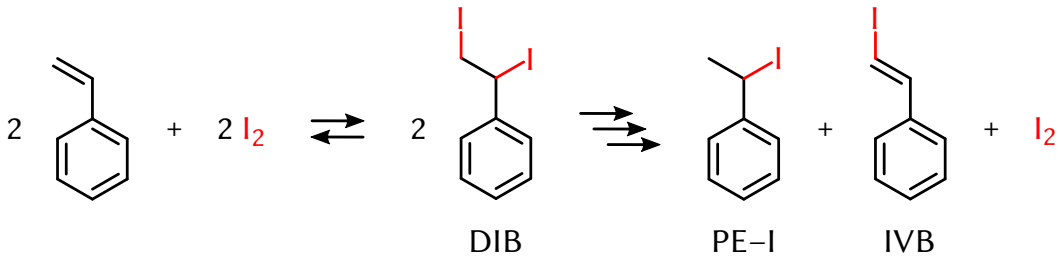

Scheme 4.9 Reactivity of I_2 toward St (net reaction),[174–176] for abbreviations see text.

facing page. While polymerization rates are distinctly higher compared to the system with $[MMMP]_0 = 50\,mmol\,L^{-1}$ at 22 °C, $\overline{M}_n$ values close to $\overline{M}_{n,theo}$ are obtained. Slightly higher $\overline{M}_n$ values can be observed for the PE–I system, indicating slightly slower (re)initiation compared to CP–I. However, in this context, it should be stated that $C_{tr} = 4.0$[59] for PE–I in ITPs of St at 60 °C. Thus, if (re)initiation was solely governed by DT, $\overline{M}_n$ values should start at about $5000\,g\,mol^{-1}$ at low monomer conversion (cf. Equation 2.16 on page 21). This indicates the positive impact of UV-induced C–I-bond cleavage and the significance of RT for the present system. No difference between PE–I and CP–I can be observed in terms of $Đ$ values, which are distinctly lower compared to the systems at 22 °C and decrease to about 1.7. Although even lower $Đ$ values are generally obtained for thermally initiated ITPs of St at even higher temperatures, the presented systems clarify that iodine-mediated polymerization is also feasible with UV initiation.

4.4.5 Comments on the reactivity of styrene toward iodine

In the last part of this section, an effect is briefly presented that might be important when UV-initiated iodine-mediated polymerizations of St are conducted. Whereas other monomer classes such as acrylates[24] and methacrylates[25,101] show no significant reactivity toward I_2 under the here investigated conditions, when I_2 is dissolved in St at room temperature, the initially reddish solution gradually decolorizes. This is due to a pronounced interaction of the vinyl double bond of St with I_2. As presented in Scheme 4.9, I_2 reversibly adds to St to form diiodoethyl benzene (DIB), which is then expected to react further via an ionic mechanism to yield PE–I and iodovinyl benzene (IVB), while effectively consuming molecular I_2.[174–176] For conven-

tional ITP systems, this reaction is arguably insignificant, as no C−I-bond cleavage and thus generation of I_2 occurs. However, it might be significant for UV-initiated polymerizations. Although only little is known about the kinetics and the influence of parameters such as reactant concentrations or UV irradiation, I_2 consumption potentially reduces the crucial RT steps of polySt$^\bullet$ with free iodine. In addition, although both DIB and IVB might eventually release and reintroduce iodine for the reversible deactivation of polySt$^\bullet$, both compounds are expected to be slow iodo CTAs[93] and their impact (adverse or beneficial) on the polymerization kinetics remains unclear at the moment. At the end of the day, the reactivity of St toward I_2 should be kept in mind when further investigations of UV-initiated iodine-mediated polymerizations of St are carried out.

4.4.6 Conclusions on styrene polymerizations

While UV-initiated iodine-mediated polymerizations of St are generally feasible with a conventional photoinitiator, it was shown that for the presented conditions, reasonably high molar masses can only be obtained for very low polymerization rates. As this is a general issue for polymerizations of St at room temperature, there are basically only two solutions when high molar masses are desired: (i) accepting low polymerization rates or (ii) applying conditions under which propagation is more pronounced toward termination (e. g., higher temperature, higher pressure,[177] using solvents such as ionic liquids[178]). The impact of reactivity of St toward I_2 is unclear at the moment and should be kept in mind when studying further UV-initiated systems with St.

CHAPTER 5

Future perspectives on iodine-mediated polymerizations

The insights into both the analysis and development of novel iodine-mediated systems that were gained in Chapter 3 and 4 offer various points of further progress in this field. Possible promising future studies are thus presented in the following.

Photoinitiation at elevated temperatures

In general, one of the big advantages of photoinitiation is its potential to conveniently produce polymer without being restricted to a certain polymerization temperature. Even though the focus of the present thesis was laid on UV-initiated polymerizations at *room temperature,* it was partly demonstrated that these systems may also be applied to *elevated temperatures.* Several facts indeed indicate why studying the developed photosystems at higher temperatures might be especially worthwhile.

As it was presented for the polymerizations of St, to obtain fairly high molar masses with reasonable polymerization rates in the first place, high temperatures were needed (Figure 4.26 on page 126 versus Figure 4.27 on page 130). The $\overline{M}_n$ and $Đ$ values respectively obtained at room temperature and 60 °C also indicate that polymerizing St at higher temperatures is beneficial for chain-growth control.

For BMA, higher temperatures were presented as a tool to obtain faster polymerization without suffering from lower chain-growth control. This is opposed to the effect for different initiator concentrations at room temperature (cf. Figure 4.20 and 4.21 on pages 107–108). The fact that for a similar control of chain growth, polymerizations at higher temperatures are faster, also indicates that more highly defined polymer could be obtained for lower initiator concentrations at higher temperatures compared to room temperature.

Another incentive to apply higher temperatures was already mentioned in the context of BA polymerizations and the extensive testing of potentially active RTCP catalysts. In kinetic studies of RTCPs of St from 60 °C to 100 °C, all of the investigated catalysts—including NIS, GeI_4, and SnI_4—led to systematically lower chain-growth control as temperatures decreased.[85] This makes it especially worthwhile to revaluate the impact of RTCP catalysts at higher temperatures. Preferably, catalysts are systematically applied for all three monomers, as successful RTCPs have only been obtained for polymerizations of styrenics and methacrylates up to today. In this context, the impact of different radiated wavelengths might be tested as well. Whereas the here applied 366 nm was partly beneficial because of induced C–I-bond cleavage, it also resulted in a pronounced decomposition of iodo catalysts.

Initiator cocktail

As it was demonstrated in Figure 3.6 on page 53, the application of an initiator cocktail for RITP led to smooth polymerization with a short inhibition period. While this is already beneficial in the context of common RITP, it offers huge potential to obtain well-defined polymer in combination with UV irradiation. As it was shown, the impact of incessant C–I-bond cleavage is higher for slower polymerization. Therefore, additional irradiation of a well-composed initiator-cocktail system directly addresses the two adverse effects in RITP, namely (i) long inhibition and (ii) only moderate chain-growth control. It thus offers the possibility of obtaining highly defined polymer in a very efficient way by employing rather simple and basic substances.

ESI-MS analysis

Iodine chain-end functionality of polyMMA obtained from common RITP-based RTCP systems was clarified in Section 3.3.2 on page 45. The reactivity of catalysts toward initiation or termination (or other side-reactions) is ar-

guably too small to yield a detectable extent of chains under such conditions. To get access to potential reactions of the catalysts, systems with much higher catalyst concentrations could be investigated. In this context, even the effect of rate retardation via cross-termination could be systematically examined. As it was demonstrated by polymerization-rate studies by Goto et al.,[26,27,85] the extent of rate retardation can be specifically quantified by the ratio between conventional irreversible termination (polymer$^{\bullet}$ + polymer$^{\bullet}$) and cross-termination (polymer$^{\bullet}$ + G$^{\bullet}$) (cf. page 27). This ratio can indeed be potentially determined via ESI-MS through the relative intensities of the signals from conventional dead chains and chains terminated via cross-termination. As a matter of course, the method still has to prove applicability and might face obstacles (e. g., cross-termination products have the be stable, conventional dead chains and cross-termination chains should have similar ionization probabilities[98]). However, considering the high importance of rate retardation for practical applications and the capability to study various systems and conditions, it seems worthwhile to test the potential of the method. As a general comment, since the inhibition period is a rather unpredictable factor in this context, CP–I might be applied via the semi-in-situ approach developed in Chapter 4 (cf. Experimental Section 10.1.3.1 on page 218).

Part III

Band broadening in size-exclusion chromatography

In this second major part of the thesis, band-broadening (BB) effects in size-exclusion chromatography (SEC) are presented and discussed. The part starts with a theoretical background on the principles of SEC and its inherent BB behavior. In Chapter 7 on page 153, the experimentally obtained influence of operating parameters on the extent of BB is presented. The impact of BB on molar-mass determination of polymer—in particular of polymer produced by means of (quasi-)living polymerizations—is demonstrated via a series of simulations in Chapter 8 on page 173. Potential correction techniques for the obtained effects will be presented and discussed eventually. A part of the content of the presented chapters has already been published and is reused with permisson from Wolpers, A.; Russell, G. T.; Vana, P. *Macromol. Theory Simul.* **2011**, *20*, 667–674.

CHAPTER 6

Theoretical background: size-exclusion chromatography and band broadening

6.1 Basics of size-exclusion chromatography

6.1.1 Historical background

First developments in the separation of macromolecules via size exclusion go back to the year of 1955, when Lathe and Ruthven showed that columns filled with swollen starch grains can be used to separate proteins with molar masses of hundreds of $\mathrm{kg\,mol^{-1}}$.[44,179] In subsequent works, Porath and Flodin used dextran gels as filling material and introduced the term *gel-filtration chromatography* (GFC).[180] At this time, the employed packing material was swellable only in *aqueous* media and thus application still limited to water-soluble macromolecules. (To the present day, the term GFC is indeed frequently used when talking about aqueous SEC systems, even though it is incorrect since separation is based on permeation rather than filtration.) Attempts of establishing systems for lipophilic synthetic polymer were made by using polySt-network beads. However, achieving high cross-linkage—which was necessary for a favorable high rigidity of the filling material—turned out to be very challenging.[181,182] After several studies of the solvent influence on the extent of cross-linkage and porosity,[183–185] John C. Moore of The Dow Chemical Company presented and patented the first SEC instrument based on rigid St–divinylbenzene copolymer networks

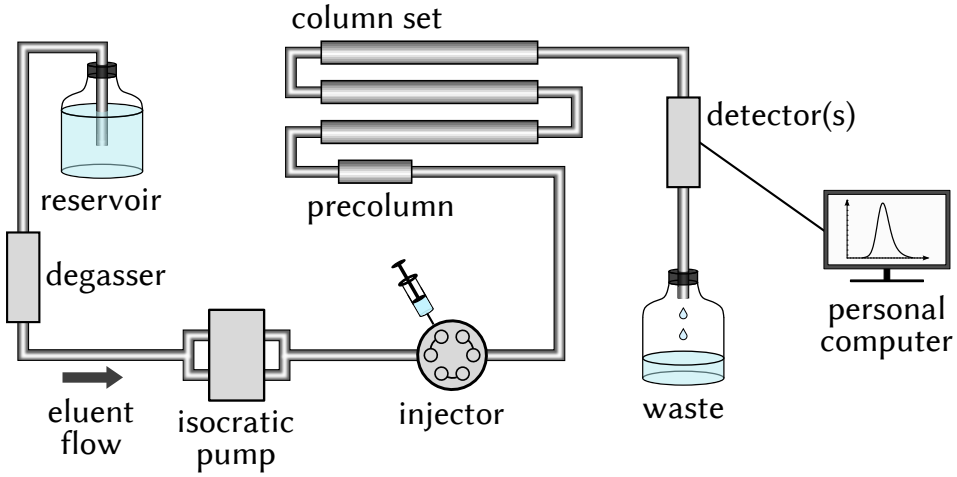

Figure 6.1 Schematic representation of a typical SEC setup.[48,187,188]

in 1964.[46,186] In collaboration with the Waters Corporation (at that time Waters Associates), SEC setups for lipophilic polymer were constructed on an industrial scale and commercialized. The introduction of SEC led to fast evaluations of polymer samples' MMDs within about 1 h, while before, this normally was a matter of weeks.[45] In addition, SEC experiments were straightforward and easy to conduct, which led to an instant success in the world of polymer analysis. In fact, since its breakthrough invention, SEC has not lost its worldwide top position and is by far the most common method for molar-mass determination of synthetic polymer.

6.1.2 Typical experimental setup

Figure 6.1 schematically shows a typical SEC setup.[48,187,188] It basically consists of a reservoir for the eluent, a degasser, an isocratic pump, an injector, separation columns and one or several detector(s). The choice of the **eluent** serving as the mobile phase (MP) is determined by its ability to solve the polymer sample while ideally having only little other effects such as interactions with the stationary phase (SP) inside the separation columns. Nowadays, there is a wide range of different systems available, including polar organic, nonpolar organic, halogenated, and aqueous ones. The MP is **degassed** to mainly prevent (i) reactions of potentially dissolved oxygen with the analyte or the SEC hardware and (ii) alteration of the detector signal. In addition, gas bubbles could form inside the isocratic HPLC **pump** and impede a regular eluent flow. To further stabilize the

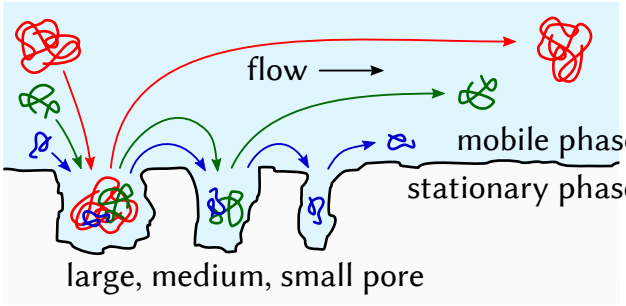

Figure 6.2 Simplified principle of size separation in SEC: big molecules visit less pores than small molecules and therefore elute earlier.

flow rate, a pulse dampener adjusted to the pump's design is generally installed as well. After the **injection**, which is normally achieved via an autosampling valve-injection system, the analyte passes the precolumn and the successive **separation columns.** Typical filling materials are porous (bio)polymer-network particles (or called *gel* when swollen in the eluent environment) with distinct pore-size distributions similar to the analyte-size distribution. The temperature of the columns is commonly regulated by an oven. Typical operating temperatures are 25 to 50 °C below the eluent's boiling point, leading to a rather low viscosity and high column pressure, which is beneficial for both resolution and the duration of an SEC experiment. The analyte is eventually detected in the **detector cell.** There are two general types of detectors, namely (i) concentration-sensitive (e. g., refractive index, UV light) and (ii) molar-mass-sensitive ones (e. g., light scattering, viscosimetry). Each detector type has respective advantages and disadvantages and the combination of different detector types even offers multiple possibilities to study into polymer properties such as chemical composition or constitution.[189] The most commonly applied type in routine experiments is the refractive-index detector, which measures the polymer-concentration-dependent relative refractive index of the solution. Refractive-index detection works linearly over a wide range of polymer concentrations, the polymer molecules do not require any specially active groups, and its sensitivity is nearly independent of the polymer type. The detector signal is recorded and displayed by a **personal computer** (PC). In modern SEC setups, the PC can also regulate injection, acquisition time, as well as operating parameters such as flow rate, pressure, and temperature of both the column set and the detector cells.

6.1.3 Separation principle

In SEC, polymer molecules are separated by their size in solution, which corresponds to their hydrodynamic volume, V_h. The highly porous SP allows molecules to diffuse into the pores, where their motion is mainly governed by relatively slow self-diffusion and not by the flow of the MP. Small molecules visit more pores than big ones, spend more time in the SP, and elute later (cf. Figure 6.2 on the previous page). (In this context, it should be stated that generally, the pores are interconnected and therefore, nonarbitrary flow is also expected inside the SP particles, which leads to a complex penetration and permeation behavior of the macromolecules.[190,191]) Ideally, separation is solely governed by entropic effects and no enthalpic polymer–polymer or polymer–SP interactions exist,[192] which is normally achieved by a good solvent that interacts strongly with the polymer. In addition, the solvent should be compatible with the SP in terms of stability and swellability. As a rule of thumb, the more polar the macromolecules are, the more polar the solvent and the SP should be and vice versa.

6.1.4 Molar-mass determination

6.1.4.1 Hydrodynamic volume and molar mass

As stated above, polymer molecules are separated by V_h rather than their molar mass, M, while M is normally the quantity of interest. However, within a distinct polymer class (e. g., linear polySt), V_h is directly proportional to M via[193]

$$V_h = \frac{[\eta] \cdot M}{2.5 \cdot N_A} , \tag{6.1}$$

with the Avogadro number, N_A, and the intrinsic viscosity (or Staudinger index), $[\eta]$. Here, $[\eta]$ is the characteristic value for the polymer class and given by the reduced viscosity of the polymer, η_{red}, for low polymer concentrations, [polymer]:

$$\lim_{[\text{polymer}] \to 0} \eta_{red} = [\eta] , \tag{6.2}$$

with

$$\eta_{red} = \frac{\eta_{[\text{polymer}]} - \eta_0}{[\text{polymer}] \cdot \eta_0} , \tag{6.3}$$

where $\eta_{[\text{polymer}]}$ is the viscosity of the solution with [polymer] and η_0 is the viscosity of the pure solvent.

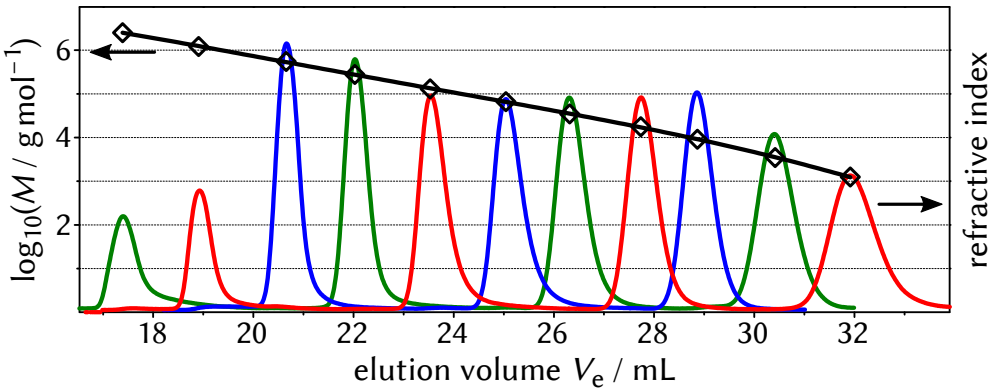

Figure 6.3 Exemplary chromatograms of polySt-standard kits recorded during a calibration process (right ordinate). The resulting pairs of $\log_{10}(M_{peak})$ (given by manufacturer of the standards) and $V_{e,peak}$ are fitted with a polynomial and yield the calibration function (left ordinate).

6.1.4.2 Calibration process

Although Equation 6.1 on the facing page provides a relation between M and V_h, the complex and highly individual processes during an SEC experiment do not allow for a universal relation between V_h and the retention behavior of a polymer chain.[48] The most reliable way to correlate retention—or the volume of elution of the MP, V_e—with M is indeed by experimental calibration rather than theoretical considerations, which makes SEC a *relative* method to determine MMDs.

Direct calibration For the most common calibration technique in SEC, polymer standards with narrow MMDs are used, which are generally acquired by purchase. After the standards are measured, the V_e values at the peak position of the obtained chromatograms, $V_{e,peak}$, are assigned to M values at the peak position of the MMDs, M_{peak}, which are specified by the manufacturer of the standards (see Figure 6.3). This leads to an almost linear relation between *logarithmized* $\log(M_{peak})$ and $V_{e,peak}$ values,[194] which are then fitted linearly or polynomially to yield the calibration function so as to translate V_e into $\log(M)$ values ($V_e = V_{e,peak}$, $M = M_{peak}$). An internal low-molar-mass standard (e. g., toluene) is usually employed to counter potential flow fluctuations during the experiment.

Universal calibration The direct-calibration method is applicable only within the same polymer class, that means when $[\eta]$ of the polymer used for calibration matches $[\eta]$ of the polymer eventually measured (cf. Equation 6.1 on page 142). For many polymer classes, standards can be either expensive or not even purchasable at all. In this case, so-called universal calibration can be employed if a direct calibration function of another polymer class exists. Generally, when two analyte molecules 1 and 2 eluate at the same V_e value, they have the same V_h. According to Equation 6.1, this leads to

$$[\eta]_1 \cdot M_1 = [\eta]_2 \cdot M_2 \ . \tag{6.4}$$

In this relative context, a polymer's $[\eta]$ value can be expressed by the empirical Mark–Houwink (MH) equation[195]

$$[\eta] = K \cdot M^a \tag{6.5}$$

and the MH parameters K and a, which depend on the polymer class, solvent, and temperature. If a calibration function for polymer 1 exists and the MH parameters of both polymer 1 and 2 are known, M_2 can be calculated through

$$\log_{10}(M_2) = \frac{1}{1+a_2} \cdot \log_{10}\left(\frac{K_1}{K_2}\right) + \frac{1+a_1}{1+a_2} \cdot \log_{10}(M_1) \ . \tag{6.6}$$

K and a can be experimentally determined via viscosimetry for example. In addition, they are tabulated in the literature[196] for a variety of polymer–solvent–temperature combinations. In practice, universal calibration leads to the fact that an SEC setup is often calibrated with one or two common polymer classes (e. g., linear polySt, linear polyMMA) while other classes are usually covered by applying the MH equation. If neither polymer standards nor MH parameters for a certain polymer class are available, absolute molar masses can be obtained without the need of calibration through the combination of concentration-sensitive and molar-mass sensitive detectors (e. g., refractive index and light scattering, refractive index and viscosimetry).[197,198]

6.1.5 Separation range

To effectively separate polymer, the SP should feature a pore-size distribution (PSD) covering the size distribution of the macromolecules.[48] Depending on the conditions during the production of the polymer-network particles, PSDs are often very limited to a certain range. To cover a wider size range of macromolecules, either (i) several columns with different PSDs

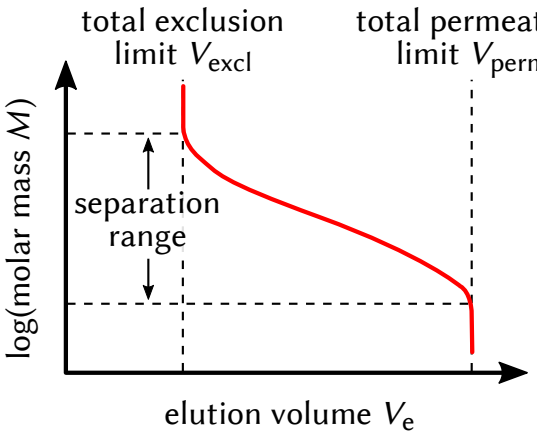

Figure 6.4 Typical log(M) separation range resulting from the V_e range between V_{excl} and V_{perm}. In case of $V_e < V_{excl}$, the analyte molecules are bigger than the biggest pore of the SP. In case of $V_e > V_{perm}$, the analyte molecules are so small that they can access all of the effective pore volume.

are connected in series or (ii) polymer-network particles with different PSDs are mixed in one single column. In the latter case, a number of columns are often connected in series as well to increase resolution. However, even a wide PSD is practically limited and hence limits the separation range of molar masses. Figure 6.4 shows a typical function of log(M) versus V_e values. All molecules that are bigger than the biggest pore elute at the total exclusion limit, V_{excl}. All molecules that are so small that they access all of the effective pore volume elute at the total permeation limit, V_{perm}.

6.2 Band broadening in size-exclusion chromatography

BB in SEC distorts the shape of measured MMDs and affects characteristic values frequently determined in the analysis of polymer (e. g., mean values, inflection points).[199–201] Because of the omnipresence of SEC, the interest in BB is obvious and the International Union of Pure and Applied Chemistry (IUPAC) organized projects to study the cause, the impact, and the correction of BB in SEC experiments.[47,199] In this context, investigating BB seems worthwhile not only for the sake of BB itself. It also helps to sharpen the understanding of the complex effects during size-exclusion separation in general, which serves as a basis for the development of more sophisticated and effective future SEC devices and techniques.[48,202] In the following, after a brief description of common methods to quantify BB, an overview of prevalent concepts of the indeed special BB behavior in SEC will be presented.

6.2.1 Determination of band broadening

The shape of an SEC trace can be considered as a combination of the true shape of the analyte's MMD and the shape of BB, i. e., the BB function (BBF). A common strategy to estimate the BBF is hence to measure precisely known MMDs. In this context, one can for example use (i) unimolar substances, (ii) Poisson-distributed polymer standards produced via anionic polymerization, or (iii) any polymer whose MMD was determined by a method not prone to BB. However, respective drawbacks exist for all three approaches. (i) Compared to normal polymer, unimolar substances are generally very small and can cover only the low-molar-mass region of the separation range. Still, *quasi*-unimolar polymer with very narrow MMDs can be produced via fractionation (e. g., by means of SEC or *temperature gradient interaction chromatography*, TGIC) and was shown to give reliable BB results.[203,204] (ii) Side reactions in anionic polymerization procedures can lead to deviations from ideal Poisson distributions. To date, only polySt has indeed been proven to reliably yield Poisson-shaped MMDs from anionic polymerizations,[203,205,206] while for a few other polymers classes, the MMDs can be considered as close-to-Poissonian.[207] (iii) MMDs are difficult to obtain with methods alternative to SEC. MALDI-MS is an option,[206,208] however, very high molar masses are often not accessible, the results can be altered by artifacts, and special care has to be taken during the experiments.[96,209]

When the true MMD is known, BB can then be determined from the difference between the true MMD and the experimental result through an educated guess of the general shape of the BBF. This can be done by comparing characteristics of the distributions (e. g., inflection points, width at certain heights)[210,211] or by simulating the complete experimentally obtained distribution with a computational broadening routine.

Other approaches exist that do *not* require knowing the true shape of the analyzed MMD, such as the combination of concentration- and molar-mass-sensitive detectors,[212,213] reverse-flow[214] and recycle techniques.[215] However, they are rather complex and very prone to errors when experimental parameters are not chosen wisely.

6.2.2 Size-exclusion chromatography as liquid chromatography

Mechanistically, SEC is a type of liquid chromatography (LC) with a simplified model of analyte molecules being either in the MP or the SP, while

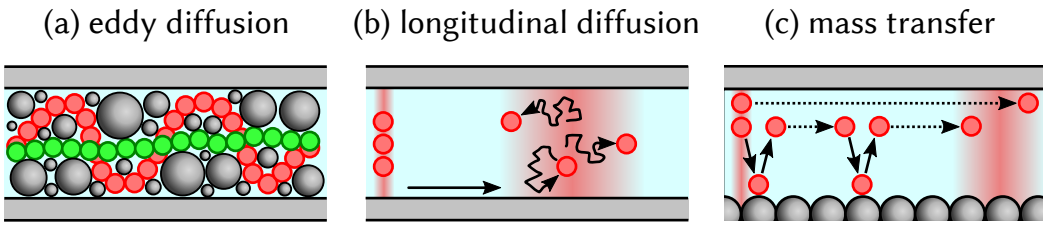

Figure 6.5 General mechanisms causing symmetric Gaussian broadening in a chromatographic experiment.

the amount of time spent in each of the two phases determines analyte retention. Many interpretations[47] of BB in SEC are based on the fundamental stochastic *rate theory* for chromatography. It was originally advanced for gas chromatography (GC) and LC systems by famous works of Giddings and Eyring,[216,217] and van Deemter et al.[218] in the mid-1950s. In this regard, two distinct first-order rate coefficients determine the transfer of analyte molecules from the MP to the SP and from the SP back to the MP. This chromatographic principle led to the well-known van Deemter equation, which relates chromatographic resolution with the flow rate of the MP. According to this equation, BB occurs because of three general reasons, which are presented in Figure 6.5: (a) eddy diffusion (the effect that two similar analyte molecules can have different pathways), (b) longitudinal diffusion (self-diffusion of analyte molecules with and opposed to the flow), and (c) mass transfer between the MP and the SP (the actual chromatographic effect). Although BB is expected to be much more complex in SEC—as will be pointed out in the next section—the van Deemter terms are still frequently used to interpret BB, especially in terms of its symmetric Gaussian behavior. In this context, Gaussian broadening was found to be mainly caused by (a) eddy diffusion and (c) mass transfer, whereas (b) longitudinal diffusion is much less pronounced[219] and even negligible for $M > 30\,000\,\mathrm{g\,mol^{-1}}$.[220] This is a result of the rather low self-diffusion coefficients, D, of macromolecules ($D \sim V_\mathrm{h}^{-1/3}$).[221]

6.2.3 Skewing as inherent band-broadening effect

A brief look at chromatograms is often enough to spot that Gaussian broadening is a rather rough estimation as pronounced signal asymmetry and *positive* skewing (tailing toward *higher* V_e, see Figure 6.6 on the next page) is normally obtained. Skewing can be caused by several effects such as a truly

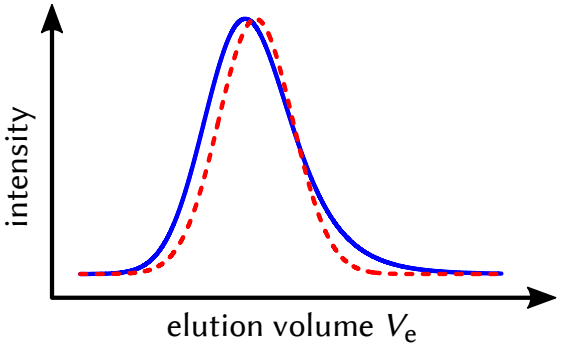

Figure 6.6 Symmetric signal (broken line) and asymmetric signal with a positive skew (tailing toward higher V_e) (unbroken line).

asymmetric MMD, a nonlinear detector response, a nonlinear molar-mass calibration, or strongly unsuitable operating conditions. However, the overwhelming majority of experimental findings[47] leave little doubt that the BBF is inherently skewed even for sophisticated SEC setups and conditions. These findings are supported by theoretical considerations and simulations of SEC retention. Skewing in SEC is expected to be basically caused by two effects, (i) insufficient lateral diffusion of the analyte and (ii) rare mass transfer between the MP and the SP, which will be described in more detail in the following.

Insufficient lateral diffusion The rather slow self-diffusion of macromolecules leads to effects distinctly different from common LC of low-molar-mass substances. For a significant time during an SEC experiment, the eluent has a more or less parabolic flow-velocity profile. That includes (i) regions of low velocity near stationary elements such as column/capillary walls or the SP and (ii) regions of higher velocity for an increasing distance from these elements. For low-molar-mass analytes, self-diffusion is fast and leads to an effective averaging of lateral positions and thus positions of lower and higher flow velocity. However, the higher the analyte's molar mass is, the less pronounced is the averaging, which was shown to result in highly skewed exponential-like elution profiles.[204,222] Insufficient lateral diffusion is expected to be mainly an *extracolumn* effect occurring inside the interconnecting capillaries and to be highly dependent on their inner diameter. While this effect also seems to exist between SP particles inside the separation columns,[223] it is much less pronounced since (i) the distance between particles is much smaller than between capillary walls and (ii) the particles lead to a pronounced turbulence impeding a parabolic flow profile. Indeed,

more pronounced skewing is again expected when larger and therefore less densely packed SP particles are used.[223]

Rare mass transfer The other main reason for skewing is rare mass transfer of analyte molecules between the MP and the SP. Supported by experimental results, both simulations[204] and theoretical calculations[224–227] have shown that ingress–egress processes of the analyte (equivalent to MP–SP mass transfer) play an essential role for the occurrence of chromatographic skewing. Basically, once a polymer molecule is located in the SP, the probable duration until its egression follows a highly skewed and exponential-like distribution. For the case of not only one but many pore visits, this distribution gradually transforms into a narrower and more symmetric Gaussian shape.[204] However, even for frequent mass transfer, slight skewness is still observed.

6.2.4 Symmetric broadening and skewing

6.2.4.1 Quantification: the exponentially modified Gaussian model

Obvious skewing effects have led to approaches to quantify BB more elaborately than with a simple Gaussian distribution. A BBF providing excellent results in several studies[47] is the so-called *exponentially modified Gaussian* (EMG) function.[228,229] While mathematical detail on the EMG function will be presented in Section 7.1.3 on page 155, here, only the individual quantification of symmetric broadening and asymmetric skewing will be explained. The EMG function is deduced from a convolution product between a symmetric Gaussian and an asymmetric exponentially decaying function. The more pronounced symmetric broadening is, the higher is the standard deviation of the Gaussian function, σ_G. The more pronounced skewing is, the higher is the parameter of the exponential function, τ. The overall standard deviation (= broadness), σ, and the overall skewness, γ, of the EMG function is given by

$$\sigma = \sqrt{{\sigma_G}^2 + \tau^2} \quad \text{and} \quad \gamma = 2(\tau/\sigma)^3 \,. \tag{6.7}$$

Both σ_G and τ thus contribute to both σ and γ. The higher both σ_G and τ are, the broader the BBF is, while the lower σ_G and the higher τ is, the more skewed it is.

6.2.4.2 Behavior during SEC analysis

The EMG function has proven to be highly suitable to express experimental BB results for both high- and low-molar-mass polymer.[47] In this context, several studies indicate that the BBF in SEC is nonuniform, which means that the EMG parameters σ_G and τ are not constant over the complete V_e or M range. In addition, BB strongly depends on factors such as operating parameters and individual SEC-hardware elements. Part of these effects will be pointed out in the context of the investigated extent of BB for different operating conditions in Section 7.2 on page 159, while comprehensive communications can be found in the literature.[48,230] In the following, a brief overview of the frequently obtained trends of σ_G and τ as a function of V_e will be presented.

Skewing In many literature studies,[47,204,211,213] τ values were shown to generally decrease with increasing V_e. This trend is indeed in accordance with the above-mentioned two main mechanisms that cause skewing, namely (i) the insufficient lateral diffusion and (ii) the rare mass transfer. The lower M (= higher V_e) of a molecule is, (i) the faster is its self-diffusion and thus the more pronounced is its averaging of lateral positions. In addition, lower M leads to (ii) a higher number of visited pores. For very few visits and V_e close to V_{excl}, τ values increase even drastically.[204] In this regard, if M is so high that part of the polymer's MMD is expected to be totally excluded from the SP, the chromatogram is highly distorted and prediction or observation of the BBF is impossible.[231]

Symmetric broadening In contrast to τ, literature results for σ_G are slightly more ambiguous. While there is general agreement on the fact that σ_G is less sensitive to different V_e values than τ, there are studies in which σ_G (i) slightly increases,[211,213,225] (ii) is almost constant,[204] or (iii) exhibits a rather complex behavior[204,211,219,232] with increasing V_e. This discrepancy can also be found for theoretical considerations: while a more sophisticated van Deemter equation[233,234] (upgraded by the concept of obstructed diffusion) predicts a decreasing broadness for higher V_e, the stochastic Giddings–Eyring–Carmichael model[225,227] predicts an increasing broadness. Although this controversy is still not fully decided, huge experimental evidence exists that even if σ_G might not systematically increase for lower V_e, both the overall broadness σ (= combination of σ_G

and τ, see Equation 6.7 on page 149) and the overall skewness γ often do.[47,204,211,213,219]

6.2.4.3 Complex band-broadening behavior

The behavior of both σ_G and τ versus V_e can sometimes be slightly scattered and the above-described trends are evident only after the analysis of a large number of polymer samples (depending on the robustness of the employed determination method).[204,211] It should also be noted that each SEC device is indeed highly individual (even if constructed similarly) and that every single hardware element and joint has its own contribution to the overall shape of BB, depending on its inner volume and geometry.[188,235] For example, while the dead-end pore model with a stagnant flow zone in the SP simplifies theoretical considerations, in reality, the pores are expected to behave as internally connected capillaries with individual flow regimes.[190,236] This makes separation highly dependent on complex factors such as the inner convection and the tortuosity of the SP and challenges the simple concept of mass transfer.[234] Decoiled polymer chains can also (partially) enter pores that should theoretically be too small for permeation, which leads to unexpectedly long retention after the chains trudged through the close pore structure of the SP.[237,238] Partial penetration may also contribute to degradation of macromolecules upon flow-induced shearing at the surface of the SP, further distorting SEC results.[239] In fact, these are just a few examples where SEC deviates from its more or less expected behavior. The partly ambiguous trends of BB for different V_e further clarify that the extent of BB cannot be generally predicted for a specific SEC setup. As BB is affected by the interplay of various individual effects, it is highly recommended to experimentally determine BB for the *complete* SEC setup and under the operating conditions eventually used for routine measurement.[188,219] When either a single hardware element is replaced or operating conditions are changed, BB should be redetermined. In this regard, even for an untouched SEC setup, the BB behavior could change after some time, for example because of gradually clogging particle filters or separation columns.[240]

CHAPTER 7

Influence of operating parameters on the extent of band broadening for narrow-distribution polymer

In the here presented section, the influence of several operating parameters on the extent of BB is investigated for narrow-distribution polymer. For this, polySt standards were measured for different (i) injection volumes, V_{inj}, (ii) concentrations, [polymer], (iii) flow rates, v_{flow}, and (iv) column temperatures, T_{col}. The four parameters were chosen since they can often be easily adjusted when the conditions used for routine measurements prove to be unsuitable for the analysis of the designated analyte (e. g., detector signal too high/low, limited amounts of analyte available, degradation effects of polymer). In this context, the narrow polySt standards are particularly applicable since (i) their true MMDs are generally known, (ii) they are employed in the crucial calibration process, and (iii) they resemble polymer commonly obtained from (quasi-)living polymerization ((Q)LP) systems such as well-controlled RDRPs. Indeed, some of the observed effects are expected to be more pronounced for narrow- than for broad-distribution polymer, which will be clarified in the course of this section. BB is quantified by applying a simulated broadening routine using the EMG function and its parameters σ_G and τ to model the experimentally obtained chromatograms. The impact of various operating conditions (including the here considered ones) on BB has already been extensively investigated in the past.[48] However, to the best of knowledge, this was mainly conducted in terms of general broadness, skewness, and chromatographic resolution rather than in terms of an

individual evaluation of σ_G and τ. As will be clarified in the course of the section, the EMG model is indeed especially suitable to express the obtained effects. The used method is very robust since (almost) the entire distribution is regarded rather than only a few characteristic points. It is described in more detail in the following while the results are presented in Section 7.2 on page 159.

7.1 Method

7.1.1 Estimation of calibration functions

To translate simulated MMDs into simulated elution chromatograms, SEC calibration functions were determined for the respective experimental conditions. Conveniently, the polySt samples eventually used for the estimation of BB were the polySt standards also used for the routine calibration process, so that no additional measurements had to be conducted. As described in Section 6.1.4.2 on page 143, the measured $V_{e,peak}$ values were assigned to the $\log_{10}(M_{peak})$ values provided by the manufacturer (cf. Experimental Section 10.1.6 on page 221) by means of the SEC software *WinGPC UniChrom* version 8.2. The $V_{e,peak}$ value of the internal standard toluene served as a fixpoint and was set to 36.930 mL for each measurement. The obtained pairs of values were fit with a 5^{th}-order polynomial, giving the individual calibration parameters a_{cal} to f_{cal} of the calibration function

$$y = a_{cal} \cdot x^5 + b_{cal} \cdot x^4 + c_{cal} \cdot x^3 + d_{cal} \cdot x^2 + e_{cal} \cdot x + f_{cal} \,, \tag{7.1}$$

with $y = V_e$ and $x = \log_{10}(M)$, or $y = \log_{10}(M)$ and $x = V_e$, respectively ($V_e = V_{e,peak}$, $\log_{10}(M) = \log_{10}(M_{peak})$). All calibration functions were checked to ensure a reasonable behavior between neighboring calibration points and to avoid overfitting.

7.1.2 Simulation of unbroadened elution chromatograms

The chain-length distributions (CLDs) of the polySt standards produced via anionic polymerization can be very well expressed via the Poisson distribution[203,205,206]

$$x_i = \frac{\nu^i \cdot \exp(-\nu)}{i!} \,, \tag{7.2}$$

where x_i is the probability of a chain with a chain length of i, and ν is the kinetic (average) chain length. The factorial part of the equation causes mathematical limitations for the program used for broadening (Excel, Microsoft Office 2010, Microsoft®, see below) and prevents simulations of complete CLDs for $\nu \gtrsim 700$. In that case, instead of a Poissonian, a Gaussian distribution of the following form is applied:

$$x_i = \frac{1}{\sqrt{2\pi \cdot \nu}} \cdot \exp\left(-\frac{(i-\nu)^2}{2\nu}\right) , \tag{7.3}$$

which approximates a Poissonian for high ν values.[241] To assess the significance of the difference between applying a Poissonian and a Gaussian distribution, BB parameters σ_G and τ were determined for experimentally obtained chromatograms of polySt standards with $\nu < 700$ according to the method described in this section on the basis of CLDs by both Equation 7.2 and 7.3. The results are given in Appendix B.3 on page 237 and show that EMG parameters for the Poissonian and the Gaussian CLDs become more alike as ν increases and that they differ by less than 1 % for $\nu > 300$. This justifies the use of Gaussian CLDs for $\nu > 700$ in the present work.

The CLDs of the form "x_i versus i" are then transformed into MMDs of the typical chromatographic form obtained from a refractive-index detector, "intensity versus $\log_{10}(M)$". While $\log_{10}(M) = \log_{10}(i \cdot M_{St})$, the calculation of the intensity of the refractive-index detector, RI, is described in detail by Hutchinson et al.[242] and given by

$$\mathrm{RI} = x_M \cdot M^2 , \tag{7.4}$$

with the probability x_M of a macromolecule with a molar mass of M. Values of $\log_{10}(M)$ can then be transformed into V_e by applying the calibration function described in the previous section. When all steps are conducted up to this point, a hypothetically unbroadened (= true) elution chromatogram, $\mathrm{RI}^{\mathrm{unbr}}(V_e)$, of a polySt standard is obtained.

7.1.3 The exponentially modified Gaussian model

Broadening $\mathrm{RI}^{\mathrm{unbr}}(V_e)$ gives the broadened chromatogram, $\mathrm{RI}(V_e)$, which is eventually used for modeling the experimentally measured chromatogram and obtained by applying Tung's equation[243]

$$\mathrm{RI}(V_e) = \int_0^\infty g\left(V_e, V_e^0\right) \cdot \mathrm{RI}^{\mathrm{unbr}}\left(V_e^0\right) \mathrm{d}V_e^0 , \tag{7.5}$$

where $g(V_e, V_e^0)$ is the BBF at the position $V_e = V_e^0$. Illustratively, $RI^{unbr}(V_e)$ is divided into many dV_e. For every division, a BBF $g(V_e, V_e^0)$ is created at the position of the division, V_e^0, with the intensity of $RI^{unbr}(V_e^0)$. $RI(V_e)$ is then obtained by adding up the respective BBFs. In the present work, this process was conducted numerically and is more precisely explained in the next section.

The BBF of choice was the EMG function. As described in Section 6.2.4.1 on page 149, it combines the two different BB effects of (i) symmetric broadening and (ii) skewing by a convolution product of a Gaussian and a decaying exponential function:[228,229]

$$g\left(V_e, V_e^0\right) = \frac{1}{\sqrt{2\pi}\cdot\sigma_G\cdot\tau}\cdot\underbrace{\left(\exp\left(-\frac{\left[\left\{V_e - V_e^0\right\} + \tau\right]^2}{2{\sigma_G}^2}\right)\right)}_{f_1(V_e)} * \underbrace{\left(\exp\left(-\frac{V_e - V_e^0}{\tau}\right)\right)}_{f_2(V_e)}, \tag{7.6}$$

with the convolution operator "$*$" and $f_1(V_e) * f_2(V_e) = \int_0^{V_e} f_1(u)\cdot f_2(V_e - u)\mathrm{d}u$ as well as the bound convolution variable u. It should be noted that the Gaussian function is centered at $V_e^0 - \tau$. This leads to the distribution's average V_e value of V_e^0 so that the average V_e value of $RI(V_e)$ is independent of both σ_G and τ. The EMG function only gives valid values in case of $\sigma_G > 0$ and $\tau > 0$. For $\sigma_G = 0$, it is therefore reduced to the exponentially decaying part while for $\tau = 0$, it is reduced to the Gaussian part. For $\sigma_G = \tau = 0$, there is no broadening and the BBF becomes the Dirac delta function.

7.1.4 Broadening simulation of unbroadened elution chromatograms

In order to apply EMG broadening to $RI^{unbr}(V_e)$, Equation 7.5 and 7.6 were used. The broadening procedure as well as the quantification of σ_G and τ (see next section) were numerically conducted with the Excel application of the Microsoft Office 2010 package by Microsoft®. Figure 7.1 on the facing page presents a schematic example of a utilized Excel sheet. The unbroadened elution chromatogram $RI^{unbr}(V_e)$ is given in columns A & B. The corresponding V_e values were chosen to equal the *equidistant* ones

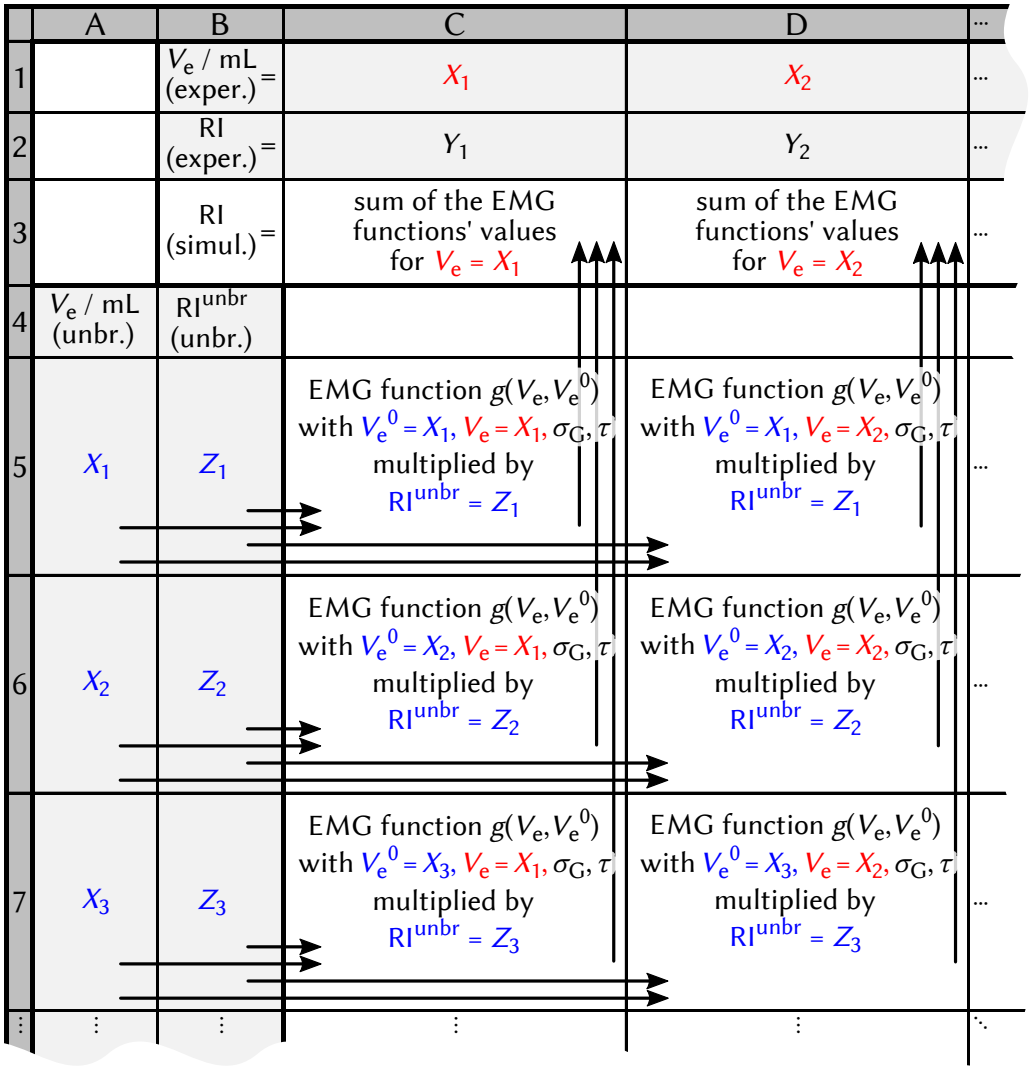

Figure 7.1 Schematic example of an Excel sheet used for the broadening process of an ideal or unbroadened (unbr.) elution chromatogram (columns A & B) by applying an EMG function for certain values of σ_G and τ. V_e values (blue $X_1, X_2, \ldots$) are predetermined by the experimentally obtained (exper.) elution chromatogram (rows 1 & 2). Row 3 gives RI values of the simulated (simul.) broadened chromatograms for the respective V_e values given in row 1. RI (simul) is derived from the sum of the values of the EMG functions (row $5, 6, \ldots$) for the respective V_e values. After normalizing RI (exper.) and RI (simul.) to the same maximum intensity, best-fit procedures can be conducted by minimizing the differences between row 2 and 3.

of the experimentally obtained chromatogram (rows 1 & 2) determined by the SEC software (see below), so that blue X_1 = red X_1, blue X_2 = red X_2, etc. In this context, it should be stated that the original simulation of $\mathrm{RI}^{\mathrm{unbr}}(V_\mathrm{e})$ according to the previous sections results in nonequidistant V_e values differing from the experimental V_e values in row 1. Therefore, $\mathrm{RI}^{\mathrm{unbr}}(V_\mathrm{e})$ is translated into a distribution with the equidistant V_e values via an interpolation procedure presented in Appendix B.2 on page 236. This is necessary to achieve an unbiased broadening result. From row 5 and column C on, EMG functions for certain values of σ_G and τ were created row-wisely (for the practically applied EMG function see Appendix B.1 on page 235). Here, the V_e values of $\mathrm{RI}^{\mathrm{unbr}}(V_\mathrm{e})$ (blue X values) correspond to V_e^0, and the V_e values of the experimentally obtained chromatogram (red X values) correspond to V_e. The EMG functions are weighted with the $\mathrm{RI}^{\mathrm{unbr}}$ values (Z values) according to Equation 7.5 on page 155. The simulated RI values of the broadened chromatogram (row 3) are eventually calculated by summing up all EMG functions' values for the same V_e value, i. e., within one column.

7.1.5 Fitting procedure of experimentally obtained elution chromatograms

Fitting of an experimentally obtained chromatogram was conducted by first normalizing both the experimentally obtained and the simulated chromatogram to the same maximum intensity (row 2 and 3 in Figure 7.1 on the preceding page). Then, the difference between row 2 and 3 was minimized via the least-squares method by variation of the EMG parameters σ_G and τ, and of the kinetic chain length, ν. In this context, ν influences the shape of $\mathrm{RI}^{\mathrm{unbr}}(V_\mathrm{e})$ and its position along the V_e axis (column A & B). The fitting procedure was conducted with the Excel add-in program *Solver* using the Generalized Reduced Gradient (GRG2) algorithm.[244] Fitting was proceeded for intensities higher than 25 % of the maximum intensity since some chromatograms were not completely baseline-separated owing to the usage of polymer kits rather than discrete polymer standards. Both σ_G and τ were assumed to be constant over the complete signal range, which is a reasonable assumption in case of narrow-distribution polymer standards ($\Delta V_\mathrm{e} < 1.5\,\mathrm{mL}$).[47] The distance between adjacent V_e values was 0.016 mL and determined by the SEC software.

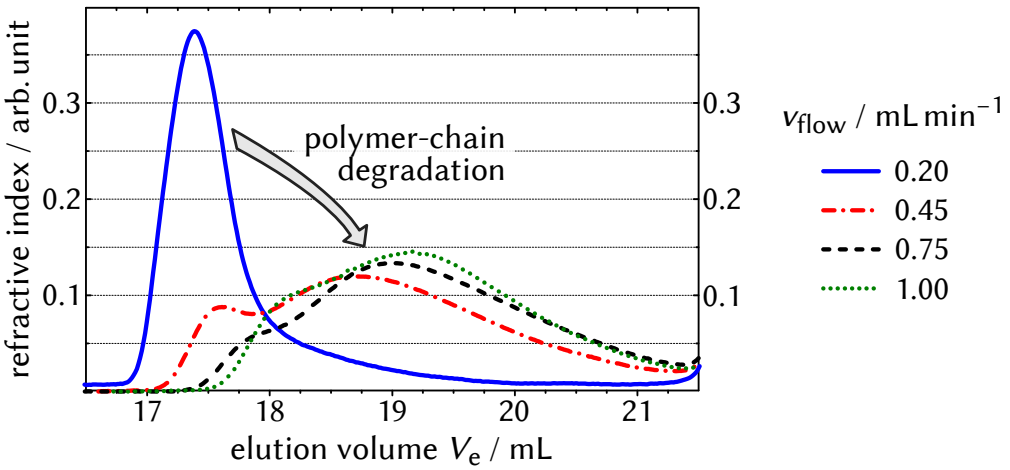

Figure 7.2 Elution chromatograms indicating flow-induced degradation of high-molar-mass polymer (M_{peak} = 2 520 000 g mol^{-1}): for v_{flow} > 0.20 mL min^{-1}, the signal is strongly distorted and shifted toward higher V_e (lower M). Other operating parameters: [polymer] = 4 g L^{-1}, V_{inj} = 40 µL, T_{col} = 35 °C.

7.2 Results and discussion

PolySt standards were measured for different values of V_{inj} and [polymer] (presented in Section 7.2.1 on the next page), and v_{flow} and T_{col} (presented in Section 7.2.2 on page 167), while BB parameters σ_G and τ were determined as described in the previous section. SEC setup 2 was used (cf. Experimental Section 10.2.4 on page 223). It should be noted that standards for low and very high molar masses were excluded from this process. While the low-molar-mass signals were partially superimposed by system signals, the highest-molar-mass standard (M_{peak} = 2 520 000 g mol^{-1}) showed distinct flow-induced degradation for v_{flow} > 0.20 mL min^{-1}, as presented in Figure 7.2. This effect is indeed especially pronounced for high molar masses and expected to be caused by extensional strains of polymer chains.[239] Out of the remaining signals eventually used to establish the respective calibration function, the ones with the highest and the lowest $V_{e,peak}$ value were not modeled as well. This is because the calibration function reliably covers only the area between these two $V_{e,peak}$ values, thus, half of the respective signals (exceeding the calibration function) is not covered. As a result, for every condition, BB was consistently determined for the polySt standards with M_{peak} from 9130 g mol^{-1} (V_e ≈ 29 mL) to 549 000 g mol^{-1} (V_e ≈ 21 mL).

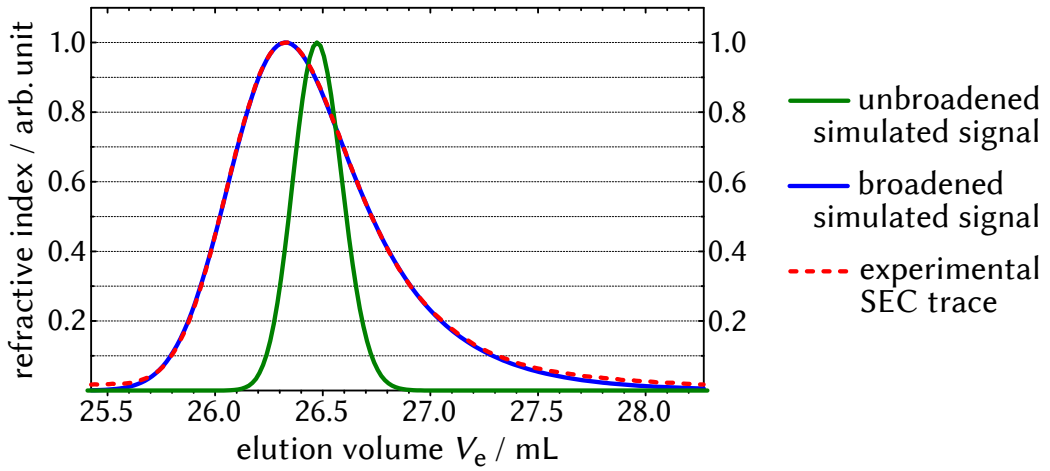

Figure 7.3 Exemplary best-fit result of a polySt standard's SEC trace (all curves normalized to the same maximum intensity). The best-fit EMG parameters are $\sigma_G = 0.18\,\text{mL}$ and $\tau = 0.34\,\text{mL}$, with the correlation coefficient $r = 1.000$. Operating parameters: $V_{inj} = 10\,\mu\text{L}$, [polymer] $= 4\,\text{g}\,\text{L}^{-1}$, $v_{flow} = 1.00\,\text{mL}\,\text{min}^{-1}$, and $T_{col} = 35\,^\circ\text{C}$.

Quality of the fitting process

Figure 7.3 shows a clearly skewed exemplary experimental SEC trace and the corresponding simulated best-fit broadened and unbroadened signal. The high quality of the fit is evident and the correlation coefficient, r, for the fitted intensities $> 25\,\%$ equals 1.000, while the lowest value obtained for any standard in the present work is $r = 0.997$. This clarifies very good agreement and supports the EMG model to be a suitable BBF. An important additional result is the shift of $V_{e,peak}$ toward lower V_e after BB is applied, as a consequence of the positive skewness. Since $V_{e,peak}$ is crucial for the calibration process, this shift plays an important role for subsequent molar-mass determination, which will be discussed more deeply in Section 8 on page 173.

7.2.1 Injection volumes and sample concentrations

For constant values of v_{flow} ($1.00\,\text{mL}\,\text{min}^{-1}$) and T_{col} ($35\,^\circ\text{C}$), chromatograms were measured for [polymer] $= 4\,\text{g}\,\text{L}^{-1}$ and $8\,\text{g}\,\text{L}^{-1}$. In either case, V_{inj} was set to 10 µL, 40 µL, 70 µL, and 100 µL. The parameter values were chosen as they cover the typical region for the routine analysis of unknown polymer. In this regard, the choice is normally a compromise between a variety of things

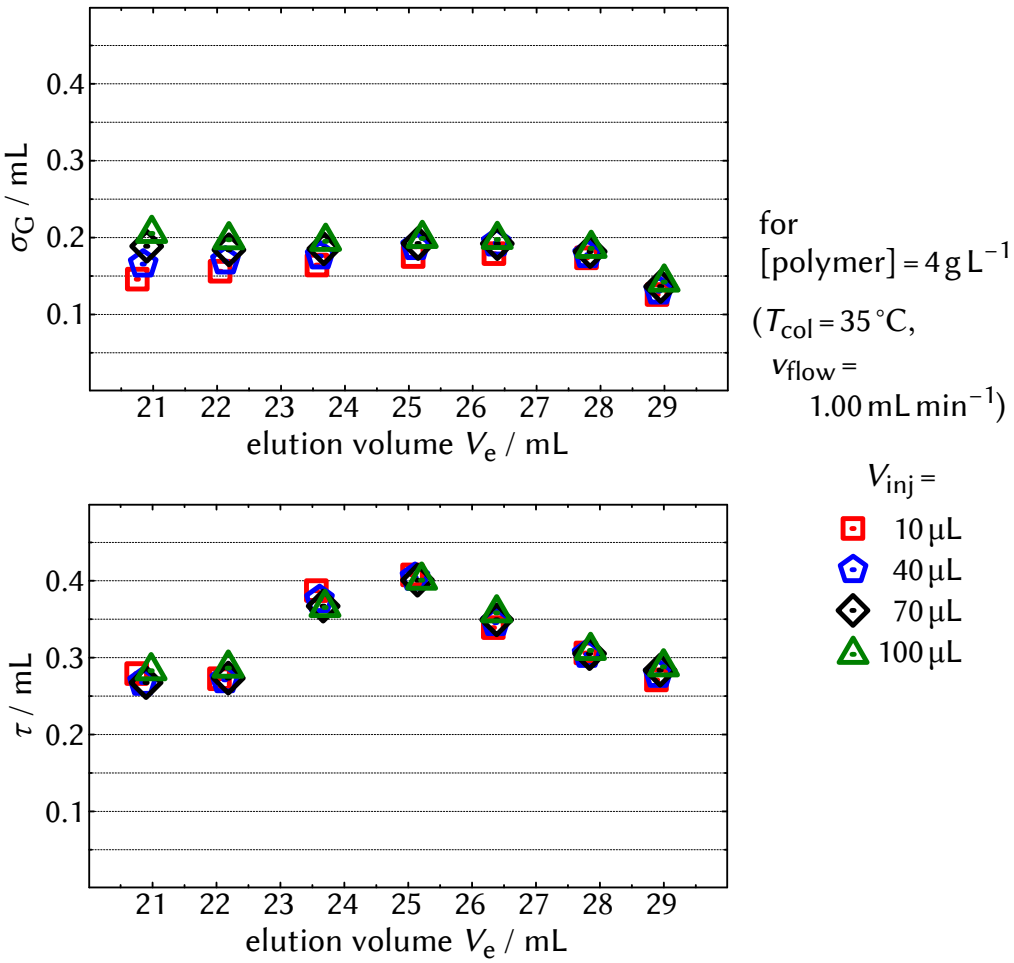

Figure 7.4 Exemplary EMG parameters, σ_G and τ, as a function of V_e (= $V_{e,peak}$) for polySt standards measured under the indicated operating conditions.

such as a high signal-to-noise ratio, staying in the linear-detection region, preventing analyte–analyte interactions or viscosity effects, or simply the available mass of the sample.

7.2.1.1 V_e dependence of band broadening

For [polymer] = 4 g L^{-1}, the determined EMG parameters σ_G and τ as a function of V_e (= $V_{e,peak}$ of the respective signals) are exemplarily given in Figure 7.4. Here, it will be focused on the impact of V_e on the EMG parameters, while the general impact of V_{inj} will be discussed at a later stage.

Both σ_G and τ are in the order of values commonly obtained in literature studies. In agreement with the above-mentioned literature finding that σ_G is only little sensitive to V_e, σ_G is rather constant between 0.15 and 0.20 mL. In contrast, τ is much more sensitive to V_e. For decreasing V_e values, τ starts to increase, reaches a maximum at $V_e \approx 25$ mL, and then decreases eventually, varying between 0.25 and 0.40 mL. As described above, τ was generally found to have an increasing trend for decreasing V_e because of slower self-diffusion and fewer pore visits of larger polymer molecules. However, here, this trend is only observed for medium- and low-molar-mass standards with $V_e > 24$ mL. This behavior was not fully resolved within the present work. While it might stem from the highly individual and hardly tangible interplay of the distinct SEC-hardware elements, another potential reason could be based on the nature of the used standards. According to the manufacturer,[1] the measured polySt standards are guaranteed to be produced exclusively via anionic polymerization up to molar masses of only about 100 000 g mol^{-1} (corresponding to a V_e value between 24 and 25 mL). For higher molar masses, the standards might be produced via other polymerization techniques (e. g., coordinative, radical) and subsequently fractionated to obtain narrow MMDs. Thus, the assumption of Poisson-distributed MMDs is highly doubtful in these cases and the determined EMG parameters might not reflect the true extent of BB. The absolute values for low V_e should therefore be treated with caution. However, the major aim of the here presented experiments is not to absolutely quantify the impact of V_e on EMG broadening—this has already been done in extensive literature studies[47]—but to determine the *change* of BB parameters depending on operating conditions. Therefore, the general divergence of MMDs from the Poissonian shape is not crucial as long as standards of the same production line are analyzed and compared.

7.2.1.2 Mass-dependent band broadening

To clarify the general impact of V_{inj} and [polymer], the seven σ_G and τ values over the complete V_e range were respectively combined to average σ_G and τ values. Detailed EMG parameters similar to Figure 7.4 are given in Appendix B.4 on page 238 for every conducted SEC experiment. In this context, it should be stated that the basic trends are rather close to the ones observed in Figure 7.4. In Figure 7.5 on the next page, the average EMG parameters as well as the standard deviation, σ (see Equation 6.7 on page 149),

[1] Polymer Standards Service (PSS), Mainz, Germany; telephone conversation; June 2013.

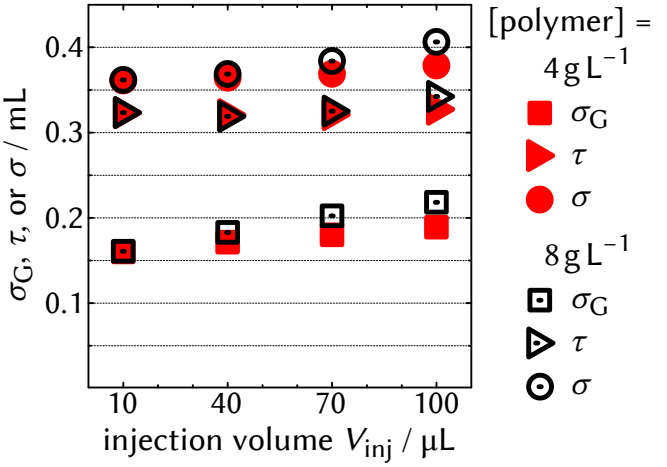

Figure 7.5 Average values of EMG parameters, σ_G and τ, and standard deviations, σ, as a function of V_{inj} for polySt standards and [polymer] as indicated. Other operating parameters: $v_{flow} = 1.00\,mL\,min^{-1}$, $T_{col} = 35\,°C$.

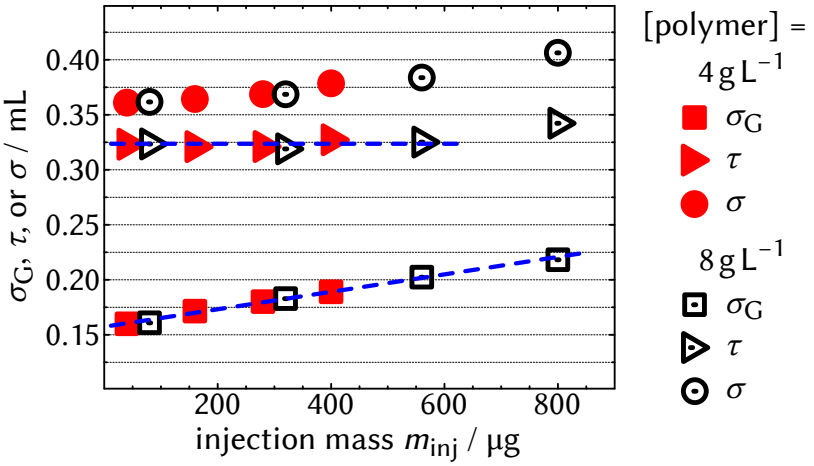

Figure 7.6 Average values of EMG parameters, σ_G and τ, and standard deviations, σ, from Figure 7.5 as a function of m_{inj} (= $V_{inj} \cdot$ [polymer]). The dashed lines are given to guide the eye.

as a function of V_{inj} are presented for [polymer] = $4\,g\,L^{-1}$ and $8\,g\,L^{-1}$. For $4\,g\,L^{-1}$, τ is almost independent of V_{inj} with values of about 0.32 mL. For σ_G, a small but systematical increase is observed with increasing V_{inj} as it is about 0.03 mL higher for $V_{inj} = 100\,\mu L$ than for 10 µL. The same trend can be observed for [polymer] = $8\,g\,L^{-1}$, while there, the effect is about twice as pronounced and σ_G increases by 0.06 mL from $V_{inj} = 10\,\mu L$ to 100 µL. Up to $V_{inj} = 70\,\mu L$, τ is almost identical to the case of [polymer] = $4\,g\,L^{-1}$, whereas for 100 µL, it is slightly higher.

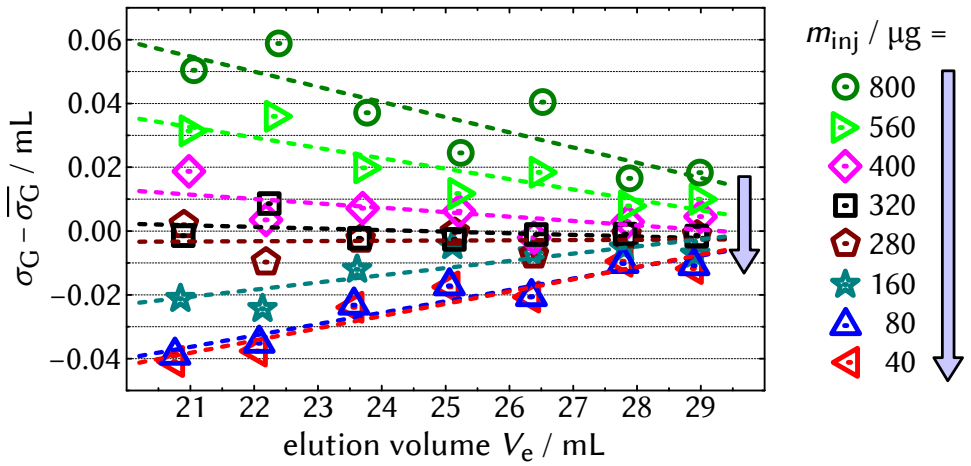

Figure 7.7 Difference of σ_G of polySt standards for m_{inj} as indicated (cf. Figure 7.6 on the previous page) to the average σ_G value of the respective standard for all m_{inj}, $\overline{\sigma_G}$. The linear best-fit is given for each m_{inj}.

The results for σ_G indicate that their determining factor is indeed the injection mass, m_{inj} (= $V_{inj} \cdot$ [polymer]). In Figure 7.6 on the previous page, the EMG parameters of Figure 7.5 are presented as a function of m_{inj} rather than V_{inj}. Except for the already mentioned value for $m_{inj} = 800\,\mu g$, τ is independent of m_{inj}. In contrast, σ_G linearly increases with higher m_{inj}, irrespectively of the actual V_{inj} or [polymer] value. Indeed, the contribution of V_{inj} to the total variance of the Gaussian broadening, ${\sigma_G}^2$, can be estimated via[245] ${\sigma_{inj}}^2 = 1/12 \cdot {V_{inj}}^2$ and is smaller than 2 % for every experiment. Generally higher σ_G values for higher m_{inj} can be ascribed to a higher local viscosity of the solution when more polymer is solved, which leads to more pronounced BB and is sometimes referred to as *viscous fingering*.[246]

A look back at Figure 7.4 on page 161 indicates that σ_G does not increase by the same extent for every polymer standard. In fact, the dependence on m_{inj} is higher for lower V_e, since higher-molar-mass polymer has a more pronounced impact on the local viscosity. In Figure 7.7, for all m_{inj}, the σ_G values of every standard are given as the difference to the average σ_G value of the same standard for all m_{inj}, $\overline{\sigma_G}$ (consequently, the sum for each standard equals zero). While σ_G is generally higher for high m_{inj}, it is evident that the impact of m_{inj} on σ_G becomes more pronounced for lower V_e.

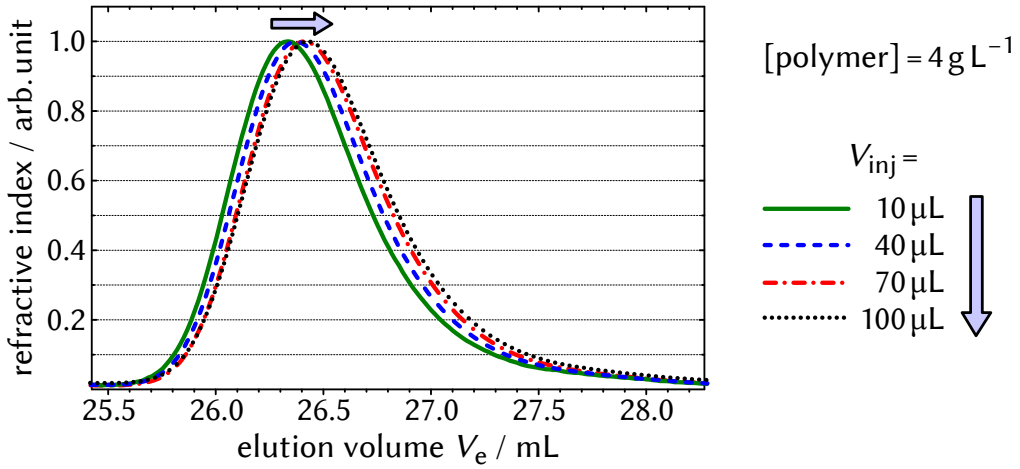

Figure 7.8 Elution chromatograms of a polySt standard with M_{peak} = 34 800 g mol^{-1} (all normalized to the same maximum intensity) for experimental conditions as indicated. For higher V_{inj}, the signal shifts to higher V_e. Other operating parameters: v_{flow} = 1.00 mL min^{-1}, T_{col} = 35 °C.

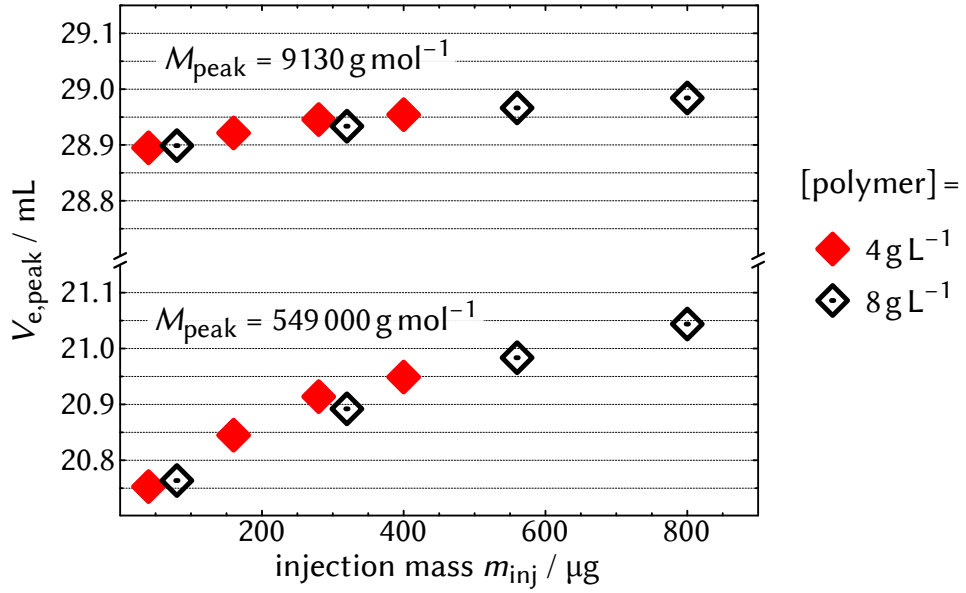

Figure 7.9 V_e at peak position, $V_{e,peak}$, of the chromatograms of the lowest- (top) and the highest-molar-mass polySt standard (bottom) as a function of m_{inj}. Other operating parameters: v_{flow} = 1.00 mL min^{-1}, T_{col} = 35 °C.

7.2.1.3 Impact on $V_{e,peak}$

Besides its impact on the extent of BB, m_{inj} significantly affects the retention behavior of the polymer standards. Figure 7.8 on the preceding page exemplarily shows the chromatograms of the standard with M_{peak} = 34 800 g mol^{-1} for [polymer] = 4 g L^{-1} and different V_{inj}. For higher V_{inj}, retention is longer and the signal is shifted to higher V_e. This effect is a special feature of SEC and not observed in other LC methods.[48] It is mainly assigned to lower effective V_h of polymer chains when a higher number of chains compete for space in solution.[247] This effect was found to be more pronounced for larger macromolecules,[247] which can be illustrated by comparing retention of the lowest- and the highest-molar-mass standard (see Figure 7.9 on the previous page). While for M_{peak} = 9130 g mol^{-1}, $V_{e,peak}$ shifts about +0.1 mL from m_{inj} = 40 to 800 µg, it shifts about +0.3 mL for M_{peak} = 549 000 g mol^{-1}. As mentioned above, a shift of $V_{e,peak}$ can be very crucial for the calibration process and potentially affects subsequent molar-mass determination, which will be discussed in more detail in Section 8 on page 173.

It should be stated that for common SEC analysis, it is recommended reducing m_{inj} until no significant impact on the shape (= BBF) or retention of a chromatogram is observed.[248] This way, avoidable noninstrumental effects that distort molar-mass determination are minimized. As presented, this holds especially true when high-molar-mass polymer is analyzed, while low-molar-mass polymer is much less affected even for high m_{inj}. In addition, these effects are expected to be much less pronounced as MMDs become broader and polymer molecules more dispersed along the columns. As a rule of thumb, for reasonable m_{inj} values in the range of the ones applied here, these effects are significant for $Đ < 1.15$, so that the here obtained variations of σ_G and $V_{e,peak}$ are closely related to the narrow-distribution polymer standards and do not generally hold true for all polymer. As a side note, while no significant difference in σ_G or $V_{e,peak}$ is observed between m_{inj} = 40 µg and 80 µg, no calibration procedures should be conducted for $m_{inj} > 80$ µg for the here used SEC setup. Otherwise, errors are expected especially for high molar masses.

7.2.1.4 Polymer stability in solution

Polymer chains are usually less stable and more prone to decomposition when in solution rather than in their solid state.[249] Indeed, manufactur-

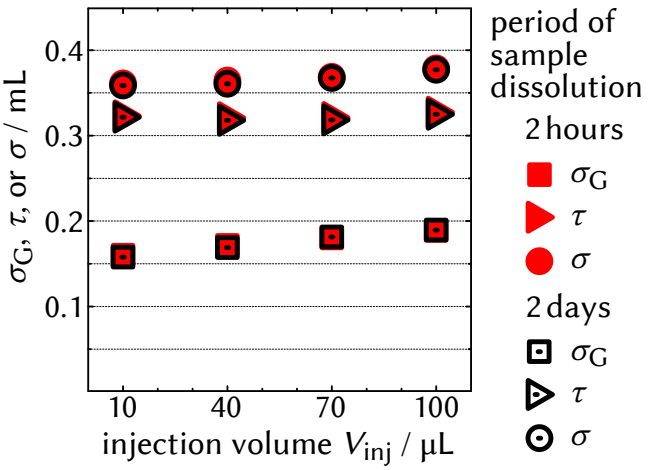

Figure 7.10 Average values of EMG parameters, σ_G and τ, and standard deviations, σ, as a function of V_{inj} for polySt standards and different periods of sample dissolution as indicated. Other operating parameters: [polymer] = 4 g L^{-1}, v_{flow} = 1.00 mL min^{-1}, T_{col} = 35 °C.

ers of polymer standards recommend keeping the period between sample dissolution and measurement short. While one has to be aware of this effect when conducting SEC experiments in general, it might be especially important for studying the impact of v_{flow} on the extent of BB, which will be presented in the next section. In this context, for the lowest v_{flow}, the measurement of one single polymer sample takes several hours, during which subsequent samples are pending in the autosampler. To test the significance for the employed polySt standards, the results in Figure 7.5 on page 163 for [polymer] = 4 g L^{-1}—which were measured after 2 h of sample dissolution—were compared to results of measurements under identical conditions, except that the dissolution period was extended to 2 d. The almost identical results are presented in Figure 7.10 and indeed show that decomposition does not take place for polySt within at least 2 d. In addition, the results indicate the high quality of reproducibility of the SEC experiments. This can also be seen in the retention behavior, as the respective $V_{e,peak}$ values for all standards and V_{inj} statistically differ by only about 0.015 mL on average (data not shown).

7.2.2 Flow rate and temperature

7.2.2.1 Impact on band broadening

Investigations of the impact of v_{flow} and T_{col} on the extent of BB were conducted similarly to the impact of V_{inj} and [polymer] in the previous

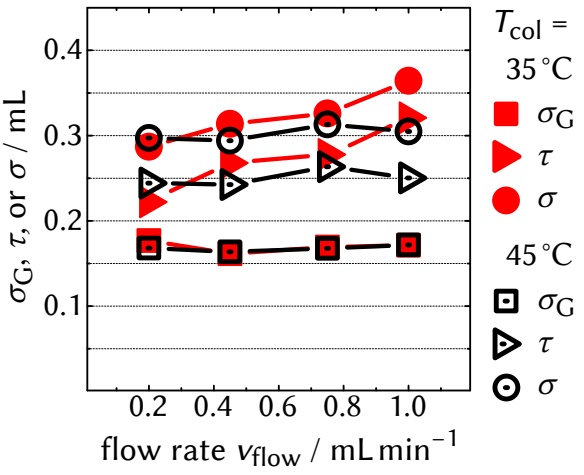

Figure 7.11 Average values of EMG parameters, σ_G and τ, and standard deviations, σ, as a function of v_{flow} for polySt standards and T_{col} as indicated. Other operating parameters: [polymer] = 4 g L^{-1}, V_{inj} = 40 µL.

section. PolySt standards were measured at either T_{col} = 35 °C or 45 °C for v_{flow} = 0.20 mL min^{-1}, 0.45 mL min^{-1}, 0.75 mL min^{-1}, and 1.00 mL min^{-1}, while V_{inj} = 40 µL and [polymer] = 4 g L^{-1} remained unchanged. The resulting average values of σ_G, τ, and σ are given in Figure 7.11. σ_G is remarkably independent of both T_{col} and v_{flow} with consistent values of about 0.17 mL. On the contrary, τ is sensitive to changes in both v_{flow} and T_{col}. For T_{col} = 35 °C, τ significantly increases for higher v_{flow} with a difference of 0.10 mL between v_{flow} = 0.20 mL min^{-1} and 1.00 mL min^{-1}. This result is consistent with findings in the literature indicating higher skewness for higher v_{flow}.[191,223] It is also in agreement with the prevalent concepts of skewing: for lower v_{flow}, SEC experiments take longer and therefore polymer molecules have more time (i) for lateral diffusion to average radial positions and (ii) to perform a greater number of pore visits. For T_{col} = 45 °C, this effect is much less pronounced and over the complete v_{flow} range, τ only slightly varies between 0.24 mL and 0.27 mL. To the best of knowledge, no thorough investigation of the impact of T_{col} on skewing exists in the literature. However, skewness should generally decrease with higher T_{col}, since higher temperatures and the resulting lower viscosity of the eluent leads to faster self-diffusion of the analyte. Lower skewing is indeed generally obtained for T_{col} = 45 °C with the average τ value being 0.02 mL smaller than for 35 °C. While the lower sensitivity of τ to v_{flow} at T_{col} = 45 °C remains unclear at the moment, it might indicate that under conditions that lead to reduced skewing, the impact of parameters like v_{flow} on skewing is less pronounced than under conditions for which skewing is generally higher.

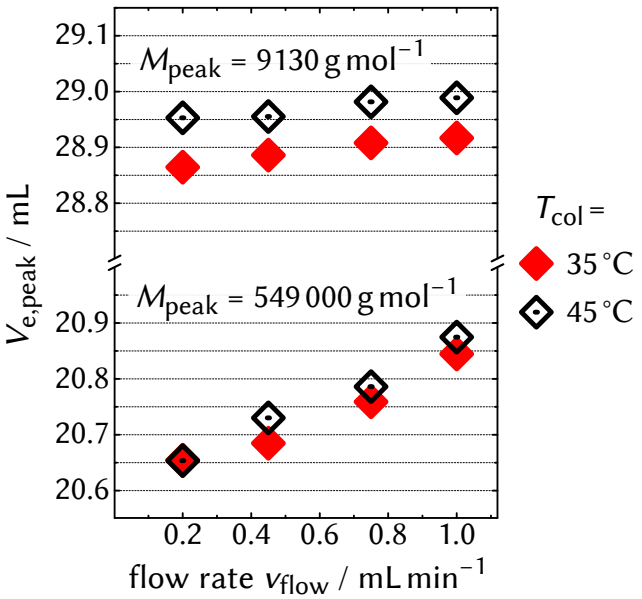

Figure 7.12 V_e at peak position, $V_{e,peak}$, of the chromatograms of the lowest- (top) and the highest-molar-mass polySt standard (bottom) as a function of v_{flow} with T_{col} as indicated. Other operating parameters: [polymer] = 4 g L^{-1}, V_{inj} = 40 µL.

Low- and high-molar-mass polymer

Similar to the higher sensitivity of σ_G toward m_{inj} for high-molar-mass polymer presented in Figure 7.7 on page 164, τ is also more sensitive to v_{flow} for high than for low molar masses. In this context, the linear best-fit of τ versus V_e (as in Figure 7.7) leads to $\Delta\tau$ = 0.07 mL for $V_e \approx$ 29 mL and to $\Delta\tau$ = 0.13 mL for $V_e \approx$ 21 mL between v_{flow} = 0.20 mL min^{-1} and 1.00 mL min^{-1} (data not shown).

7.2.2.2 Impact on $V_{e,peak}$

Similar to m_{inj}, variations of both v_{flow} and T_{col} affect retention behavior and shift the standards' $V_{e,peak}$ values. As presented in Figure 7.12, higher v_{flow} leads to later elution, while this effect is more pronounced for high molar masses with $\Delta V_{e,peak} \approx$ +0.05 mL for M_{peak} = 9130 g mol^{-1} and $\Delta V_{e,peak} \approx$ +0.20 mL for M_{peak} = 549 000 g mol^{-1} from v_{flow} = 0.20 mL min^{-1} to 1.00 mL min^{-1} for both T_{col}. In contrast, from T_{col} = 35 °C to 45 °C, $\Delta V_{e,peak}$ is more pronounced for *low* than for high molar masses (+0.08 mL versus +0.03 mL on average). Only a few literature studies about the influence of v_{flow} and T_{col} on SEC retention exist[48] and the crucial mechanisms are not fully understood yet. Reliable interpretations are difficult to give since obtained trends often are contradictory or seem to highly depend on the individual SEC system. Theoretically, retention is expected to be indepen-

dent of v_{flow} since it should not influence the equilibrium of the analyte between the MP and SP.[250] However, in some studies, retention is affected by v_{flow}, which led to complex concepts that assume flow-dependent failure of the entropic separation model,[48,251] thus influencing the extent of SP–MP mass-transfer. SP–MP mass-transfer might be also individually affected by the flow-dependent operating pressure and its impact on analyte and pore dimensions.[251] In addition, the flow-dependent velocity profile inside the columns and tubes is also expected to influence retention.[252]

Concepts for the impact of T_{col} are generally more consistent and yet highly individual for the used SEC system. As a rather straightforward effect, T_{col} influences the solubility and therefore V_h of polymer chains. While this is sometimes referred to as negligible for T_{col} changes by a few tens of °C, general statements should be made with caution in this context. Whether V_h increases or decreases in a significant matter or not depends on the polymer, the solvent, and the temperature region. For example, for the here investigated system of linear polySt in THF, smaller V_h are expected from T_{col} = 35 °C to 45 °C as the intrinsic viscosity $[\eta]$ was shown to decrease by about 3 %.[253] This is indeed in accordance with the observed higher $V_{e,peak}$ values. Besides the impact of T_{col} on V_h, literature studies revealed that for systems with significant nonideal interactions between the polymer and the SP, higher temperatures can lead to lower interactions and therefore faster elution.[254] In addition, changes of T_{col} might also affect the swelling behavior and porosity of the SP.[255]

The fact that the presented trends of $V_{e,peak}$ in Figure 7.12 are systematical for both v_{flow} and T_{col} indicate that noncontrary mechanisms might be involved here. However, it should again be noted that by the current state of knowledge, these trends are expected to be highly individual for the given SEC system and that general predictions about the impact of v_{flow} or T_{col} on retention are difficult to make. Therefore, it is recommended estimating a potential shift of $V_{e,peak}$ by experiment rather than by theoretical considerations or by relying on literature results. It is a matter of course that individual calibration is required for different values of v_{flow} and T_{col}.

7.3 Concluding remarks

The presented results show how variations of fundamental operating parameters affect both the BB and the retention behavior of narrow-distribution polymer. In this context, it should be emphasized that the EMG function

appears to be highly suitable to model the BBF in SEC. At first sight, this seems to be evident from the excellent fitting of experimentally obtained chromatograms exemplarily shown in Figure 7.3 on page 160. However, several other mathematical functions exist that are also considered to be adequate to express skewed chromatograms.[256] The much more exceptional effect here is that the EMG parameters σ_G and τ are individually affected by the change of certain experimental conditions. In this context, it is shown that m_{inj} affects σ_G while τ remains constant, whereas for different v_{flow} and T_{col}, it is the other way around. This finding does not only support the EMG function as a reliable model to empirically describe BB. It does even support the aforementioned theories of BB in SEC with its separable mechanisms causing (i) symmetric Gaussian broadening and (ii) exponential-like skewing. It should be noted that this is remarkable also because of the low complexity of the EMG function, which extends the classic Gaussian approach by only *one* individual parameter. Originally, the EMG function was in fact mainly introduced as a simple model to better express the obviously skewed shape of SEC traces in order to more precisely determine plate counts or chromatographic resolution.[235,257] In addition, as stated during the discussion of the here obtained results, the impact of fundamental operating parameters has already been investigated[48] in terms of *general* broadness and asymmetry (via individual asymmetry factors). In this context, it should be noted that both σ_G and τ contribute to both the standard deviation σ and the skewness γ of an EMG function (cf. Equation 6.7 on page 149). Therefore, a change of an operating parameter most likely results in a change of both σ and γ—for example, a constant τ and higher σ_G leads to a higher σ and lower γ, while a constant σ_G and higher τ leads to a higher σ and higher γ. This makes the separate consideration of σ_G and τ rather than the classic σ and γ worthwhile and helps to unambiguously assign the impact of certain parameters on BB.

CHAPTER 8

Impact of band broadening on molar-mass determination in (quasi-)living polymerizations

In this section, the impact of BB on molar-mass determination will be presented on the basis of both simulation and experimental results. Special focus will be laid on the analysis of (Q)LP systems such as well-controlled RDRPs, as effects might be of particular importance for the interpretation of the iodine-mediated polymerizations presented in Part II of this thesis. Previously, there have been studies of the impact of BB on MMDs obtained from PLP[258] and steady-state polymerization,[201,259] for example. In addition, models introduced by Hamielec and Ray express what effect BB can generally have on MMDs' average molar-mass values.[260,261] However, to the best of knowledge, there has never been a systematic investigation of how BB affects analysis of (Q)LP systems.

BB will be simulated applying EMG broadening to Poisson-distributed polymer as it is ideally obtained from (Q)LP systems. The impact of σ_G and τ on the characteristic $\overline{M}_n$ (or $\overline{DP}_n$) and $Đ$ values of the simulated MMDs will be displayed as a function of monomer conversion, which is very common for the analysis of (Q)LP systems. As will then be further clarified by a thorough quantitative evaluation in Section 8.2.2 on page 186, the found effects are expected to be molar-mass-dependent and therefore particularly significant for the analysis of gradually growing polymer that evolves through different molar-mass regions of the SEC separation range. In fact, the obtained results remarkably resemble trends frequently found in analyses of (Q)LP systems.

Eventually, strategies will be discussed to avoid the revealed pitfalls in SEC analysis and to enable more reliable molar-mass determination of polymer.

Before the results will be presented, the method to obtain broadened MMDs will be explained in the following. It should again be noted that the impact of BB on molar-mass determination is already present during the crucial calibration process, since BB is an inherent feature of SEC, whether it is during calibration or during the eventual measurement of the analyte.

8.1 Method

8.1.1 Calibration functions

As BB—particularly skewing—affects chromatograms not only in terms of broadness but also in terms of $V_{e,peak}$ (cf. Figure 7.3 on page 160), individual calibration functions were simulated for every investigated combination of σ_G and τ. For this, elution chromatograms of polySt standards were measured over the complete SEC separation range and σ_G and τ were respectively determined similar to the parameter estimation in Section 7. Besides the extent of BB, this procedure gives the shape of the unbroadened (= true) chromatogram $RI^{unbr}(V_e)$ for the case of $\sigma_G = \tau = 0\,mL$ (see Figure 7.3 on page 160). On the basis of $RI^{unbr}(V_e)$, for every standard, broadened chromatograms were systematically simulated for different values of σ_G and τ and individual apparent calibration functions were created by means of the resulting $V_{e,peak}$ values. In this context, it should be noted that for all the simulations presented in this section, EMG parameters were assumed to be uniform, i. e., constant over the complete V_e range. As already mentioned, this is not expected to occur in reality, however, it simplifies interpretation of the observed effects. The so-created calibration functions were then implemented in the BB routine for the investigated simulated analyte MMDs, which is described in the following.

8.1.2 MMD simulations

In a typical procedure, an unbroadened Poissonian MMD with a specific initial $\overline{DP}_n$ value, $\overline{DP}_n^0$ (= ν), is simulated and translated into an unbroadened elution chromatogram via the true calibration function for $\sigma_G = \tau = 0\,mL$. Subsequently, the chromatogram is broadened with certain values of σ_G and τ to obtain the broadened chromatogram, which is finally retranslated into the broadened MMD by applying the calibration function for the used σ_G

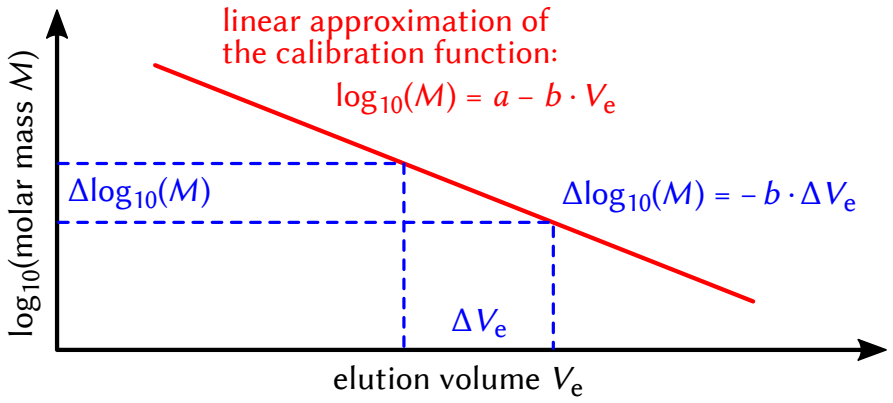

Figure 8.1 Linear approximation of a calibration function in SEC with the intercept and the slope value, a and $-b$, respectively.

and τ values. The apparent $\overline{DP}_n$ and $Đ$ of the broadened MMD are then determined.

8.2 Results and discussion

8.2.1 (Quasi-)living polymerization

8.2.1.1 Dispersity

Simulations were conducted for six different Poissonian polySt MMDs with $\overline{DP}_n^0$ = 50, 100, 150, 200, 250, and 300. The increasing true $\overline{DP}_n^0$ values mimic an increasing monomer conversion during polymerization, which is linearly linked with the expected $\overline{DP}_n^0$ in case of (Q)LPs (with $\overline{DP}_n^0$ = 300 for full monomer conversion). The obtained apparent $\overline{DP}_n$ and $Đ$ values are then displayed as a function of $\overline{DP}_n^0$ giving the common representation of $\overline{DP}_n$ (or $\overline{M}_n$) and $Đ$ versus monomer conversion. The calibration functions simulated for this section are based on chromatograms obtained from SEC setup 1 (cf. Experimental Section 10.2.4 on page 223). For the investigated V_e region, the slope of the calibration function can be approximated with $b \approx 0.26\,\mathrm{mL}^{-1}$. The b value is essential for the universal evaluation of BB effects on molar-mass determination among different SEC setups since a certain broadness on the V_e scale (= ΔV_e) has a bigger impact on the $\log_{10}(M)$ scale (= $\Delta \log_{10}(M)$) when the calibration function is steeper (= has a high b value, see Figure 8.1). Notably, calibration functions usually obtained

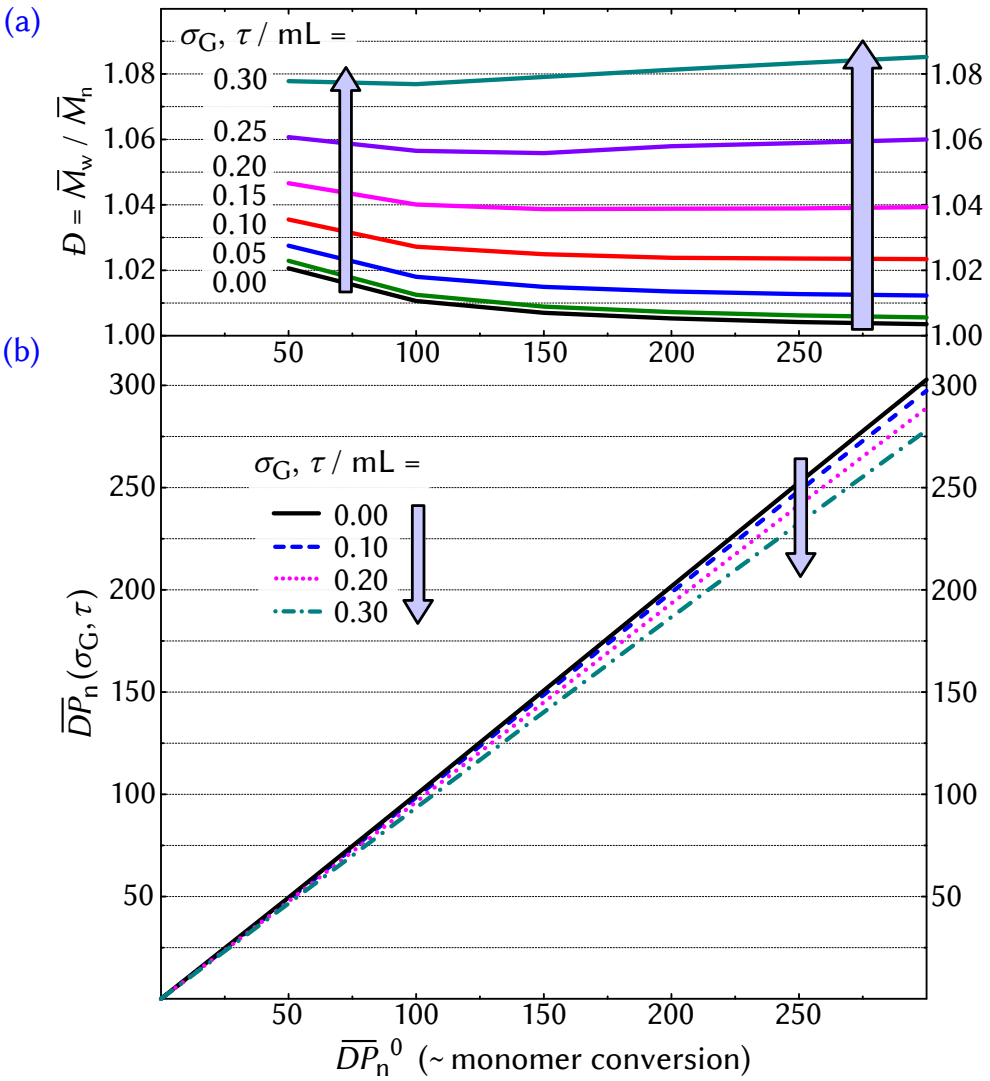

Figure 8.2 Apparent (a) $Đ$ and (b) $\overline{DP}_n$ values versus the initial (true) $\overline{DP}_n^0$ of the unbroadened Poissonian MMD for different EMG parameters from $\sigma_G = \tau = 0.00$ mL to 0.30 mL as indicated (slope of the calibration function: $b \approx 0.26\,\text{mL}^{-1}$).

slightly deviate from linear behavior, which can lead to remarkable effects concerning BB, which will be discussed in the following.

In Figure 8.2a on the current page, plots of apparent $Đ$ as a function of $\overline{DP}_n^0$ are presented for MMDs that underwent BB with $\sigma_G = \tau$ increasing together from 0.00 mL to 0.30 mL in steps of 0.05 mL. For $\sigma_G = \tau = 0.00$ mL (no BB), the Poisson result $Đ = 1 + 1/\overline{DP}_n^0$ is correctly obtained. Note the

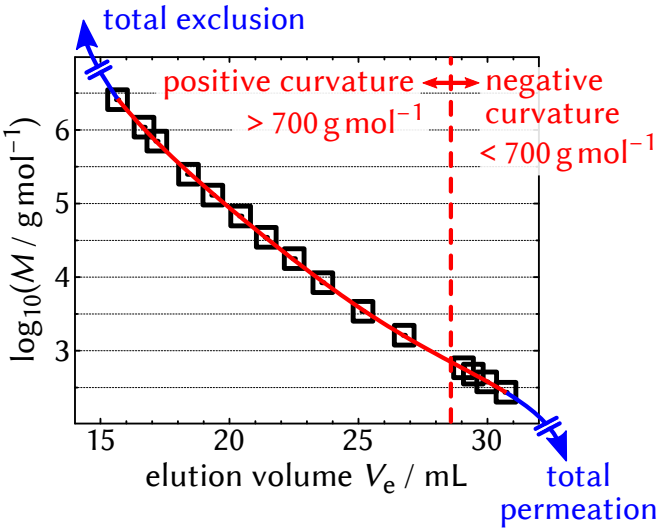

Figure 8.3
Calibration points ($\log_{10}(M_{peak})$ versus $V_{e,peak}$) for SEC setup 1 fitted by a calibration function (5^{th}-degree polynomial) with indicated regions of positive and negative curvature.

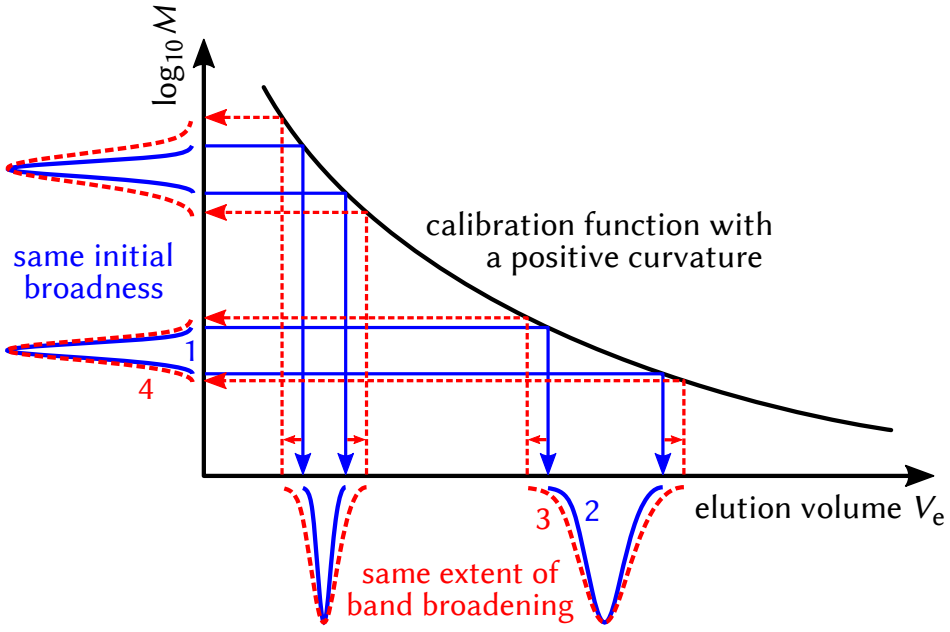

Figure 8.4 Illustration of the effect of an SEC calibration function ($\log_{10}(M)$ versus V_e) with a positive curvature on the apparent (broadened) MMDs. The initially unbroadened MMDs (1, full lines, $\log_{10}(M)$ axis) are translated into unbroadened chromatograms (2, full lines, V_e axis). Then, the same extent of band broadening is applied to both chromatograms giving rise to the broadened chromatograms (3, broken lines, V_e axis). After retranslation into broadened MMDs (4, broken lines, $\log_{10}(M)$ axis), the effect of higher broadening for higher $\log_{10}(M)$ can clearly be observed.

natural descending trend of this equation for increasing $\overline{DP}_n^0$. As expected, $Đ$ increases as BB becomes stronger. For $\sigma_G = \tau \geq 0.20\,\text{mL}$, $Đ$ even defies the descending trend at high $\overline{DP}_n^0$. In other words, the influence of BB on $Đ$ is so pronounced at high $\overline{DP}_n^0$ that it overrides the natural trend of $Đ$ for increasing $\overline{DP}_n^0$. This remarkable effect—namely that the same extent of BB has a higher impact on MMD broadness for high $\overline{DP}_n^0$—can be attributed to the individual nature of the involved calibration functions. As mentioned above, in a rough approximation, calibration functions have a linear trend and a constant b value. However, more often than not, they bear significant curvatures and gradually changing b values over the complete V_e (and $\log_{10}(M)$) range. For the here employed SEC setup, the experimental calibration curve is presented in Figure 8.3 on the preceding page and has a wide positive-curvature region while turning into a negative curvature for the oligomeric regime $< 700\,\text{g mol}^{-1}$. This behavior is indeed reasonable as it represents the trends expected from the concept of total exclusion and total permeation. As a consequence of positive curvature, the same amount of BB on the V_e axis has a higher impact on the $\log_{10}(M)$ axis when BB occurs for low V_e. This effect is schematically illustrated in Figure 8.4 on the previous page. In this context, it should be noted that for the typical chromatographic scaling of an SEC-derived MMD (RI versus $\log_{10}(M)$), the $Đ$ value remains constant if the MMD is shifted (without being stretched) along the $\log_{10}(M)$ axis. In other words, when the broadness of an MMD in an RI-versus-$\log_{10}(M)$ diagram is higher than the broadness of another MMD, its $Đ$ value is higher as well, irrespective of the actual position along the $\log_{10}(M)$ axis.

It is worth mentioning that this effect might also be involved in the finding that BB seemingly increases with increasing M_{peak} of polymer standards,[206] even if the BBF is close to uniform. In this regard, it is important to also be aware that a linear or almost linear shape of the calibration function only works for molar masses given on a *logarithmic* scale. In case of a *linear* molar-mass scale, the same extent of BB in an elution chromatogram covers a much wider molar-mass range for high than for low molar masses. BB could thus be mistakenly considered as much more pronounced for higher molar masses when SEC-derived MMDs are compared with MMDs obtained from methods such as MALDI-MS, which are commonly given on a linear molar-mass scale.

Notably, the effect presented in Figure 8.4 strongly depends on the individual (and rather unpredictable) nature of the calibration function. In case of a linear region (zero curvature), BB would affect $Đ$ values equally. In case

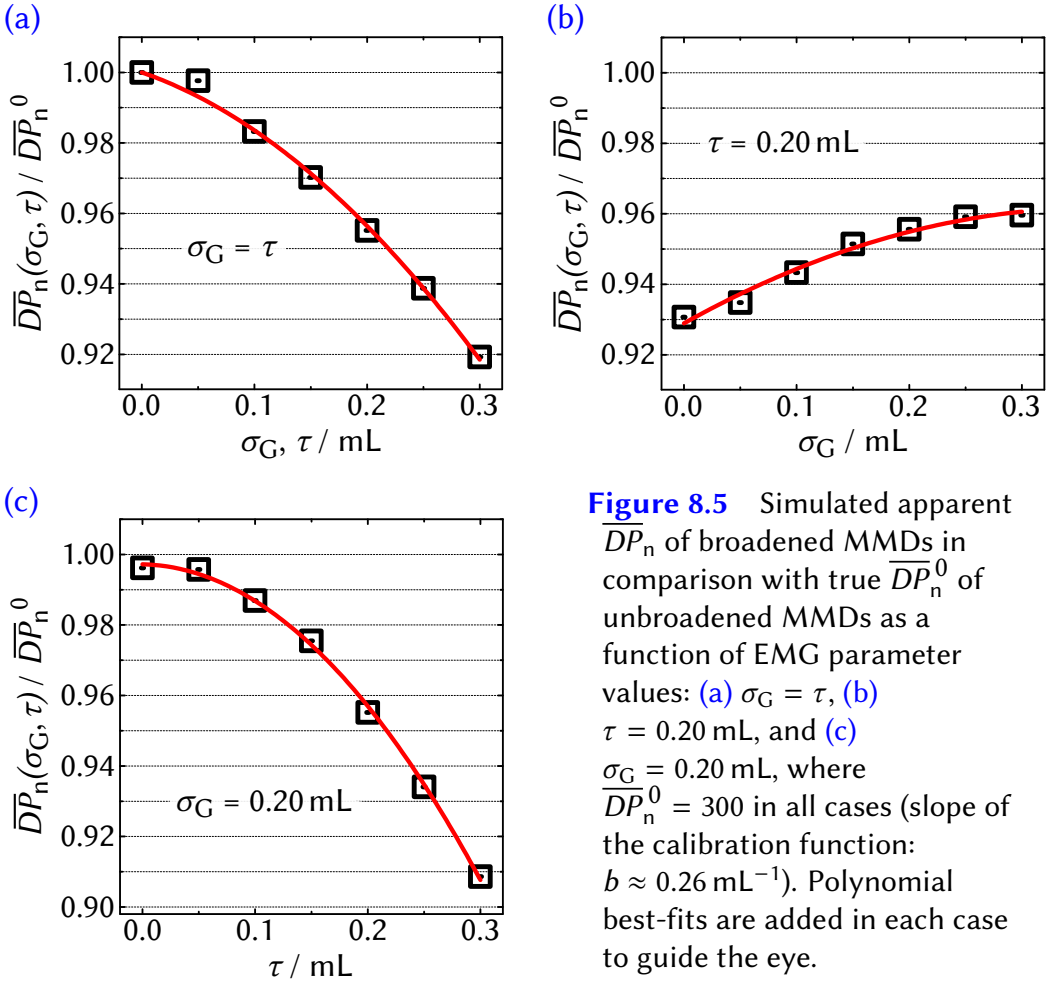

Figure 8.5 Simulated apparent $\overline{DP}_n$ of broadened MMDs in comparison with true $\overline{DP}_n^0$ of unbroadened MMDs as a function of EMG parameter values: (a) $\sigma_G = \tau$, (b) $\tau = 0.20\,\text{mL}$, and (c) $\sigma_G = 0.20\,\text{mL}$, where $\overline{DP}_n^0 = 300$ in all cases (slope of the calibration function: $b \approx 0.26\,\text{mL}^{-1}$). Polynomial best-fits are added in each case to guide the eye.

of a region with a negative curvature, BB would even have a higher impact for *low* molar masses. However, these two cases are arguably less striking since they do not challenge the naturally descending trend of $Đ$.

8.2.1.2 Number-average degree of polymerization

Figure 8.2b shows that for all extents of BB, $\overline{DP}_n$ increases almost linearly for increasing $\overline{DP}_n^0$, while lower slopes are obtained for higher σ_G and τ. Figure 8.5a on this page illustrates this in an alternative way by giving the ratio between $\overline{DP}_n$ and $\overline{DP}_n^0$ as a function of $\sigma_G = \tau$ for $\overline{DP}_n^0 = 300$. In agreement with Figure 8.2b, the plot shows a downward trend and increasing deviation of $\overline{DP}_n$ from $\overline{DP}_n^0$ with increasing EMG parameter values. The downward

deviation up to about 8 % from the true $\overline{DP}_\mathrm{n}^{\,0}$ value for a reasonable extent of BB indicates that this effect is rather significant. Figures 8.5b and 8.5c give $\overline{DP}_\mathrm{n}/\overline{DP}_\mathrm{n}^{\,0}$ obtained from simulations for a fixed value of 0.20 mL for either τ or σ_G so as to illustrate the individual effect of each EMG parameter. In Figure 8.5c, higher τ values cause a strong decrease of $\overline{DP}_\mathrm{n}$, almost the same as in Figure 8.5a. On the other hand, there is a less pronounced sensitivity of $\overline{DP}_\mathrm{n}$ to σ_G in Figure 8.5b, in which it actually trends slightly *closer* to $\overline{DP}_\mathrm{n}^{\,0}$ as σ_G increases. Taken together, the results of Figure 8.5 amount to a clear illustration of the finding that BB leads to downward deviations of apparent $\overline{DP}_\mathrm{n}$ from true $\overline{DP}_\mathrm{n}^{\,0}$ values, which is mainly due to τ, whereas σ_G only has a slight but opposed impact on $\overline{DP}_\mathrm{n}$.

The observed trends for different σ_G and τ can be explained by the individual influence of the parameters on the shape of the obtained chromatogram. In case of $\sigma_\mathrm{G} = \tau = 0.00\,\mathrm{mL}$, the chromatogram is almost symmetric for $\overline{DP}_\mathrm{n}^{\,0} = 300$. (Indeed, symmetry decreases for lower $\overline{DP}_\mathrm{n}^{\,0}$ values, which will be discussed later in Section 8.2.2.2 on page 188.) This symmetry leads to nearly identical values of $V_\mathrm{e,peak}$ and the average elution volume, $\overline{V_\mathrm{e}}$. An increasing skewing of the chromatogram through BB leads to a higher divergence of $V_\mathrm{e,peak}$ from $\overline{V_\mathrm{e}}$, more precisely to lower $V_\mathrm{e,peak}$ values compared with $\overline{V_\mathrm{e}}$ (since skewing is toward higher V_e values). As $V_\mathrm{e,peak}$ is used in the calibration process and assigned to a given M_peak value, lower $V_\mathrm{e,peak}$ in relation to $\overline{V_\mathrm{e}}$ would lead to lower $\overline{M}_\mathrm{n}$ ($\sim \overline{DP}_\mathrm{n}$) in relation to the *by definition/calibration* constant M_peak value after transforming the chromatogram into an MMD. This effect is illustrated in Figure 8.6 on page 182 for the chromatograms and MMDs with $\overline{DP}_\mathrm{n}^{\,0} = 300$, $\sigma_\mathrm{G} = 0.20\,\mathrm{mL}$, and different τ values. While the $V_\mathrm{e,peak}$ values of the chromatograms are gradually shifted to lower V_e, $\overline{V_\mathrm{e}}$ remains constant (since EMG broadening does not affect $\overline{V_\mathrm{e}}$). When the chromatograms are then translated into MMDs via the respective calibration functions, M_peak is at the same position for every τ value while $\overline{M}_\mathrm{n}$ is inherently lower for higher τ. In this context, the higher intensities at the low-molar-mass side of the MMDs can clearly be observed.

Difference between $V_\mathrm{e,peak}$ and $\overline{V_\mathrm{e}}$

Since the skewness of the EMG function is given by $\gamma = 2(\tau/\sigma)^3$, the ratio between τ and σ ($= \sqrt{{\sigma_\mathrm{G}}^2 + \tau^2}$) plays a crucial role in the shifting of $V_\mathrm{e,peak}$. Notably, the overall skewness of the simulated chromatogram differs from $2(\tau/\sigma)^3$ since the EMG function is employed on a true distribution that

Table 8.1 Simulated influence of the EMG parameters σ_G and τ on $V_{e,peak}$ and $\overline{V_e}$ of an elution chromatogram of Poisson-distributed polySt for $\overline{DP_n}^0 = 300$. Differences of $V_{e,peak}$ and $\overline{V_e}$ are given as an indicator of skewness (slope of the used calibration function: $b \approx 0.26\,mL^{-1}$).

σ_G / mL	τ / mL	$V_{e,peak}$ / mL	$\overline{V_e}$ / mL	$V_{e,peak} - \overline{V_e}$ / mL
0.00	0.00	21.62	21.62	0.00
0.05	0.00	21.62	21.62	0.00
0.10	0.00	21.62	21.62	0.00
0.15	0.00	21.62	21.62	0.00
0.20	0.00	21.62	21.62	0.00
0.25	0.00	21.62	21.62	0.00
0.30	0.00	21.62	21.62	0.00
0.00	0.00	21.62	21.62	0.00
0.00	0.05	21.62	21.62	0.00
0.00	0.10	21.58	21.62	−0.04
0.00	0.15	21.55	21.62	−0.07
0.00	0.20	21.51	21.62	−0.11
0.00	0.25	21.47	21.62	−0.15
0.00	0.30	21.43	21.62	−0.19
0.00	0.20	21.51	21.62	−0.11
0.05	0.20	21.53	21.62	−0.09
0.10	0.20	21.54	21.62	−0.08
0.15	0.20	21.55	21.62	−0.07
0.20	0.20	21.57	21.62	−0.05
0.25	0.20	21.58	21.62	−0.04
0.30	0.20	21.58	21.62	−0.04
0.20	0.00	21.62	21.62	0.00
0.20	0.05	21.62	21.62	0.00
0.20	0.10	21.61	21.62	−0.01
0.20	0.15	21.59	21.62	−0.03
0.20	0.20	21.57	21.62	−0.05
0.20	0.25	21.54	21.62	−0.08
0.20	0.30	21.50	21.62	−0.12

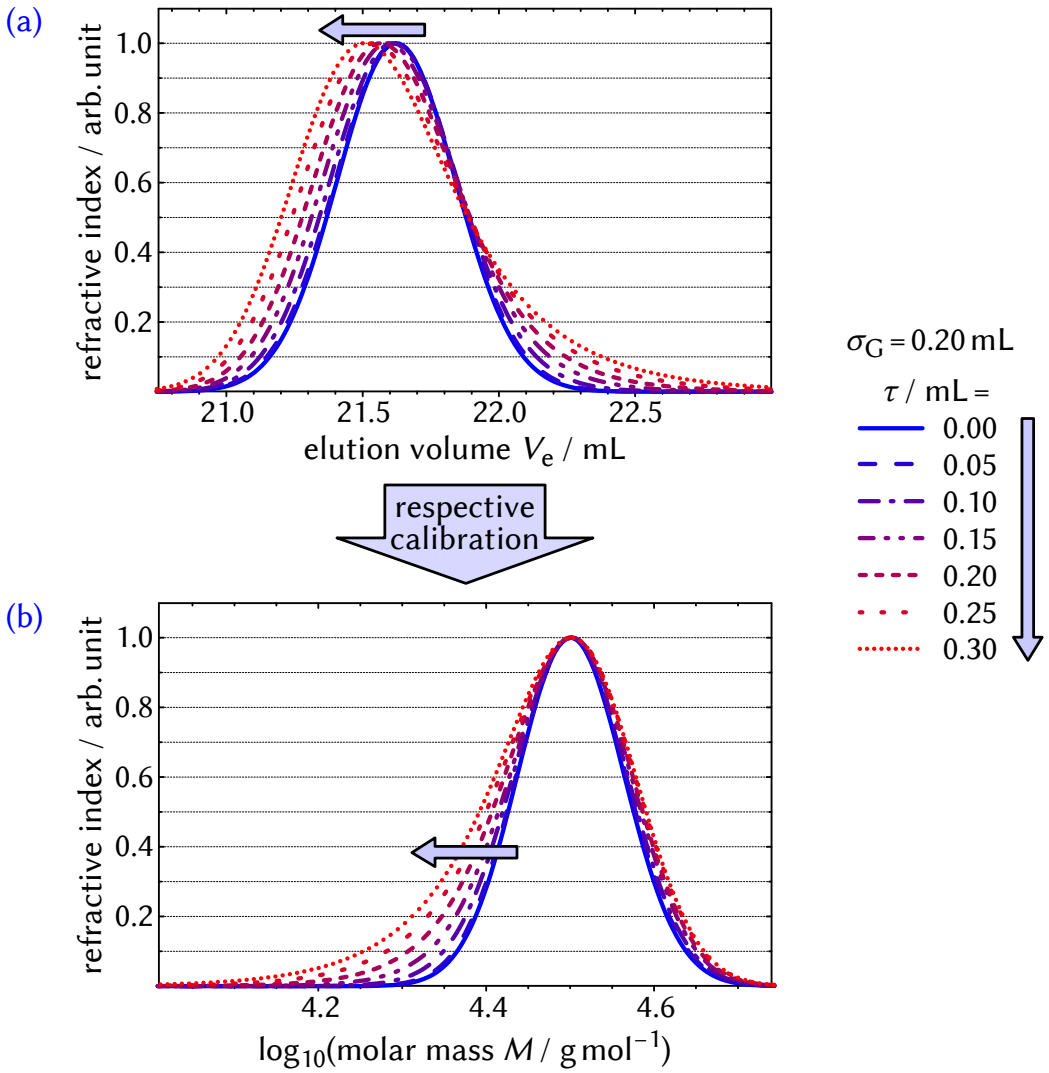

Figure 8.6 Simulated (a) elution chromatograms and (b) MMDs for Poisson-distributed polySt samples with $\overline{DP}_n^0 = 300$ and EMG parameters σ_G and τ as indicated. For ease of comparison, all curves are normalized to the same maximum intensity; slope of the calibration function: $b \approx 0.26\,\mathrm{mL}^{-1}$.

itself contributes broadening and skewing to the overall values,[210] which will be described more precisely at a later stage. Notwithstanding this, it is evident from this skewness relationship that the qualitative effects are for high τ to cause strong skewing while high σ_G increases the symmetry of the distribution. This is supported by Table 8.1 on the previous page, which

gives $V_{e,peak}$ and $\overline{V_e}$ values of chromatograms with $\overline{DP}_n^0 = 300$ for varying values of σ_G and τ while the other parameter is constant at either 0.00 mL or 0.20 mL. In this context, the difference between $V_{e,peak}$ and $\overline{V_e}$ is an indicator of skewness. Since the chromatograms show rather high symmetry for $\tau =$ 0.00 mL, increasing values of σ_G do not affect $V_{e,peak}$. In contrast, increasing τ introduces skewness and shifts $V_{e,peak}$ toward lower values. With fixed values of 0.20 mL for one of the EMG parameters, their competing influence on skewing is clarified. The same values of τ lead to smaller differences between $V_{e,peak}$ and $\overline{V_e}$ for $\sigma_G = 0.20$ mL than they do for $\sigma_G = 0.00$ mL. In addition, an increasing value of σ_G for $\tau = 0.20$ mL even causes reduced differences, as it lowers the skewness of the chromatogram. Both effects can be observed in Figure 8.5b and 8.5c on page 179 and clarify the correlation between the difference of $V_{e,peak}$ and $\overline{V_e}$ and the downward deviation of $\overline{DP}_n$ from $\overline{DP}_n^0$. In this context, the difference between $V_{e,peak}$ and $\overline{V_e}$ provides the basis for a universal quantification and further elucidation of the obtained effect, which will be thoroughly discussed in Section 8.2.2 on page 186. As a general comment, the effect would of course lead to *upward* deviations of $\overline{DP}_n$ from $\overline{DP}_n^0$ in case of *negative* SEC skewing (tailing toward lower V_e values). However, this has indeed not been obtained in any of the numerous literature studies so far.[47,210]

8.2.1.3 Experimentally observed skewing effect

The impact of skewing can also be observed for the SEC results obtained *experimentally* in the context of BB-parameter determination in Section 7. The most significant effect is expected for different v_{flow} at $T_{col} = 35\,°C$ since the highest variation of τ was observed in this case. Elution chromatograms and respective MMDs of the standard with $M_{peak} = 34\,800\,g\,mol^{-1}$ are presented in Figure 8.7 on the following page for this set of experiments. Respective σ_G and τ values are given in the figure caption; for reasons of clarity, the distributions for $v_{flow} = 0.45\,mL\,min^{-1}$ are omitted since the determined EMG parameters are almost equal to the case of $v_{flow} = 0.75\,mL\,min^{-1}$. While skewness increases for higher v_{flow}, $\overline{M}_n$ systematically decreases about 4 % from the slowest to the fastest flow. Notably, the effect appears to be smaller than in Figure 8.6 on the preceding page, which is simply due to τ increasing by only about 0.1 mL in total from an already existing skewing with $\tau = 0.26$ mL. Thus, even the highest apparent $\overline{M}_n$ is expected to be lower than the true $\overline{M}_n$ value. In contrast to simulations, experimentally obtained $\overline{M}_n$ results are of course prone to potential uncertainties during the ex-

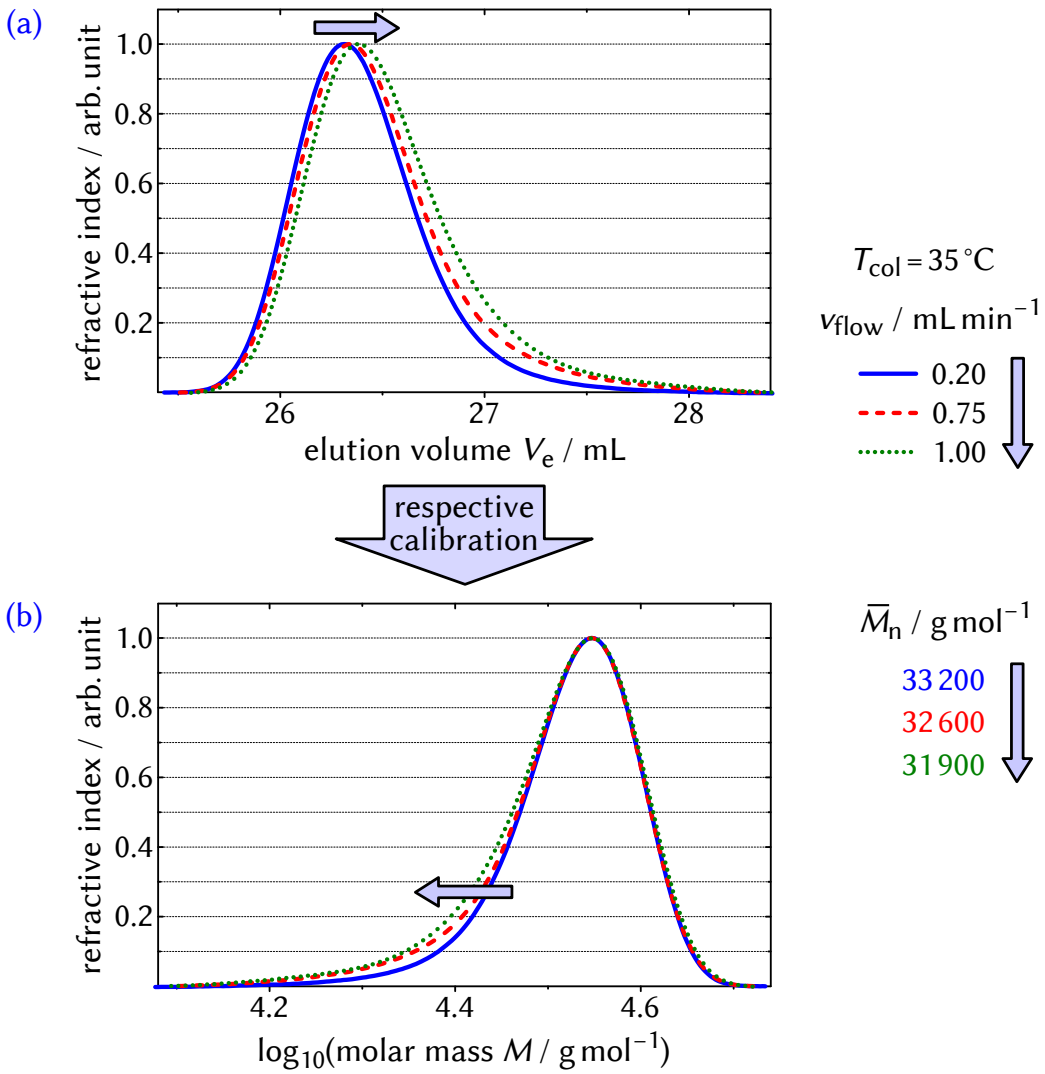

Figure 8.7 (a) Experimentally obtained elution chromatograms for the same polySt standard (M_{peak} = 34 800 g mol^{-1}) at different flow rates, v_{flow}, (cf. Figure 7.11 on page 168) and (b) respective MMDs (all curves are normalized to the same maximum intensity). For higher skewness of the elution chromatogram, lower $\overline{M}_n$ values are obtained: v_{flow} = 0.20 mL min^{-1} (σ_G = 0.19 mL, τ = 0.26 mL); 0.75 mL min^{-1} (0.19 mL, 0.30 mL); 1.00 mL min^{-1} (0.19 mL, 0.35 mL). Slope of the calibration functions: $b \approx 0.21$ mL^{-1}.

periment or data interpretation.[248,262,263] However, the more pronounced low-molar-mass sides of the MMDs clearly reflect the trend of the determined $\overline{M}_n$ values. In addition, the distributions serve as a good example to emphasize that $V_{e,peak}$ values do not necessarily have to decrease to obtain lower $\overline{M}_n$ values. $V_{e,peak}$ could also increase or stay constant. The crucial quantity is indeed how much $V_{e,peak}$ is shifted *in relation to* $\overline{V}_e$, which is basically determined by the extent of BB, i. e., the interplay of σ_G and τ. This will be further clarified in the next section.

8.2.2 Impact of band broadening: further elucidation and universal quantification

In this section, the specific reasons for the previously presented BB effect will be fundamentally clarified. This allows for a comprehensive understanding and a reliable universal quantification of the impact of BB on the obtained molar masses. On the basis of this elucidation, the influence of σ_G and τ as well as of the shape of both the polymer standards' MMDs and the analytes' MMDs can be further demonstrated. This leads to potential correction techniques, which will be eventually discussed. In a brief anticipation, the impact is expected to be more pronounced as molar masses increase, which is especially relevant for the analysis of (Q)LP systems.

Broadening effect and calibration effect As a working assumption that will be illustrated in the following, BB basically leads to two separable effects, namely (i) the broadening of the polymer standards' chromatograms affecting their $V_{e,peak}$ values and (ii) the broadening of the analyte's chromatogram. Henceforth, the first effect will be referred to as *calibration effect*—as it originates from the calibration process—and the latter as *broadening effect.* Both effects will be quantitatively discussed in detail in the following, which will be mostly done in terms of MMDs ($\log_{10}(M)$ scale) with EMG parameters $\sigma_G \cdot b$ and $\tau \cdot b$ rather than chromatograms (V_e scale) with σ_G and τ. This ensures universal applicability of the presented quantitative effects on molar-mass determination (cf. Figure 8.1 on page 175).

8.2.2.1 Broadening effect

In early works, Hamielec and Ray showed that symmetric BB does not only influence the broadness of an MMD, i. e., its $Đ$ value, but also its $\overline{M}_n$ value. They quantified this effect for the assumption of a linear SEC calibration function and simple Gaussian broadening.[260,261] In further works, Yau et al. applied this effect to the more sophisticated EMG model as part of the so-called GPCV3 method, which is an improved version of the Hamielec method for SEC calibration using broad polymer standards.[48,264] In this context, for the assumption of a linear calibration function and a uniform BBF (i. e., $\sigma_G \cdot b$ and $\tau \cdot b$ are constant), the correlation between the true $\overline{M}_n$ value of an MMD (without BB), $\overline{M}_n$(true), and the apparent $\overline{M}_n$ value (with BB), $\overline{M}_n$(app), can be expressed via

$$\overline{M}_n(\text{true}) \overset{\text{BB}}{=} r_{\text{BB,n}} \cdot \overline{M}_n(\text{app}) \,, \tag{8.1}$$

and the correction term

$$r_{\mathrm{BB,n}} = \frac{\exp\left(\frac{1}{2}\cdot\{\sigma_{\mathrm{G}}\cdot b\cdot\ln(10)\}^2 - \tau\cdot b\cdot\ln(10)\right)}{1-\tau\cdot b\cdot\ln(10)}\,, \tag{8.2}$$

for $\tau\cdot b\cdot\ln(10) < 1$. The correlation between the respective $\overline{M}_{\mathrm{w}}$ values can be expressed via

$$\overline{M}_{\mathrm{w}}(\mathrm{true}) \overset{\mathrm{BB}}{=} r_{\mathrm{BB,w}}\cdot\overline{M}_{\mathrm{w}}(\mathrm{app})\,, \tag{8.3}$$

and the correction term

$$\begin{aligned} r_{\mathrm{BB,w}} = \exp&\left(-\tfrac{1}{2}\cdot\{\sigma_{\mathrm{G}}\cdot b\cdot\ln(10)\}^2 - \tau\cdot b\cdot\ln(10)\right)\\ &\cdot\{1+\tau\cdot b\cdot\ln(10)\}\,, \end{aligned} \tag{8.4}$$

for $\tau\cdot b\cdot\ln(10) > -1$.[48,264] In case of $\sigma_{\mathrm{G}}\cdot b = \tau\cdot b = 0$, $r_{\mathrm{BB,n}} = r_{\mathrm{BB,w}} = 1$, whereas in any other case, $r_{\mathrm{BB,n}} > 1$ and $r_{\mathrm{BB,w}} < 1$, which results in $\overline{M}_{\mathrm{n}}(\mathrm{app}) < \overline{M}_{\mathrm{n}}(\mathrm{true})$ and $\overline{M}_{\mathrm{w}}(\mathrm{app}) > \overline{M}_{\mathrm{w}}(\mathrm{true})$. This behavior is indeed reasonable in terms of an increasing apparent $Đ$ value, $Đ(\mathrm{app}) = \overline{M}_{\mathrm{w}}(\mathrm{app})/\overline{M}_{\mathrm{n}}(\mathrm{app})$, as BB increases. In contrast, the impact on $\overline{M}_{\mathrm{n}}$ might be counterintuitive since EMG broadening does not affect the mean value of a distribution. However, it should be noted that this only holds true in the dimensions in which EMG broadening actually occurs, namely the chromatographic RI-versus-$\log_{10}(M)$ dimension. There, the mean value of $\log_{10}(M)$, $\overline{\log_{10}(M)}$, remains unaffected indeed. Consequently, while $\overline{M}_{\mathrm{n}}$ is the mean value of the MMD on an x_M-versus-M scale, the deviation between $\log_{10}(\overline{M}_{\mathrm{n}})$ and $\overline{\log_{10}(M)}$ is generally higher for broader MMDs. This could be validated for the here conducted numerical simulations by applying EMG broadening for different values of $\sigma_{\mathrm{G}}\cdot b$ and $\tau\cdot b$ on an RI-versus-$\log_{10}(M)$ scale. The resulting changes in both $\overline{M}_{\mathrm{n}}$ and $\overline{M}_{\mathrm{w}}$ (or $\overline{DP}_{\mathrm{n}}$ and $\overline{DP}_{\mathrm{w}}$) could be accurately predicted by Equation 8.1 to 8.4 (see Appendix B.5 on page 244).

While $\sigma_{\mathrm{G}}\cdot b$ and $\tau\cdot b$ are included differently in Equation 8.2 (and 8.4), their impacts are rather similar for $\sigma\cdot b\,(=\sqrt{(\sigma_{\mathrm{G}}\cdot b)^2+(\tau\cdot b)^2}) < 0.5$. However, for higher $\sigma\cdot b$ values, both $\overline{M}_{\mathrm{n}}(\mathrm{app})$ and $\overline{M}_{\mathrm{w}}(\mathrm{app})$ values are slightly smaller for higher $\tau\cdot b$ than for higher $\sigma_{\mathrm{G}}\cdot b$, while this divergence becomes more pronounced as $\sigma\cdot b$ increases.[48,264] The quantitative impact of constant $\sigma_{\mathrm{G}}\cdot b$ and $\tau\cdot b$ values on both $\overline{M}_{\mathrm{n}}(\mathrm{app})$ and $\overline{M}_{\mathrm{w}}(\mathrm{app})$ is independent of the actual shape of the MMD (e. g., unimodal, multimodal, narrow, broad).[48,229,260,264]

8.2.2.2 Calibration effect

Correction term

When BB occurs during the calibration process, the standard's $V_{\mathrm{e,peak}}$ shifts relatively to $\overline{V_{\mathrm{e}}}$. As $\overline{V_{\mathrm{e}}}$ remains untouched, for specific σ_{G} and τ, the shift can be straightforwardly quantified as

$$\begin{aligned}\Delta V_{\mathrm{e}}(\sigma_{\mathrm{G}},\tau) &= \left(V_{\mathrm{e,peak}}(\sigma_{\mathrm{G}},\tau) - \overline{V_{\mathrm{e}}}\right) - \left(V^{0}_{\mathrm{e,peak}} - \overline{V_{\mathrm{e}}}\right)\\ &= V_{\mathrm{e,peak}}(\sigma_{\mathrm{G}},\tau) - V^{0}_{\mathrm{e,peak}}\,,\end{aligned} \tag{8.5}$$

where $V^{0}_{\mathrm{e,peak}}$ corresponds to $V_{\mathrm{e,peak}}$ for the hypothetically true case of no BB. As mentioned above, when $\Delta V_{\mathrm{e}}(\sigma_{\mathrm{G}},\tau)$ is translated to the $\log_{10}(M)$ scale, both $V_{\mathrm{e,peak}}(\sigma_{\mathrm{G}},\tau)$ and $V^{0}_{\mathrm{e,peak}}$ are *by calibration* set to the same $\log_{10}(M_{\mathrm{peak}})$ value. For constant $\sigma_{\mathrm{G}}\cdot b$ and $\tau\cdot b$ values, this results in a shift of the mean values of the MMD according to

$$\begin{aligned}-b\cdot\Delta V_{\mathrm{e}}(\sigma_{\mathrm{G}},\tau) &= \left(\overline{\log_{10}(M)}^{\,0} - \log_{10}(M_{\mathrm{peak}})\right)\\ &\quad - \left(\overline{\log_{10}(M)}(\sigma_{\mathrm{G}}\cdot b,\tau\cdot b) - \log_{10}(M_{\mathrm{peak}})\right)\\ &= \overline{\log_{10}(M)}^{\,0} - \overline{\log_{10}(M)}(\sigma_{\mathrm{G}}\cdot b,\tau\cdot b)\\ &= \Delta\log_{10}(M)(\sigma_{\mathrm{G}}\cdot b,\tau\cdot b)\,,\end{aligned} \tag{8.6}$$

with the shifted mean value $\overline{\log_{10}(M)}(\sigma_{\mathrm{G}}\cdot b,\tau\cdot b)$ and the mean value for the hypothetically true case of no BB, $\overline{\log_{10}(M)}^{\,0}$. It should be noted that even though $\tau\cdot b>0$, when skewing is described in the context of MMDs and $\log_{10}(M)$, it is always toward *lower* $\log_{10}(M)$ values (cf. Figure 8.6 on page 182). Considering that $\overline{\log_{10}(M)}^{\,0}$ can be regarded as a true and $\overline{\log_{10}(M)}(\sigma_{\mathrm{G}}\cdot b,\tau\cdot b)$ as an apparent $\log_{10}(M)$ value, this leads to

$$\begin{aligned}\Delta\log_{10}(M)(\sigma_{\mathrm{G}}\cdot b,\tau\cdot b) &\overset{\mathrm{cal}}{=} \log_{10}(M(\mathrm{true})) - \log_{10}(M(\mathrm{app}))\\ &\overset{\mathrm{cal}}{=} \log_{10}\left(\frac{M(\mathrm{true})}{M(\mathrm{app})}\right)\,,\end{aligned} \tag{8.7}$$

which gives the correction term of the calibration effect

$$r_{\mathrm{cal}} \overset{\mathrm{cal}}{=} \frac{M(\mathrm{true})}{M(\mathrm{app})} \overset{\mathrm{cal}}{=} 10^{\Delta\log_{10}(M)(\sigma_{\mathrm{G}}\cdot b,\tau\cdot b)}\,. \tag{8.8}$$

Therefore, if the shift of the polymer standard's $\overline{\log_{10}(M)}$ value upon BB is known, the deviation of the apparent from the true molar masses can

be estimated. It should be noted that for the assumption that the true and the apparent calibration function share the same b, the apparent calibration function is just shifted along the $\log_{10}(M)$ axis by $\Delta \log_{10}(M)(\sigma_G \cdot b, \tau \cdot b)$. In that case, the calibration effect influences molar masses (e. g., $\overline{M}_n$, $\overline{M}_w$, molar mass at the inflection points) equally and independently of the shape of the analyte's MMD. This will be shown more precisely at a later stage.

In the following, a fundamental approach will be presented to quantify the impact of certain parameters on the crucial $\Delta \log_{10}(M)(\sigma_G \cdot b, \tau \cdot b)$ value. The approach is based on the assumption that both a hypothetically unbroadened and a broadened MMD (or chromatogram) of a Poissonian polymer standard can be expressed through an EMG function (at least partly, see below), for which the distance between the mean value and the peak position is unambiguously defined by its parameters $\sigma_G \cdot b$ and $\tau \cdot b$.

Molar-mass distributions as EMG functions

Mean value and peak position of an EMG function As stated above, the difference between the mean value and the peak position of an EMG function is defined by its parameters σ_G and τ (here: $\sigma_G \cdot b$ and $\tau \cdot b$). The difference can in fact be precisely calculated, however, this involves a somewhat complex conversion of a *scaled complementary error function.*[265] A much simpler expression was therefore developed by numerically determining the difference for a variety of distinct EMG parameters and finding an appropriate best-fit function. In the context of MMDs in SEC, the following empirical expression was obtained:

$$\begin{aligned}\Delta_{EMG} \log_{10}(M)(\sigma_G \cdot b, \tau \cdot b) &= \overline{\log_{10}(M)} - \log_{10}(M_{peak}) \\ &= -\tau \cdot b \cdot \left(1 + 0.3750 \cdot \left(\frac{\sigma_G \cdot b}{\tau \cdot b}\right)^{0.8433}\right)^{-3.756},\end{aligned} \tag{8.9}$$

with $\tau \cdot b > 0$ and $\sigma_G \cdot b \geq 0$, while for $\tau \cdot b = 0$, the distribution is symmetric and $\Delta_{EMG} \log_{10}(M) = 0$. The fitting quality is excellent and for the evaluated range of $\sigma_G \cdot b$ and $\tau \cdot b$ from 0 to 3, the highest deviation between the numerically determined $\Delta_{EMG} \log_{10}(M)$ value and the one obtained via Equation 8.9 is 0.0004, which corresponds to a difference in molar masses of < 0.1 % (cf. Equation 8.8 on the preceding page). It should be stated that Equation 8.9 is expected to be a good approximation even if $\sigma_G \cdot b$ and $\tau \cdot b$ are higher than 3, since $\Delta_{EMG} \log_{10}(M)$ is proportional to $\tau \cdot b$ for a fixed $(\sigma_G \cdot b)/(\tau \cdot b)$ value, which is also inherent in the above-mentioned exact

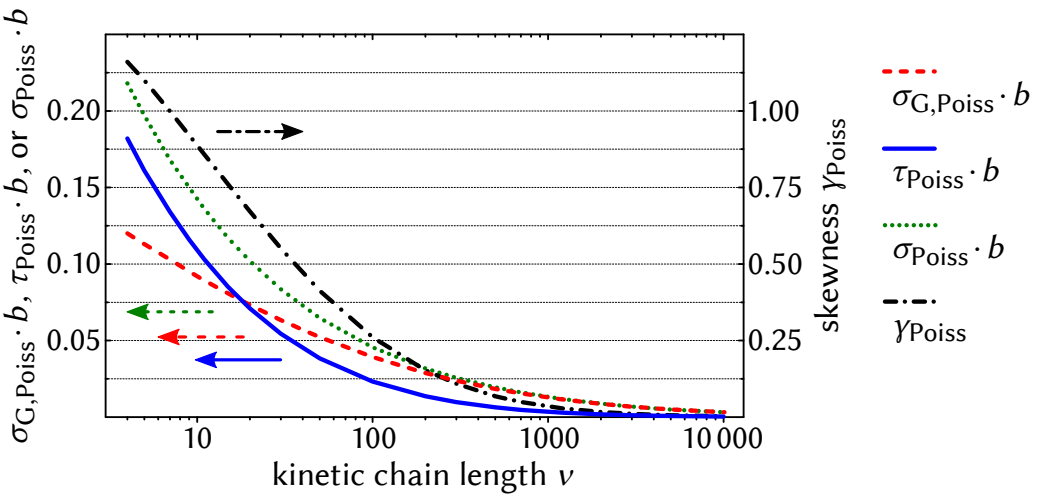

Figure 8.8 EMG parameters $\sigma_{G,Poiss} \cdot b$ and $\tau_{Poiss} \cdot b$ obtained from best-fits of Poissonian MMDs translated to chromatographic dimensions as a function of the MMDs' ν values (see Equation 8.10 and 8.11 on the next page). The standard deviation $\sigma_{Poiss} \cdot b$ and skewness γ_{Poiss} of the distributions calculated from the EMG parameters are given as well.

mathematical expression.[265] While the validity could be confirmed for various combinations of $\sigma_G \cdot b$ and $\tau \cdot b > 3$, no systematical analysis was conducted in the course of the presented work. It should also be stressed that Equation 8.9 is valid for EMG functions in general with $\overline{\log_{10}(M)}$ being the mean value, $\log_{10}(M_{peak})$ the peak position and $\sigma_G \cdot b$ and $\tau \cdot b$ being the classic EMG parameters σ_G and τ, respectively. Therefore, it could as well be used to calculate the difference between $\overline{V_e}$ and $V_{e,peak}$ of an elution chromatogram, for example. However, it should be noted that for a classic EMG function having a *positive* skewness, the difference is always positive and the prefactor should be τ rather than $-\tau$.

Unbroadened Poissonian MMDs Vega and Schnöll-Bitai have shown that when Poissonian MMDs are translated to chromatographic RI-versus-$\log_{10}(M)$ dimensions, they can be well-described via EMG functions skewed toward lower $\log_{10}(M)$ values (like EMG broadening is).[210] They developed expressions of respective $\sigma_G \cdot b$ and $\tau \cdot b$ values as a function of the Poissonian ν value for $50 \leq \nu \leq 400$, which become invalid for either $\nu < 50$ or $\nu > 400$.[210] To expand the ν range, Poissonian MMDs were systematically simulated for various ν values from 4 to 10 000, translated to

chromatographic dimensions, and fitted with EMG functions. It should be noted that the logarithmic character of the $\log_{10}(M)$ axis makes the shape of the resulting distribution independent of the molar mass of the monomeric unit. Excellent fitting was observed for every single distribution and the following empirical expressions were obtained:

$$\sigma_{\mathrm{G,Poiss}} \cdot b = 0.1532 \cdot \left(1 - \exp\left(-1 \cdot \left(\frac{\nu}{8.710}\right)^{-0.5108}\right)\right) , \tag{8.10}$$

$$\tau_{\mathrm{Poiss}} \cdot b = 0.3110 \cdot \left(1 - \exp\left(-1 \cdot \left(\frac{\nu}{3.318}\right)^{-0.7570}\right)\right) . \tag{8.11}$$

More detailed information about the procedure and the best-fits of the distinct values is presented in Appendix B.6 on page 245. Indeed, for $50 \leq \nu \leq 400$, $\sigma_{\mathrm{G,Poiss}} \cdot b$ and $\tau_{\mathrm{Poiss}} \cdot b$ agree very well with the data given by Vega and Schnöll-Bitai. In Figure 8.8 on the preceding page, $\sigma_{\mathrm{G,Poiss}} \cdot b$ and $\tau_{\mathrm{Poiss}} \cdot b$ as well as the resulting standard deviations $\sigma_{\mathrm{Poiss}} \cdot b$ and skewness values γ_{Poiss} (cf. Equation 6.7 on page 149) are presented as a function of ν. All parameters decrease with increasing ν, so that for low-molar-mass standards, the hypothetically unbroadened MMD can be regarded as relatively broad and skewed, while high-molar-mass standards can be regarded as narrow and symmetric.

Convolution of two EMG functions Based on the facts that (i) convolution (= broadening) is a commutative mathematical operation and that (ii) the convolution of two Gaussian distributions with the respective standard deviations $\sigma_{\mathrm{G},1}$ and $\sigma_{\mathrm{G},2}$ again give a Gaussian distribution with the standard deviation $\sigma_{\mathrm{G},3} = \sqrt{{\sigma_{\mathrm{G},1}}^2 + {\sigma_{\mathrm{G},2}}^2}$, Vega and Schnöll-Bitai[210] also showed that the convolution between two EMG functions $\mathrm{EMG}(\sigma_{\mathrm{G},1}, \tau_1)$ and $\mathrm{EMG}(\sigma_{\mathrm{G},2}, \tau_2)$ can again be well-approximated with another EMG function via

$$\mathrm{EMG}(\sigma_{\mathrm{G},1}, \tau_1) * \mathrm{EMG}(\sigma_{\mathrm{G},2}, \tau_2) \approx \mathrm{EMG}\left(\sqrt{{\sigma_{\mathrm{G},1}}^2 + {\sigma_{\mathrm{G},2}}^2}, \tau_1\right) \quad \text{for } \tau_1 \gg \tau_2 \tag{8.12}$$

or

$$\mathrm{EMG}(\sigma_{\mathrm{G},1}, \tau_1) * \mathrm{EMG}(\sigma_{\mathrm{G},2}, \tau_2) \approx \mathrm{EMG}\left(\sqrt{{\sigma_{\mathrm{G},1}}^2 + {\sigma_{\mathrm{G},2}}^2}, \tau_2\right) \quad \text{for } \tau_1 \ll \tau_2 . \tag{8.13}$$

This approximation is very good in case of either $\tau_1 \gg \tau_2$ or $\tau_1 \ll \tau_2$, while the more alike τ_1 and τ_2 are, the more the convolution product deviates

from an EMG function given by Equation 8.12 or 8.13. This behavior was confirmed in a systematical numerically conducted EMG broadening procedure of EMG functions for several values of $\sigma_{G,1}$, τ_1, $\sigma_{G,2}$, and τ_2 (data not shown). However, even though Equation 8.12 or 8.13 are less fulfilled for similar τ_1 and τ_2 values, still reasonably skewed distributions are obtained in these cases that could be mostly approximated by EMG functions with other parameters. In a trial-and-error process, it was found that convolution of two EMG functions EMG($\sigma_{G,1}$, τ_1) and EMG($\sigma_{G,2}$, τ_2) results in a distribution for which the difference between its mean value and its peak position strongly resembles the respective difference for an EMG function with the parameters

$$\sigma_{G,3} = \sqrt{{\sigma_{G,1}}^2 + {\sigma_{G,2}}^2} \tag{8.14}$$

and

$$\tau_3 = \sqrt[3]{{\tau_1}^3 + {\tau_2}^3}\,. \tag{8.15}$$

In the context of SEC broadening, this correlation offers a way to express the crucial difference between $\overline{\log_{10}(M)}$ and $\log_{10}(M_{peak})$ of a broadened polymer standard, while this broadened polymer standard can be regarded as a convolution product between the hypothetically unbroadened Poissonian distribution, EMG($\sigma_{G,1} = \sigma_{G,Poiss} \cdot b, \tau_1 = \tau_{Poiss} \cdot b$), and the BBF, EMG($\sigma_{G,2} = \sigma_G \cdot b, \tau_2 = \tau \cdot b$). In fact, systematically conducted convolutions with reasonable values of $\sigma_{G,Poiss} \cdot b$, $\tau_{Poiss} \cdot b$, $\sigma_G \cdot b$, and $\tau \cdot b$ have shown that this approach is very suitable within the here relevant value range. In this context, $\sigma_{G,Poiss} \cdot b$ and $\tau_{Poiss} \cdot b$ were predetermined by ν while $\sigma_G \cdot b$ and $\tau \cdot b$ were varied from 0 to $1/\ln(10)$ (as this is the inherent limitation of $\tau \cdot b$ for $r_{BB,n}$ in Equation 8.2 on page 187). In accordance with the above-mentioned facts, it was found that (i) the more alike $\tau_{Poiss} \cdot b$ and $\tau \cdot b$ are and (ii) the higher $\tau_{Poiss} \cdot b$ and $\tau \cdot b$ are compared to $\sigma_{G,Poiss} \cdot b$ and $\sigma_G \cdot b$, the more the difference between $\overline{\log_{10}(M)}$ and $\log_{10}(M_{peak})$ of the convolution product deviates from the respective difference for an EMG function with the total parameters

$$\sigma_{G,tot} \cdot b = \sqrt{(\sigma_{G,Poiss} \cdot b)^2 + (\sigma_G \cdot b)^2} \tag{8.16}$$

and

$$\tau_{tot} \cdot b = \sqrt[3]{(\tau_{Poiss} \cdot b)^3 + (\tau \cdot b)^3}\,. \tag{8.17}$$

Nevertheless, even in the most unfavorable extreme cases found for (i) the lowest $\nu = 4$ ($\sigma_{G,Poiss} \cdot b = 0.12$, $\tau_{Poiss} \cdot b = 0.18$) and $\sigma_G \cdot b \to 0$, $\tau \cdot b = 0.18$,

as well as for (ii) the highest $\nu = 10\,000$ ($\sigma_{\mathrm{G,Poiss}} \cdot b = 0.0041$, $\tau_{\mathrm{Poiss}} \cdot b = 0.0007$) and $\sigma_{\mathrm{G}} \cdot b \to 0$, $\tau \cdot b = 1/\ln(10)$, this deviation results in molar-mass errors of only about 3 % and 2 %, respectively. Indeed, for more realistic BB parameters, this error generally drops below 1 %, which illustrates the high applicability of this approach, as will also be presented at a later stage.

As stated above, Equation 8.14 to 8.17 on the facing page were found by trial-and-error and still lack a solid mathematical basis at this point. Therefore, the existence of a more accurate correlation between the difference of $\overline{\log_{10}(M)}$ and $\log_{10}(M_{\mathrm{peak}})$ and the combined BB parameters cannot be ruled out. While Equation 8.14 and 8.16 reflect the convolution of the two Gaussian parts, Equation 8.15 and 8.17 simulate the behavior that the bigger one of the two τ values is more significant for the resulting τ value, as it is the case in Equation 8.12 and 8.13 on page 191. The found expressions strongly simplify the structural correlation between the unbroadened and the broadened MMD of the polymer standard and thus enable a straightforward interpretation of the general concepts of the calibration effect.

Difference between unbroadened an broadened polymer standard

With the facts stated so far, it is possible to describe the difference between the $\overline{\log_{10}(M)}$ and the $\log_{10}(M_{\mathrm{peak}})$ value for (i) an unbroadened standard via $\Delta_{\mathrm{EMG}} \log_{10}(M)(\sigma_{\mathrm{G,Poiss}} \cdot b, \tau_{\mathrm{Poiss}} \cdot b)$ (Equation 8.9, 8.10, and 8.11 on pages 189–191) and for (ii) a broadened standard via $\Delta_{\mathrm{EMG}} \log_{10}(M)(\sigma_{\mathrm{G,tot}} \cdot b, \tau_{\mathrm{tot}} \cdot b)$ (Equation 8.9, 8.10, 8.11, 8.16, and 8.17 on pages 189–192). As both chromatograms share the same $\log_{10}(M_{\mathrm{peak}})$ value after calibration, the crucial $\Delta \log_{10}(M)(\sigma_{\mathrm{G}} \cdot b, \tau \cdot b)$ value (cf. Equation 8.6 on page 188) can be expressed via

$$\begin{aligned} \Delta \log_{10}(M)(\sigma_{\mathrm{G}} \cdot b, \tau \cdot b) = &\Delta_{\mathrm{EMG}} \log_{10}(M)(\sigma_{\mathrm{G,Poiss}} \cdot b, \tau_{\mathrm{Poiss}} \cdot b) \\ &- \Delta_{\mathrm{EMG}} \log_{10}(M)(\sigma_{\mathrm{G,tot}} \cdot b, \tau_{\mathrm{tot}} \cdot b) \end{aligned} \tag{8.18}$$

and r_{cal} can be calculated according to Equation 8.8 on page 188.

8.2.2.3 Simulation of the calibration effect

Separation of the calibration effect from the broadening effect

To check the universal applicability of r_{cal}, simulations of apparent molar masses for different extents of BB were conducted similarly to the simulations for the (Q)LP system presented in Section 8.2.1 on page 175. Since

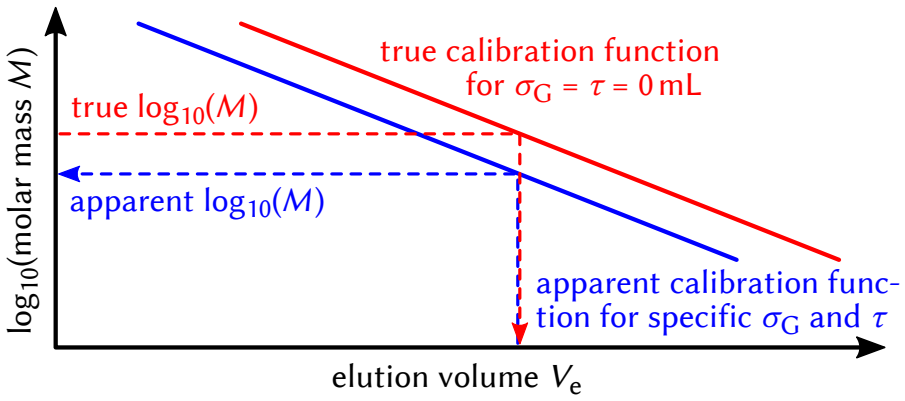

Figure 8.9 Illustration of simulating the calibration effect.

there, the results are obtained from both (i) broadening analytes' MMDs and (ii) applying respective calibration functions, they are affected by both (i) the broadening and (ii) the calibration effect. To separate the calibration effect from the broadening effect, here, BB was simulated just for the Poissonian standards during calibration and *not* for the analytes' MMDs. In this context, a hypothetically unimolecular polySt analyte with the true chain length i was translated to the V_e scale by applying the true calibration function for no BB. Then, the obtained V_e value was directly retranslated to the apparent $\log_{10}(M)$ (or i) value by applying the apparent calibration function for distinct BB parameters. The procedure is illustrated in Figure 8.9.

Chain-length-dependent calibration effect

Simulations were conducted for three different true $i = 20$, 500, and 5000. The apparent i values were determined for σ_G and τ from 0.0 mL to 0.5 mL in steps of 0.1 mL. The resulting (interpolated) deviations of the apparent from the true i values are given in Figure 8.10a ($i = 20$), 8.11a ($i = 500$), and 8.12a ($i = 5000$) on pages 195–197. The observed trends generally support the previously presented findings of the competing behavior between σ_G and τ with a lower apparent i for low σ_G and high τ. For the lowest $i = 20$, it can be observed that for low τ and high σ_G, a striking upward rather than a downward deviation from the true i is obtained. This stems from the fact that for low ν values, the hypothetically true chromatograms of the polymer standards already have a pronounced skewness (see γ_{Poiss} in Figure 8.8 on page 190). Symmetric BB counteracts this skewness and the difference between $V_{e,peak}$ and $\overline{V_e}$ becomes even *lower* than for the unbroad-

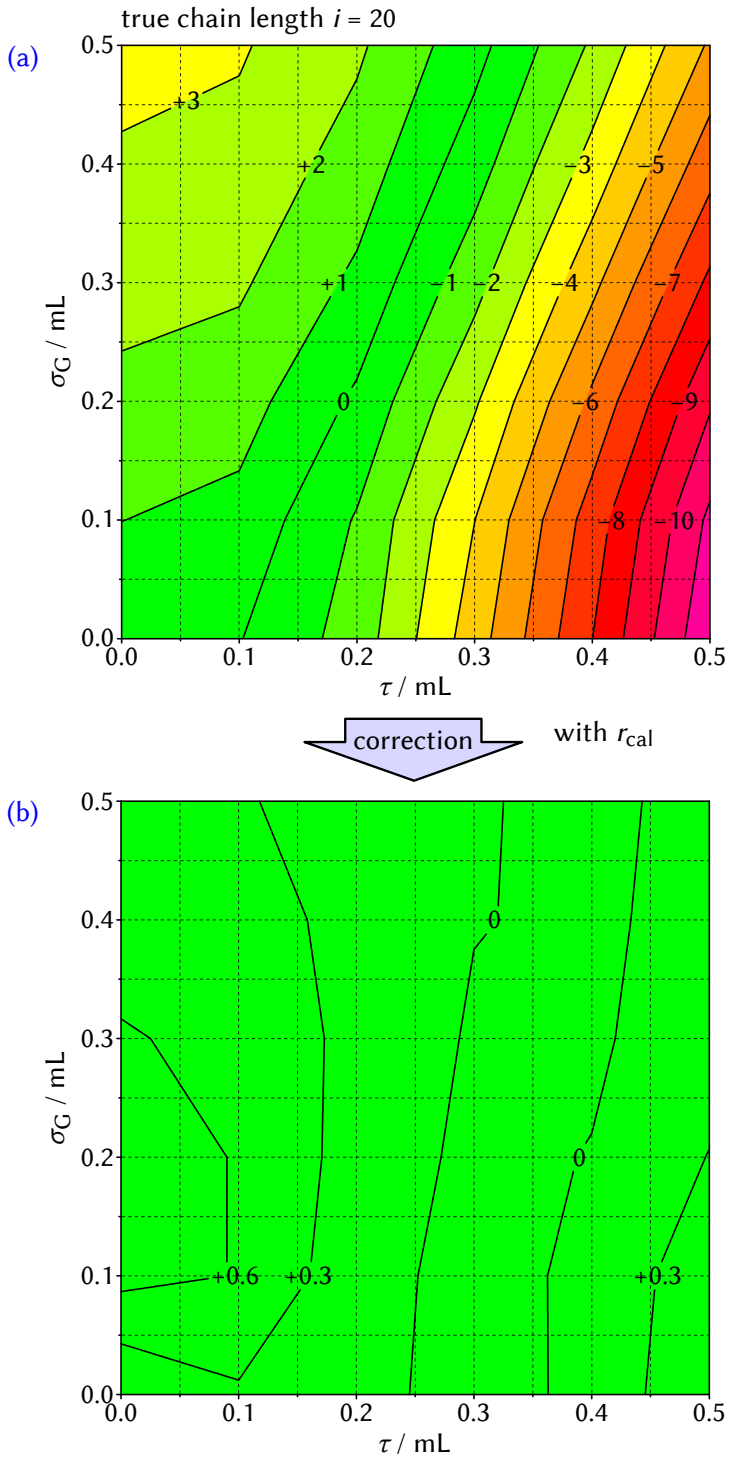

Figure 8.10 (a) Calibration-effect-caused deviations (in %) of the simulated apparent chain length from the true chain length $i = 20$ for different BB parameters σ_G and τ and (b) corrected deviations (with r_{cal}); local slope of the true calibration function $b = 0.298\,\mathrm{mL}^{-1}$.

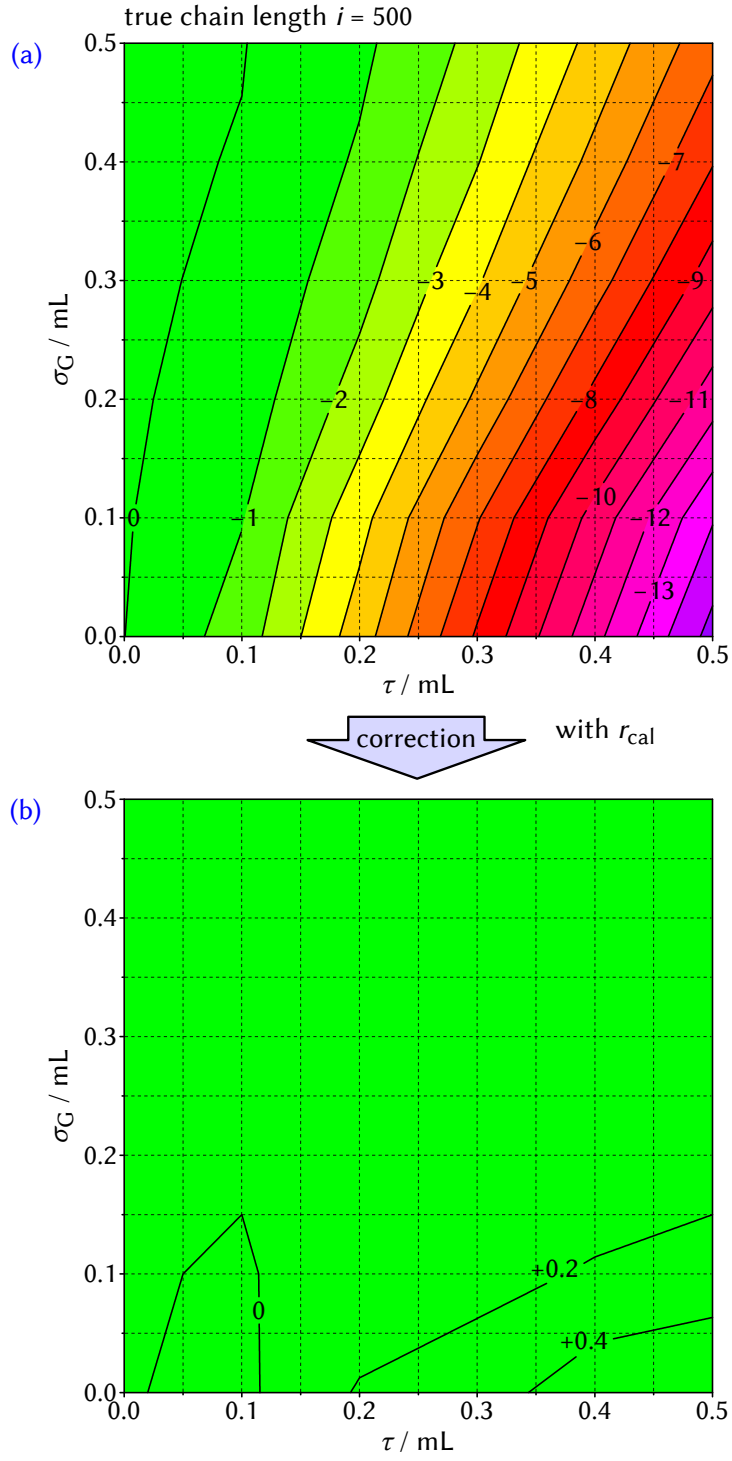

Figure 8.11 (a) Calibration-effect-caused deviations (in %) of the simulated apparent chain length from the true chain length $i = 500$ for different BB parameters σ_G and τ and (b) corrected deviations (with r_{cal}); local slope of the true calibration function $b = 0.207\ \text{mL}^{-1}$.

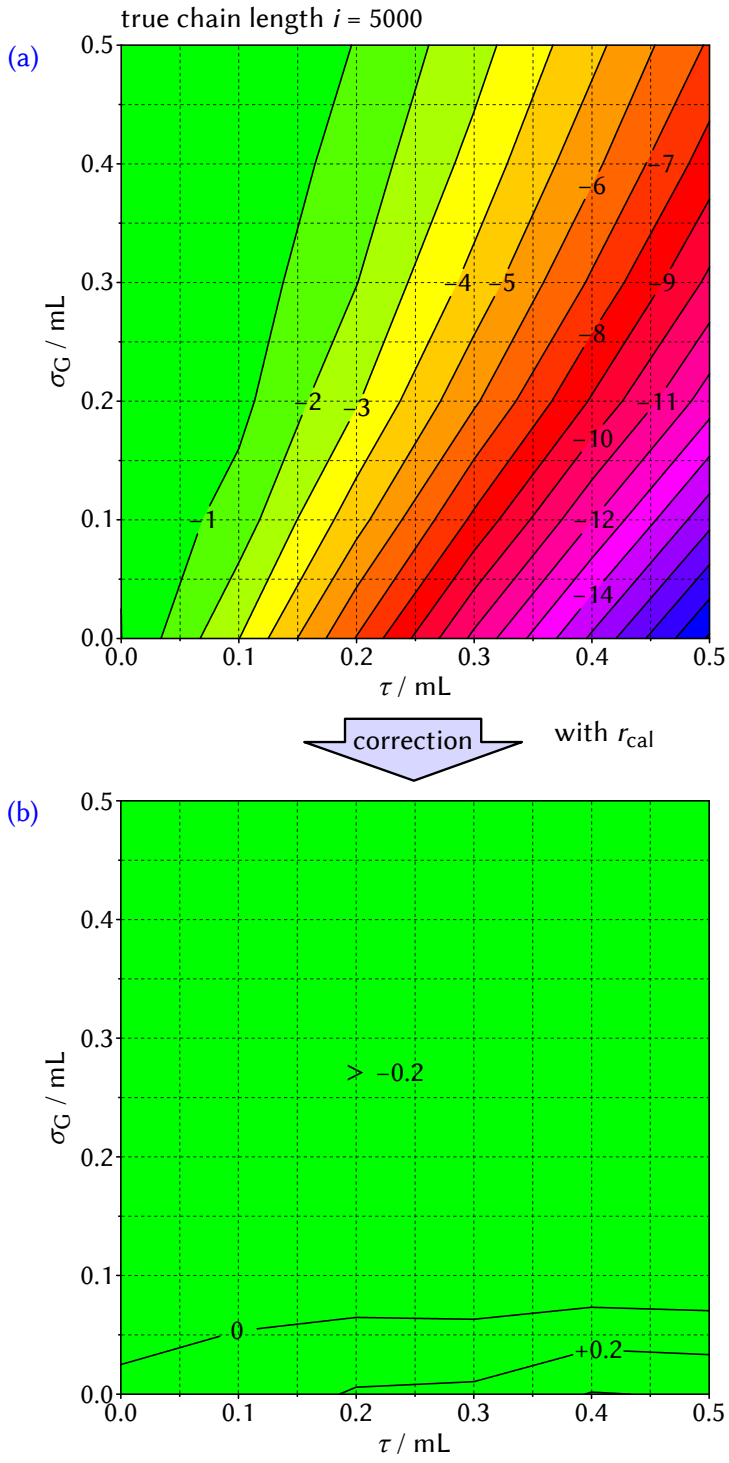

Figure 8.12 (a) Calibration-effect-caused deviations (in %) of the simulated apparent chain length from the true chain length $i = 5000$ for different BB parameters σ_G and τ and (b) corrected deviations (with r_{cal}); local slope of the true calibration function $b = 0.212\,\mathrm{mL}^{-1}$.

ened case (and the apparent calibration function in Figure 8.9 on page 194 is shifted to higher V_e for low i). This effect is less pronounced for higher ν (= lower γ_{Poiss}). For $i = 500$, the upward deviation is only about +0.1 % for $\sigma_G = 0.5$ mL and $\tau = 0.0$ mL, while for $i = 5000$, there is basically no deviation from the true i value.

As an additional effect, apparent i values are lower and more strongly affected by SEC skewing for higher true i. This is due to the fact that for lower ν, the standards' σ_{Poiss} values are higher. As the general broadness of the true chromatogram is higher, the same extent of skewing causes a lower shift of $V_{e,peak}$ and therefore a less pronounced calibration effect.

Application of the correction term r_{cal}

The apparent i values were corrected via r_{cal} (cf. Equation 8.8 on page 188 and 8.18 on page 193) and the deviation of the corrected from the true i values are presented in Figure 8.10b, 8.11b, and 8.12b. For this, $\sigma_{G,Poiss}$ and τ_{Poiss} were respectively calculated for $\nu = 20$, 500, and 5000 according to $\nu = i$. It should be noted that although r_{cal} and the apparent local shift of the calibration function is determined by ν, the calibration functions are *actually* affected by the standards involved in the calibration process, which are located at $i \approx 12$, 33, 88, 169, 334, 634, 1250, 2660, and 5270 (cf. Experimental Section 10.1.6 on page 221). However, as these standards are well-distributed along the $\log_{10}(M)$ range with three standards per order of magnitude ($\Delta \log_{10}(M) = 1$), the calculated effect on a hypothetical standard with a certain ν value (e. g., 20, 500, 5000) nicely conforms with the actually obtained interpolated effect on the two neighboring standards. The respectively used local b values were taken from the true calibration function and $i = 20$, 500, or 5000, and are given in the figure captions. Since the downward shift for low $V_{e,peak}$ is always more pronounced than for high $V_{e,peak}$ standards when BB is applied, b of the apparent calibration functions is always slightly lower than of the true calibration function. However, this effect is rather theoretical as it generally leads to molar-mass deviations below 0.1 %.

To put it simply, as the most striking result, r_{cal} effectively corrects the simulated calibration effect in every single case and reduces deviations from the true i values between +3 % and −18 % to absolute deviations of distinctly < 1 % for the complete σ_G and τ range. Still existing small deviations are generally ascribed to a combination of the approximations and uncertainties involved in the derivation of r_{cal} and to the numerically conducted simulation

procedure. It should be emphasized that r_{cal} was theoretically derived from scratch and correction was not achieved by just calculating back the initially obtained deviations from the true i values. The fact that r_{cal} effectively describes the rather different behavior of the apparent i values for i = 20, 500, *and* 5000 demonstrates that the different impact of low and high-molar-mass standards and their quantitative sensitivity to BB is well-understood. In this context, the shifting of the standards' $V_{e,peak}(\sigma_G, \tau)$ values in relation to $V^0_{e,peak}$ could be unambiguously identified as the crucial factor. These findings serve as a solid basis for the reasonable assessment of several effects in molar-mass analysis of (Q)LP systems (such as chain-length dependence), which will be presented at a later stage.

8.2.2.4 Simulation of the overall effect

Simulations were conducted similarly to the previous section, however, (i) rather than assuming a hypothetically unimolecular, here, the analyte's MMD was again Poissonian for which (ii) EMG broadening was applied as well. The results thus describe the *overall* effect of BB (broadening effect and calibration effect), which would be practically obtained in a real SEC experiment. In fact, these simulations correspond to the ones conducted in Section 8.2.1 on page 175, while here, the emphasis lies on the quantification of the overall effect.

The common BB procedure was applied for Poissonian MMDs with a true $\overline{DP}_n^0$ value of 500. As no striking effects were observed for other $\overline{DP}_n^0$ values—apart from the above-mentioned influence of the standards' ν values—data is not shown for these cases. The deviations of the resulting apparent $\overline{DP}_n$ values from $\overline{DP}_n^0$ are presented in Figure 8.13a on the following page. They resemble the deviations obtained for the sole calibration effect in Figure 8.11a on page 196. However, in agreement with the concept of the additional broadening effect, the apparent $\overline{DP}_n$ values are generally lower, which is particularly pronounced for high σ_G and τ. For both cases σ_G = 0.5 mL, τ = 0.0 mL and σ_G = 0.0 mL, τ = 0.5 mL, the apparent value is about 3 % lower than for the sole calibration effect, while for $\sigma_G = \tau$ = 0.5 mL, it is even about 7 % lower. This also leads to the remarkable effect that for high σ_G values, $\overline{DP}_n$ values again decrease rather than increase and defy the trend determined by the calibration effect. As a side note, this effect is indeed not obtained in Figure 8.5 on page 179 since the $\overline{DP}_n$ values are presented for a smaller σ_G and τ range. The quantitative difference between the apparent $\overline{DP}_n$ values obtained in Figure 8.5 and Figure 8.13 can be mainly

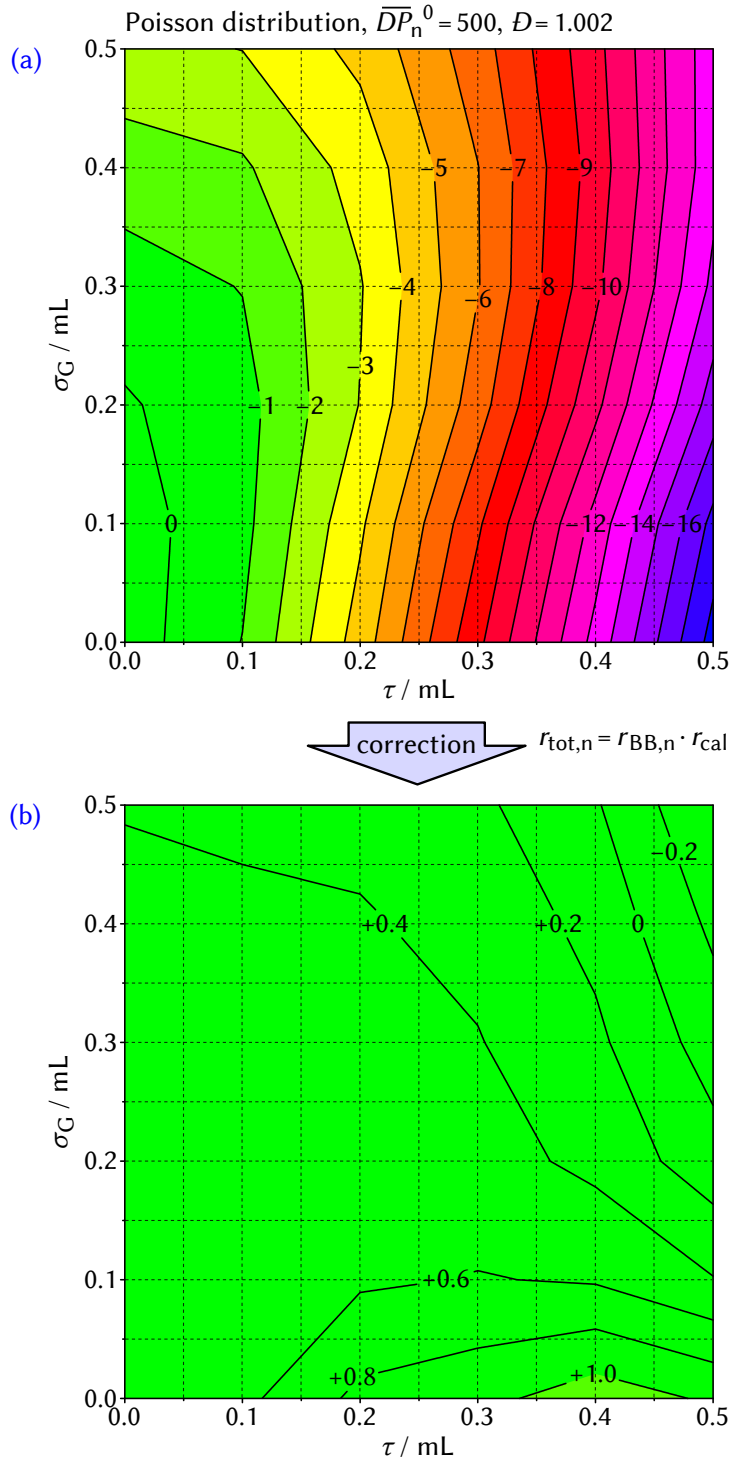

Figure 8.13 (a) Overall deviations (in %) of the simulated apparent $\overline{DP}_n$ from the true $\overline{DP}_n^{\,0} = 500$ of a Poisson-distributed MMD for different BB parameters σ_G and τ and (b) corrected deviations (with $r_{tot,n}$); local slope of the true calibration function $b = 0.207\,\text{mL}^{-1}$.

ascribed to different local b values. Altogether, the illustrated interplay of the broadening and the calibration effect makes it clear that τ is the much more crucial BB parameter when it comes to the downward deviation of the apparent $\overline{DP}_\mathrm{n}$ from the true $\overline{DP}_\mathrm{n}^{\,0}$ values.

Application of the overall correction term

The apparent $\overline{DP}_\mathrm{n}$ values were corrected similarly to the sole calibration effect, while the used total correction factor $r_\mathrm{tot,n}$ is a combination of $r_\mathrm{BB,n}$ and r_cal:

$$\overline{M}_\mathrm{n}(\mathrm{true}) = r_\mathrm{BB,n} \cdot r_\mathrm{cal} \cdot \overline{M}_\mathrm{n}(\mathrm{app}) = r_\mathrm{tot,n} \cdot \overline{M}_\mathrm{n}(\mathrm{app})\,. \tag{8.19}$$

The ν value was chosen to be $\nu = \overline{DP}_\mathrm{n}^{\,0} = 500$. Deviations of the corrected $\overline{DP}_\mathrm{n}$ values from the true $\overline{DP}_\mathrm{n}^{\,0}$ values are presented in Figure 8.13b. Again, the quality of the correction is very good as absolute deviations are mainly below 1 % throughout the complete σ_G and τ range. This clarifies that the broadening and the calibration effect, which were both individually presented in Appendix B.5 on page 244 and Section 8.2.2.3 on page 193, are the two crucial effects that determine the overall deviation of the apparent $\overline{DP}_\mathrm{n}$ values. Thus, for the assessment of potential BB-related effects on molar-mass determination, these two effects have to be evaluated individually, as will be presented at a later stage.

Impact on broad analyte's MMDs

As stated above, for constant $\sigma_\mathrm{G} \cdot b$ and $\tau \cdot b$ values, the impact of the *broadening effect* on the apparent $\overline{M}_\mathrm{n}$ and $\overline{M}_\mathrm{w}$ values is independent of the shape of the analyte's MMD. This also holds true for the calibration effect, which influences analyte's molar masses in general, whereas it should be noted that because of the presented chain-length dependence of r_cal, higher and lower molar masses of the analyte are theoretically affected slightly differently. It is a matter of course that the significance of this effect is mainly determined by the broadness of the MMD, since broader MMDs cover a wider range of individual ν and thus r_cal values. While the impact of differently shaped MMDs is not thoroughly considered within the here presented work, at this point, simulation results of apparent $\overline{DP}_\mathrm{n}$ values for an analyte's MMD much broader than a Poissonian will be discussed exemplarily. For this, a Schulz–Flory CLD of the form

$$x_i = (i-1) \cdot \alpha^{(i-2)} \cdot (1-\alpha)^2 \tag{8.20}$$

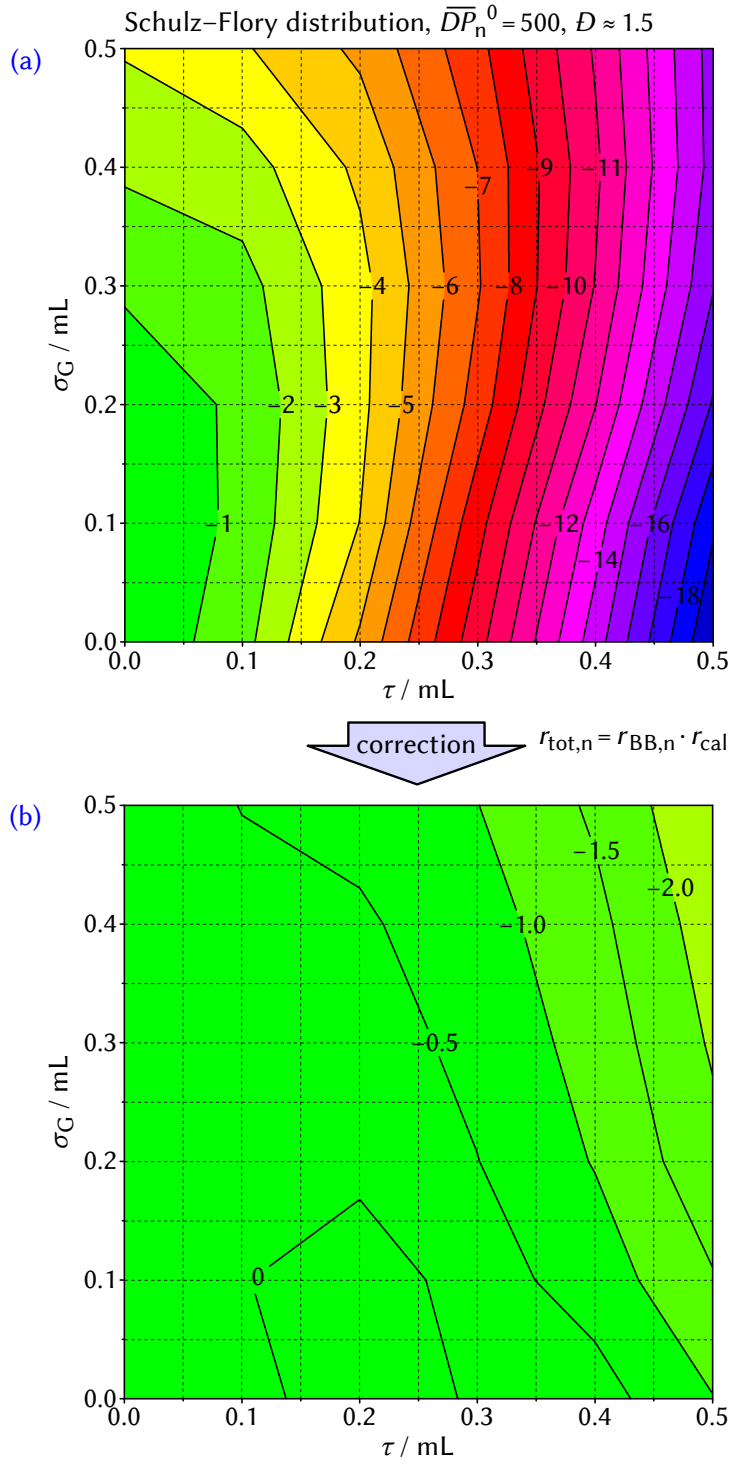

Figure 8.14 (a) Overall deviations (in %) of the simulated apparent $\overline{DP}_n$ from the true $\overline{DP}_n^0 = 500$ of a Schulz–Flory-distributed MMD for different BB parameters σ_G and τ and (b) corrected deviations (with $r_{tot,n}$); local slope of the true calibration function $b = 0.207\,\mathrm{mL}^{-1}$.

was investigated, where $\alpha = 1 - 2/\nu = 1 - 2/\overline{DP}_\mathrm{n}^0 = 1 - 2/500 = 0.996$, giving a polySt MMD with $\overline{DP}_\mathrm{n}^0 = 500$ and $Đ \approx 1.5$. As stated in the context of polymerization kinetics in Chapter 2, $Đ \approx 1.5$ is ideally obtained in conventional RPs if macroradicals terminate exclusively via combination, while it also reflects a typical broadness for only moderately controlled RDRP systems (such as ITPs).

Deviations of apparent $\overline{DP}_\mathrm{n}$ values are presented in Figure 8.14a on the preceding page. As expected, the results strongly resemble the ones for the narrow Poissonian MMD. After applying $r_\mathrm{tot,n}$—which is equal to $r_\mathrm{tot,n}$ for the Poissonian MMD as the same local b value is used—the corrected $\overline{DP}_\mathrm{n}$ values in Figure 8.14b are about 1 % to 2 % lower than for the Poissonian MMD. This results from the above-mentioned fact that a broader MMD covers a wider range of the calibration function with varying b values. Indeed, while the maximum spread of the Poissonian is lower than 2 mL, the one of the Schulz–Flory distribution is about 7 mL, covering molar masses from about 10 000 g mol^{-1} to 300 000 g mol^{-1}. In this context, the b values on the low- and the high-molar-mass side (0.257 mL^{-1} and 0.212 mL^{-1}, respectively) are slightly higher than at the center (0.207 mL^{-1}), which leads to a more pronounced BB effect than it is estimated by $r_\mathrm{tot,n}$, which uses the local center value. This leads to lower apparent $\overline{DP}_\mathrm{n}$ values than for the narrow Poissonian MMD.

These results exemplarily show potential differences between the analysis of narrow and broad MMDs that can occur in a *real* SEC experiment with a *nonlinear* calibration function. In this context, universal quantification is difficult as molar masses are individually affected by the shape of the chromatogram, the position and the range of the covered V_e values, and the calibration function. However, it should be emphasized that the most relevant region for these effects is located at the center of the chromatogram where intensities are high. Therefore, even if the condition of constant $\sigma_\mathrm{G} \cdot b$ and $\tau \cdot b$ values is not completely fulfilled, the obtained $r_\mathrm{tot,n}$ might serve as a good approximation. Indeed, even though the Schulz–Flory distribution covers more than threefold the V_e range of the Poissonian distribution, the impact on the apparent $\overline{DP}_\mathrm{n}$ values is rather similar and $r_\mathrm{tot,n}$ highly suitable in both cases. In this context, the equation of $r_\mathrm{tot,n}$ even offers a simple possibility to assess the influence of potential variations ($\sigma_\mathrm{G} \cdot b$, $\tau \cdot b$, ν) on the outcome of apparent molar masses.

Dispersity values

As a general comment, since the calibration effect has a similar impact on $\overline{M}_\mathrm{n}$ and $\overline{M}_\mathrm{w}$, apparent $Đ$ values, $Đ\,(\mathrm{app})$, are expected to be mainly influenced by just the broadening effect.[48,264] This could also be observed for the here conducted simulations (data not shown). With $\overline{M}_\mathrm{w}(\mathrm{true}) = r_\mathrm{tot,w} \cdot \overline{M}_\mathrm{w}(\mathrm{app})$ and $r_\mathrm{tot,w} = r_\mathrm{BB,w} \cdot r_\mathrm{cal}$, the true $Đ$ value is given by

$$\begin{aligned} Đ\,(\mathrm{true}) = \frac{\overline{M}_\mathrm{w}(\mathrm{true})}{\overline{M}_\mathrm{n}(\mathrm{true})} &= \frac{r_\mathrm{tot,w} \cdot \overline{M}_\mathrm{w}(\mathrm{app})}{r_\mathrm{tot,n} \cdot \overline{M}_\mathrm{n}(\mathrm{app})} = \frac{r_\mathrm{BB,w} \cdot r_\mathrm{cal} \cdot \overline{M}_\mathrm{w}(\mathrm{app})}{r_\mathrm{BB,n} \cdot r_\mathrm{cal} \cdot \overline{M}_\mathrm{n}(\mathrm{app})} \\ &= \frac{r_\mathrm{BB,w} \cdot \overline{M}_\mathrm{w}(\mathrm{app})}{r_\mathrm{BB,n} \cdot \overline{M}_\mathrm{n}(\mathrm{app})} = \frac{r_\mathrm{BB,w}}{r_\mathrm{BB,n}} \cdot Đ\,(\mathrm{app})\,. \end{aligned} \tag{8.21}$$

This is indeed reasonable since the $Đ$ value of an MMD is not affected when it is simply shifted along the $\log_{10}(M)$ axis, as it was described in the context of Figure 8.4 on page 177.

8.2.3 Chain-length-dependent impact of band broadening on (Q)LP systems

The thorough quantitative analysis of the impact of BB on the apparent molar-mass values presented in the previous sections allows to further assess the effects expected in the analysis of (Q)LP systems. As the most characteristic feature of (Q)LPs, they yield continuously growing macromolecules, which evolve through a rather wide range of SEC separation. Although the BBF was assumed to be uniform for the conducted simulations, the literature results presented in the introductory Section 6.2.4.2 on page 150 illustrate that this is most likely not the case for real systems. While the precise behavior and the absolute extent of BB might be strongly individual, both the overall standard deviation σ and the skewness γ generally increase with decreasing V_e. Together with the facts stated in context of the broadening and calibration effect, this leads to the conclusion that apparent $\overline{M}_\mathrm{n}$ values are not only expected to be generally lower than the true ones. This downward deviation is even expected to become more pronounced as molar-masses increase. This is caused by three independent effects coexisting during SEC analysis:

#1 As σ $(= \sqrt{{\sigma_\mathrm{G}}^2 + \tau^2})$ of the BBF generally increases for lower V_e, $r_\mathrm{BB,n}$ increases as well.

Table 8.2 Determined BB parameters σ_G and τ and local b values for Poissonian polySt standards presented in Figure 7.4 on page 161 (V_{inj} = 10 µL) and resulting deviations (dev.) of $\overline{M}_n$(app) from $\overline{M}_n$(true) calculated from the correction term $r_{tot,n}$ (= $r_{BB,n} \cdot r_{cal}$).

M_{peak} / g mol^{-1}	σ_G / mL	τ / mL	b / mL^{-1}	$r_{BB,n}$	r_{cal} [a]	$r_{tot,n}$	dev. of $\overline{M}_n$(app)
3470 [b]	0.114	0.181	0.286	1.011	1.017	1.028	−2.7 %
9130	0.126	0.271	0.260	1.018	1.071	1.090	−8.3 %
17 600	0.174	0.306	0.235	1.020	1.083	1.105	−9.5 %
34 800	0.179	0.339	0.210	1.019	1.095	1.116	−10.4 %
66 000	0.175	0.408	0.202	1.024	1.128	1.155	−13.4 %

[a] With $\nu = M_{peak}/M_{St}$; [b] σ_G and τ values for this standard were omitted for reasons of consistent comparison in Figure 7.4 on page 161, but could be determined for this specific set of data.

#2 As γ of the BBF generally increases for lower V_e, r_{cal} increases as well. As stated in Section 8.2.2.1 on page 186, for a constant value of σ and increasing γ/σ, even $r_{BB,n}$ slightly increases, since τ has a higher impact than σ_G. However, within the here investigated extent of BB, this effect is rather theoretical and not significant.

#3 As the Poissonian polymer standard's ν value increases for lower V_e values, σ_{Poiss} decreases (cf. Figure 8.8 on page 190). Lower σ_{Poiss} makes the standard's $V_{e,peak}$ value more prone to BB, so that higher-molar-mass standards yield a higher r_{cal} even for identical $\sigma_G \cdot b$ and $\tau \cdot b$ values.

In Table 8.2, the expected deviation of $\overline{M}_n$(app) from $\overline{M}_n$(true) is exemplarily presented for the Poissonian-shaped polySt standards from M_{peak} = 3470 g mol^{-1} to 66 000 g mol^{-1} measured in the context of the BB parameter estimation (cf. Figure 7.4 on page 161, V_{inj} = 10 µL). Values of $r_{BB,n}$ and r_{cal} were calculated from the determined σ_G and τ values and the local b values of the calibration function. As M_{peak} increases, the downward deviation of $\overline{M}_n$(app) increases from −2.7 % to −13.4 % from M_{peak} = 3470 g mol^{-1} to 66 000 g mol^{-1}. In this regard, the specific behavior of the calibration function with lower b values for higher M_{peak} even attenuates this effect. If the calibration function was linear in this region and b was universally set to the average value of 0.239 mL^{-1}, the calculated deviation would almost increase

tenfold from −1.7 % to −16.3 %. Even if the generally observed trends of the BBF's σ and γ value (effect #1 and #2) were much less pronounced and all σ_G and τ values were constant and hypothetically set to the average values of $0.153\,\mathrm{mL}^{-1}$ and $0.301\,\mathrm{mL}^{-1}$, respectively, the deviation would still increase twofold from −5.8 % to −11.1 % just because of effect #3.

8.3 Concluding remarks on BB effects and potential correction techniques

8.3.1 Impact of BB on molar-mass determination for (Q)LP systems

The reliable relation between the retention behavior and the molar mass of polymer molecules is the key to successful SEC analysis. While general retention is affected by various parameters such as the employed operating conditions and hardware, this rather unpredictable dependence is taken into account by calibration with peak positions of narrow polymer standards. However, as shown by extensive simulations and experiments, BB effects are *not* and might result in strong systematical deviations of the determined apparent molar masses from the true ones. While these BB effects apply to MMDs in general, their impact on the analysis of (Q)LP systems draws special attention within the here presented work. The fact that the obtained simulation results align with trends often found in the literature assumes relevance. For example, it is regularly found that the variation of $\overline{M}_n$ with monomer conversion is slightly below the ideal linear increase,[266] exactly as in Figure 8.2b on page 176. As it was clarified, this effect is even expected to be chain-length-dependent and to become more pronounced as molar masses increase during polymerization. Usually, this deviation is ascribed to the occurrence of irreversible termination reactions and formation of dead polymer, especially when it becomes more pronounced as polymerization proceeds. It should be emphasized that there is no denying this mechanistic cause. In fact, it is even obtained for the kinetic simulations presented in Chapter 4 in Figure 4.22 on page 114, which give perfectly true $\overline{M}_n$ values. However, it seems reasonable to suggest that BB could be contributing to the deviation. After all, the reality of BB is as undeniable as that of termination. In this context, it is also possible that this effect obscures molar masses that are higher than the ideal ones, which could indicate a gradual depletion of

living chains. There, the apparent molar masses might actually be closer to the ideal ones than the true molar masses.

Literature results from (Q)LP systems also display variation of $Đ$ with monomer conversion that mirrors that of Figure 8.2a on page 176. In particular, the increase rather than decrease of $Đ$ at high monomer conversion is common.[266] This is usually taken as evidence that a (Q)LP becomes less ideal as conversion increases, for example through the occurrence of side reactions or irreversible termination. Indeed, this conclusion appears especially reasonable when the obtained $\overline{M}_\mathrm{n}$ values more and more deviate from the ideal ones. Again, this explanation is not disputed. However, it seems plausible to suggest that a portion of the observed variation of $Đ$ is simply an apparent effect due to BB rather than a real mechanistic effect. As this effect is obtained already for uniform BB, it is of course expected to be more pronounced when BB increases for higher molar masses.

As a general comment, those who spend their lives poring over SEC results from (Q)LPs will find the MMDs of Figure 8.6 on page 182 to be hauntingly familiar. These MMDs are generated by nothing more than simulated SEC broadening of Poisson distributions. Given the thousands of studies there have been in which SEC has been used to evaluate the success of (Q)LPs and their suitability for special applications, it seems remarkable that the present is the first systematic investigation of how BB affects this process.

8.3.2 About the awareness of BB effects and potential correction techniques

In the following concluding part, techniques will be discussed that potentially allow for a correction and compensation of the presented BB effects. As a side note, these techniques do not include a correction of SEC resolution, namely the effect that BB leads to a smoothening of chromatograms and a possible loss of information—e. g., merging peaks, disappearing shoulders. Indeed, such corrections require complex and error-prone deconvolution and inversion procedures,[199] which do not fall within the scope of the presented work. Eventually, it will be outlined how the here obtained results debunk popular misconceptions about BB in SEC and that categorically ruling out significant impacts on molar-mass determination might be grossly negligent.

8.3.2.1 Applying the correction terms $r_{\mathrm{tot,n}}$ and $r_{\mathrm{tot,w}}$

From an academic point of view, $r_{\mathrm{tot,n}}$ and $r_{\mathrm{tot,w}}$ clarify the individual BB effects and enable to test how different values of $\sigma_{\mathrm{G}} \cdot b$, $\tau \cdot b$, or ν quantitatively affect the outcome of SEC experiments. As presented, the terms can also be applied to effectively correct experimentally obtained molar masses when the extent of BB is known. Indeed, when the behavior of σ_{G} and τ along the separation range is known—for example, from the analysis of the polymer standards used for calibration—individual correction functions $r_{\mathrm{tot,n}}(V_{\mathrm{e}})$ and $r_{\mathrm{tot,w}}(V_{\mathrm{e}})$ can be established. They can then be used to calculate the correction values at the center of the analyte's chromatogram, e. g., at $V_{\mathrm{e}} \approx \overline{V_{\mathrm{e}}}$. As demonstrated, this seems especially suitable for narrow MMDs, which cover only small variations of $r_{\mathrm{tot,n}}$ and $r_{\mathrm{tot,w}}$. However, it should be stated that the practical applicability and the robustness of this method still requires to be thoroughly investigated in terms of complicating factors such as the broadness of the analytes' MMDs, nonuniform BBFs, and experimental noise or fluctuations. This also holds true for the correction techniques presented in the following, while potential strategies of investigation will be more precisely discussed in the outlook chapter on page 213.

8.3.2.2 Determination of the true calibration function

Using the true calibration function for SEC analysis rather than the apparent one is probably the most straightforward method to correct for the calibration effect (*not* the broadening effect). The true calibration function is obtained by assigning M_{peak} to true $V^0_{\mathrm{e,peak}}$ values of the hypothetically unbroadened chromatograms of the standards. In this regard, $V^0_{\mathrm{e,peak}}$ values can be determined from the EMG parameter estimation, as the hypothetically unbroadened signal is automatically obtained during this procedure (see Figure 7.3 on page 160).

In an even simpler approach, when $\overline{V_{\mathrm{e}}}$ of a standard is known, the expected difference to $V^0_{\mathrm{e,peak}}$ can be calculated from $\sigma_{\mathrm{G,Poiss}}$ and τ_{Poiss}. In this context, the determination of $\overline{V_{\mathrm{e}}}$ is arguably less robust than the one of $V_{\mathrm{e,peak}}$, especially when it comes to handling the low-intensity parts of the chromatogram. However, more reliable $\overline{V_{\mathrm{e}}}$ values might be obtained when the higher intensities of the chromatograms are fitted with a suitable distribution function (e. g., EMG), as it was conducted in the context of EMG parameter estimation.

When chromatograms of polymer standards are strongly skewed, it is sometimes recommended assigning M_{peak} *directly* to $\overline{V_{\mathrm{e}}}$ rather than $V_{\mathrm{e,peak}}$. Partly, this can indeed be regarded as a good approximation also for slightly skewed chromatograms, since for Poissonian MMDs with $\nu > 100$, the difference between $\overline{\log_{10}(M)}^{\,0}$ and $\log_{10}(M_{\mathrm{peak}})$ (∼ difference between $\overline{V_{\mathrm{e}}}$ and $V^{0}_{\mathrm{e,peak}}$) corresponds to a molar-mass error of below 1 %. This fact is expected to hold true for high-molar-mass standards in general—not only for Poissonians—as they are usually narrow on the chromatographic scale and the difference between $\overline{\log_{10}(M)}^{\,0}$ and $\log_{10}(M_{\mathrm{peak}})$ is low compared to the difference induced by BB. For $\nu < 100$, however, this approximation should be applied with caution, as the difference between $\overline{\log_{10}(M)}^{\,0}$ and $\log_{10}(M_{\mathrm{peak}})$ becomes more pronounced and calibration with $\overline{V_{\mathrm{e}}}$ rather than $V^{0}_{\mathrm{e,peak}}$ results in an overestimation of molar masses of about 10 % for $\nu = 10$ and still about 5 % for $\nu = 20$. Considering the molar-mass deviations in Figure 8.10 on page 195, this means that for most of the BB parameters, the calibration correction with $\overline{V_{\mathrm{e}}}$ would lead to less accurate results than no correction at all. It is therefore recommended to consistently factor in the natural deviation of $\overline{\log_{10}(M)}^{\,0}$ from $\log_{10}(M_{\mathrm{peak}})$ irrespectively of ν, as the extra effort is rather small. Advantages of the described method are that (i) $\sigma_{\mathrm{G}} \cdot b$ and $\tau \cdot b$ values do not have to be known and (ii) nonuniformity of the BBF is automatically considered when the true calibration function is applied. As mentioned above, it should be noted that the broadening effect is not factored in here. However, as indicated in Table 8.2 on page 205, for reasonable extents of BB, the broadening effect might be generally less significant than the calibration effect, so that this method can be regarded as more than half the struggle to improve molar-mass accuracy. Individual functions of $r_{\mathrm{BB,n}}(V_{\mathrm{e}})$ and $r_{\mathrm{BB,w}}(V_{\mathrm{e}})$ might of course be applied in addition.

8.3.2.3 Analysis of well-known polymer

A method to directly determine functions of $r_{\mathrm{tot,n}}(V_{\mathrm{e}})$ and $r_{\mathrm{tot,w}}(V_{\mathrm{e}})$ is measuring polymer with well-known true $\overline{M}_{\mathrm{n}}$ and $\overline{M}_{\mathrm{w}}$ values.[204] The ratios of the true molar-mass averages and the respective apparent ones then directly yield $r_{\mathrm{tot,n}}$ and $r_{\mathrm{tot,w}}$. This simple back calculation of the obtained deviations is applicable since both the calibration and the broadening effect are valid irrespectively of the shape of the MMD. While this technique thus requires no specific shape of the employed MMDs, ideally, they are again narrow so that they cover only a small V_{e} range (e. g., the standards used for calibration).

It is a matter of course that accurate true $\overline{M}_n$ and $\overline{M}_w$ values and general reliable information about the true MMDs are highly desired—whether they are obtained from own experiments or provided by the manufacturer. Indeed, this holds true for any process involving polymer standards, which will be addressed in the following.

8.3.2.4 Knowing the polymer standards

When polymer is used for calibration or any other kind of quantitative consideration (e. g., BB, correction), the accuracy of this process depends on how well its true MMD is known. It should therefore be noted that in the context of relative SEC, the *true* molar-mass values determined by correction are more of the ones obtained in the *ideal case of no BB.* In addition, the above-described correction techniques are based on knowing either (i) how much $V_{e,peak}$ is influenced by a certain extent of BB, (ii) where $V^0_{e,peak}$ should be without BB, or (iii) what the true values of $\overline{M}_n$ and $\overline{M}_w$ are. This illustrates how beneficial it can be to have comprehensive knowledge about the standards and that specification through M_{peak} (which is indeed often the only one) is not sufficient to assess the impact of BB on apparent molar masses. While incomplex linear polySt standards (and a few other classes) can be regarded as Poissonian (or close-to-Poissonian)[207] *when produced under respectively suitable anionic polymerization conditions,* information about the actual production technique is generally not provided. In addition, the standards are usually specified by means of SEC so that the user is left in the dark about the true MMDs. Ideally, instead of giving only little specific information, the manufacturer provides the complete MMD measured by a method not prone to BB, such as MALDI-MS.[208,209] Even if it is not possible to rigorously determine MMDs (e. g., at high molar masses), any additional (rough) information on the expected shape of the true MMD helps to more accurately determine molar masses. This clarifies why a closer collaboration between the users and the manufacturers of polymer standards is highly recommended.

8.3.2.5 Misconceptions about BB

While the here presented results unambiguously demonstrate the impact of BB on molar-mass determination, they also reveal misconceptions about BB in SEC that can sometimes be found in the literature. For example, it is sometimes suggested that only narrow MMDs are significantly affected,

while there is no impact on broad MMDs when modern SEC setups are used. This belief arguably stems from the fact that at a first glance, BB distorts narrow MMDs much more evidently than broad MMDs. However, as frequently stated, both the broadening and the calibration effect are independent of the analyte's MMD. Another misconception is that *even if* these narrow MMDs are affected by BB, this only happens in terms of general broadness (e. g., $Đ$, points of inflection), whereas $\overline{M}_\mathrm{n}$ values are not influenced. This belief probably originates from the fact that BB has no impact on the average value of the elution chromatogram. However, as described, this does not hold true for either the calibration or broadening effect in terms of molar masses. Therefore, a significant impact of BB must not be ruled out just because a broad MMD is analyzed or $\overline{M}_\mathrm{n}$ values are determined.

It shall be emphasized that besides BB, molar-mass determination is of course affected by statistical errors during the experiment, which are as inherent as BB itself. However, in recently conducted round-robin tests,[267] the respective analysis of identical polymer in different laboratories demonstrated the nowadays generally high repeatability (= *intra*laboratory reproducibility) for organic-phase SEC. (Indeed, the obtained statistical variation of $V_\mathrm{e,peak}$ for the SEC experiments after 2 h and 2 d of sample dissolution in Section 7.2.1 on page 160 leads to a standard deviation of molar-mass results below 1 %.) The quality of *inter*laboratory reproducibility is somewhat lower, but it was also shown that it can be drastically improved when general guidelines of measurement and data processing are followed.[263,267,268] (For example, the obtained shift of $V_\mathrm{e,peak}$ in Figure 7.9 on page 165 and 7.12 on page 169 clarify how important low m_inj during calibration and generally constant experimental conditions are for successful molar-mass analyses.) However, even if these guidelines are rigorously followed and statistical errors are minimized, the *systematical* errors introduced by BB cannot be ruled out. In this context, BB is in fact hardly addressed when it comes to reproducibility of SEC results, which is presumably due to the above-mentioned misconceptions. Based on the here presented results, it is highly probable that BB contributes to the obtained uncertainties between several different SEC setups with different BB behavior. This is supported by the finding that $\overline{M}_\mathrm{w}$ values are generally more robust than $\overline{M}_\mathrm{n}$ values in round-robin tests, an effect which is under discussion and still unclear at the moment.[267] Whereas BB causes apparent $\overline{M}_\mathrm{n}$ values to generally decrease because of both the broadening and the calibration effect, the impact on $\overline{M}_\mathrm{w}$ is contrary; while the broadening effect leads to *higher* apparent $\overline{M}_\mathrm{w}$, the calibration

effect gives *lower* ones, so that the two effects somewhat compensate each other. This makes $\overline{M}_w$ more robust toward BB than $\overline{M}_n$, which might also be responsible for the finding that the deviation from the true values is often higher for $\overline{M}_n$ than for $\overline{M}_w$.[204] For all that, reliable interpretations of the relationship between reproducibility and BB can only be found if BB effects are taken account of in future round-robin tests.

As a general comment, BB can be very individual, which prohibits universal assessments about its impact on molar-mass determination. As a matter of course, the extent of BB for a certain SEC setup might be so low that the expected molar-mass deviation is irrelevant for the obtained results and their utilization. However, at the end of the day, every man is the architect of his own fortune and no one can dodge responsibility to at least estimate how significantly his results are affected by BB.

CHAPTER 9

Future perspectives on molar-mass correction

The thorough elucidation of the impact of BB on molar-mass determination presented in the previous chapter provides a strong basis for the development of correction techniques. Potential techniques were discussed in detail from Section 8.3.2.1 to 8.3.2.3 on pages 208–209. They include overall correction through application of the V_e-dependent correction terms $r_{tot,n}(V_e)$ and $r_{tot,w}(V_e)$, which can be determined either by knowing the extent of BB or by measuring explicitly known polymer. In addition, correction of the calibration effect can be achieved by finding the true calibration function. This can be accomplished either by modeling experimental chromatograms of the polymer standards or by calculating the hypothetically expected difference between their mean values and their peak values.

Within the simplified context of the simulations presented in this thesis—i. e., a constant extent of BB for the complete V_e range and no experimental uncertainties—all correction techniques are expected to be very reliable. However, correction becomes valuable not before it proves itself under less ideal/simplified conditions and in actual experiments. As discussed, all techniques have their individual advantages and disadvantages, and it is highly desired to check the respective applicability for molar-mass correction. In this regard, complementary simulation and experimental studies offer the possibility for a comprehensive evaluation of this issue.

Simulations As constant σ_G and τ values are not expected in real SEC experiments, a more sophisticated simulation model with V_e-dependent σ_G and τ values could be applied for the determination of $\overline{M}_n$(app) values similarly to the simulations presented in this thesis. By this means, the impact of specific BB behavior (more/less increasing, decreasing, fluctuating) and the potential of the specific correction techniques can be determined in a more realistic scenario. In fact, the impact of different trends of σ_G and τ can be barely investigated by experiment as they are normally rather predetermined by the SEC setup, even for different conditions (cf. Figure 7.4 on page 161). As a concrete problem, strategies might be developed to choose suitable values of V_e for the calculation of $r_{tot,n}(V_e)$ and $r_{tot,w}(V_e)$. As it was indicated in the context of Figure 8.14 on page 202, for broad-distribution analytes, calculation of $r_{tot,n}(V_e)$ at the center of the chromatogram can lead to inaccurate results. Average $r_{tot,n}$ values—potentially weighted with the intensities of the chromatogram—that cover a wider V_e range might improve correction in that case.

Experiments The applicability of the individual correction techniques should also be tested experimentally. In this context, identical polymer samples could be systematically measured for different extents of BB. This is feasible by using different SEC setups and/or varying operating conditions. While individual BB leads to individual $\overline{M}_n$(app), after correction, the obtained $\overline{M}_n$(true) values should be rather similar for the same polymer. This allows for a consistency check that strongly supports the applicability of a specific correction technique even if the true $\overline{M}_n$ value is not accurately known. As a brief example, applying $r_{tot,n}$ (via $\sigma_G \cdot b$, $\tau \cdot b$) to the experimentally obtained $\overline{M}_n$ values in Figure 8.7 on page 184 ($\overline{M}_n$(app) = 33 200 g mol^{-1}, 32 600 g mol^{-1}, and 31 900 g mol^{-1}) leads to rather similar *corrected* $\overline{M}_n$ values ($\overline{M}_n$(true) = 35 700 g mol^{-1}, 35 600 g mol^{-1}, and 35 700 g mol^{-1}). For a number of polymer samples and experimental conditions, the individual correction techniques can be evaluated and compared, and the applicability for real experiments can be systematically investigated.

Routine correction

As the ultimate goal, highly applicable correction techniques might then be implemented in software of SEC devices. This way, automatic BB correction might become part of routinely conducted calibration processes or of the eventual analysis of polymer.

Part IV

Experimental part

In this part, information on the employed materials, analytical methods, as well as the conducted kinetic simulations and polymerization procedures are given.

CHAPTER 10

Experimental information

10.1 Materials

10.1.1 Monomers

The monomers used in this work are presented in Figure 10.1. Styrene (St) (Aldrich, ≥ 99 %) was purified through an alumina column and stored at −21 °C. Methyl methacrylate (MMA) (99 %, Aldrich), *n*-butyl methacrylate (BMA) (99 %, Aldrich), and *n*-butyl acrylate (BA) (≥ 99 %, Aldrich) were all purified through an alumina column and stored at 3 °C.

10.1.2 Radical initiators

The radical initiators used in this work are presented in Figure 10.2 on the following page. 1,1′-Azobis(cyclohexanecarbonitrile) (ACCN) (Aldrich,

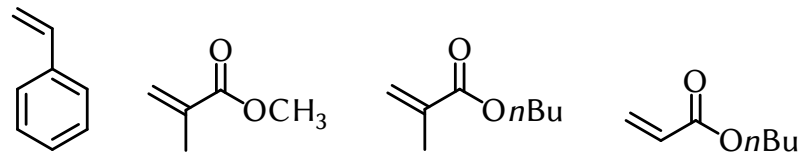

St MMA BMA BA

Figure 10.1 Monomers used in this work. For abbreviations see text.

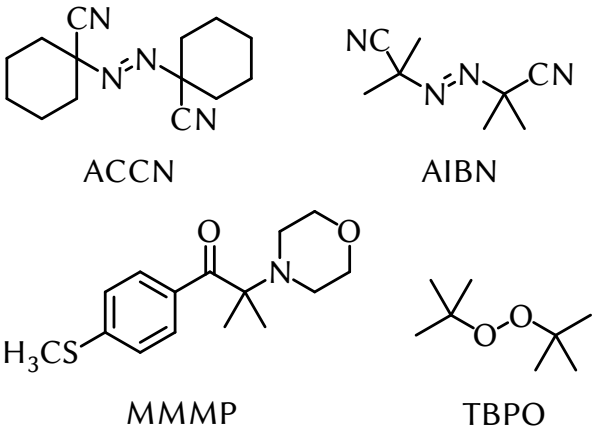

Figure 10.2 Radical initiators used in this work. For abbreviations see text.

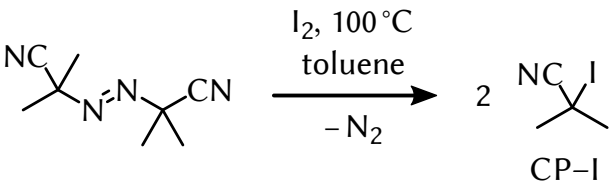

Scheme 10.1 Preparation of cyanopropyl iodide (CP–I) inspired by Bałczewski and Mikołajczyk.[147]

98 %) and 2,2′-azobis(2-methylpropionitrile) (AIBN) (Fluka, ≥ 98.0 %) were recrystallized from acetone and toluene and stored at 3 °C. 2-Methyl-4′-(methylthio)-2-morpholinopropiophenone (MMMP) (Aldrich, 98 %), stored in the dark at room temperature, and di-*tert*-butyl peroxide (TBPO) (Aldrich, 98 %), stored at 3 °C, were used as received.

10.1.3 Chain-transfer agents

10.1.3.1 Preparation of cyanopropyl iodide in toluene

The preparation of cyanopropyl iodide (CP–I) was inspired by Bałczewski and Mikołajczyk (Scheme 10.1).[147] A solution of I_2 (0.17 g, 0.67 mmol, 1.0 equiv) and AIBN (0.27 g, 1.6 mmol, 2.4 equiv) in toluene (6.3 g) was heated at 100 °C in an 8 mL glass vial under an argon atmosphere in the dark. After 15 min to 60 min (depending on the subsequent utilization), the solution was cooled down rapidly. The light yellow solution of the product in toluene was stored at −21 °C for 1 d at the longest and used without purification. By ^{1}H-NMR (formation of CP–I) and UV/vis spectroscopy (consumption of I_2), the yield was estimated to be > 99 % (cf. Section 4.2.3 on page 73).

Characterization: ^{1}H NMR (300.14 MHz, $CDCl_3$, room temperature): δ = 2.13 (s, 6 H, CH_3) ppm.

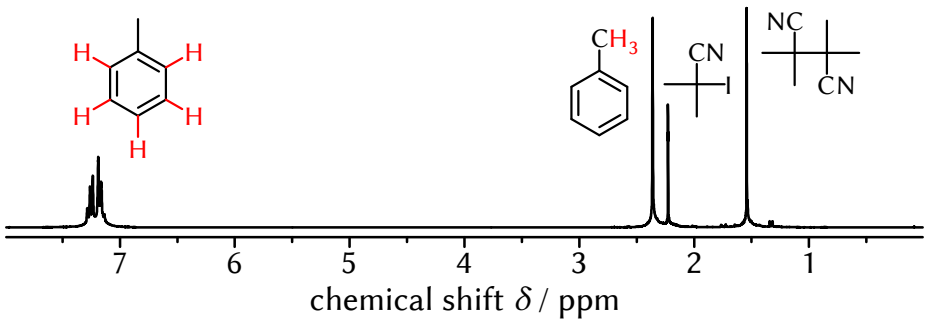

Figure 10.3 ^{1}H-NMR spectrum (300.14 Hz, $CDCl_3$, room temperature) of a solution of I_2 and AIBN in toluene after being heated at 100 °C for 60 min.

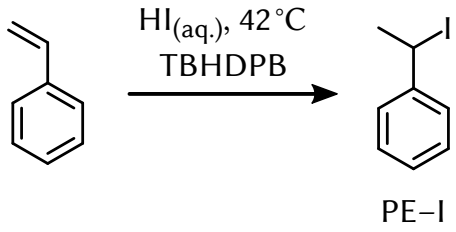

Scheme 10.2 Synthesis of phenylethyl iodide (PE–I) inspired by Matyjaszewski et al.[58]

Approach for higher CP–I concentrations More highly concentrated solutions of CP–I in toluene were obtained by carrying out the above-described procedure for higher concentrations of the reactants: I_2 (0.038 g, 0.15 mmol, 1.0 equiv), AIBN (0.079 g, 0.48 mmol, 3.2 equiv), toluene (0.21 g). In this regard, the initially slightly muddy mixture turned into a homogeneous solution at temperatures higher than room temperature. By means of UV/vis spectroscopy, the consumption of I_2 was estimated to be > 99 %. A ^{1}H-NMR spectrum (300.14 Hz, $CDCl_3$, room temperature) measured after the reaction time of 60 min is presented in Figure 10.3.

10.1.3.2 Synthesis of phenylethyl iodide

The synthesis of phenylethyl iodide (PE–I) was inspired by Matyjaszewski et al. (Scheme 10.2).[58] Hydroiodic acid (14 mL, 9.6 g, ≥ 47 g g^{-1}, 75 mmol, 3.0 equiv) was added to a solution of tributylhexadecylphosphonium bromide (TBHDPB) (1.3 g, 2.5 mmol, 0.10 equiv) in styrene (2.9 mL, 2.6 g, 25 mmol, 1.0 equiv). The two-phase mixture was stirred at 42 °C until the aqueous and the organic phase reversed (ca. 4–9 h). Afterwards, the mixture was stirred for additional 2 h.

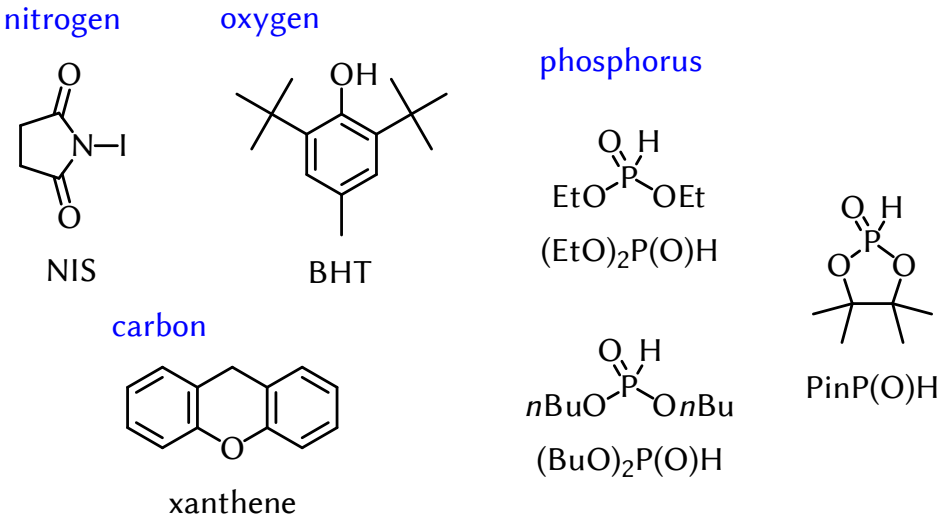

Figure 10.4 Nitrogen-, oxygen-, phosphorus-, and carbon-centered reversible-chain-transfer catalysts used in this work. For abbreviations see text.

Subsequently, ethyl acetate (20 mL) was added to the mixture. The organic phase was successively washed with distilled water (1 × 20 mL), a saturated aqueous solution of sodium carbonate (3 × 20 mL), and again distilled water (3 × 20 mL). It was dried over sodium sulfate. The raw product was purified by means of column chromatography at silica gel with pentane as the eluent. The product was received as a yellow liquid (3.1 g, 13 mmol, 54 %). It was stored at −21 °C.

Characterization: $R_f = 0.39$ (pentane); ^{1}H NMR (300.14 MHz, $CDCl_3$, room temperature): $\delta = 2.24$ (d, $^3J_{HH} = 7.1$ Hz, 3 H, CH_3), 5.43 (q, $^3J_{HH} = 7.1$ Hz, 1 H, CH), 7.23–7.37 (m, 3 H, H2, H4, H6), 7.44–7.51 (m, 2 H, H3, H5) ppm; ^{13}C NMR (75.48 MHz, $CDCl_3$, rt): $\delta = 26.1$ (CH_3), 28.9 (CH), 126.5 (C2, C6), 127.9 (C4), 128.7 (C3, C5), 145.3 (C1) ppm.

10.1.4 Reversible-chain-transfer catalysts

The nitrogen-, phosphorus-, oxygen-, and carbon-based reversible-chain-transfer catalysts used in this work are presented in Figure 10.4.

Germanium- and tin-based Germanium(IV) iodide (GeI_4) (Aldrich, 99.99 %) and tin(IV) iodide (SnI_4) (ABCR, 95 %) were used as received and stored at 3 °C.

Nitrogen-based *N*-iodosuccinimide (NIS) (Aldrich, 95 %) was used as received and stored at 3 °C.
Phosphorus-based Diethyl phosphonate ($(EtO)_2P(O)H$) (ABCR, 95 %) and dibutyl phosphonate ($(BuO)_2P(O)H$) (Aldrich, 96 %) were used as received and stored at 3 °C. 4,4,5,5-tetramethyl-1,3,2-dioxaphospholane 2-oxide (PinP(O)H) was externally[1] obtained (synthesis described elsewhere[269,270]) and stored in the dark at room temperature.
Oxygen-based 3,5-Di-*tert*-butylhydroxytoluene (BHT) (Aldrich, ≥ 99 %) was used as received and stored in the dark at room temperature.
Carbon-based Xanthene (Aldrich, 99 %) was used as received and stored in the dark at room temperature.

10.1.5 Miscellaneous

Solvents The solvents used in this work were obtained by common chemical retailers. They were used as received and stored at room temperature.
Iodine Molecular iodine (I_2) (Aldrich, 99.8 %) was used as received and stored in the dark at room temperature.

10.1.6 Polystyrene standards

For the experiments on the impact of operating parameters on the obtained SEC chromatograms (cf. Section 7 on page 153), polystyrene (polySt) standards obtained from Polymer Standards Service (PSS) were employed. They were stored in the dark at room temperature. They consist of three polySt standard kits—specified as green, red, and white—with four almost baseline-separated MMDs in each kit. Information about M_{peak}, $\overline{M}_w$, $\overline{M}_n$, and m of the respective MMDs is provided by PSS (see Table 10.1 on the next page).

10.2 Analytical methods

10.2.1 Electrospray-ionization mass-spectrometry

Electrospray-ionization mass-spectrometry (ESI-MS) spectra were measured with a Bruker Daltonik micrOTOF ESI–time-of-flight–mass-spectrometer. In a typical procedure, spectra were obtained in the positive ion mode at a spray

[1] Dr. Christoph Kornhaaß, Workgroup Prof. Dr. Lutz Ackermann, Institut für Organische und Biomolekulare Chemie, Georg-August-Universität Göttingen, Tammannstr. 2, D-37077 Göttingen, Germany.

Table 10.1 Information for the polySt standard kits—specified as green, red, and white—given by the manufacturer PSS.

green

M_{peak} / g mol^{-1}	$\overline{M}_w$ / g mol^{-1}	$\overline{M}_n$ / g mol^{-1}	m / mg
2 520 000	2 460 000	2 300 000	2.0
277 000	271 000	265 000	4.0
34 800	34 000	32 700	4.0
3470	3460	3260	4.0

red

M_{peak} / g mol^{-1}	$\overline{M}_w$ / g mol^{-1}	$\overline{M}_n$ / g mol^{-1}	m / mg
1 210 000	1 170 000	1 070 000	2.0
130 000	125 000	120 000	4.0
17 600	17 300	16 900	4.0
1250	1250	1100	4.0

white

M_{peak} / g mol^{-1}	$\overline{M}_w$ / g mol^{-1}	$\overline{M}_n$ / g mol^{-1}	m / mg
549 000	552 000	537 000	4.0
66 000	60 500	59 300	4.0
9130	8900	8650	4.0
474	570	492	4.0

voltage of 4.5 kV, a capillary temperature of 180 °C, and a dry-gas flow of 4 L min^{-1}. Analyte samples were dissolved in a THF–methanol mixture with or without the addition of ionization agents (e. g., formic acid, ammonium acetate) and introduced into the electrospray interface by injection via a syringe pump with a flow of 3 µL min^{-1}.

10.2.2 EPR spectroscopy

EPR measurements were performed on a Bruker EPR CW/transient spectrometer system Elexsys-II 500T with an ER 41122SHQE-LC cavity (Bruker) equipped with a grid.

10.2.3 NMR spectroscopy

NMR spectra were recorded using either a Varian Unity 300 (300 MHz) or a Varian Mercury 300 (300 MHz) system. They were measured at room temperature with an analyte concentration of about 40 g L^{-1} in deuterated solvent. The residual proton signal was respectively taken as the internal standard.

10.2.4 Size-exclusion chromatography

Two different SEC setups were used for molar-mass determination in the present work. They are referred to as "SEC setup 1" and "SEC setup 2" and are described in the following. For both setups, THF was used as the eluent at 35 °C with a flow rate of 1 mL min^{-1}, if not stated differently. Both setups were calibrated with polySt and polyMMA standards of low dispersities manufactured by PSS with toluene as the internal standard. Molar masses of polyBMA[271] and polyBA[272] were determined according to the principle of universal calibration (cf. Section 6.1.4.2 on page 143). If not stated differently, the concentration of the polymer samples was 5 g L^{-1} while the injection volume was 50 µL.

10.2.4.1 SEC setup 1

The setup consisted of an isocratic HPLC pump (Waters 515), an autosampler (JASCO AS-2055-plus), a PSS SDV (styrene–divinylbenzene copolymer-network) precolumn (8 × 50 mm), three PSS SDV separation columns (8 × 300 mm; particle size = 5 µm; pore size = 10^5, 10^3, and 10^2 Å), a refractive-index detector (Waters 2410), and a UV detector (Viscotek VE 3210).

10.2.4.2 SEC setup 2

The Agilent 1260 Infinity system consisted of an isocratic HPLC pump, an autosampler, a PSS SDV precolumn (8 × 50 mm), three PSS SDV separation columns (8 × 300 mm; particle size = 10 µm; pore size = 10^6, 10^5, and 10^3 Å), and a refractive-index detector.

10.2.5 UV/vis spectroscopy

Optical absorption spectroscopy was performed with a Cary 300 Scan or a Shimadzu UV-2450 photospectrometer in solution against the pure solvent, using either Heraeus quartz cuvettes (thickness of 2 mm) or Hellma

quartz cuvettes (thickness of 10 mm). The spectra were recorded at room temperature, if not stated differently.

10.3 Kinetic simulations

Kinetic simulations were performed using the program package Predici©.[151–153] The applied simulation models consisted of the initial concentrations of all reaction components and the individual chemical reactions with the respective rate coefficients. The main results are approximations of the polymeric products' complete MMDs and/or their respective moments and mean values, as well as the concentrations of the remaining reagents, which are obtained via a numerical time integration of differential equations over the predetermined final reaction time. The program package uses a method of approximation for countable differential equation systems (discrete Galerkin *h*–*p* method) and a special time discretization.[153] Simulations were performed using Predici© version 6.4.6 on an Intel Core i7-3630QM, 2.4 GHz computer.

10.4 Polymerization procedures

10.4.1 Thermally initiated RITP-based systems

In a typical procedure, prior to polymerization, a solution of I_2 (0.11 g) and AIBN (0.14 g) in MMA (8.7 g) was degassed via three consecutive freeze–pump–thaw cycles in the dark. Under an argon atmosphere, the solution was then divided into several distinct 8 mL glass vials (ca. 1–2 mL each), which were subsequently heated in a shaken thermostated block heater at 80 °C in the dark. After determined reaction times, glass vials were rapidly cooled down and polymeric products were isolated by evaporation of the residual monomer. Monomer conversion was determined gravimetrically.

10.4.2 Photoinitiated systems

In a typical procedure, 0.13 g of the CP–I solution (see Section 10.1.3.1 on page 218) was added to a solution of MMMP (56 mg) in BMA (3.5 g). Prior to polymerization, the solution (ca. 4 mL in an 8 mL borosilicate-glass vial) was purged with argon for 20 min in the dark. The solution was then stirred in a thermostated water bath at 22 °C. The solution was irradiated with a

UV lamp (Hg-vapor lamp with an optical bandpass filter at 366 nm, 8 W, Herolab UV Hand Lamp) from a distance of 7 cm (intensity = 4.5 mW cm^{-2}). After determined reaction times, samples were taken via syringe through a septum while purging with argon. For some BA polymerizations, separate glass vials were used. The polymeric products were isolated by evaporation of the residual monomer and solvent. Monomer conversion was determined gravimetrically.

Appendices

APPENDIX A

UV-initiated iodine-mediated polymerizations

A.1 Polymerizations of BA

A.1.1 Crystallographic analysis of [MMMP−H]$^+$I$^-$

A batch of crystals of compound [MMMP−H]$^+$I$^-$ suitable for single crystal X-ray diffraction was grown from a solution of [MMMP−H]$^+$I$^-$ in toluene and acetone. A crystal of the dimensions (0.25 × 0.10 × 0.06) mm was se-

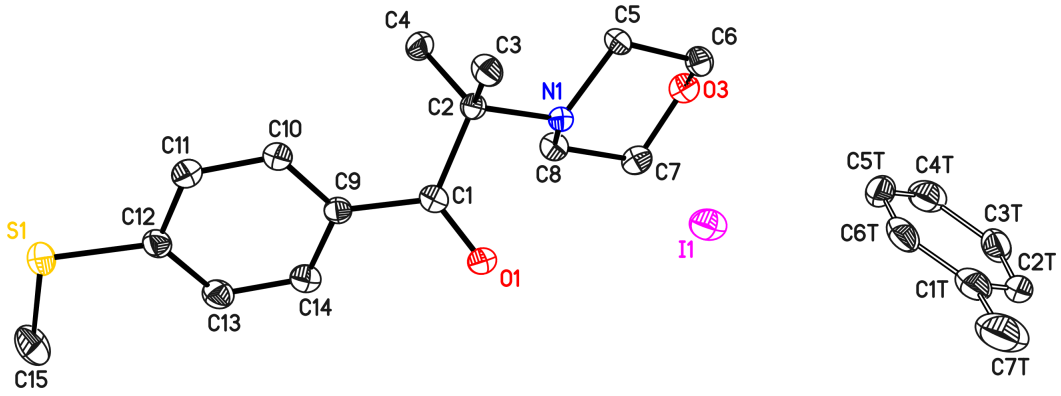

Figure A.1 Crystallographic structure of [MMMP−H]$^+$I$^-$ co-crystallized with toluene; C = carbon, I = iodine, N = nitrogen, O = oxygen, S = sulfur. For additional information see text.

lected and mounted on the tip of a glass fiber. A complete dataset up to a resolution of 0.79 Å with an average multiplicity of 8.6 and an internal agreement factor of $R_{\text{int}} = 4.76\,\%$ was collected using a Bruker Apex2 Ultra diffractometer with rotating Molybdenum anode, Incoatec focusing mirror optics and Bruker Kryoflex 2 crystal cooling device. The sample temperature was kept at 101 K throughout the data collection. Data reduction was performed with SAINT.[273] SADABS[274] was used for absorption correction and scaling of the data. The structure was solved with Direct Methods and a full-matrix least-squares structure refinement against F^2 with SHELXL was carried out.[275] Compound $[\text{MMMP}-\text{H}]^+\text{I}^-$ crystallized in monoclinic space group $C2/c$ (unit cell constants: $a = 25.879(10)$ Å, $b = 10.205(3)$ Å, $c = 16.311(5)$ Å, $\beta = 114.04(2)^\circ$) with 0.5 molecules of toluene per molecule of $[\text{MMMP}-\text{H}]^+\text{I}^-$. Hydrogen atom positions and displacement parameters were calculated using a riding model. The toluene molecule was situated on a special position. Its carbon atom positions and displacement parameters were refined using similarity restraints. The refinement converged at a final wR2 (all data) of 9.90 %, R1 ($I > 2\sigma$) of 3.80 % and with a goodness-of-fit of 1.014 (see Figure A.1 on the preceding page).[1]

A.1.2 Hydrogen abstraction from PADs

A solution of $(\text{BuO})_2\text{P(O)H}$ in TBPO (v/v = 1 : 1) was irradiated with a Hg-vapor lamp with 500 W (LAX 1450/SH2/5,500W, Müller) in a quartz tube through a grid inside the EPR device described in the Experimental Section 10.2.2 on page 222 at room temperature. The resulting spectrum is given in Figure A.2 on the facing page.

A.1.3 UV-initiated decomposition of SnI_4

A solution of SnI_4 in toluene with $[SnI_4]_0 = 0.55 \times 10^{-3}\,\text{mol}\,\text{L}^{-1}$ was irradiated similarly to the polymerization experiments in Section 4.2.7 on page 97. After different periods of time, samples were taken and measured via UV/vis spectroscopy. The results are shown in Figure A.3 on page 232. The decomposition of SnI_4 according to $SnI_4 \xrightarrow{h \cdot \nu} Sn + 2\ I_2$[166,167] is indicated by the decreasing signal of SnI_4 at $\lambda \approx 360$ nm and the increasing signal of I_2 at $\lambda \approx 500$ nm. Based on the intensity at $\lambda = 400$ nm (lowest absorption of I_2,

[1] The procedure was conducted by Dr. Jakob Hey, Workgroup Prof. Dr. Dietmar Stalke, Institut für Anorganische Chemie, Georg-August-Universität Göttingen, Tammannstr. 4, D-37077 Göttingen, Germany.

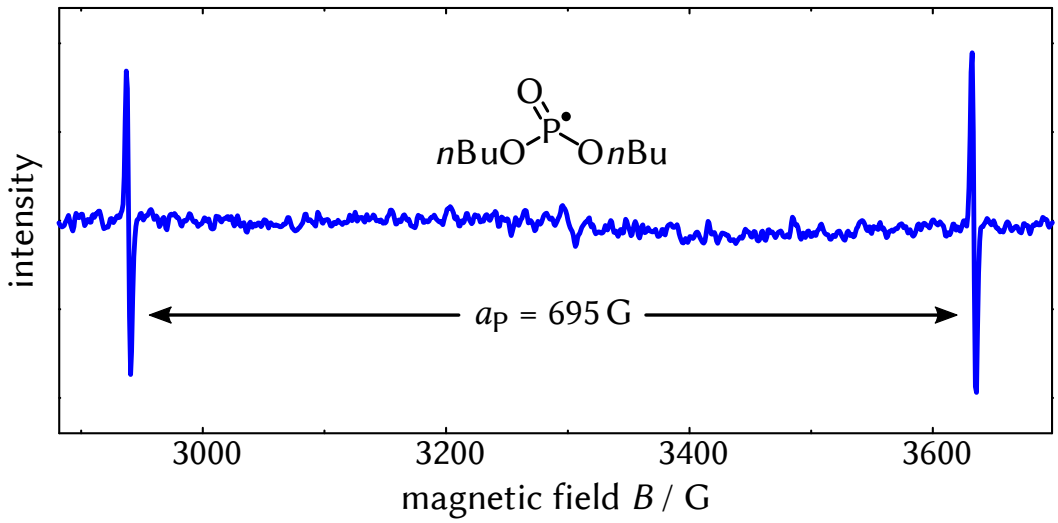

Figure A.2 EPR spectrum of the indicated species upon UV irradiation with TBPO at room temperature.

cf. Figure 4.1 on page 64), the extent of decomposition of SnI_4 was estimated to be at about 12 % after 150 min.

A.2 Polymerizations of BMA

A.2.1 Determination of C_{ex}

Kinetic simulations by means of the program package Predici were used to determine the exchange constant $C_{ex} = k_{ex}/k_p$ for iodine transfer in polymerizations of BMA. C_{ex} was obtained through the transfer constant $C_{tr} = k_{tr}/k_p$ of CP–I, which is structurally similar to polyBMA–I ($C_{tr} \approx C_{ex}$). C_{tr} was determined by modeling experimentally obtained $\overline{M}_n$ values as a function of monomer conversion for an ITP of BMA with CP–I in bulk at 60 °C (in the dark). The reaction components in their initial concentrations are given in the bottom rows of Table A.1 on page 234. The reactions and respective rate coefficients implemented in the simulation are presented in Scheme A.1 on page 233 and Table A.1. In this context, rate coefficients were taken from the literature as indicated (for further explanations see Section 4.3.5.1 on page 110. A best-fit procedure according to the least-squares method was performed in order to obtain k_{ex}, while the rest of the

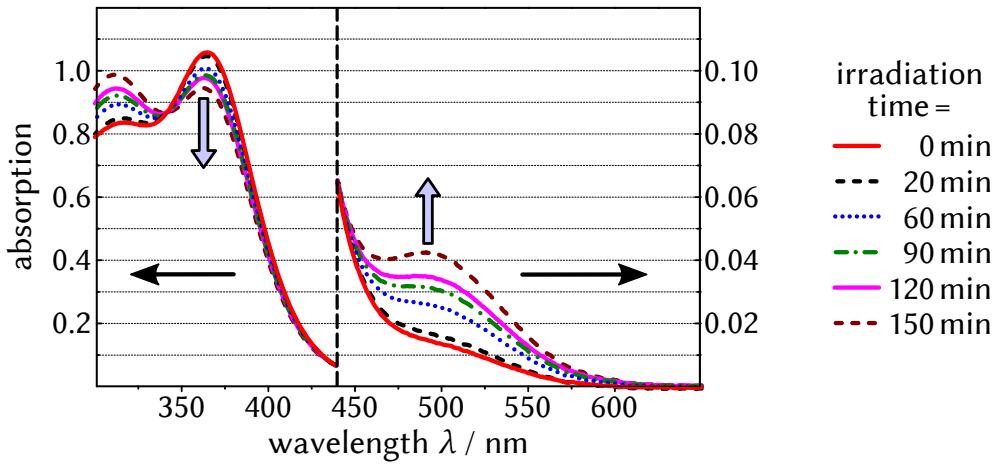

Figure A.3 UV/vis spectra of SnI_4 in toluene ($[SnI_4]_0 = 0.55 \times 10^{-3}$ mol L^{-1}) UV-irradiated for different times as indicated. For details see text. Thickness of quartz cuvette: 2 mm.

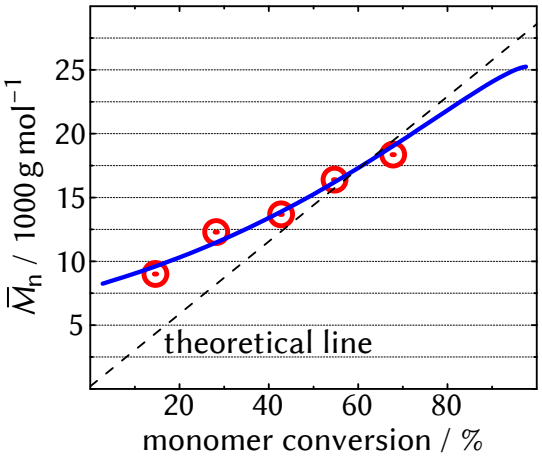

Figure A.4 Experimentally obtained $\overline{M}_n$ values as a function of monomer conversion of an ITP of BMA with CP–I in bulk at 60 °C (for initial concentrations see Table A.1 on page 234). The best-fit simulation is given for $k_{ex} = 3.5 \times 10^3$ L mol^{-1} s^{-1}.

rate coefficients remained constant. The results are shown in Figure A.4. k_{ex} was determined to be 3.5×10^3 L mol^{-1} s^{-1}, leading to $C_{ex} = k_{ex}/k_p = 3.6$.

A.2.2 Determination of k_{hc}

The rate coefficient k_{hc} of the homolytic C–I-bond-cleavage reaction of CP–I used for the kinetic simulations described in Section 4.3.5.1 on page 110 was determined. For this, a dilute solution of CP–I in toluene (prepared according to Section 4.2.3 on page 73) was saturated with air and then irradiated with a lamp distance of 7 cm similar to the polymerization experiments in Chapter 4

(a) conventional radical polymerization

radical formation & initiation

$$\text{(I)}\quad \text{AIBN} \xrightarrow{k_{dec}} f\times \text{In}^\bullet + f\times \text{In}^\bullet$$

$$\text{(II)}\quad \text{In}^\bullet + \text{BMA} \xrightarrow{k_{ini}} \text{polyBMA}^\bullet(1)$$

propagation

$$\text{(III)}\quad \text{polyBMA}^\bullet(i) + \text{BMA} \xrightarrow{k_p} \text{polyBMA}^\bullet(i+1)$$

irreversible termination

$$\text{(IV)}\quad \begin{matrix}\text{polyBMA}^\bullet(i)\\ +\ \text{polyBMA}^\bullet(j)\end{matrix} \xrightarrow[=k_t(i,i);\ i\approx j]{k_t} \begin{matrix}\delta_t\times\ \text{polyBMA}_{dead}(i)\\ +\ \text{polyBMA}_{dead}(j)\\ \&\\ (1-\delta_t)\times\ \text{polyBMA}_{dead}(i+j)\end{matrix}$$

(b) iodine-transfer polymerization

pre-equilibrium degenerative chain-transfer

$$\text{(V)}\quad \text{polyBMA}^\bullet(i) + \text{CP–I} \xrightarrow{k_{ex}} \text{polyBMA–I}(i) + \text{CP}^\bullet$$

$$\text{(VI)}\quad \text{polyBMA–I}(i) + \text{CP}^\bullet \xrightarrow{k_{ex}} \text{polyBMA}^\bullet(i) + \text{CP–I}$$

reinitiation

$$\text{(VII)}\quad \text{CP}^\bullet + \text{BMA} \xrightarrow{k_{ini}} \text{polyBMA}^\bullet(1)$$

main equilibrium degenerative chain-transfer

$$\text{(VIII)}\quad \begin{matrix}\text{polyBMA}^\bullet(i)\\ +\ \text{polyBMA–I}(j)\end{matrix} \xrightarrow{k_{ex}} \begin{matrix}\text{polyBMA–I}(i)\\ +\ \text{polyBMA}^\bullet(j)\end{matrix}$$

Scheme A.1 Reactions and corresponding rate coefficients implemented for the simulations of ITP of BMA in bulk at 60 °C (for the values of the coefficients see Table A.1 on the next page).

on page 61. Under these conditions, the formed $CP^\bullet$ is expected to react much more likely with the dissolved oxygen than with the free iodine (especially when iodine concentration is low), so that reversible termination of $CP^\bullet$ with iodine is suppressed. The resulting accumulation of I_2 was quantified via UV/vis spectroscopy, allowing to calculate the amount of decomposed CP–I. The integrated rate law of the decomposition reaction gives

$$[\text{CP–I}] = [\text{CP–I}]_0 \cdot \exp(-k_{hc} \cdot t) \tag{A.1}$$

Table A.1 Kinetic parameters for the simulations of ITP of BMA in bulk at 60 °C (see Scheme A.1 on the previous page for the respective reactions).

coefficient	value	reference
k_{dec}	$1.1 \times 10^{-5}\,s^{-1}$	106
f	0.6	105,107
k_{ini}	$9770\,L\,mol^{-1}\,s^{-1} = 10 \times k_p$	155,156,169
k_p	$977\,L\,mol^{-1}\,s^{-1}$	169
k_t	$2.9 \times 10^8 \cdot i^{-0.65}\,L\,mol^{-1}\,s^{-1}$ $(i \leq 50)$ $5.0 \times 10^7 \cdot i^{-0.20}\,L\,mol^{-1}\,s^{-1}$ $(i > 50)$	141
δ_t	0.6	98,110
k_{ex}	$3.5 \times 10^3\,L\,mol^{-1}\,s^{-1}$	–
$[BMA]_0$	$5.9\,mol\,L^{-1}$	–
$[CP{-}I]_0$	$30 \times 10^{-3}\,mol\,L^{-1}$	–
$[AIBN]_0$	$9.6 \times 10^{-3}\,mol\,L^{-1}$	–

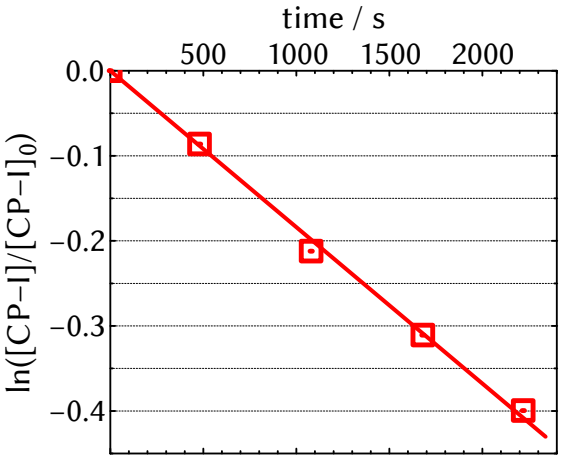

Figure A.5 Experimental data of the photoinduced decomposition of CP−I and linear best-fit according to Equation A.2. The slope of the best-fit is determined to be $-1.8 \times 10^{-4}\,s^{-1}$.

or

$$\ln\left([CP{-}I]/[CP{-}I]_0\right) = -k_{hc} \cdot t\,, \tag{A.2}$$

while

$$[CP{-}I]/[CP{-}I]_0 = 1 - [I_2]/[I_2]_{max}\,, \tag{A.3}$$

with the initial concentration of CP−I, $[CP{-}I]_0$, and the maximum possible $[I_2]$ (for full decomposition of CP−I), $[I_2]_{max}$, which is predetermined by the amount of I_2 employed for the preparation of CP−I. The linear best-fit in Figure A.5 confirms the first-order rate of Equation A.2 and leads to $k_{hc} = 1.8 \times 10^{-4}\,s^{-1}$.

APPENDIX B

Band broadening in size-exclusion chromatography

B.1 The EMG function

The (unnormalized) convolution product between a Gaussian and a decaying exponential function is given by

$$h\left(V_\mathrm{e}, V_\mathrm{e}^0\right) = \underbrace{\exp\left(-\frac{\left[\left\{V_\mathrm{e} - V_\mathrm{e}^0\right\} + \tau\right]^2}{2{\sigma_\mathrm{G}}^2}\right)}_{f_1(V_\mathrm{e})} * \underbrace{\exp\left(-\frac{V_\mathrm{e} - V_\mathrm{e}^0}{\tau}\right)}_{f_2(V_\mathrm{e})}, \tag{B.1}$$

with the convolution operator "$*$" and $f_1(V_\mathrm{e}) * f_2(V_\mathrm{e}) = \int_0^{V_\mathrm{e}} f_1(u) \cdot f_2(V_\mathrm{e} - u)\mathrm{d}u$ as well as the bound convolution variable u. For application, the convolution product was determined by means of the computer algebra system Maple (version 13, Maplesoft®):

$$\begin{aligned} h\left(V_\mathrm{e}, V_\mathrm{e}^0\right) = \exp\left(-\frac{2\tau \cdot V_\mathrm{e} - 2\tau \cdot V_\mathrm{e}^0 + 2\tau^2 - {\sigma_\mathrm{G}}^2}{2\tau^2}\right) \cdot \sigma_\mathrm{G} \\ \cdot \left[\mathrm{erf}\left(\frac{\tau \cdot V_\mathrm{e} - \tau \cdot V_\mathrm{e}^0 + \tau^2 - {\sigma_\mathrm{G}}^2}{\sqrt{2}\sigma_\mathrm{G} \cdot \tau}\right) + \mathrm{erf}\left(\frac{\tau \cdot V_\mathrm{e}^0 - \tau^2 + {\sigma_\mathrm{G}}^2}{\sqrt{2}\sigma_\mathrm{G} \cdot \tau}\right)\right] \end{aligned} \tag{B.2}$$

with the so-called error function

$$\mathrm{erf}(x) = \frac{2}{\sqrt{\pi}} \cdot \int_0^x \exp\left(-s^2\right) \mathrm{d}s, \tag{B.3}$$

	A	B	C	D	E
1	nonequidistant			equidistant	
2	V_e	RI	dummy value	V_e	RI
3	0	0	=MATCH(D1; $A$3:$A$9)=1	1	=TREND(OFFSET($B$3; C3−1;0;2;1);OFFSET($A$3; C3−1;0;2;1);D3)=0.5
4	2	1	=MATCH(D2; $A$3:$A$9)=2	2	=TREND(OFFSET($B$3; C4−1;0;2;1);OFFSET($A$3; C4−1;0;2;1);D4)=1
5	3.1	2	...=2	3	...=1.9
6	3.5	2	...=4	4	...=1.8
7	4.5	1.6	...=5	5	...=1.4
8	6	1			
9	7	0			

Figure B.1 Schematic example of an Excel sheet used for the interpolation of data points to obtain elution chromatograms with equidistant V_e values. For details on the Excel functions see text.

and the bound variable s.

B.2 Interpolation of data points via Microsoft Excel

The routine of simulating MMDs (Poissonian, Schulz–Flory) and translating them into elution chromatograms leads to chromatograms with nonequidistant V_e values. Chromatograms with *equidistant* V_e values are necessary for an unbiased broadening procedure and were calculated via linear interpolation by means of Microsoft Excel® using the implemented `MATCH`, `TREND`, and `OFFSET` functions. A small example is presented in Figure B.1. The `MATCH(lookup_value;lookup_array)` function finds the largest value within the `lookup_array` that is less than or equal to the `lookup_value`, while the values in the `lookup_array` must be placed in ascending order. The function then returns the relative position of the found value within the `lookup_array`. The `OFFSET(reference;rows;cols;height;width)` function returns a range (`height` and `width`) of values having a position

Table B.1 EMG parameters σ_G and τ obtained by modeling experimental elution chromatograms of polySt standards with kinetic chain lengths $\nu < 600$ based on simulations of either Poissonian or Gaussian MMDs. $\Delta\sigma_G$ and $\Delta\tau$ give the percentage deviation of the Gaussian from the Poissonian values.

	Poissonian		Gaussian			
ν	σ_G / mL	τ / mL	σ_G / mL	τ / mL	$\Delta\sigma_G$	$\Delta\tau$
31	0.153	0.076	0.151	0.034	−1.6 %	−55.8 %
80	0.132	0.146	0.143	0.128	9.3 %	−12.1 %
160	0.171	0.165	0.175	0.161	1.9 %	−2.6 %
330	0.179	0.180	0.179	0.179	−0.1 %	−0.8 %
590	0.161	0.275	0.160	0.273	−0.6 %	−0.4 %

of `rows` rows and `cols` columns away from the `reference` cell. The `TREND(known_y's;known_x's;new_x's)` function returns an ordinate value for a desired abscissa value `new_x's` from a linear fit of data points with ordinate values `known_y's` and abscissa values `known_x's`. The here described interpolation procedure is especially useful during the EMG parameter estimation presented in Section 7 on page 153. In that context, the expected chain length ν of the polymer standard's CLD is varied simultaneously with σ_G and τ, which requires an instant calculation of the corresponding chromatogram.

B.3 Poissonian versus Gaussian MMDs

The impact of using Gaussians instead of Poissonians as simulated MMDs of the high-molar-mass polySt standards was evaluated (cf. Section 7.1.2 on page 154). For this, EMG parameters were determined for experimentally obtained chromatograms according to the method described in Section 7.1 for kinetic chain lengths $\nu < 600$ based on either a Poissonian (Equation 7.2 on page 154) or a Gaussian MMD (Equation 7.3). The results are given in Table B.1. The higher ν is, the smaller is the deviation of the EMG parameters, $\Delta\sigma_G$ and $\Delta\tau$, respectively, as the shapes of the distributions become more and more alike. For $\nu > 300$, deviations are lower than 1 %, which demonstrates that the Gaussian distribution is a suitable function to replace the Poissonian for higher ν. It should be noted that the here used chromatograms were measured by means of a different SEC setup (SEC setup 1, cf. Experimental

Table B.2 Determined $\overline{\log_{10}(M)}$, $\overline{DP}_n$, and $\overline{DP}_w$ values of the EMG-broadened distributions presented in Figure B.7 on page 244. $\overline{DP}_n$ and $\overline{DP}_w$ values predicted by the GPCV3 model by Yau et al. are given for each case.

$\sigma_G \cdot b = \tau \cdot b$ [a]	$\overline{\log_{10}(M / \text{ g mol}^{-1})}$ [b]	$\overline{DP}_n$	$\overline{DP}_n$ (GPCV3) [c]	$\overline{DP}_w$	$\overline{DP}_w$ (GPCV3) [d]
0.023	4.171	499	499	501	501
0.046	4.171	494	494	505	505
0.069	4.171	487	487	512	512
0.092	4.171	476	476	522	522
0.115	4.171	463	463	534	534

[a] For $\sigma_G = \tau$ from 0.1 mL to 0.5 mL with $b = 0.23\,\text{mL}^{-1}$; [b] on RI-versus-$\log_{10}(M)$ scale; [c] see Equation 8.1 and 8.2 on pages 186–187; [d] see Equation 8.3 and 8.4 on page 187.

Section 10.2.4 on page 223) than the ones described in Section 7 and σ_G and τ values deviate from the there obtained ones.

B.4 EMG parameters for full V_e range

In this section, the EMG parameters, σ_G and τ, as well as the standard deviations, σ, obtained for the SEC measurements of the polySt standards discussed in Section 7.2 on page 159 are presented for the complete V_e range. Parameters are given for [polymer] = $4\,\text{g L}^{-1}$ (Figure B.2 on the facing page) and $8\,\text{g L}^{-1}$ (Figure B.3 on page 240) for $V_{inj} = 10\,\mu\text{L}$, 40 µL, 70 µL, and 100 µL and constant $T_{col} = 35\,^\circ\text{C}$ and $v_{flow} = 1.00\,\text{mL min}^{-1}$. In this context, parameters for [polymer] = $4\,\text{g L}^{-1}$ and an extended dissolution period of 2 d are given in Figure B.4 on page 241. Parameters for $T_{col} = 35\,^\circ\text{C}$ (Figure B.5 on page 242) and 45 °C (Figure B.6 on page 243) for $v_{flow} = 0.20\,\text{mL min}^{-1}$, $0.45\,\text{mL min}^{-1}$, $0.75\,\text{mL min}^{-1}$, and $1.00\,\text{mL min}^{-1}$, and constant [polymer] = $4\,\text{g L}^{-1}$ and $V_{inj} = 40\,\mu\text{L}$ are presented as well.

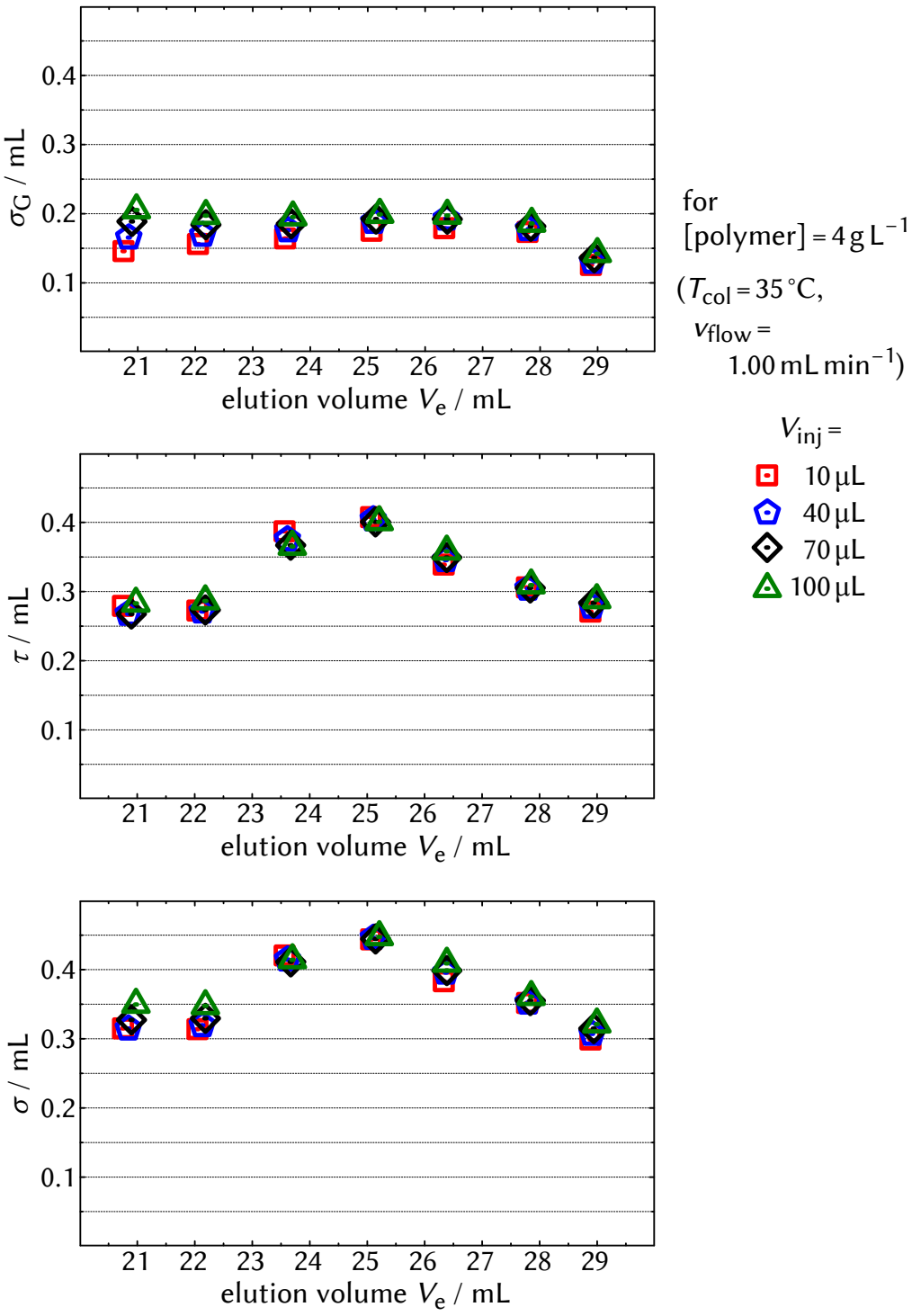

Figure B.2 EMG parameters, σ_G and τ, and standard deviation, σ, as a function of V_e (= $V_{e,peak}$) for polySt standards measured under the indicated operating conditions.

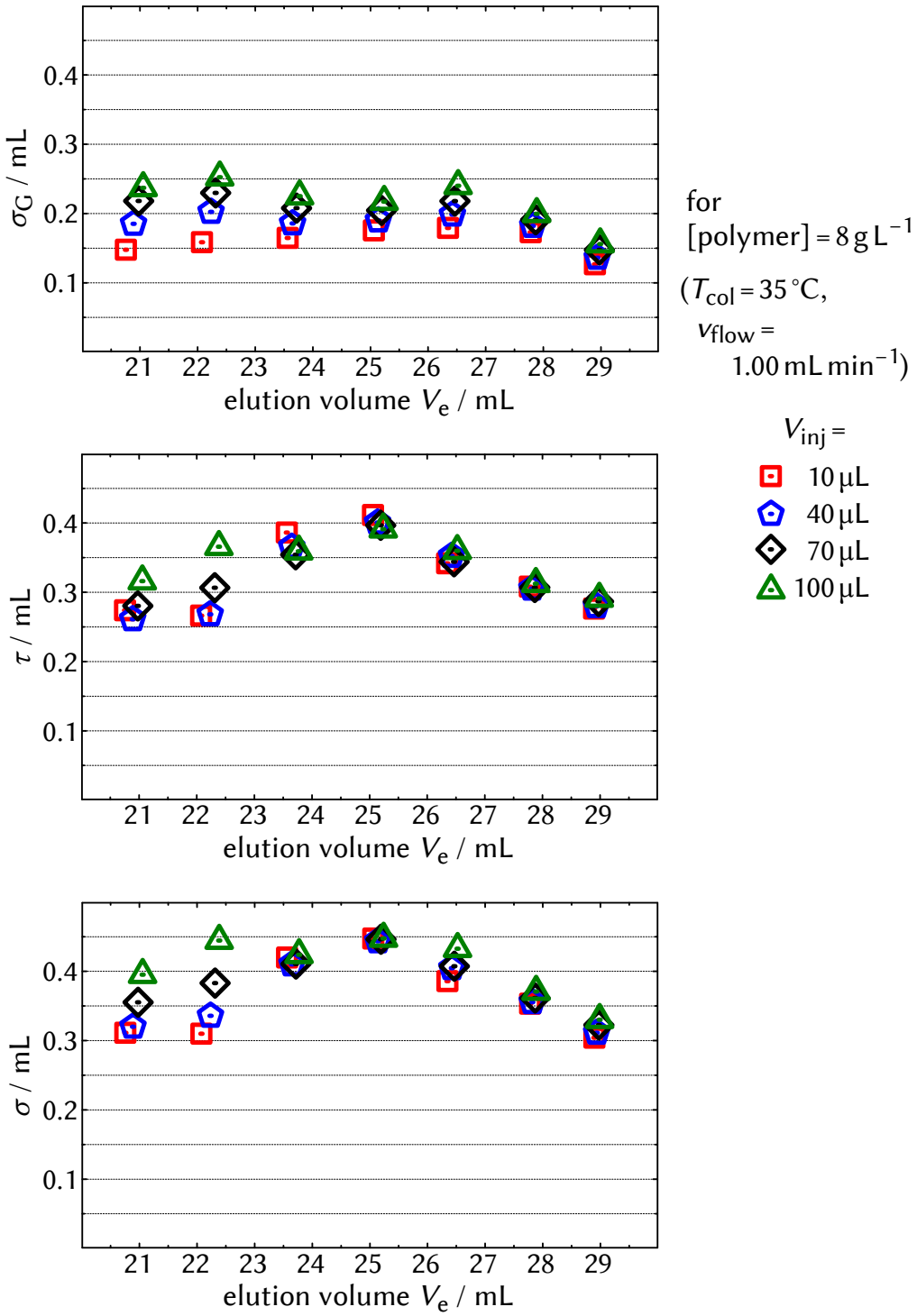

Figure B.3 EMG parameters, σ_G and τ, and standard deviation, σ, as a function of V_e (= $V_{e,peak}$) for polySt standards measured under the indicated operating conditions.

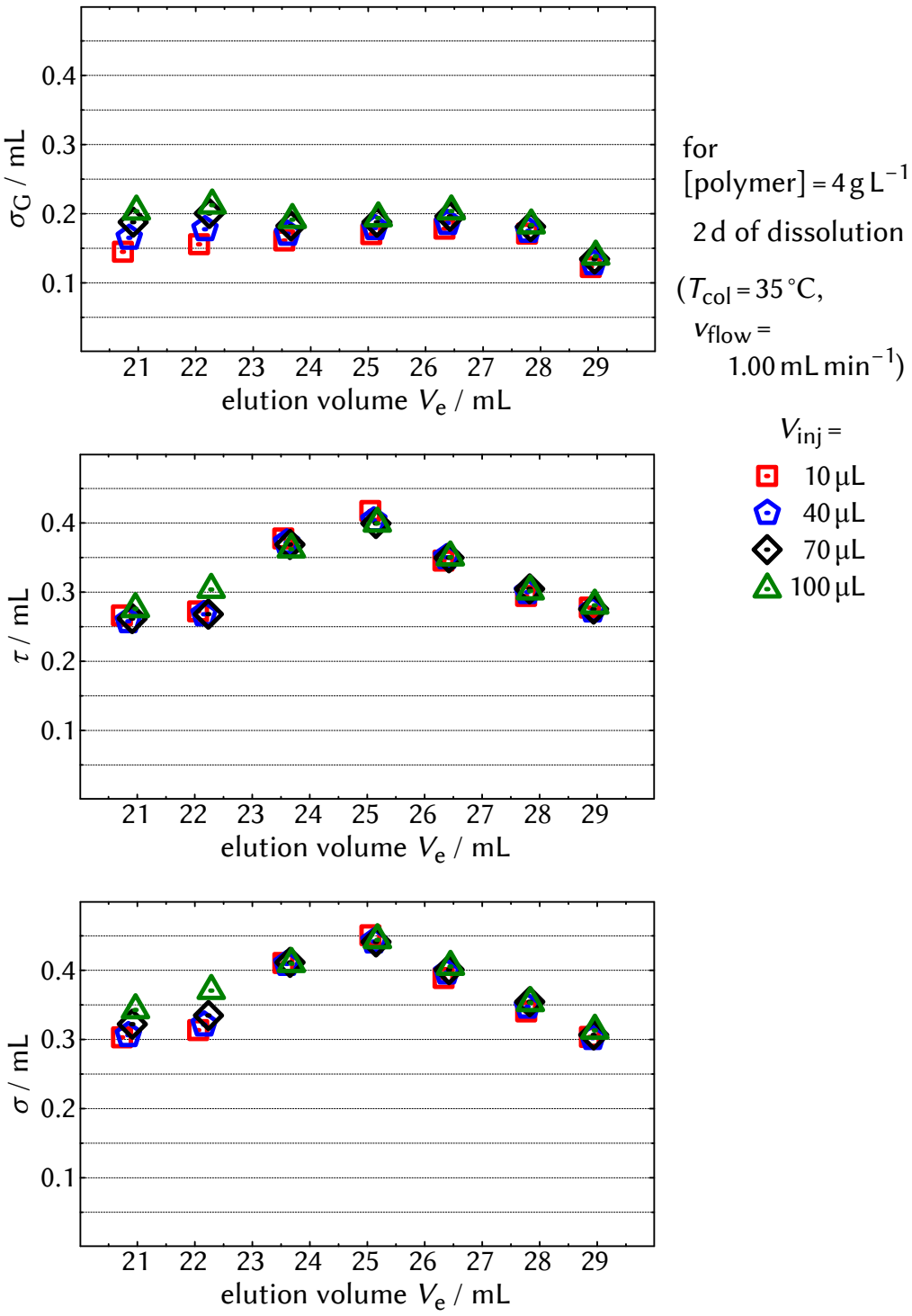

Figure B.4 EMG parameters, σ_G and τ, and standard deviation, σ, as a function of V_e (= $V_{e,peak}$) for polySt standards measured under the indicated operating conditions.

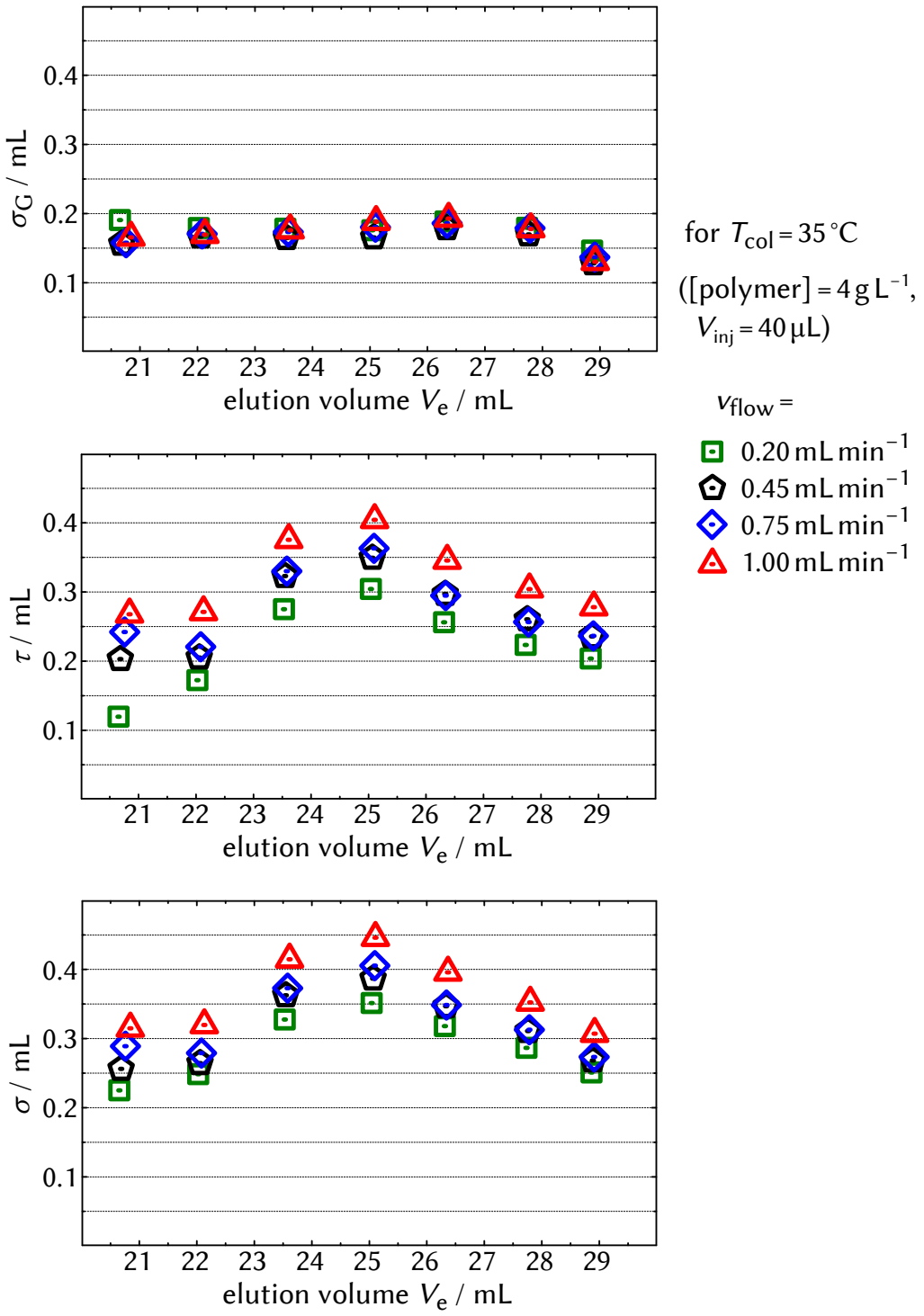

Figure B.5 EMG parameters, σ_G and τ, and standard deviation, σ, as a function of V_e (= $V_{e,peak}$) for polySt standards measured under the indicated operating conditions.

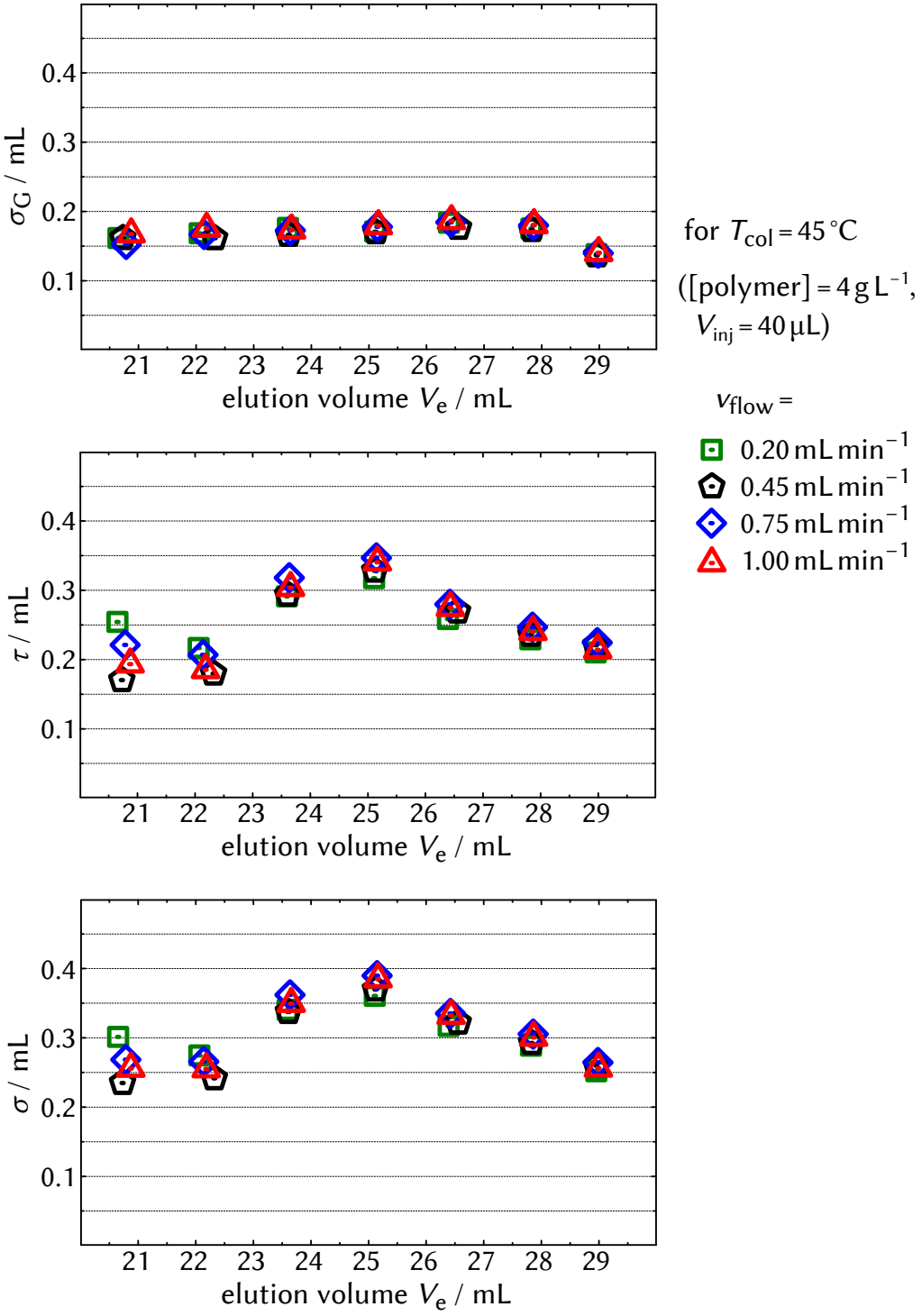

Figure B.6 EMG parameters, σ_G and τ, and standard deviation, σ, as a function of V_e (= $V_{e,peak}$) for polySt standards measured under the indicated operating conditions.

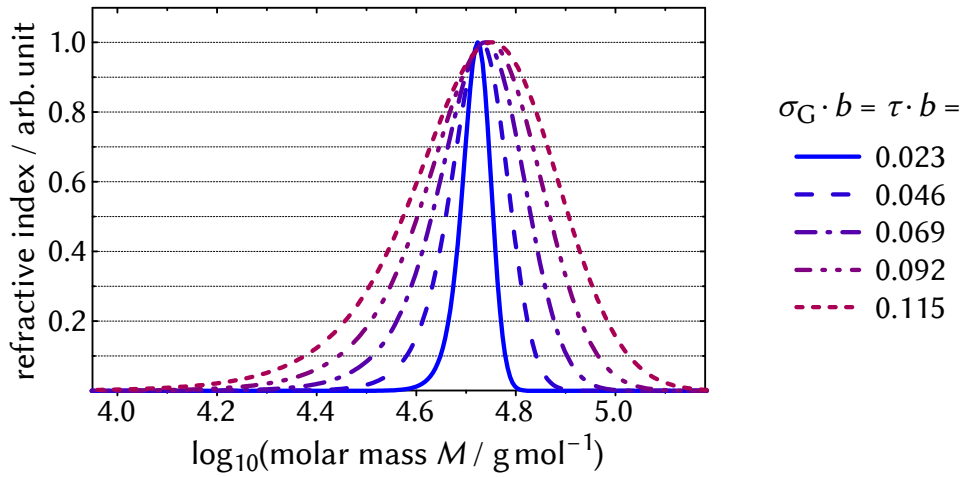

Figure B.7 Simulations of EMG broadening for hypothetically unimolecular polySt with $i = 500$ and different values of $\sigma_G \cdot b = \tau \cdot b$. For every distribution, $\overline{\log_{10}(M)}$, $\overline{DP}_n$, and $\overline{DP}_w$ are given in Table B.2 on page 238. For ease of comparison, all distributions are normalized to the same maximum intensity.

B.5 Numerical simulation of the broadening effect by Yau et al.

Simulations of EMG broadening were conducted for hypothetically unimolecular polySt with $i = 500$, which corresponds to $\log_{10}(M/\,\mathrm{g\,mol^{-1}}) = 4.171$. Broadening was applied directly on the $\log_{10}(M)$ scale, i. e., without translation to (and retranslation from) the V_e scale by using EMG parameters $\sigma_G \cdot b = \tau \cdot b$ with $b = 0.23\,\mathrm{mL^{-1}}$ and $\sigma_G = \tau$ from 0.1 mL to 0.5 mL (see Figure B.7). It should be noted that negative skewing toward *lower* values cannot be reliably expressed by the here used EMG function so that the distributions were obtained by flipping positively skewed distributions horizontally. The respective number- and weight-average degrees of polymerization, $\overline{DP}_n$ and $\overline{DP}_w$, were determined, which are given in Table B.2 on page 238. While the average $\log_{10}(M)$ value on the RI-versus-$\log_{10}(M)$ scale, $\overline{\log_{10}(M)}$, remains constant, $\overline{DP}_n$ decreases and $\overline{DP}_w$ increases with increasing EMG parameters. In this context, the quantitative impact on both $\overline{DP}_n$ and $\overline{DP}_w$ is accurately predicted by Equation 8.1 to 8.4 on pages 186–187 involved in the GPCV3 calibration method by Yau et al.[48,264]

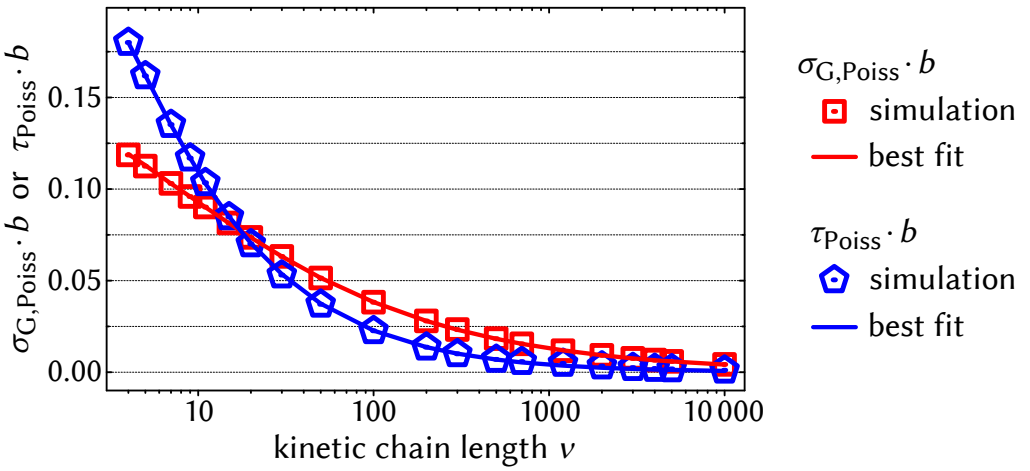

Figure B.8 EMG parameters, $\sigma_G \cdot b$ and $\tau \cdot b$, of the EMG functions used for fitting simulated Poissonian CLDs for different ν translated to chromatographic scaling (RI versus $\log_{10}(i)$) and respective best-fit functions as given in Equation B.4 and B.5.

B.6 EMG parameters of Poissonian CLDs

Poissonian CLDs were simulated for different kinetic chain lengths ν and translated to chromatographic scaling, namely RI versus $\log_{10}(i)$ (for procedure see Section 7.1.2 on page 154). In this context, CLDs rather than MMDs are used, as the logarithmic nature of i (or M) makes the shape of the resulting distribution independent of M_{mon}. In this context, it should be noted that *negatively* skewed distributions are obtained on an RI-versus-$\log_{10}(M)$ scale (which turn to positively skewed when translated to the V_e dimension). Therefore, similar to Section B.5 on the preceding page, the RI-versus-$\log_{10}(M)$ distributions were flipped horizontally before EMG fits were applied. For $\nu > 700$, Gaussian CLDs were used as good approximations for Poissonian CLDs (cf. Section B.3 on page 237). Best-fit EMG parameters were determined for simulated CLDs for $4 \leq \nu \leq 10\,000$, which are displayed in Figure B.8 together with the found best-fit equations

$$\sigma_{G,Poiss} \cdot b = 0.1532 \cdot \left(1 - \exp\left(-1 \cdot \left(\frac{\nu}{8.7105}\right)^{-0.5108}\right)\right) \tag{B.4}$$

and

$$\tau_{Poiss} \cdot b = 0.3110 \cdot \left(1 - \exp\left(-1 \cdot \left(\frac{\nu}{3.3185}\right)^{-0.7570}\right)\right) . \tag{B.5}$$

APPENDIX C

Abbreviations

Abbreviations and acronyms

[X]	concentration of species X
$[X]_0$	initial concentration of species X
$X^\bullet$	radical of species X
α_{mon}	fractional monomer conversion
a	intercept of the SEC calibration function ($\log_{10}(M)$ versus V_e) or Mark–Houwink parameter
A	(fragment of) ATRP catalyst
a_P	coupling constant of P-centered radical
al.	from *et al.,* et alia (= and others)
ACCN	1,1′-azobis(cyclohexanecarbonitrile)
AIBN	2,2′-azobis(2-methylpropionitrile)
arb.	from *arb. unit,* arbitrary unit
ATRP	atom-transfer radical polymerization
b	negative slope of the SEC calibration function ($\log_{10}(M)$ versus V_e)
B	magnetic field
BA	*n*-butyl acrylate
BB	band broadening

BBF	band-broadening function
BHT	3,5-di-*tert*-butyl-hydroxytoluene
BMA	*n*-butyl methacrylate
Bn	benzyl
C_x	($= k_x/k_p$) reaction constant of reaction x; **ex:** exchange, **tr:** transfer, **tr^{-1}:** transfer back-reaction
cat.	catalyst
CCy	cyanocyclohexyl
CLD	chain-length distribution
cf.	confer
CP	cyanopropyl
CP–I	cyanopropyl iodide
CRP	controlled radical polymerization
CTA	chain-transfer agent
δ	chemical shift in NMR spectroscopy
δ_t	($= k_{td}/k_t$) termination mode
d	doublet
D	diffusion coefficient
$Đ$	($= \overline{M}_w/\overline{M}_n = \overline{DP}_w/\overline{DP}_n$) dispersity
DIB	diiodoethyl benzene
$\overline{DP}_n$	number-average degree of polymerization
$\overline{DP}_n^0$	initial (true) $\overline{DP}_n$ value for simulations
$\overline{DP}_{n,target}$	targeted $\overline{DP}_n$ value for full monomer conversion
$\overline{DP}_w$	weight-average degree of polymerization
DT	degenerative chain-transfer
ϵ	extinction coefficient
e. g.	exempli gratia (= for example)
EMG	exponentially modified Gaussian
EPR	electron paramagnetic resonance
ESI-MS	electrospray ionization mass spectrometry
exp.	experimental
f	initiator efficiency
FD	first deactivation
γ	skewness
G	(fragment of) RTCP catalyst

GC	gas chromatography
GFC	gel-filtration chromatography
GPC	gel-permeation chromatography
η	viscosity
η_{red}	reduced viscosity
$[\eta]$	intrinsic viscosity
h	Planck constant
Hal	halogen
HOMO	highest occupied molecular orbital
HPLC	high-performance liquid chromatography
i	chain length
i. e.	id est (= that is)
In	initiator (fragment)
ini.	initiator
ITP	iodine-transfer polymerization
IUPAC	International Union of Pure and Applied Chemistry
IVB	iodovinyl benzene
K	Mark–Houwink parameter
K_{RT}	constant of RT equilibrium
k_x	reaction-rate coefficient of reaction x; **a:** activation in the RT mechanism, **a,RT:** activation in the reversible chain-transfer mechanism, **act:** pseudo-first-order activation in the reversible-deactivation mechanism, **da:** deactivation in the RT mechanism, **da,RT:** deactivation in the reversible chain-transfer mechanism, **deact:** pseudo-first-order deactivation in the reversible-deactivation mechanism, **dec:** decomposition, **ex:** exchange, **hc:** homolytic C−I-bond cleavage, **ini:** initiation, **iod:** termination with iodine, **p:** propagation, **t:** termination, **tc:** termination via combination, **td:** termination via disproportionation, **tr:** transfer, $\mathbf{tr^{-1}}$: transfer back-reaction
λ	wavelength
LC	liquid chromatography
$\overline{\log_{10}(M)}$	average $\log_{10}(M)$ value of an MMD on chromatographic scaling
$\overline{\log_{10}(M)}^{0}$	average $\log_{10}(M)$ value of a hypothetically unbroadened MMD on chromatographic scaling

LUMO	lowest unoccupied molecular orbital
m	multiplet
m	mass
m_{inj}	injection mass
M	molar mass
M_{peak}	molar mass at the peak position of an MMD
M_{X}	molar mass of species X; **BA:** *n*-butyl acrylate, **BMA:** *n*-butyl methacrylate, **CP–I:** cyanopropyl iodide, **CTA:** chain-transfer agent, **MMA:** methyl methacrylate, **mon:** monomer, **PE–I:** phenylethyl iodide, **St:** styrene
$\overline{M}_{\mathrm{n}}$	number-average molar mass
$\overline{M}_{\mathrm{n,theo}}$	theoretical number-average molar mass
$\overline{M}_{\mathrm{w}}$	weight-average molar mass
MA	methyl acrylate
MALDI	matrix-assisted laser desorption/ionization
MH	Mark–Houwink
MMA	methyl methacrylate
MMD	molar-mass distribution
MMMP	2-methyl-4′-(methylthio)-2-morpholinopropiophenone
mon.	monomer
mon. conv.	monomer conversion
MP	mobile phase
MS	mass spectrometry
ν	kinetic chain length or frequency
N	number
N_{A}	Avogadro number
NIS	*N*-iodosuccinimide
NMP	nitroxide-mediated polymerization
NMR	nuclear magnetic resonance
NS	*N*-succinimidyl (fragment)
PAD	*H*-phosphonic acid derivative
PC	personal computer
PE–I	phenylethyl iodide
PMDTA	*N*,*N*,*N*′,*N*′,*N*″-pentamethyldiethylenetriamine
polyX	polymer of species X
polyX(n)	polymer of species X with a chain length of n

polyX$^{=}$	polymer of species X with an unsaturated end-group
polyX^{H}	polymer of species X with a saturated end-group
PRE	persistent-radical effect
PSD	pore-size distribution
PSS	Polymer Standards Service
q	quartet
(Q)LP	(quasi-)living polymerization
r	correlation coefficient
R	organic moiety or (fragment of) the (re)initiating species
r_x	correction factor for BB effects in SEC; x = **BB,n:** broadening effect on $\overline{M}_n$, **BB,w:** broadening effect on $\overline{M}_w$, **cal:** calibration effect, **tot,n:** broadening and calibration effect on $\overline{M}_n$, **tot,w:** broadening and calibration effect on $\overline{M}_w$
R_f	retention factor
R_x	reaction rate of reaction x; **dec:** decomposition, **p:** propagation, **t:** termination
RAFT	reversible addition–fragmentation chain-transfer
RDRP	reversible-deactivation radical polymerization
rel. int.	relative intensity
RI	intensity of the refractive-index detector
RI^{unbr}	intensity of the refractive-index detector for a hypothetically unbroadened chromatogram
RITP	reverse iodine-transfer polymerization
RP	radical polymerization
RT	reversible termination
RTCP	reversible chain-transfer catalyzed polymerization
σ	standard deviation
σ_{Poiss}	σ of a Poissonian on chromatographic scaling
σ_G	EMG parameter of the Gaussian function
$\sigma_{G,Poiss}$	σ_G parameter of a Poissonian on chromatographic scaling
s	singlet
SDV	styrene–divinylbenzene
SEC	size-exclusion chromatography
simul.	simulated
SP	stationary phase
St	styrene

τ	EMG parameter of the exponential function
τ_{Poiss}	τ parameter of a Poissonian on chromatographic scaling
t_{inh}	inhibtion time
$t_{\text{inh,theo}}$	theoretical inhibition time
T_{col}	column temperature
*t*BuO	*tert*-butoxy (fragment)
TBHDPB	tributylhexadecylphosphonium bromide
TBPO	di-*tert*-butyl peroxide
TEMPO	(2,2,6,6-tetramethyl-piperidin-1-yl)oxyl
TERP	organotellurium-mediated polymerization
TGIC	temperature gradient interaction chromatography
THF	tetrahydrofuran
UV	ultraviolet
UV/vis	ultraviolet/visible
v_{flow}	flow rate
V_{e}	elution volume
$\overline{V_{\text{e}}}$	average V_{e} value of chromatogram
$V_{\text{e,peak}}$	elution volume at the peak position of a chromatogram
$V^0_{\text{e,peak}}$	elution volume at the peak position of a hypothetically unbroadened chromatogram
V_{excl}	total exclusion limit
V_{h}	hydrodynamic volume
V_{inj}	injection volume
V_{perm}	total permeation limit
VAc	vinyl acetate
x	probability
X	capping agent in the context of RDRPs
z	charge

Units

%	percent (10^{-2})
A	ampere
Å	angstrom (10^{-10} m)
°C	Celsius
d	day (86 400 s)

equiv	equivalent
g	gram (10^{-3} kg)
G	gauss ($10^{-4}\,\mathrm{kg\,A^{-1}s^{-2}}$)
h	hour (3600 s)
Hz	hertz ($1\,\mathrm{s^{-1}}$)
L	liter ($10^{-3}\,\mathrm{m^3}$)
m	meter
min	minute (60 s)
mol	mole
ppm	parts per million (10^{-6})
s	second
V	volt ($1\,\mathrm{kg\,m^2\,A^{-1}s^{-3}}$)
W	watt ($1\,\mathrm{kg\,m^2\,s^{-3}}$)

Unit prefixes

c	centi (10^{-2})
G	giga (10^{9})
k	kilo (10^{3})
μ	micro (10^{-6})
m	milli (10^{-3})
M	mega (10^{6})
n	nano (10^{-9})

Bibliography

[1] Staudinger, H.; Fritschi, J. *Helv. Chim. Acta* **1922**, *5*, 785–806.

[2] Tsitsilianis, C. In *Macromolecular engineering: precise synthesis, materials properties, applications*; Matyjaszewski, K., Gnanou, Y., Leibler, L., Eds.; Wiley-VCH, 2007; Vol. 4; pp 839–873.

[3] Matyjaszewski, K., Davis, T. P., Eds. *Handbook of Radical Polymerization*; Wiley-Interscience: Hoboken, New Jersey, 2002.

[4] Buback, M. *Makromol. Chem.* **1990**, *191*, 1575–1587.

[5] Shipp, D. A. *Polym. Rev.* **2011**, *51*, 99–103.

[6] Jenkins, A. D.; Jones, R. G.; Moad, G. *Pure Appl. Chem.* **2010**, *82*, 483–491.

[7] Webster, O. W. *Science* **1991**, *251*, 887–893.

[8] Lacroix-Desmazes, P.; Tonnar, J. In *Polymer Science: A Comprehensive Reference*; Matyjaszewski, K., Müller, M., Eds.; Elsevier: Amsterdam, 2012; pp 159–180.

[9] Wang, J.-S.; Matyjaszewski, K. *J. Am. Chem. Soc.* **1995**, *117*, 5614–5615.

[10] Kato, M.; Kamigaito, M.; Sawamoto, M.; Higashimura, T. *Macromolecules* **1995**, *28*, 1721–1723.

[11] Matyjaszewski, K. *Macromolecules* **2012**, *45*, 4015–4039.

[12] Chiefari, J.; Chong, Y. K.; Ercole, F.; Krstina, J.; Jeffery, J.; Le, T. P. T.; Mayadunne, R. T. A.; Meijs, G. F.; Moad, C. L.; Moad, G.; Rizzardo, E.; Thang, S. H. *Macromolecules* **1998**, *31*, 5559–5562.

[13] Moad, G.; Rizzardo, E.; Thang, S. H. *Aust. J. Chem.* **2012**, *65*, 985–1076.

[14] Percec, V.; Ramirez-Castillo, E.; Hinojosa-Falcon, L. A.; Popov, A. V. *Journal of Polymer Science Part A: Polymer Chemistry* **2005**, *43*, 2185–2187.

[15] Boutevin, B.; David, G.; Boyer, C. In *Oligomers-Polymer Composites-Molecular Imprinting*; Gong, B., Sanford, A. R., Ferguson, J. S., Eds.; Springer, 2007; pp 31–135.

[16] Gaynor, S. G.; Wang, J.-S.; Matyjaszewski, K. *Macromolecules* **1995**, *28*, 8051–8056.

[17] Tatemoto, M.; Shimizu, T. In *Modern Fluoropolymers*; Scheirs, J., Ed.; Wiley: New York, 1997; Chapter 30.

[18] David, G.; Boyer, C.; Tonnar, J.; Ameduri, B.; Lacroix-Desmazes, P.; Boutevin, B. *Chem. Rev.* **2006**, *106*, 3936–3962.

[19] Kowalczuk-Bleja, A.; Sierocka, B.; Muszyński, J.; Trzebicka, B.; Dworak, A. *Polymer* **2005**, *46*, 8555–8564.

[20] Terayama, Y.; Kobayashi, M.; Takahara, A. *Chem. Lett.* **2007**, *36*, 1280–1281.

[21] Jo, S.-M.; Lee, W.-S.; Ahn, B.-S.; Park, K.-Y.; Kim, K.-A.; Paeng, I.-S. R. *Polym. Bull.* **2000**, *44*, 1–8.

[22] Stenzel-Rosenbaum, M. H.; Davis, T. P.; Fane, A. G.; Chen, V. *Angew. Chem.* **2001**, *113*, 3536–3540.

[23] Teodorescu, M. *Eur. Polym. J.* **2001**, *37*, 1417–1422.

[24] Lacroix-Desmazes, P.; Severac, R.; Boutevin, B. *Macromolecules* **2005**, *38*, 6299–6309.

[25] Boyer, C.; Lacroix-Desmazes, P.; Robin, J.-J.; Boutevin, B. *Macromolecules* **2006**, *39*, 4044–4053.

[26] Goto, A.; Zushi, H.; Hirai, N.; Wakada, T.; Tsujii, Y.; Fukuda, T. *J. Am. Chem. Soc.* **2007**, *129*, 13347–13354.

[27] Goto, A.; Tsujii, Y.; Fukuda, T. *Polymer* **2008**, *49*, 5177–5185.

[28] Goto, A.; Nagasawa, K.; Shinjo, A.; Tsujii, Y.; Fukuda, T. *Aust. J. Chem.* **2009**, *62*, 1492–1495.

[29] Goto, A.; Hirai, N.; Nagasawa, K.; Tsujii, Y.; Fukuda, T.; Kaji, H. *Macromolecules* **2010**, *43*, 7971–7978.

[30] Fouassier, J.-P. *Photoinitiated Polymerisation: Theory and Applications*; Rapra Technology Ltd.: Shawbury, Shrewsbury, U.K., 1998.

[31] Yagci, Y.; Jockusch, S.; Turro, N. J. *Macromolecules* **2010**, *43*, 6245–6260.

[32] Tehfe, M. A.; Louradour, F.; Lalevée, J.; Fouassier, J.-P. *Appl. Sci.* **2013**, *3*, 490–514.

[33] Tasdelen, M. A.; Çiftci, M.; Uygun, M.; Yagci, Y. In *Progress in Controlled Radical Polymerization: Mechanisms and Techniques*; Matyjaszewski, K., Sumerlin, B. S., Tsarevsky, N. V., Eds.; American Chemical Society: Washington, DC, 2012; pp 59–72.

[34] Yamago, S.; Nakamura, Y. *Polymer* **2013**, *54*, 981–994.

[35] Otsu, T.; Yoshida, M. *Makromol. Chem., Rapid Commun.* **1982**, *3*, 127–132.

[36] Otsu, T.; Yoshida, M.; Tazaki, T. *Makromol. Chem., Rapid Commun.* **1982**, *3*, 133–140.

[37] Kwak, Y.; Matyjaszewski, K. *Macromolecules* **2010**, *43*, 5180–5183.

[38] Fors, B. P.; Hawker, C. J. *Angew. Chem., Int. Ed.* **2012**, *51*, 8850–8853.

[39] Zhang, H.; Deng, J.; Lu, L.; Cai, Y. *Macromolecules* **2007**, *40*, 9252–9261.

[40] Ran, R.; Yu, Y.; Wan, T. *J. Appl. Polym. Sci.* **2007**, *105*, 398–404.

[41] Koumura, K.; Satoh, K.; Kamigaito, M. *Macromolecules* **2008**, *41*, 7359–7367.

[42] Tonnar, J.; Pouget, E.; Lacroix-Desmazes, P.; Boutevin, B. *Macromol. Symp.* **2009**, *281*, 20–30.

[43] Ohtsuki, A.; Goto, A.; Kaji, H. *Macromolecules* **2013**, *46*, 96–102.

[44] Lathe, G. H.; Ruthven, C. R. *Biochem. J.* **1956**, *62*, 665–674.

[45] Ettre, L. S. *LC GC N. Am.* **2005**, *23*, 752–761.

[46] Moore, J. C. *J. Polym. Sci. General Papers* **1964**, *2*, 835–843.

[47] Meira, G. R.; Netopilík, M.; Potschka, M.; Schnöll-Bitai, I.; Vega, J. *Macromol. Symp.* **2007**, *258*, 186–197.

[48] Striegel, A. M.; Yau, W. W.; Kirkland, J. J.; Bly, D. D. *Modern Size-Exclusion Liquid Chromatography: Practice of Gel Permeation and Gel Filtration Chromatography*, 2nd ed.; John Wiley & Sons, Inc.: Hoboken, NJ, 2009.

[49] Goto, A.; Fukuda, T. *Prog. Polym. Sci.* **2004**, *29*, 329–385.

[50] Braunecker, W. A.; Matyjaszewski, K. *Prog. Polym. Sci.* **2007**, *32*, 93–146.

[51] Nicolas, J.; Guillaneuf, Y.; Lefay, C.; Bertin, D.; Gigmes, D.; Charleux, B. *Prog. Polym. Sci.* **2013**, *38*, 63–235.

[52] Georges, M. K.; Veregin, R. P. N.; Kazmaier, P. M.; Hamer, G. K. *Macromolecules* **1993**, *26*, 2987–2988.

[53] Fischer, H. *Chem. Rev.* **2001**, *101*, 3581–3610.

[54] Matyjaszewski, K.; Gaynor, S.; Greszta, D.; Mardare, D.; Shigemoto, T. *J. Phys. Org. Chem.* **1995**, *8*, 306–315.

[55] Laidler, K. J. *Pure Appl. Chem.* **1996**, *68*, 149–192.

[56] Jenkins, A. D.; Kratochvil, P.; Stepto, R. F. T.; Suter, U. W. *Pure Appl. Chem.* **1996**, *68*, 2287–2311.

[57] Flory, P. J. *Principles of polymer chemistry*; Cornell University Press: Ithaca, NY, 1953.

[58] Matyjaszewski, K.; Gaynor, S.; Wang, J.-S. *Macromolecules* **1995**, *28*, 2093–2095.

[59] Goto, A.; Ohno, K.; Fukuda, T. *Macromolecules* **1998**, *31*, 2809–2814.

[60] Starks, C. M. *Free Radical Telomerization*; Academic Press Inc.: New York, NY, 1974.

[61] Blanksby, S. J.; Ellison, G. B. *Accounts Chem. Res.* **2003**, *36*, 255–263.

[62] Lonsdale, D. E.; Johnston-Hall, G.; Fawcett, A.; Bell, C. A.; Urbani, C. N.; Whittaker, M. R.; Monteiro, M. J. *J. Polym. Sci. Polym. Chem.* **2007**, *45*, 3620–3625.

[63] Ford, M.; Water, W. A. *J. Chem. Soc. Abstr.* **1951**, 1851–1855.

[64] Boutevin, B.; Piétrasanta, Y.; Bauduin, G. *Makromol. Chem.* **1985**, *186*, 283–295.

[65] Müller, A. H. E.; Zhuang, R.; Yan, D.; Litvinenko, G. *Macromolecules* **1995**, *28*, 4326–4333.

[66] O'Brien, J. L.; Gornick, F. *J. Am. Chem. Soc.* **1955**, *77*, 4757–4763.

[67] Mayo, F. R. *J. Am. Chem. Soc.* **1943**, *65*, 2324–2329.

[68] Moad, G.; Barner-Kowollik, C. In *Handbook of RAFT polymerization*; Barner-Kowollik, C., Ed.; John Wiley & Sons, 2008.

[69] Lansalot, M.; Farcet, C.; Charleux, B.; Vairon, J.-P.; Pirri, R. *Macromolecules* **1999**, *32*, 7354–7360.

[70] Buback, M.; Egorov, M.; Gilbert, R. G.; Kaminsky, V.; Olaj, O. F.; Russell, G. T.; Vana, P.; Zifferer, G. *Macromol. Chem. Phys.* **2002**, *203*, 2570–2582.

[71] Barner-Kowollik, C.; Buback, M.; Egorov, M.; Fukuda, T.; Goto, A.; Olaj, O. F.; Russell, G. T.; Vana, P.; Yamada, B.; Zetterlund, P. B. *Prog. Polym. Sci.* **2005**, *30*, 605–643.

[72] Müller, A. H. E.; Yan, D.; Litvinenko, G.; Zhuang, R.; Dong, H. *Macromolecules* **1995**, *28*, 7335–7338.

[73] Goto, A.; Fukuda, T. *Macromolecules* **1997**, *30*, 4272–4277.

[74] Müller, A. H. E.; Litvinenko, G.; Yan, D. *Macromolecules* **1996**, *29*, 2346–2353.

[75] Fukuda, T.; Terauchi, T.; Goto, A.; Ohno, K.; Tsujii, Y.; Miyamoto, T.; Kobatake, S.; Yamada, B. *Macromolecules* **1996**, *29*, 6393–6398.

[76] Sato, E.; Hagihara, T.; Matsumoto, A. *ACS Appl. Mater. Interfaces* **2012**, *4*, 2057–2064.

[77] Kuroda, T.; Tanaka, A.; Taniyama, T.; Minami, H.; Goto, A.; Fukuda, T.; Okubo, M. *Polymer* **2012**, *53*, 1212–1218.

[78] Taniyama, T.; Kuroda, T.; Minami, H.; Okubo, M. *Polym. J.* **2012**, *44*, 1082–1086.

[79] Yorizane, M.; Nagasuga, T.; Kitayama, Y.; Tanaka, A.; Minami, H.; Goto, A.; Fukuda, T.; Okubo, M. *Macromolecules* **2010**, *43*, 8703–8705.

[80] Kitayama, Y.; Yorizane, M.; Minami, H.; Okubo, M. *Polym. Chem.* **2012**, *3*, 1394–1398.

[81] Kitayama, Y.; Yorizane, M.; Minami, H.; Okubo, M. *Macromolecules* **2012**, *45*, 2286–2291.

[82] Goto, A.; Hirai, N.; Wakada, T.; Nagasawa, K.; Tsujii, Y.; Fukuda, T. *Macromolecules* **2008**, *41*, 6261–6264.

[83] Wolpers, A.; Ackermann, L.; Vana, P. *Macromol. Chem. Phys.* **2011**, *212*, 259–265.

[84] Bai, L.; Zhang, L.; Liu, Y.; Pan, X.; Cheng, Z.; Zhu, X. *Polym. Chem.* **2013**, *4*, 3069–3076.

[85] Goto, A.; Wakada, T.; Fukuda, T.; Tsujii, Y. *Macromol. Chem. Phys.* **2010**, *211*, 594–600.

[86] Vana, P.; Goto, A. *Macromol. Theory Simul.* **2010**, *19*, 24–35.

[87] Kwak, Y.; Goto, A.; Fukuda, T. *Macromolecules* **2004**, *37*, 1219–1225.

[88] Farcet, C.; Lansalot, M.; Pirri, R.; Vairon, J. P.; Charleux, B. *Macromol. Rapid Commun.* **2000**, *21*, 921–926.

[89] Iovu, M. C.; Matyjaszewski, K. *Macromolecules* **2003**, *36*, 9346–9354.

[90] Tonnar, J.; Lacroix-Desmazes, P. *ACS Symp. Ser.* **2009**, *1024*, 65–79.

[91] Shin, H. C.; Oh, H. G.; Lee, K.; Lee, B. H.; Choe, S. *Polymer* **2009**, *50*, 4299–4307.

[92] Tonnar, J.; Severac, R.; Lacroix-Desmazes, P.; Boutevin, B. *Polym. Prepr. (Am. Chem. Soc., Div. Polym. Chem.)* **2008**, *49*, 68.

[93] Wright, T.; Chirowodza, H.; Pasch, H. *Macromolecules* **2012**, *45*, 2995–3003.

[94] Charles, L. *Mass Spectrom. Rev.* **2013**, 1–21.

[95] Barner-Kowollik, C.; Davis, T. P.; Stenzel, M. H. *Polymer* **2004**, *45*, 7791–7805.

[96] Ladavière, C.; Lacroix-Desmazes, P.; Delolme, F. *Macromolecules* **2009**, *42*, 70–84.

[97] Buback, M.; Frauendorf, H.; Günzler, F.; Vana, P. *Polymer* **2007**, *48*, 5590–5598.

[98] Buback, M.; Günzler, F.; Russell, G. T.; Vana, P. *Macromolecules* **2009**, *42*, 652–662.

[99] Buback, M.; Frauendorf, H.; Günzler, F.; Huff, F.; Vana, P. *Macromol. Chem. Phys.* **2009**, *210*, 1591–1599.

[100] Bartlett, P. D.; Kwart, H. *J. Am. Chem. Soc.* **1950**, *72*, 1051–1059.

[101] Lissi, E. A.; Aljaro, J. *J. Polym. Sci. Polym. Lett.* **1976**, *14*, 499–502.

[102] Rosman, H.; Noyes, R. M. *J. Am. Chem. Soc.* **1958**, *80*, 2410–2415.

[103] Foldiak, G.; Schuler, R. H. *J. Phys. Chem.* **1978**, *82*, 2756–2757.

[104] LaVerne, J. A.; Wojnarovits, L. *J. Phys. Chem.* **1994**, *98*, 12635–12640.

[105] Denisov, E. T.; Denisova, T. G.; Pokidova, T. S. *Handbook of Free Radical Initiators*; John Wiley & Sons, Inc.: Hoboken, NJ, 2003.

[106] AKZO Nobel Chemicals, *Initiators for High Polymers*; 2006.

[107] Stickler, M. *Makromol. Chem.* **1986**, *187*, 1765–1775.

[108] McCombie, H.; Saunders, B. C.; Stacey, G. J. *J. Am. Chem. Soc.* **1945**, 921–922.

[109] Timperley, C. M.; Waters, M. J. *Chem. Commun.* **2001**, 797–798.

[110] Nikitin, A. N.; Hutchinson, R. A.; Hesse, P. *Macromol. Chem. Phys.* **2013**, *214*, 2670–2682.

[111] Audi, G.; Bersillon, O.; Blachot, J.; Wapstra, A. H. *Nucl. Phys. A* **2003**, *729*, 3–128.

[112] Coca, S.; Jasieczek, C. B.; Beers, K. L.; Matyjaszewski, K. *J. Polym. Sci., Part A: Polym. Chem.* **1998**, *36*, 1417–1424.

[113] Borman, C. D.; Jackson, A. T.; Bunn, A.; Cutter, A. L.; Irvine, D. J. *Polymer* **2000**, *41*, 6015–6020.

[114] Nonaka, H.; Ouchi, M.; Kamigaito, M.; Sawamoto, M. *Macromolecules* **2001**, *34*, 2083–2088.

[115] Jackson, A. T.; Bunn, A.; Priestnall, I. M.; Borman, C. D.; Irvine, D. J. *Polymer* **2006**, *47*, 1044–1054.

[116] Chiantore, O.; Trossarelli, L.; Lazzari, M. *Polymer* **2000**, *41*, 1657–1668.

[117] Dohi, T.; Takenaga, N.; Goto, A.; Maruyama, A.; Kita, Y. *Org. Lett.* **2007**, *9*, 3129–3132.

[118] Mielniczak, G.; Łopusiński, A. *Synthetic Commun.* **2003**, *33*, 3851–3859.

[119] Nguyen, D. H.; Vana, P. *Aust. J. Chem.* **2006**, *59*, 549–559.

[120] Beuermann, S.; Buback, M.; Davis, T. P.; Gilbert, R. G.; Hutchinson, R. A.; Olaj, O. F.; Russell, G. T.; Schweer, J.; van Herk, A. M. *Macromol. Chem. Phys.* **1997**, *198*, 1545–1560.

[121] Günzler, K. F. *Ph. D. thesis: Kinetische Analyse radikalischer Polymerisationen durch Endgruppenbestimmung mit Hilfe der ESI-Massenspektrometrie*; Sierke Verlag: Göttingen, Germany, 2008.

[122] Barner-Kowollik, C.; Beuermann, S.; Buback, M.; Castignolles, P.; Charleux, B.; Coote, M. L.; Hutchinson, R. A.; Junkers, T.; Lacík, I.; Russell, G. T.; Stach, M.; van Herk, A. M. *Polym. Chem.* **2014**, *5*, 204–212.

[123] Guillaneuf, Y.; Bertin, D.; Gigmes, D.; Versace, D.-L.; Lalevée, J.; Fouassier, J.-P. *Macromolecules* **2010**, *43*, 2204–2212.

[124] Tasdelen, M. A.; Çiftci, M.; Yagci, Y. *Macromol. Chem. Phys.* **2012**, *213*, 1391–1396.

[125] Yamago, S.; Ukai, Y.; Matsumoto, A.; Nakamura, Y. *J. Am. Chem. Soc.* **2009**, *131*, 2100–2101.

[126] Nakamura, Y.; Yamago, S. *Beilstein J. Org. Chem.* **2013**, *9*, 1607–1612.

[127] Koumura, K.; Satoh, K.; Kamigaito, M. *Macromolecules* **2009**, *42*, 2497–2504.

[128] Koumura, K.; Satoh, K.; Kamigaito, M. *J. Polym. Sci. Polym. Chem.* **2009**, *47*, 1343–1353.

[129] Asandei, A. D.; Adebolu, O. I.; Simpson, C. P. *J. Am. Chem. Soc.* **2012**, *134*, 6080–6083.

[130] Ishibashi, H.; Haruki, S.; Uchiyama, M.; Tamura, O.; Matsuo, J.-i. *Tetrahedron Lett.* **2006**, *47*, 6263–6266.

[131] Sakota, N.; Nagasaki, T.; Sakai, S. *Polym. J.* **1971**, *2*, 192–198.

[132] Yada, H.; Tanaka, J.; Nagakura, S. *Bull. Chem. Soc. Jpn.* **1960**, *33*, 1660–1667.

[133] Goto, A.; Suzuki, T.; Ohfuji, H.; Tanishima, M.; Fukuda, T.; Tsujii, Y.; Kaji, H. *Macromolecules* **2011**, *44*, 8709–8715.

[134] Fox, R. B.; Isaacs, L. G.; Stokes, S. *J. Polym. Sci. General Papers* **1963**, *1*, 1079–1086.

[135] Fox, R. B.; Isaacs, L.; Stokes, S.; Kagarise, R. E. *J. Polym. Sci. General Papers* **1964**, *2*, 2085–2092.

[136] Torikai, A.; Ohno, M.; Fueki, K. *J. Appl. Polym. Sci.* **1990**, *41*, 1023–1032.

[137] Torikai, A.; Kato, H.; Fueki, K.; Suzuki, Y.; Okisaki, F.; Nagata, M. *J. Appl. Polym. Sci.* **1993**, *50*, 2185–2190.

[138] Greenwood, N. N.; Earnshaw, A. *Chemistry of the Elements*; Reed Educational and Professional Publishing Ltd: Woburn, MA, 1997.

[139] Miessler, G. L.; Tarr, D. A. *Inorganic Chemistry*; Prentice Hall: Upper Saddle River, NJ, 2003.

[140] Buback, M.; Kuelpmann, A. *Macromol. Chem. Phys.* **2003**, *204*, 632–637.

[141] Barth, J.; Buback, M.; Hesse, P.; Sergeeva, T. *Macromolecules* **2009**, *42*, 481–488.

[142] Barth, J.; Buback, M.; Russell, G. T.; Smolne, S. *Macromol. Chem. Phys.* **2011**, *212*, 1366–1378.

[143] Schug, J. C.; Kogan, M. J. *J. Magn. Reson.* **1973**, *11*, 406–415.

[144] Guliashvili, T.; Percec, V. *J. Polym. Sci. Polym. Chem.* **2007**, *45*, 1607–1618.

[145] Bannister, E.; Fowles, G. W. A. *J. Chem. Soc.* **1959**, 310–315.

[146] Sumarokova, T. N.; Sakenova, D. S.; Usanovich, M. I. *J. Struct. Chem.* **1966**, *7*, 365–371.

[147] Bałczewski, P.; Mikołajczyk, M. *New J. Chem.* **2001**, *25*, 659–663.

[148] Brunton, G.; Ingold, K. U. *Org. Magn. Reson.* **1975**, *7*, 527–528.

[149] Anpo, M.; Sutcliffe, R.; Ingold, K. U. *J. Am. Chem. Soc.* **1983**, *105*, 3580–3583.

[150] Davies, A. G.; Griller, D.; Roberts, B. P. *J. Am. Chem. Soc.* **1972**, *94*, 1782–1783.

[151] Deuflhard, P.; Wulkow, M. *IMPACT Comput. Sci. Eng.* **1989**, *1*, 269–301.

[152] Wulkow, M. *IMPACT Comput. Sci. Eng.* **1992**, *4*, 153–193.

[153] Wulkow, M. *Macromol. Theory Simul.* **1996**, *5*, 393–416.

[154] Nikitin, A. N.; Hutchinson, R. A.; Buback, M.; Hesse, P. *Macromolecules* **2007**, *40*, 8631–8641.

[155] Gridnev, A. A.; Ittel, S. D. *Macromolecules* **1996**, *29*, 5864–5874.

[156] Fischer, H.; Radom, L. *Angew. Chem., Int. Ed.* **2001**, *40*, 1340–1371.

[157] Asua, J. M.; Beuermann, S.; Buback, M.; Castignolles, P.; Charleux, B.; Gilbert, R. G.; Hutchinson, R. A.; Leiza, J. R.; Nikitin, A. N.; Vairon, J.-P.; van Herk, A. M. *Macromol. Chem. Phys.* **2004**, *205*, 2151–2160.

[158] Barth, J.; Buback, M.; Hesse, P.; Sergeeva, T. *Macromolecules* **2010**, *43*, 4023–4031.

[159] Smith, G. B.; Russell, G. T.; Heuts, J. P. A. *Macromol. Theory Simul.* **2003**, *12*, 299–314.

[160] Tonnar, J.; Severac, R.; Lacroix-Desmazes, P.; Boutevin, B. *Polym. Prepr. (Am. Chem. Soc., Div. Polym. Chem.)* **2008**, *49*, 187–188.

[161] Chen, M.; Moad, G.; Rizzardo, E. *J. Polym. Sci. Polym. Chem.* **2009**, *47*, 6704–6714.

[162] Dietrich, M.; Glassner, M.; Gruendling, T.; Schmid, C.; Falkenhagen, J.; Barner-Kowollik, C. *Polym. Chem.* **2010**, *1*, 634–644.

[163] Goto, A.; Kwak, Y.; Fukuda, T.; Yamago, S.; Iida, K.; Nakajima, M.; Yoshida, J.-i. *J. Am. Chem. Soc.* **2003**, *125*, 8720–8721.

[164] Yamago, S. *Chem. Rev.* **2009**, *109*, 5051–5068.

[165] Kwak, Y.; Goto, A.; Fukuda, T.; Kobayashi, Y.; Yamago, S. *Macromolecules* **2006**, *39*, 4671–4679.

[166] Grant, M. I. *Trans. Faraday Soc.* **1935**, *31*, 433–440.

[167] Bell, T. N.; Boonstra, M.; Dobud, P. A. *J. Am. Chem. Soc.* **1970**, *92*, 4521–4524.

[168] Greszta, D.; Matyjaszewski, K. *J. Polym. Sci. Polym. Chem.* **1997**, *35*, 1857–1861.

[169] Beuermann, S.; Buback, M.; Davis, T. P.; Gilbert, R. G.; Hutchinson, R. A.; Kajiwara, A.; Klumperman, B.; Russell, G. T. *Macromol. Chem. Phys.* **2000**, *201*, 1355–1364.

[170] Lecamp, L.; Youssef, B.; Bunel, C.; Lebaudy, P. *Polymer* **1997**, *38*, 6089–6096.

[171] Chong, B. Y. K.; Krstina, J.; Le, T. P. T.; Moad, G.; Postma, A.; Rizzardo, E.; Thang, S. H. *Macromolecules* **2003**, *36*, 2256–2272.

[172] Buback, M.; Gilbert, R. G.; Hutchinson, R. A.; Klumperman, B.; Kuchta, F.-D.; Manders, B. G.; O'Driscoll, K. F.; Russell, G. T.; Schweer, J. *Macromol. Chem. Phys.* **1995**, *196*, 3267–3280.

[173] Kattner, H.; Buback, M. *Macromolecules* **2015**, *48*, 309–315.

[174] Trifan, D. S.; Bartlett, P. D. *J. Am. Chem. Soc.* **1959**, *81*, 5573–5581.

[175] Fraenkel, G.; Bartlett, P. D. *J. Am. Chem. Soc.* **1959**, *81*, 5582–5590.

[176] Maschio, G.; Cerrai, P.; Giusti, P. *Polym. Bull.* **1982**, *8*, 147–153.

[177] Van Eldik, R.; Asano, T.; Le Noble, W. J. *Chem. Rev.* **1989**, *89*, 549–688.

[178] Kubisa, P. *Prog. Polym. Sci.* **2004**, *29*, 3–12.

[179] Lathe, G. H.; Ruthven, C. R. *Biochem. J.* **1955**, *60*, xxxiv.

[180] Porath, J.; Flodin, P. *Nature* **1959**, *183*, 1657–1659.

[181] Vaughan, M. F. *Nature* **1960**, *188*, 55–55.

[182] Cortis-Jones, B. *Nature* **1961**, *191*, 272–273.

[183] Lloyd, W. G.; Alfrey, T. Division of Polymer Chemistry. 139th ACS Meeting, St. Louis, MO. 1961.

[184] Alfrey, T.; Lloyd, W. G. *J. Polym. Sci.* **1962**, *62*, 159–165.

[185] Lloyd, W. G.; Alfrey, T. *J. Polym. Sci.* **1962**, *62*, 301–316.

[186] Moore, J. C. U. S. Patent 3 326 875. filed 1963.

[187] Kellner, R., Mermet, J.-M., Otto, M., Valcárcel, M., Widmer, H. M., Eds. *Analytical Chemistry*, 2nd ed.; Wiley-VCH: Weinheim, Germany, 2004.

[188] Meira, G. R.; Vega, J.; Yossen, M. In *Ewing's Analytical Instrumentation Handbook*, 3rd ed.; Cazes, J., Ed.; Marcel Dekker: New York, NY, 2005; pp 827–869.

[189] Striegel, A. M. *Anal. Chem.* **2005**, *77*, 104 A–113 A.

[190] Guttman, C. M.; DiMarzio, E. A. *Macromolecules* **1970**, *3*, 681–691.

[191] van Kreveld, M. E.; van den Hoed, N. *J. Chromatogr. A* **1978**, *149*, 71–91.

[192] Berek, D. In *Column Handbook for Size Exclusion Chromatography*; Wu, C.-s., Ed.; Academic Press: New York, NY, 1999; pp 445–457.

[193] Flory, P. F. *J. Chem. Phys.* **1945**, *13*, 453.

[194] Grubisic, Z.; Rempp, P.; Benoit, H. *J. Polym. Sci. Polym. Lett.* **1967**, *5*, 753–759.

[195] Houwink, R. *J. Prakt. Chem.* **1940**, *157*, 15–18.

[196] Kurata, M.; Tsunashima, Y. In *Polymer Handbook*, 4th ed.; Brandup, J., Immergut, E. H., Grulke, E. A., Eds.; Wiley-Interscience: New York, NY, 1999.

[197] Wyatt, P. J. *Anal. Chim. Acta* **1993**, *272*, 1–40.

[198] Reed, W. F. *Macromol. Chem. Phys.* **1995**, *196*, 1539–1575.

[199] Baumgarten, J. L.; Busnel, J.-P.; Meira, G. R. *J. Liq. Chrom. R. T.* **2002**, *25*, 1967–2001.

[200] Kornherr, A.; Olaj, O. F.; Schnöll-Bitai, I.; Zifferer, G. *Macromol. Theory Simul.* **2004**, *13*, 560–569.

[201] van Berkel, K. Y.; Russell, G. T.; Gilbert, R. G. *Macromolecules* **2005**, *38*, 3214–3224.

[202] Uliyanchenko, E.; Schoenmakers, P. J.; Van der Wal, S. *J. Chromatogr. A* **2011**, *1218*, 1509–1518.

[203] Lee, W.; Lee, H.; Cha, J.; Chang, T.; Hanley, K. J.; Lodge, T. P. *Macromolecules* **2000**, *33*, 5111–5115.

[204] Busnel, J. P.; Foucault, F.; Denis, L.; Lee, W.; Chang, T. *J. Chromatogr. A* **2001**, *930*, 61–71.

[205] Saito, T.; Lusenkova, M. A.; Matsuyama, S.; Shimada, K.; Itakura, M.; Kishine, K.; Sato, K.; Kinugasa, S. *Polymer* **2004**, *45*, 8355–8365.

[206] van Herk, A. M. *Macromol. Symp.* **2009**, *275*, 120–132.

[207] Schnöll-Bitai, I. *Chromatographia* **2003**, *58*, 375–380.

[208] Schnöll-Bitai, I.; Hrebicek, T.; Rizzi, A. *Macromol. Chem. Phys.* **2007**, *208*, 485–495.

[209] Montaudo, G.; Samperi, F.; Montaudo, M. S. *Prog. Polym. Sci.* **2006**, *31*, 277–357.

[210] Vega, J. R.; Schnöll-Bitai, I. *J. Chromatogr. A* **2005**, *1095*, 102–112.

[211] Schnöll-Bitai, I.; Vega, J.; Mader, C. *Anal. Chim. Acta* **2007**, *604*, 9–17.

[212] Yossen, M. M.; Vega, J. R.; Meira, G. R. *J. Chromatogr. A* **2006**, *1128*, 171–180.

[213] Yossen, M. M.; Vega, J. R.; Chang, T.; Meira, G. R. *J. Liq. Chromatogr. R. T.* **2012**, *35*, 79–94.

[214] Tung, L. H.; Runyon, J. R. *J. Appl. Polym. Sci.* **1969**, *13*, 2397–2409.

[215] Grubisic-Gallot, Z.; Marais, L.; Benoit, H. *J. Polym. Sci. Polym. Phys.* **1976**, *14*, 959–961.

[216] Giddings, J. C.; Eyring, H. *J. Phys. Chem.* **1955**, *59*, 416–421.

[217] Giddings, J. C. In *Dynamics of Chromatography*; Giddings, J. C., Keller, R. A., Eds.; Marcel Dekker: New York, NY, 1965.

[218] van Deemter, J. J.; Zuiderweg, F. J.; Klinkenberg, A. *Chem. Eng. Sci.* **1956**, *5*, 271–289.

[219] Schnöll-Bitai, I. *J. Chromatogr. A* **2005**, *1084*, 160–166.

[220] Striegel, A. M. *J. Chromatogr. A* **2001**, *932*, 21–31.

[221] Einstein, A. *Ann. Phys.* **1905**, *17*, 549–560.

[222] Yau, W. W.; Malone, C. P.; Suchan, H. L. *Sep. Sci.* **1970**, *5*, 259–271.

[223] Ouano, A. C.; Barker, J. A. *Sep. Sci.* **1973**, *8*, 673–699.

[224] Dondi, F.; Cavazzini, A.; Remelli, M.; Felinger, A.; Martin, M. *J. Chromatogr. A* **2002**, *943*, 185–207.

[225] Pasti, L.; Dondi, F.; van Hulst, M.; Schoenmakers, P. J.; Martin, M.; Felinger, A. *Chromatographia* **2003**, *57*, S171–S186.

[226] Felinger, A.; Pasti, L.; Dondi, F.; van Hulst, M.; Schoenmakers, P. J.; Martin, M. *Anal. Chem.* **2005**, *77*, 3138–3148.

[227] Sepsey, A.; Bacskay, I.; Felinger, A. *J. Chromatogr. A* **2014**, *1331*, 52–60.

[228] Grushka, E. *Anal. Chem.* **1972**, *44*, 1733–1738.

[229] Yau, W. W. *Anal. Chem.* **1977**, *49*, 395–398.

[230] Berek, D. *J. Sep. Sci.* **2010**, *33*, 315–335.

[231] Netopilík, M. *J. Chromatogr. A* **2006**, *1133*, 95–103.

[232] Schnöll-Bitai, I.; Mader, C. *J. Chromatogr. A* **2006**, *1137*, 198–206.

[233] Chiantore, O.; Guaita, M. *J. Liq. Chromatogr.* **1982**, *5*, 643–667.

[234] Potschka, M. *J. Chromatogr. A* **1993**, *648*, 41–69.

[235] Kirkland, J. J.; Yau, W. W.; Stoklosa, H. J.; Dilks, C. H. *J. Chromatogr. Sci.* **1977**, *15*, 303–316.

[236] Potschka, M. *Macromolecules* **1991**, *24*, 5023–5039.

[237] Liu, Y.; Radke, W.; Pasch, H. *Macromolecules* **2005**, *38*, 7476–7484.

[238] Liu, Y.; Radke, W.; Pasch, H. *Macromolecules* **2006**, *39*, 2004–2006.

[239] Striegel, A. M. *J. Liq. Chromatogr. R. T.* **2008**, *31*, 3105–3114.

[240] Simeková, M.; Berek, D. *J. Chromatogr. A* **2005**, *1084*, 167–172.

[241] Curtis, L. J. *Am. J. Phys.* **1975**, *43*, 1101–1103.

[242] Hutchinson, R. A.; Aronson, M. T.; Richards, J. R. *Macromolecules* **1993**, *26*, 6410–6415.

[243] Tung, L. H. *J. Appl. Polym. Sci.* **1966**, *10*, 1271–1283.

[244] Fylstra, D.; Lasdon, L.; Watson, J.; Waren, A. *Interfaces* **1998**, *28 (5)*, 29–55.

[245] Prüß, A.; Kempter, C.; Gysler, J.; Jira, T. *J. Chromatogr. A* **2003**, *1016*, 129–141.

[246] Norton, T. T.; Fernandez, E. J. *Ind. Eng. Chem. Res.* **1996**, *35*, 2460–2468.

[247] Bleha, T.; Bakoš, D.; Berek, D. *Polymer* **1977**, *18*, 897–904.

[248] Bruessau, R. J. *Macromol. Symp.* **1996**, *110*, 15–32.

[249] Hawkins, W. L. In *Polymer Degradation and Stabilization*; Harwood, H. J., Ed.; Springer: Berlin, Germany, 1984.

[250] Little, J. N.; Waters, J. L.; Bombaugh, K. J.; Pauplis, W. J. *J. Polym. Sci. Polym. Phys.* **1969**, *7*, 1775–1783.

[251] Aubert, J. H.; Tirrell, M. *Sep. Sci. Technol.* **1980**, *15*, 123–130.

[252] Brewer, A. K.; Striegel, A. M. *Anal. Bioanal. Chem.* **2009**, *393*, 295–302.

[253] Ahmad, N.; Bhettani, A. K.; Rashad, A. *J. Chem. Soc. Pak.* **1990**, *12*, 62–66.

[254] Boone, M. A.; Nymeyer, H.; Striegel, A. M. *Carbohyd. Res.* **2008**, *343*, 132–138.

[255] Borchard, W. *Europ. Polym. J.* **1978**, *14*, 661–664.

[256] Di Marco, V. B.; Bombi, G. G. *J. Chromatogr. A* **2001**, *931*, 1–30.

[257] Foley, J. P.; Dorsey, J. G. *Anal. Chem.* **1983**, *55*, 730–737.

[258] Buback, M.; Busch, M.; Lämmel, R. A. *Macromol. Theory Simul.* **1996**, *5*, 845–861.

[259] Konkolewicz, D.; Taylor II, J. W.; Castignolles, P.; Gray-Weale, A.; Gilbert, R. G. *Macromolecules* **2007**, *40*, 3477–3487.

[260] Hamielec, A. E.; Ray, W. H. *J. Appl. Polym. Sci.* **1969**, *13*, 1319–1321.

[261] Hamielec, A. E. *J. Appl. Polym. Sci.* **1970**, *14*, 1519–1529.

[262] Moad, G.; Moad, C. L. *Macromolecules* **1996**, *29*, 7727–7733.

[263] Held, D.; Kilz, P. In *Quantification in LC and GC: A Practical Guide to Good Chromatographic Data*; Kuss, H.-J., Kromidas, S., Eds.; Wiley-VCH: Weinheim, Germany, 2009.

[264] Yau, W. W.; Stoklosa, H. J.; Ginnard, C. R.; Bly, D. D. 12th Middle Atlantic Regional Meeting, American Chemical Society. 1978.

[265] Kalambet, Y.; Kozmin, Y.; Mikhailova, K.; Nagaev, I.; Tikhonov, P. *J. Chemometr.* **2011**, *25*, 352–356.

[266] Lutz, J.-F.; Lacroix-Desmazes, P.; Boutevin, B. *Macromol. Rapid Comm.* **2001**, *22*, 189–193.

[267] Ritter, A.; Schmid, M.; Affolter, S. *Polym. Test.* **2010**, *29*, 945–952.

[268] Mori, S. *Int. J. Polym. Anal. Ch.* **1998**, *4*, 531–546.

[269] Munoz, A.; Hubert, C.; Luche, J.-L. *J. Org. Chem.* **1996**, *61*, 6015–6017.

[270] Ackermann, L.; Althammer, A. *Org. Lett.* **2006**, *8*, 3457–3460.

[271] Hutchinson, R. A.; Beuermann, S.; Paquet, D. A.; McMinn, J. H. *Macromolecules* **1997**, *30*, 3490–3493.

[272] Hutchinson, R. A.; McMinn, J. H.; Paquet, D. A.; Beuermann, S.; Jackson, C. *Ind. Eng. Chem. Res.* **1997**, *36*, 1103–1113.

[273] Bruker, SAINT v7.68, Madison, 2009.

[274] Sheldrick, G. M. SADABS 2008/2, Göttingen, 2008.

[275] Sheldrick, G. M. *Acta Crystallogr. A* **2007**, *64*, 112–122.

Acknowledgements

For all of the people who have accompanied me on my academic path in the past years and made some contribution to this work, I want to express my deep gratitude.

First and foremost, I want to thank my main supervisor Prof. Dr. Philipp Vana for giving me the great opportunity to work on a fascinating field of research with his full support. Discussions with him have always been motivating and inspiring, and I am grateful for his trust in my competence and skills.

I want to thank my secondary supervisor Prof. Dr. Michael Buback for his guidance on my studies. I consider his insightful comments as a great contribution to my work.

I am thankful to my third supervisor Prof. Dr. Dietmar Stalke for the cooperation within the international Ph. D. program "Catalysis for Sustainable Synthesis" (CaSuS), where I could benefit from the huge expertise in the field of crystallography.

I would also like to acknowledge Prof. Dr. Peter Botschwina, Prof. Dr. Burkhard Geil, and Jun.-Prof. Dr. Ricardo Mata for being part of my thesis committee.

As for financial support and competent guidance, I want to thank the international Ph. D. program CaSuS, which has allowed me to communicate with various skilled and experienced researchers in a huge number of seminars, workshops, and conferences in Germany, as well as the United Kingdom, Italy, and China.

I feel indebted to Assoc.-Prof. Dr. Gregory Russell for what I call a planet-spanning friendship. Apart from cooperating in the research on BB

effects in SEC, he brought sagacious aspects to our exciting discussions about the science of both chemistry and football (although he still lacks the well-deserved betting gold medal).

I want to thank Dr. Hanna Steininger for coordinating the CaSuS program and Dr. Markus Hold for his kind help with administration matters.

I would like to thank Dr. Christoph Kornhaaß and Prof. Dr. Lutz Ackermann for cooperation under the CaSuS program, for providing the PAD PinP(O)H, as well as for great help in answering general questions regarding organic chemistry.

I would like to extend my thanks to Heike Rohmann and Sandra Lotze for support with experimental works as well as to Dr. Hans-Peter Vögele for valuable help in the field of spectroscopy.

I want to thank the Department of Central Analytics and Mass Spectrometry of the Institute of Organic and Biomolecular Chemistry and representatively their members Dr. Holm Frauendorf and Frank Hambloch for friendly support in obtaining and resolving mass-spectrometric data.

Great contribution to my work came from Lara Riemann, Steffen Eggers, Malte-Ole Schneemann, Björn Sölter, and Daniel Zell, who I had the luck to supervise. They worked on their projects with high interest and motivation and my special thanks go to all of them.

Discussions with Dr. Wibke Meiser, Dr. Robert Rotzoll, Dr. Johannes Barth, Dr. Jens Schrooten, and Hendrik Kattner were as helpful as their tremendous support regarding experiments and the introduction to various instruments—especially at the outset of the work.

I am very thankful to Julia Möhrke and Dennis Hübner for diligent proofreading of my thesis.

I want to thank all the past and present colleagues and group members for the friendly, supportive, and relaxed atmosphere, which I consider an indispensable factor for successful research.

I want to express deep gratitude to my fellow students Adam, Bastian, Jakob, Reent, and Stefan for their friendship.

Finally, I want to thank my family for their unconditional manifold support. That also includes my partner Linda. I consider myself incredibly lucky to have her in my life.

About the author

Arne Wolpers, * May 21, 1984, Hildesheim, Germany, German citizen.

Curriculum vitae

2010–2014 *Promotion (Ph. D. student)*, Georg-August-Universität Göttingen, final grade: "summa cum laude", supervisor: Prof. Dr. Philipp Vana.

2009–2014 *Teaching assistant*, Institut für Physikalische Chemie, Georg-August-Universität Göttingen.

2009 *Diplom (final degree)*, Georg-August-Universität Göttingen, final grade: "sehr gut", thesis title: "Mechanismus der Reversible Chain Transfer Catalyzed Polymerization" ("Mechanism of the reversible chain transfer catalyzed polymerization"), supervisor: Prof. Dr. Philipp Vana.

2005 *Vordiplom (intermediate examinations)*, Georg-August-Universität Göttingen, final grade: "gut".

2003–2009 *Student of Chemistry* at the Georg-August-Universität Göttingen, Germany.

2003 *Abitur (final secondary-school examinations)*, Bischöfliches Gymnasium Josephinum, Hildesheim, Germany, final grade: "1,7".

Publications

- "*H*-Phosphonic Acid Derivatives as Catalysts for Reversible Chain Transfer Catalyzed Polymerization (RTCP) at Ambient and High Pressure"
  A. Wolpers, L. Ackermann, P. Vana, *Macromolecular Chemistry and Physics* **2011**, *212*, 259–265.

- "The Impact of Band Broadening on Molar-Mass Determination of Narrow-Distribution Polymer by Size-Exclusion Chromatography"
  A. Wolpers, G. T. Russell, P. Vana, *Macromolecular Theory and Simulations* **2011**, *20*, 667–674.

- "UV Light as External Switch and Boost of Molar-Mass Control in Iodine-Mediated Polymerization"
  A. Wolpers, P. Vana, *Macromolecules* **2014**, *47*, 954–963.

Contributions to conferences

- "A New Phosphine Oxide as Catalyst for Reversible Chain Transfer Catalyzed Polymerization (RTCP)"
  Poster, 43rd IUPAC World Polymer Congress, "Macro2010", Glasgow, UK, **July 2010**.

- "Use of Non-Transition-Metal Catalysts in Reversible Chain Transfer Catalyzed Polymerizations (RTCPs)"
  Poster, Niedersächsisches Katalyse Symposium "NiKaS", Göttingen, **October 2010**.

- "Impact of Band Broadening on Molar-Mass Determination of Polymers via SEC"
  Poster, Niedersächsisches Katalyse Symposium "NiKaS", Göttingen, **October 2012**.

- "Impact of Band Broadening on Molar-Mass Determination of Polymers via SEC"
  Poster, European Polymer Congress, "EPF 2013", Pisa, Italy, **June 2013**.